An Analytical and Experimental Stochastic Modelling of the Resultant Force System in BTA Deep-Hole Machining and Its Influence on the Dynamics of the Machine Tool Workpiece System

Srinivasan Chandrashekhar

A Thesis

in

The Department

of

Mechanical Engineering

Presented in Partial Fulfilment of the Requirements
for the degree of Doctor of Philosophy at
Concordia University
Montréal, Québec, Canada

June 1984

DEDICATED TO LORD VINAYAKA

ABSTRACT

ABSTRACT

An Analytical and Experimental Stochastic Modelling of the Resultant Force System in BTA Deep-Hole Machining and Its Influence on the Dynamics of the Machine Tool Workpiece System

Srinivasan Chandrashekhar
Concordia University, 1984

This investigation examines in detail the interaction between the cutting tool and the workpiece in BTA machining. Equations to represent the mean and periodic cutting forces are derived using the thin shear plane model. The equations representing the periodic cutting forces can be used when a chatter analysis of the machine tool system has to be carried out. In this investigation, the region of interest is the non-chatter zone. A theoretical approach to describe the resultant force system, consisting of an axial force and torque, is quite complex and impractical. Moreover, the characteristics of the randomly varying resultant force system can only be determined by performing a series of experiments. Hence, a set of experiments are performed to establish a mathematical model for the resultant force system. These are carried out using a piezo-electric transducer, mounted on a specially designed dynamometer. The data recorded from the dynamometer are analyzed, and a mathematical model is established to represent the resultant force system.

The effect of the resultant force system on the dynamics of the machine tool is obtained by the derivation of a system model using Lagrange's equation and assumed modes method. The solutions to these equations are combined using vector addition, to obtain an expression which describes the tool tip motion, for the case of a rotating cutting

tool-stationary workpiece system. Based on the tool tip motion, a recommendation is made on the development of a microprocessor based adaptive control unit. Also, an index to define the roundness error is presented. The roundness error obtained from this index for certain machining conditions, is compared with a set of experimental values obtained under the same conditions and it is conjectured that the resultant force system is not completely balanced at the pads.

ACKNOWLEDGEMENTS

ACKNOWLEDGEMENTS

The author wishes to express his gratitude and appreciation to his thesis supervisors, Dr. T.S. Sankar, and Dr. M.O.M. Osman for initiating the project and providing continued guidance throughout the investigation.

The financial support of the Natural Sciences and Engineering Research Council Grants No. A5181 and A7104, Formation de Chercheurs et d'Action Concertee of the Government of Quebec, Grant No. G12, and the Concordia University Graduate Fellowship awarded to the author are gratefully acknowledged.

The assistance and suggestions of Mr. J. Seeger, Mr. E. Heasman, Mr. J. Frazao, Dr. K. Shankar, and the machine shop of the Faculty of Engineering and Computer Science, and the Mechanical Engineering Laboratories are gratefully acknowledged. Thanks are also due to Mrs. Ilana Crawford for typing the manuscript of the thesis.

TABLE OF CONTENTS

TABLE OF CONTENTS

LIST OF FIGURES

LIST OF FIGURES

LIST OF TABLES

LIST OF TABLES

NOMENCLATURE

NOMENCLATURE

a_1	amplitude of tool oscillation	[mm]
a_2	amplitude of wave on uncut surface	[mm]
A(t)	amplitude of vibration of the cutting tool boring bar system	[mm]
$A_s(t)$	amplitude of vibration of the spindle workpiece assembly	[mm]
ACRFE	adaptive control of random function excursion	
C	parameter representing material effect	[μm]
C_1	constant	
C_2	constant	
C_b	equivalent viscous damping of the boring bar cutting tool system	[N-sec/m]
C_s	equivalent viscous damping of the spindle workpiece assembly	[N-sec/m]
CLA	center line average	
CLAGF	center line average of generalized force	
d	diameter of the cutting tool	[mm]
d_s	diameter of spindle-workpiece assembly	[mm]
E	Young's modulus of steel	[N/m^2]
f	instantaneous value of feed	[mm/rev]
f_m	mean value of feed	[mm/rev]
F_T	tangential cutting force	[N]
F_R	radial cutting force	[N]
F_a	axial cutting force	[N]
F_{Tm}	mean tangential force	[N]

F_{Rm}	mean radial force	[N]
F_{am}	mean axial force	[N]
F_{aR}	resultant mean axial force	[N]
F_{ap}	peak axial force	[N]
$(dF_{Tm})_r$	mean tangential force on an incremental thickness "dr" of the cutting tool	[N]
$(dF_{qm})_r$	mean thrust force on an incremental thickness "dr" of the cutting tool	[N]
$(dF_{Rm})_r$	mean radial force on an incremental thickness "dr" of the cutting tool	[N]
$(dF_{sm})_r$	mean shear force on an incremental thickness "dr" of the cutting tool	[N]
$(dF_m)_r$	mean frictional force on the incremental thickness "dr" of the cutting tool	[N]
$(dF_{Nm})_r$	mean normal force on the incremental thickness "dr" of the cutting tool	[N]
G	modulus of rigidity	[N/m^2]
I	area moment of cross-section of beam	[m^4]
I_t	mass moment of inertia about transverse axis	[$kg-m^2$]
I_x	mass moment of inertia of the cutting tool-boring bar system about the axis of symmetry	[kg/m^2]
I_x^*	mass moment of inertia of the spindle workpiece assembly about the axis of symmetry	[kg/m^2]
J	polar moment of inertia	[m^4]
k	slope of shear stress compressive strength curve	
2ℓ	length of boring bar-cutting tool system	[m]

m_b	mass per unit length of the cutting tool boring bar assembly	[kg/m]
m_s	mass per unit length of the spindle-workpiece assembly	[kg/m]
MCE	mean crest excursion	
MCEGF	mean crest excursion of the generalized force	
MVE	mean valley excursion	
MVEGF	mean valley excursion of the generalized force	
m_a	number of distinct values of λ_{if} or Λ_{if}	
n	RPM of the cutting tool	
n_p	number of data points	
n_a	number of distinct values of λ or Λ	
$P_c(\lambda)$	probability distribution of crest excursion	
$P_c(\Lambda)$	probability distribution of valley excursion	
$P_c(\lambda_f)$	probability distribution of crest excursion of generalized force signal	
$P_c(\Lambda_f)$	probability distribution of valley excursion of generalized force signal	
$p(u,t)$	probability density function of the logarithm of the amplitude of vibration of the cutting tool	
$p_\Phi(\Phi,t)$	probability density function of the phase angle between the cutting tool vibration and the axial force	
$p(\tilde{y})$	joint probability density function of the elements of $\tilde{y}$	
$p_s(\omega,t)$	probability density function of the logarithm of the amplitude of vibration of the spindle workpiece assembly	

$p_{\Phi_s}(\Phi_s, t)$	probability density function of the phase angle between the spindle workpiece assembly and the axial force	
$p_s^*(\theta_s, \dot{\theta}_s)$	joint probability density function of the random variables θ_s, and $\dot{\theta}_s$	
p_i	length of the ith step	[mm]
R	resultant cutting force on the BTA tool	[N]
$(dR_m)_r$	mean resultant force on an incremental thickness "dr", of the cutting tool	[N]
$R_f(\tau)$	auto-correlation function for resultant axial force	
$R_T(\tau)$	auto-correlation function for resultant torque	
RMS	root mean square value	
RMSGF	root mean square value of the generalized force	
RMSCE	root mean square crest excursion	
RMSCEGF	root mean square crest excursion of generalized force	
RMSVE	root mean square valley excursion	
RMSVEGF	root mean square valley excursion of generalized force	
t	time	[sec]
T_m	mean cutting torque acting on the cutting tool	[N-m]
T_R	resultant torque	[N-m]
T	peak resultant torque	[N-m]
v_c	cutting velocity	[m/sec]
v_o	flow velocity of oil chip mixture	[m/sec]
α	rake angle of the cutting tool	[radians]

α_w	working rake angle of the cutting tool	[radians]
α_r	rake angle of the tool at a distance "r" from the axis	[radians]
β_r	friction angle at a distance "r" from the axis of the cutting tool	[radians]
γ	mass per unit volume	[kg/m]
γ_i	approach angle of the ith step	[radians]
δ_c	work surface and also the slope of the surface generated	
$[\Delta_x]_{av}$	average "x" component deviation of the cutting tool tip relative to the spindle workpiece assembly	[meters]
$[\Delta_y]_{av}$	average "y" component deviation of the cutting tool tip relative to the spindle-workpiece assembly	[meters]
$[\Delta_x]_{max}$	maximum "x" component deviation of the cutting tool tip relative to the spindle-workpiece assembly	[meters]
$[\Delta_y]_{max}$	maximum "y" component deviation of the cutting tool tip relative to the spindle-workpiece assembly	[meters]
$[\Delta_x]_{min}$	minimum "x" component deviation of the cutting tool tip relative to the spindle-workpiece assembly	[meters]
$[\Delta_y]_{min}$	minimum "y" component deviation of the cutting tool tip relative to the spindle-workpiece assembly	[meters]
$[\Delta_R]_{max}$	maximum value of the deviation of the cutting tool tip relative to the spindle-workpiece assembly	[meters]
$[\Delta_R]_{av}$	average value of the deviation of the cutting tool tip relative to the spindle-workpiece assembly	[meters]

$[\Delta_R]_{min}$	minimum value of the deviation of the cutting tool tip relative to the spindle-workpiece assembly	[meters]
ε_{max}	angle made by $[\Delta_R]_{max}$ with the X' axis	[radians]
ε_{av}	angle made by $[\Delta_R]_{av}$ with the X' axis	[radians]
ε_{min}	angle made by $[\Delta_R]_{min}$ with the X' axis	[radians]
ζ_i	generalized co-ordinate	
η	generalized co-ordinate	
θ	phase angle between uncut surface wave and tool oscillation	[radians]
θ_s	generalized co-ordinate	
λ	chip compression factor	
μ	co-efficient of friction	
μ_c	mass per unit length of chip oil mixture	[kg/m]
ξ_i	generalized co-ordinate	
τ	shear strength of material	[N/m^2]
τ_o	shear strength of material at zero compressive stress	[N/m^2]
Φ_1, Φ_2	mode shapes of the cutting tool-boring bar assembly	
$\phi(\omega t+\theta)$	function describing the variation of co-efficient of friction with angular velocity	
ϕ_i	instantaneous value of shear angle	[radians]
ϕ_{im}	instantaneous value of the shear angle measured relative to the mean cutting direction	[radians]
ϕ_r	mean shear angle at a distance "r" from the axis of the cutting tool	[radians]
Ψ_1, Ψ_2	mode shapes of the spindle-workpiece assembly	
ω	frequency of oscillation of tool tip	[Hz]

ω_r	natural frequency of vibration	[Hz]
ω_o	angular velocity of cutting tool	[rad/sec]
ω_b	angular velocity of cutting tool relative to spindle-workpiece assembly	[rad/sec]

CHAPTER 1

INTRODUCTION

CHAPTER 1

INTRODUCTION

Deep hole machining is known to be one of the most complex of all hole making operations, wherein the individual drilling processes are categorized by the types of tools they employ. The choice of a specific drilling process for any particular application, starts with the requirements of the hole-diameter, depth, macro- and micro errors of geometry and must include not only the production volume, but also the specific types of drilling equipment available. The sub-category of "deep-hole drilling" includes gundrilling, BTA drilling, and trepanning. One of the main features about this type of machining is that the tool holding structure is relatively slender and this adversely affects the cutting tool life, the accuracy of the finished hole, and the entire dynamical behaviour of the machine tool.

1.1 A Historical Background

Historically, hand drills were built during the new stone age [about 4000 B.C.]. The device was a bow drill consisting of a wooden shaft tipped by a sharp piece of hard stone. The shaft was rotated in a wooden frame and was loaded by a heavy piece of stone to provide the thrust. But, the actual problem of producing deep-holes was first attempted in the middle ages, when holes had to be drilled in the center of logs for use as water mains [1]. Deep-hole metal drilling was first employed in the production of gun barrels during 16th to 18th centuries in Germany with water mill as a machine tool and spade bits as cutting tools. Two barrels could be drilled simultaneously by two parallel boring spindles with the feed and thrust produced by the operator. The

first vertical gun boring machine was invented in 1713, where a cutter head mounted on the end of a boring bar was rotated by animal power, and a downward feed was given to the gun barrel. The frame of the machine, made entirely of wood, formed a part of the structure housing it [2].

The first boring machine, produced in 1758 by Verburggen, was of massive construction, and is regarded as the first example for engineering applications. Here, the axis of rotation of the gun was horizontal, and the feed motion was given to the boring tool. The cutters consisted of a spade drill with two boring cutters. Since then, with the development of science and technology many sophisticated deep-hole machining systems have been built.

1.2 Manufacturing Capability of Drilling Operations

Drilling operation involves the conversion of the material within a desired cavity into conventional chips by the relative rotation of a cutting tool and the workpiece. The manufacturing capability of each of the different drilling processes is examined in detail. This enables the determination of the important characteristics and the process capability of the BTA system as compared to other drilling processes. This also leads to the identification of the important parameters which influence the BTA deep-hole machining operation.

1.2.1 Twist Drilling

Twist drills are the most common tools used in hole making operations. They can be employed in almost any type of machine tool that can provide relative rotation and axial translation of a tool and a workpiece as well as in both pneumatic and electric portable tools.

Although twist drills are manufactured to fairly close tolerances the twist drill is not a precision tool. The tool is typically long and slender (Fig. 1.1), its helical flutes constitute a column eccentricity that further reduces rigidity under axial thrust loading, chip elimination is difficult, heating problems are aggravated, cutting speeds vary from zero at the center to a maximum at the periphery, and the depth of cut is fixed at half the diameter.

The cutting end of a twist drill presents two distinctly different features, a pair of cutting lips and the chisel edge. The symmetrical location of the cutting lips in a twist drill leads to a completely balanced force system [3]. But the drilling process becomes unstable due to any disturbance that might arise from the uneven grinding of the point angle or wear of the drill cutting edges. Such an unbalance of the force system leads to waviness and considerable runout of the drilled hole, when the hole to be drilled is very long [4,5]. This instability is the major reason why twist drills are unsuitable for drilling holes with high length to diameter ratio.

1.2.2 Half-Round Drills

The half round drill is essentially a length of round rod with approximately half its diameter ground away at the business end and a conical point which is offset to provide radial relief for the single cutting lip [3]. The flat, provides both space for chip removal and a zero degree cutting rake face. A slight back taper is incorporated behind the tip.

Correctly ground half round drills have a conical point near the cutting edge. Thus, they will start accurately in position and will have

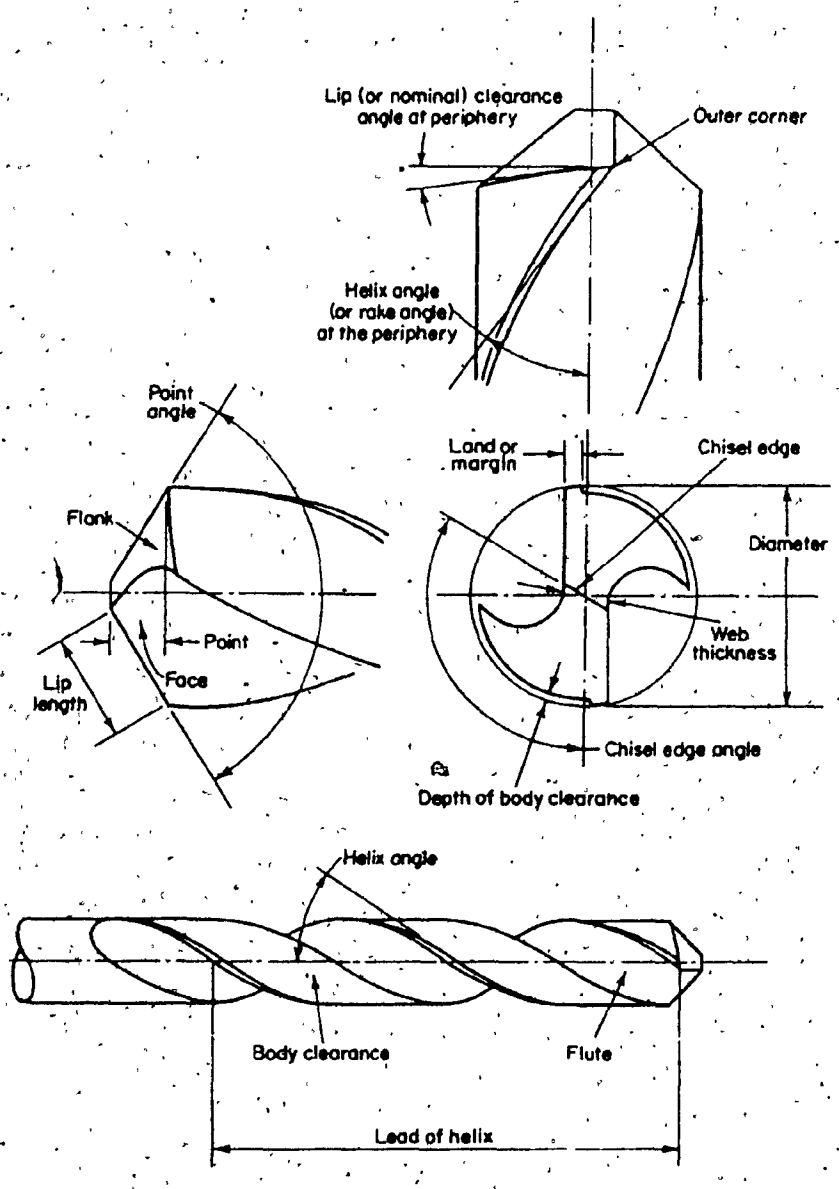

Figure 1.1: A Typical Twist Drill

no tendency to drift - even in very small diameters that are inherently flexible. In view of this, half-round drills exceed the capability of two-lipped drills on diameter tolerances and internal finish. The only drawback in half-round drills is that the chip flushing system is inefficient. Since the half-round drills are used dry, the only thing that pushes the chips are the new chips formed. In view of this, the depth-to-diameter ratio of half-round drills is generally held below 10:1 in horizontal positions or 2:1 in vertical position.

1.2.3 Microdrilling

Microdrills as the name suggests are used for machining small holes, with their largest size being 0.5 mm. These drills are two-lipped end-cutting tools of relatively simple geometry that lie somewhere between that of a half round with the second side also flattened and that of a twist drill without the helical twist.

One of the major problems is the fact that its rigidity is small, as the rigidity is approximately inversely proportional to the fourth power of diameter. The microdrills should be as short as possible, as the deflection varies as the cube of the length. The second major problem is extreme close tolerance depends upon the dimension of the hole.

1.2.4 Spade Drills

The spade drills, shown in Fig. 1.2, consists of two parts viz. a flat blade, and a shank. The two piece tool consists of a holder that has a shank at one end and is slotted to accept a mating notch at the rear end of the blade. The geometry of the blade itself bears much resemblance to the twist drill and the half round drill, but in view of the large diameters and heavy feeds involved, the rake face of each

Spade drill

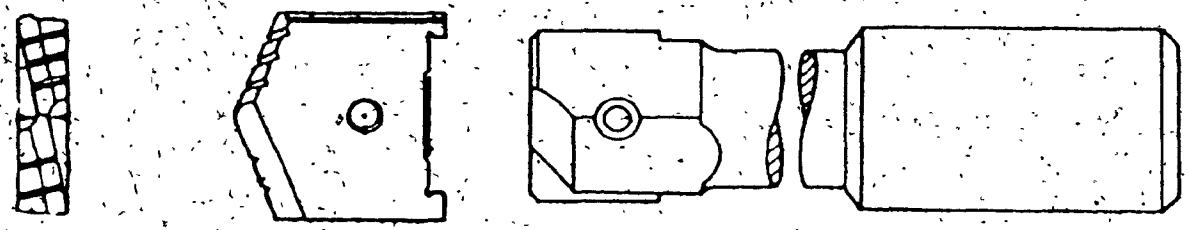

Figure 1.2: A Typical Spade Drill

cutting tip is generally ground in a manner that provides a positive rake angle of five to twelve degrees.

The elimination of chips is a vital concern in spade drilling and this is the reason for all the chip splitting and chip breaking features at the point. The chips must be reduced in size so that they can exit around the head of the holder and back out in the space between the hole ID and the holder.

Problems arise in spade drills during the breakthrough of a hole. As the point breaks through, the cutting fluid escapes through the path of least resistance, thus causing overheating and metallurgical damage to the cutting tool. Another problem is the tendency of the machine to spring back somewhat as the breakthrough relaxes the heavy thrust of the operation.

Despite these problems, spade drills are used to produce holes in which the depth to diameter ratio exceeds 40:1 in horizontal drilling, but the depth to diameter ratio never exceeds 10:1 in vertical drilling.

1.2.5 Indexable Insert Drills

The indexable insert drills are used for producing shallow holes. They not only provide the benefits of throwaway inserts, but also provide the capability of producing holes at carbide speeds.

Most of the insert drills are essentially two-flute drills with two or three inserts fixed to the business end: one insert cuts to the center, one cuts to the ID of the hole, and the third insert, if present, serves to fill the gap between the first two. Since, most designs incorporate straight flutes, the insert drill has no inherent chip pulling action. So the drill bodies provide for coolant delivery through the

tool, which is effective in washing out the chips produced. Compressed air can be fed through the coolant passage to help evacuate the dust like chips produced in drilling brittle materials.

The indexable-insert drill is unique among drilling tools in its capability to perform boring operations in addition to drilling. Surface quality of the holes produced by indexable drills is similar to that obtained by twist drilling.

1.2.6 Gundrilling

The gundrills are single lip, end-cutting tools which drill a hole in a single pass. They consist of a crimped alloy-steel tubing shank with a carbide edge tip brazed or mechanically fixed to it. The cutting edge cuts through the center on one side of the hole, leaving no area of material to be extruded. The cutting is done by the outer and inner cutting angles which meet at a point. The depth of the hole theoretically has no limit, but in practice is limited by the torsional rigidity of the shank [6].

Gundrills have a single lip cutting action. Bearing areas, and lifting forces generated by the coolant pressure counteract the radial and tangential loads. The single lip construction with its supporting bearing arrangement forces the cutting edge to cut in a true circular pattern. Due to this principle of guidance the tip follows the direction of its own axis.

Hole straightness is affected by a number of variables, such as diameter, depth, uniformity of the workpiece material, condition of the machine, sharpness of the gundrill, feeds and speeds used, and the specific technique (rotation of the tool, of the work, or counter-rotation)

used. Also, due to the single lipped construction, a pre-bored start must be made into the workpiece or a starter bushing provided to support the tool initially.

1.2.7 Ejector Drills

The ejector drill, shown in Fig. 1.3, is a special tool used for drilling. Here the coolant is introduced between the outer and inner tube. About one third of the coolant is drawn off through the annular nozzle straight back through the inner tube, moving with a sufficient velocity to set up a partial vacuum in the two chip passages. The rest of the coolant passes through a number of holes and provides cooling and lubrication of the cutting edges and the supporting pads, after which it is drawn by vacuum back through the inner tube and carried away with the chips.

The tool itself is a three-edge arrangement, two edges located on one side and the third one at 180° from the other two edges. One cutting edge starts from the periphery of the head and cuts through approximately 0.4 of the radius. The second cutting edge cuts through the center approximately 0.4 of the radius. The third one located at 180°, cuts the remainder of the area partially overlapping the area cut by the other two edges. This arrangmenet gives the tool partially balanced cutting forces, and takes some load off the supporting pads.

1.2.8 Trepanning

Trepanning is a process for making round, accurate holes from solid, requires a pressurized cutting fluid system, and employs self piloting cutting action. The main characteristics of the trepanning operation are (a) it is practical for making holes greater than 60 mm.,

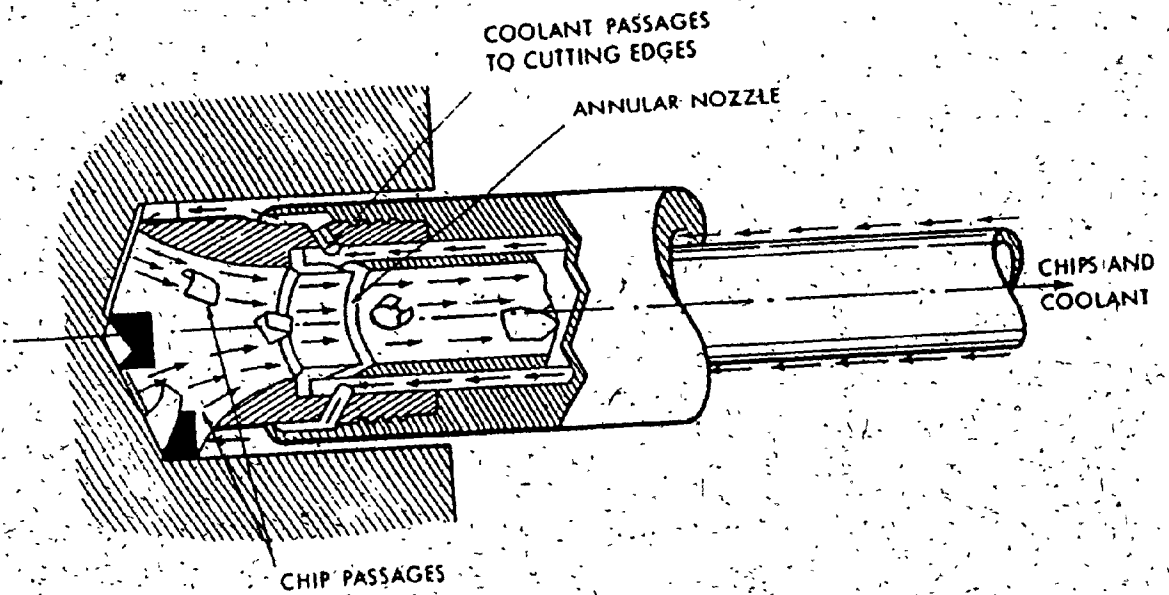

Figure 1.3: An Ejector Drill

(b) it produces a solid core instead of chips.

The trepanning tool consists of one cutting bit situated with the cutting edge protruding from the end of a tubular shaped head, and two wear pads located on the circumference at the most advantageous points to carry the cutting pressure of the bit. The head must have an appropriate chip mouth.

Trepanning tools, in general, are noted for the straightness of the hole they produce and maintain, even at extended depths. The reasons for this lie in the design of the head and in the alignment accuracy of the machine used. Once the bore is started and the wear pads fully engage the wall of the hole, the tool alone maintains size and concentricity.

1.2.9 BTA Drill

This method basically utilizes single edge cutting tools with internal chip removal. The BTA drilling head presents an asymmetrical cutting edge balanced by wear pads at approximately 90° and 180° behind the cutting edge to provide guidance after the tool has entered the workpiece through a guide bushing. Figure 1.4 shows some typical BTA tools. This tooling when integrated with a high pressure lubrication system, which removes the chips through the interior of the drill tube (boring bar), works very well, and thus helps in producing holes of high accuracy of size, parallelism, straigthness, and surface finish. The principle of the BTA deep-hole machining operation is shown in Fig. 1.5.

The BTA machining operation can be performed on every type of machine tool that has facilities for rotating a spindle or workpiece. But most often they are carried out on the following machine tools:

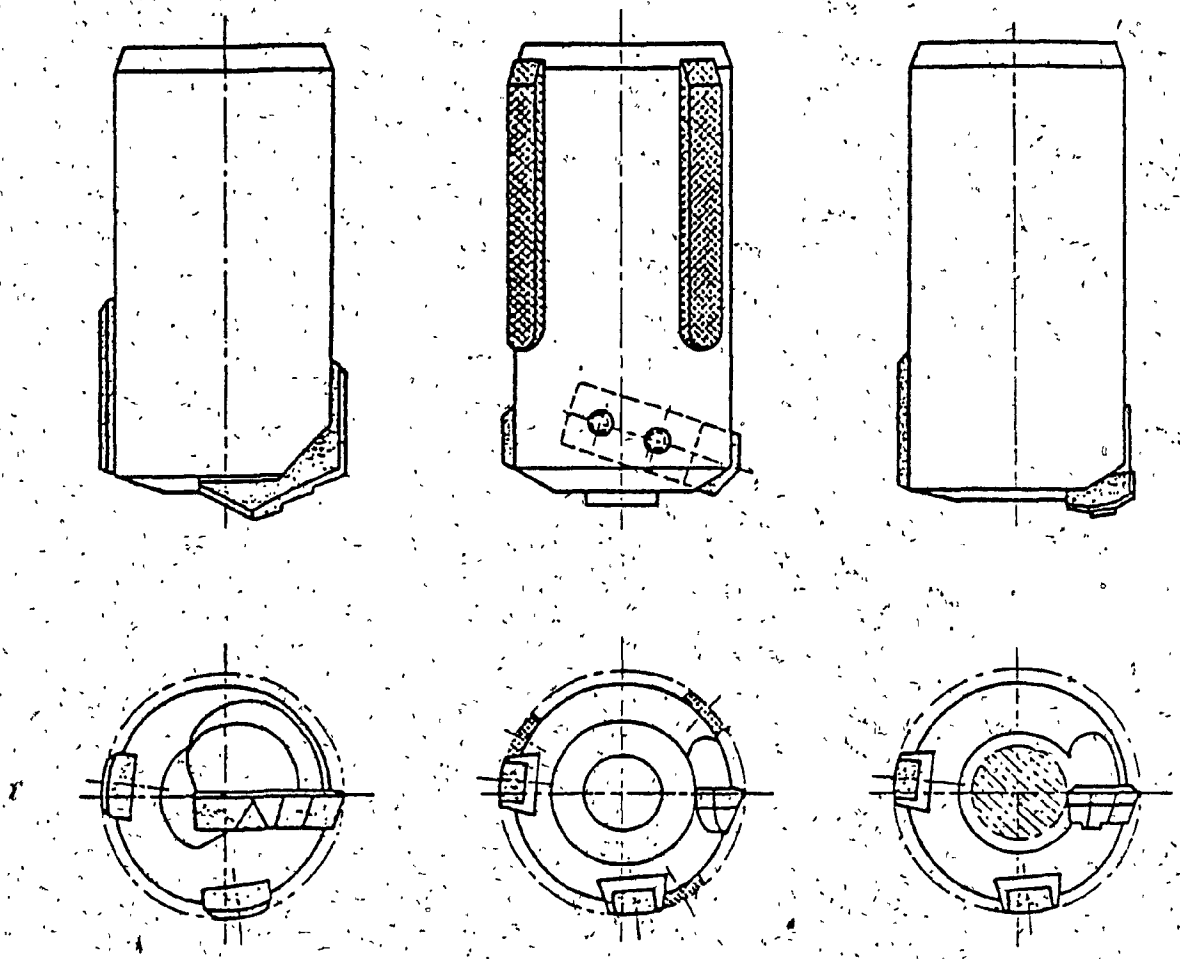

Figure 1.4: Typical BTA Tools

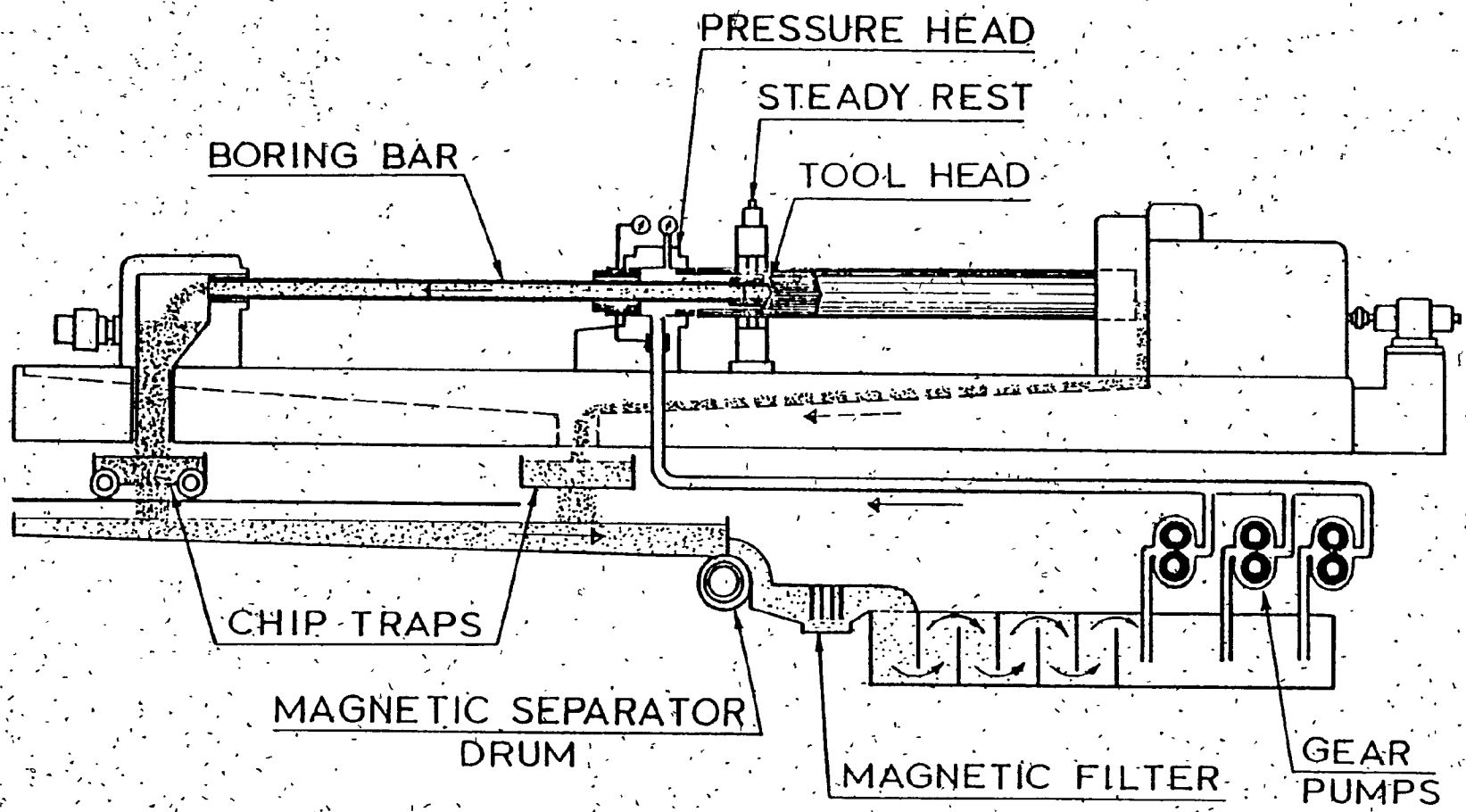

Figure 1.5: The Principle of BTA Deep-Hole Machining Operation

(a) Engine Lathe.

(b) Turret Lathe.

(c) Screw Machine.

(d) Vertical Boring Mills.

(e) Vertical Turret Lathe.

(f) Horizontal Boring Mill.

(g) Drill Press.

(h) Precision Boring Machine.

(i) Deep-Hole Drilling Machine.

Just like gundrilling, even in the BTA process either the work or the tool may be rotated or both may be rotated in opposite directions. Table 1.1 summarizes the process capability of the BTA process as compared to other drilling processes.

1.3 Literature Survey

The study and analysis of the dynamical behaviour of the machine tool in BTA drilling and its influence on the accuracy of the finished hole needs a thorough understanding of the BTA process, the mechanics of metal removal, the measurement of forces, and the methods of analyzing machine tool dynamics. Therefore, a literature survey is carried out on each of these topics and concepts introduced in some of the works described are taken as the basis for this investigation.

1.3.1 Cutting Force Models

Investigators in the metal cutting field have attempted to develop an analysis of the cutting process which gives a clear understanding of the mechanism involved and which enables a prediction of the

Table 1.1: Process Capability of Drilling Operations

	Twist Drill	Half Round	Gundrill	Spade Drill	Ejector Drill	Trepanning	BTA Drill
DIAMETER [mm]							
Typical Range	0.5 to 50	0.12 to 8	1.4 to 25	25 to 150	18 to 60	42 to 250	12 to 200
DEPTH/DIAMETER RATIO							
Min. Practical	no. min.	no. min	< 1	no. min.	1	10	1
Common Max.	5 - 10	> 10	100	> 40	50	100	100
Ultimate	> 50	> 50	200	10(vert.) >100(hor.)	> 50	> 100	> 100

cutting forces without the need for exhaustive empirical testing. The first effort in this direction was due to Merchant [7] who developed an analysis for the cutting force based on the thin shear plane model. He assumed that the process is steady, the tool is sharp, and the deformation two-dimensional. Kobayashi and Thomsen [8] agreed with Merchant's analysis, but Palmer and Oxley [9] and Okushima and Hitomi [10] disagreed and suggested an analysis based on a thick deformation zone.

Shaw, Cook, and Smith [11] extended the above analysis to three-dimensional problems and suggested methods to study the chip flow direction. An alternate procedure was given by Brown and Armarego [12] who studied the cutting forces and predicted the chip flow.

Kronenberg [13] derived an empirical equation for calculating the the force necessary to drill in steel, and Shaw and Oxford [14], applying dimensional analysis, predicted that the thrust force and torque in drilling depended on the Brinell hardness of the work material and the ratio of the chisel edge length to drill diameter. Similarly, empirical methods for determining forces and power in milling were suggested by Boston and Kraus [15], by giving an expression for the work done per chip, and Koenigsberger and Sabberwall [16] developed nomograms for giving the average force, the maximum force, and the power consumption.

All the above investigations assume that the cutting process is a steady state process and that the cutting forces have no dynamic fluctuations. Not only is this approach inaccurate in many machining processes, but also, some very important parameters such as machinability, the surface texture of the machined work, the tool life, and the power consumption depend upon the magnitude and frequency of cutting force fluctuations.

Arnold [17] assumed that the fluctuations in the cutting force arises due to the fluctuations in the depth of cut and the rake angle. He took account of these fluctuations, by introducing a linear function in the displacement of the tool and postulated a velocity principle to study the stability of the machining operation. Doi and Kato [18] proposed that the cutting force always lags behind the chip thickness fluctuations because of the time lag in the change in frictional resistance on the tool face. Thus they considered that the fluctuations of the cutting force arises due to the fluctuations in chip thickness. Experimental observations made by them during metal cutting with imposed low frequency oscillations on the tool, showed a time lag as per this theory.

Tobias and Fishwick [19,20] and Tobias [21] assumed that the dynamic cutting force is composed of components proportional to the variation in chip thickness, feed velocity, and the rotational speed. They suggested that these components could be determined from steady state machining tests. Later, Smith and Tobias [22] stated that the results obtained by Doi and Kato [18], with a forced fluctuation in the undeformed chip thickness showed a force lag only because the frequency of fluctuations were low. Basing their results on the Tobias-Fishwick model [20], they claimed that the fluctuation was only a result of machine tool chatter.

Albrecht [23] in his classical paper took into account the variation in shear angle due to sinusoidal variation in the uncut chip thickness in deriving the force relationship. The instantaneous shear angle expressions were derived from the geometric considerations which also

included the changes in cutting velocity. In a parallel investigation, Wallace and Andrew [24,25] established that the oscillating cutting forces are in phase with and proportional to the geometry of the machining process and that the speed is not a significant variable provided that no appreciable built-up edge existed. Das and Tobias [26] show the proportionality constants suggested by Tobias and Fishwick [19,20] from the steady state experimental data using the concept of universal machinability index [27]. Kainth [28,29] refined the Das-Tobias [26] approach by considering the variation of the shear angle as affected by variations in rake angle and chip thickness. This method is very involved to allow practical application in the determination of the dynamic force.

Nigm, Sadek and Tobias [30,31] used dimensional analysis to evaluate the dominant parameters and their influence on the dynamic cutting forces. They considered the variations in the instantaneous cutting conditions, the instantaneous rake angle and the instantaneous free surface slope. The model requires a number of constants to be evaluated from the steady state and dynamic cutting data in addition to using lengthy expressions.

Rubenstein [32] considered the geometrical modifications as well as the variations in strain and strain rate properties of the material due to tool oscillations. His model is based on the promise "that only those events, which have been observed during steady or quasi-steady state cutting, are assumed to occur in dynamic cutting". Thus the resulting dynamic cutting force equations obtained are non-linear and he suggested [33] a method of linearizing these equations for applications, which compared favourably with experiments [34].

Sarnicola and Boothroyd [35] showed both by experiments and theory that the work surface slope plays an important role in changing the amplitude and phase of the resulting forces. With the help of this, the existence of chatter susceptibility condition was derived [36]. Fabris and D'Souza [37] considered the dynamic cutting force as a Fourier series based on experimental results [23] and thus obtained a non-linear transfer function between the force and chip thickness.

Hanna and Tobias [38] considered the cutting force as a polynomial of third degree in terms of the uncut-chip thickness variation. The proportionality constants of the polynomial were determined from experiments under steady state cutting condition. Grasso, Nato La Diega, and Passannanti [39] derived equations for three dimensional cutting by assuming a linear force model for static cutting assuming that the tool angles and the shear plane orientation do not change during chatter. Bickel [40] was the first to recognize the stochastic nature of the cutting forces in metal cutting. He used piezo-electric devices for the cutting force measurements and proved that the degree of randomness could be a high percentage of the steady state cutting force. Based on this observation, Maragos [41] proved experimentally that the cutting forces in turning are essentially stochastic in nature and are gaussian distributed for the finishing operation. Rakhit, Sankar, and Osman [42] verified that the cutting forces in turning are random and gaussian distributed. Furthermore, a relationship between the surface texture and the cutting force fluctuations is obtained, which in turn plays an important part in the characterization of the machined surface.

Osman, Xistris, and Chahil [43] showed that the dynamic fluctuations

of torque and thrust in drilling are stationary, processes with a gaussian density function. Also, it was shown that under certain conditions the degree of randomness could be as high as 50% of the steady state value.

The various cutting force models discussed in this section bring out the influence of the different machining parameters on the cutting force. Using certain characteristics discussed, a cutting force model for the BTA deep-hole machining process, considering its salient features can be derived. Further, since the resultant force system in finish turning and drilling is random in nature, it can be expected at this stage, that the resultant force system in BTA deep-hole machining process is also random in nature, as it is both a roughing and finishing process.

1.3.2 Dynamometry

The measurement of metal cutting forces are performed either by measuring directly the deformation due to the cutting forces or by measuring the transformed deformation by a transducing element. Direct indicating dynamometers are of the mechanical type, the deformation being picked up by the dial indicators. The basic scheme of such a dynamometer is shown in Fig. 1.6. However, for achieving larger sensitivites, the deformation is often magnified by the lever system.

One of the earliest two component dynamometer was designed by Merchant [7] to measure the forces in orthogonal machining. The schematic diagram is shown in Fig. 1.7. Rosenhein, Schlesinger, and Vulf [96] used a hydraulic dynamometer in which mercury or some suitable fluid was used as a pressure transmitting medium. A three dimensional capacitive tool force dynamometer, where the cutting force is a function of the change in capacitance developed in the U.S.S.R. is shown in

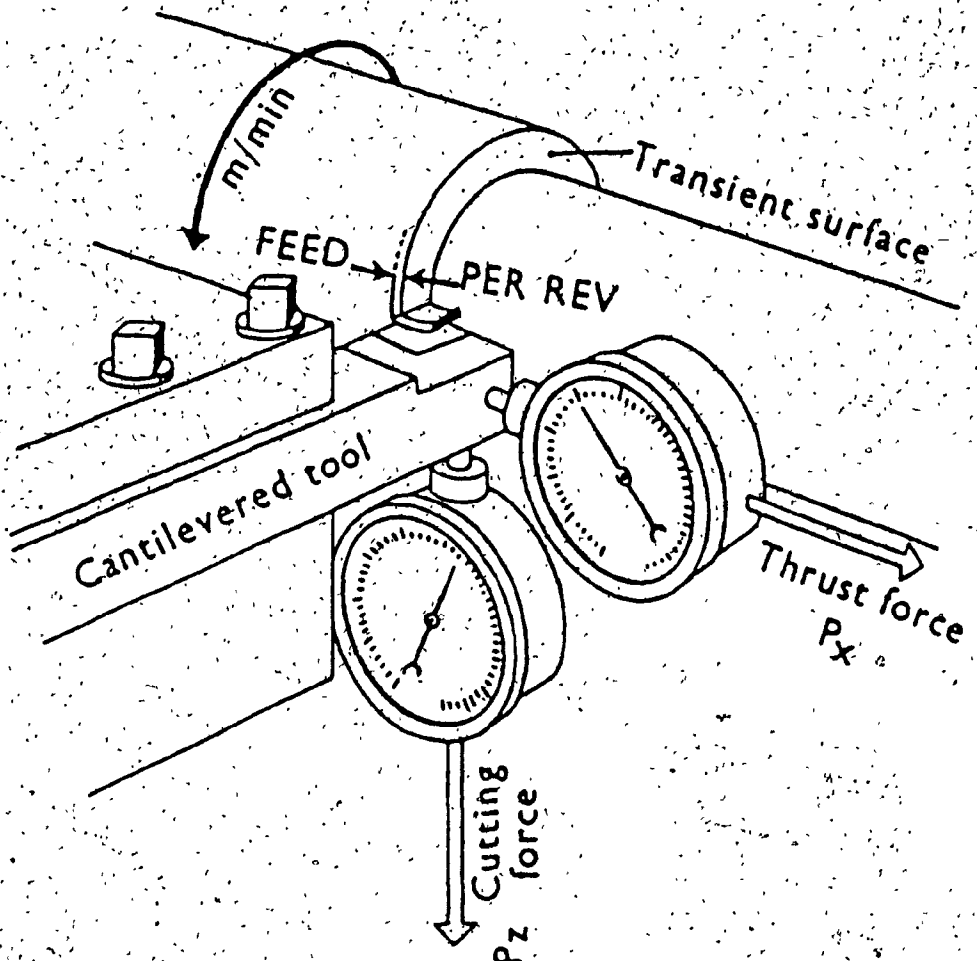

Figure 1.6: Basic Scheme of a Dynamometer

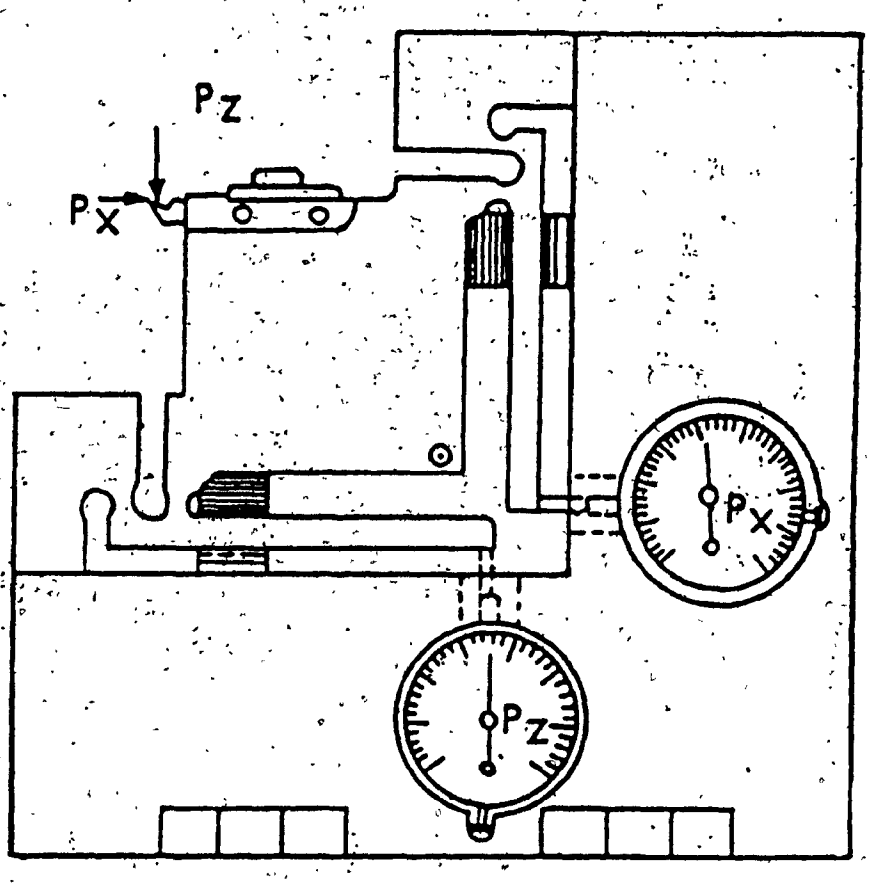

Figure 1.7: Principle of a Mechanical Tool Dynamometer

Fig. 1.8 [96]. An inductance type dynamometer used by Wallichs and Opitz [44] is shown in Fig. 1.9. Here the dynamometers employ the unbalancing of the circuit due to a change in mutual inductance caused by the mechanical deformation. The turning dynamometer used by Shaw, Cook and Lowen [45] was based on the principle of a strain gauge, where the unbalance in the wheatstone bridge indicates the cutting forces. Two sets of four gauges each were connected into two bridge circuits to enable the determination of the forces accurately. This same principle was used in an improved version lathe dynamometer by Shaw, Lowen and Marshall [46] shown in Fig. 1.10. The main element of this unit is the bar which carries the tool. The ends of the bar are rigidly clamped. Eight gauges are cemented to the central bar in the position shown in Fig. 1.10. Gauges 1-4 are attached along the top and bottom surfaces at an angle of 45° to the bar axis and are parallel to each other. These gauges measure the torsional stress produced in the bar by the vertical component of the force. Gauges 1-4 will be in tension and gauges 2-3 in compression. Similarly gauges 5-8 measure the other component of force.

A three dimensional tool force dynamometer constructed by Okushima and Hitomi [47] consists of an elastic disk which is supported at its periphery and a cutting tool installed on a circular base in the center of the disks. Strain gauges are attahced to the surface of the disk. These gauges are used for measuring the principal cutting force, the feed cutting force and the radial cutting force. Since the cutting forces were shown to be random in nature, Micheletti, Von Turkovich, and Rossetto [48] constructed a three component dynamometer capable of measuring these dynamic variations of the cutting forces accurately. This dynamometer consists of five components, a square plate tool holder, four

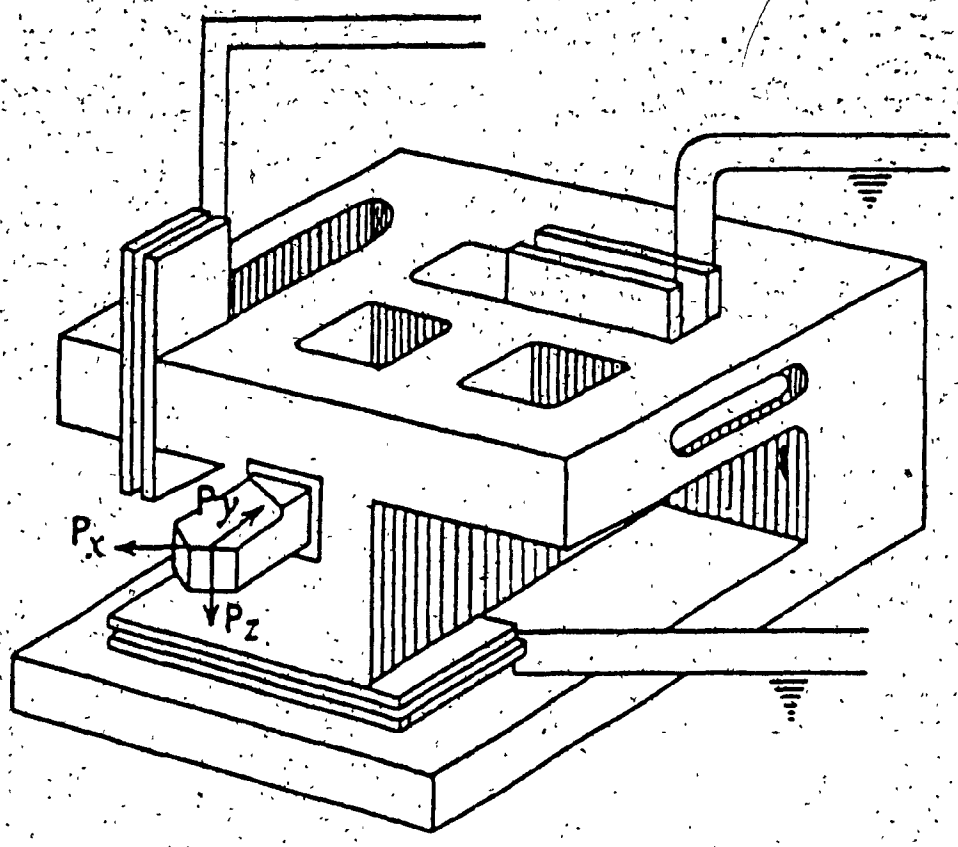

Figure 1.8: Schematic Diagram of a Capacitive Tool Force Dynamometer

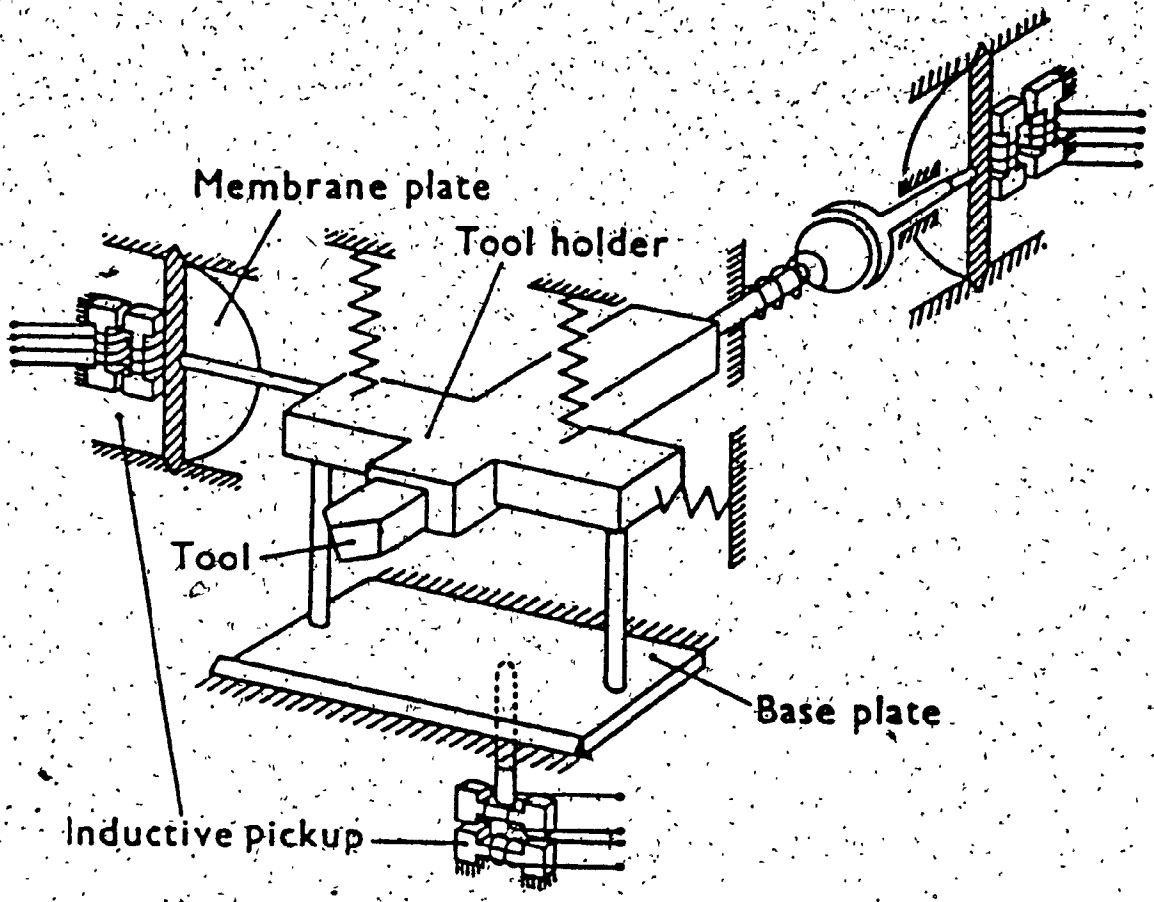

Figure 1.9: An Inductive Three Dimensional Tool Force Dynamometer

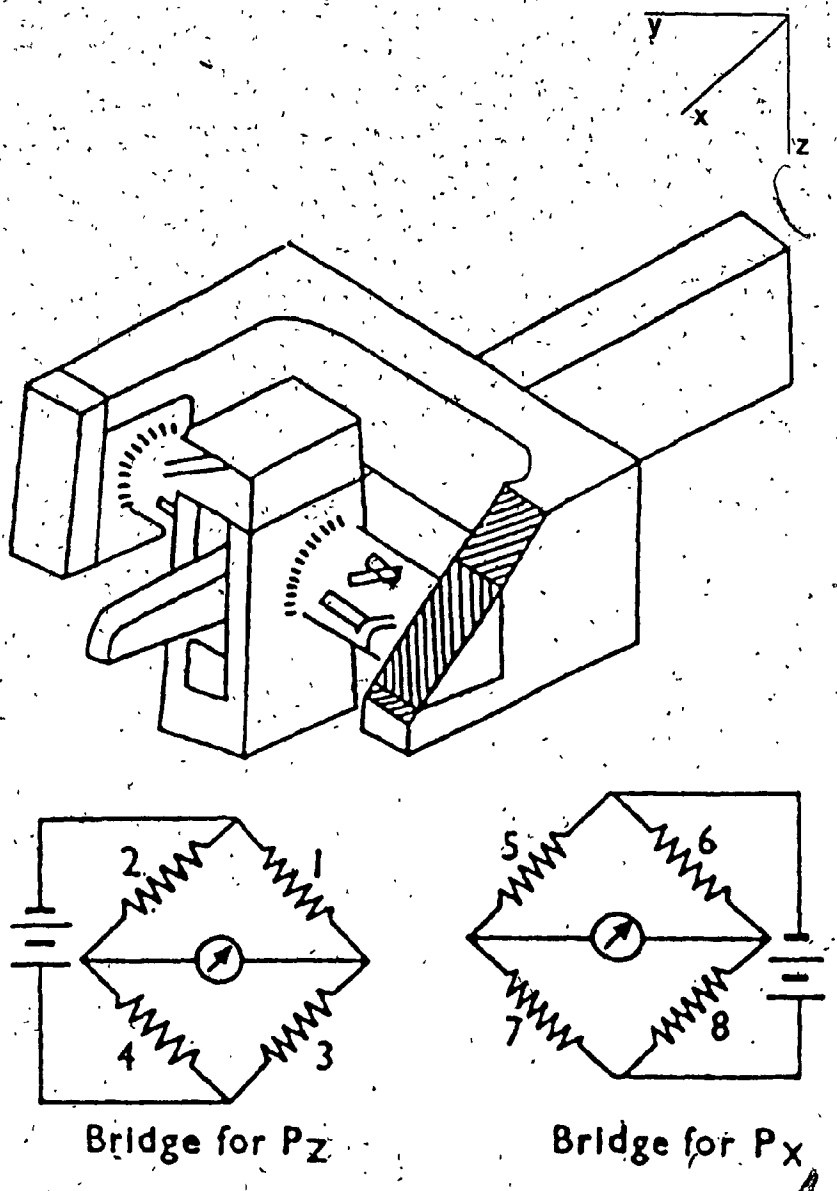

Figure 1.10: A Strain Gauge Turning Dynamometer

bolts to preload the piezo-electric cells, four piezo-electric cells, a base plate, and has a high natural frequency cover to protect the cables against the fluids.

One of the earliest types of drill dynamometer is a mechanical type used by Boston and Gilbert [49]. The work material is fixed on a vise which is free to rotate about the vertical axis. The torque is determined from the ordinate of the curve drawn over a moving paper by a pencil. Boston and Oxford [50] later designed a hydraulic type dynamometer to increase the accuracy of measurement. A lever attached to the rotatable vise presses against a plate which is in contact with a rubber diaphragm over a container. The fluid inside the container is displaced and the displacement is indicated in a mercury manometer.

Galloway [51] used a capacitance type dynamometer to further increase the accuracy of measurement. Here a lever from the rotatable vise on to which the workpiece is fixed holds one of the plates of the capacitor and moves against a spring force.

Dean and Kilburn [52] reported a simple torquemeter where the direct measurement of the angle of twist in a definite length of the shaft is utilized for determining the applied torque. Schmidt [53] fabricated a drill torquemeter where two torque plates are supported by four pins which deform elastically when the upper plate is twisted relative to the lower one.

Ghosh, Mukherjee, and Bhattacharya [54] designed a sensitive drill dynamometer based on the principle of measurement of the time interval between two recurrent magneto electric pulses to measure the dynamic fluctuations of the resultant force system. The schematic

diagram of the dynamometer is shown in Fig. 1.11. Osman, Xistris, and Chahil [43] used a two component measuring platform of the Kistler type in modelling the random fluctuations of torque and thrust in twist drilling. This dynamometer, has the following features:

(a) A measuring load cell preloaded between the base plate and the top plate with an elastic shank bolt.

(b) A protective jacket.

(c) A central hole protected with a steel tube.

(d) The maximum axial thrust and torque which could be measured are of the order of 20 KN and 100 N-m respectively.

Boston, Gilbert, and Kaiser [55] made power measurements in milling using mechanical type of dynamometer, while Schmidt [56] used calorimetric techniques for evaluating the forces at the cutting edge in high speed milling. Bendixen [57] used an inductive torque dynamometer mounted between the spindle and cutter. A coil was placed in front of the dynamometer with the core at its back. The milling torque was then determined on the basis of the air gap between the core and the coil during actual cutting. A planetary gear dynamometer was constructed by Roubik [58] to measure the tangential cutting forces in milling. The device was used to indicate the variations of cutting forces of a single point and multi-point face mill. To improve the accuracy of measurement in milling and grinding, Cook, Lowen, and Shaw [55] demonstrated the potential of a ring as a load measuring device. For milling dynamometers, four octagonal strain rings are to be placed between two flat plates. The principle of strain rings is also adapted in the design of grinding dynamometers.

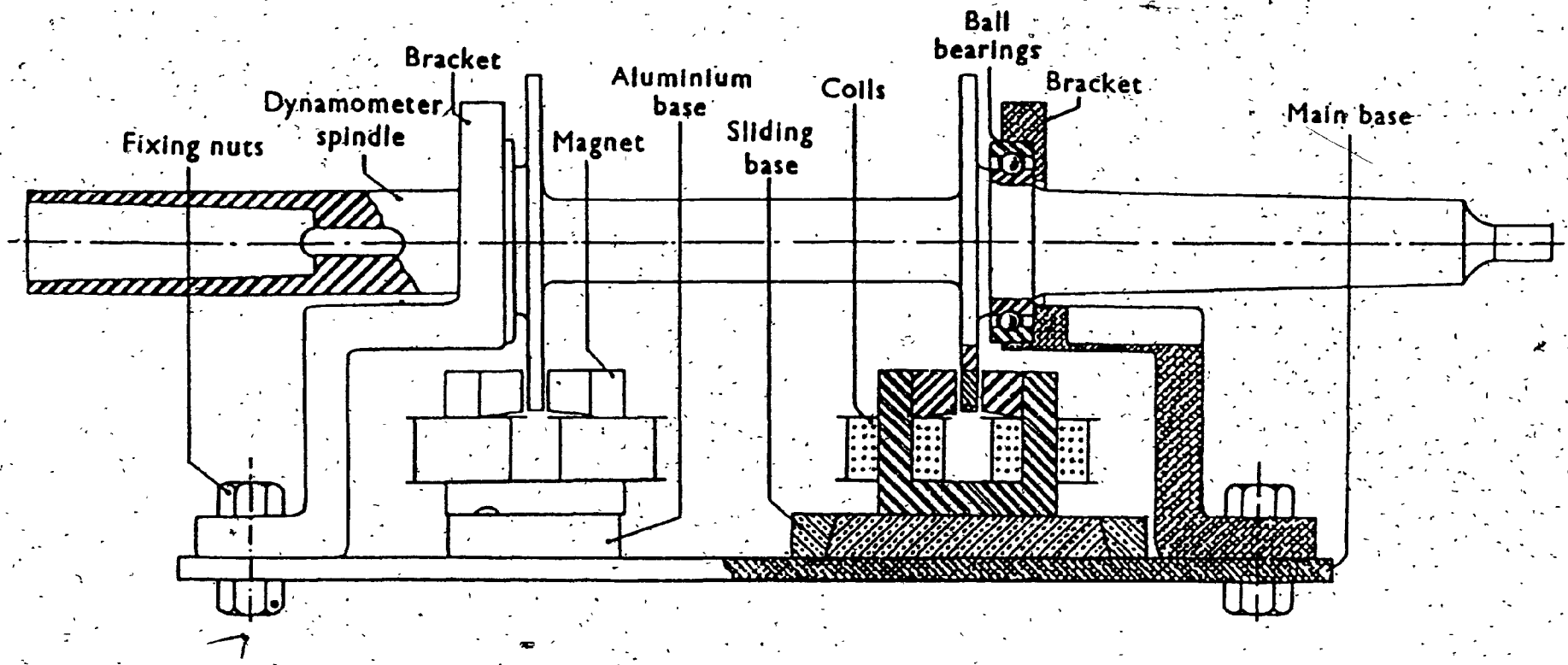

Figure 1.11: Drill Torquemeter Based on a Recurrent Pulse Technique

Griffths [60] adopted a dynamometer consisting of a thin wall tube to which strain gauges were cemented to measure the mean value of static thrust and torque. Here, the pilot bush and workpiece are situated at one end of the thin wall tube dynamometer and the other end is clamped to the welded bracket which itself is bolted to the pressure head. Sakuma, Taguchi and Kinjo [61] measured the torque and thrust using a dynamic strain meter and a direct recording electro-magnetic oscillograph by two axis cross type strain gauges bonded on the periphery of the boring bar near its mounting holder.

Del Taglia and Tani [62] proposed a method for measuring all the three components of forces in boring using a combination of a dynamometric table and an angular position transducer. The dynamometric table measures the axial component of the cutting force and the angular position transducer gives the radial and tangential force.

Sun, Chang, Wang and Lui [63] proposed a piezo-electric shank type dynamometer and have used it to measure the cutting forces in turning operation. Here the piezo-electric quartz three component transducer is placed in an oval opening of the tool shank to reduce the cross-correlation. The various dynamometers presented in this section enable (a) the choosing of the right kind of transducer, (b) to design a dynamometer structure to not only suit the needs of the machine, but also minimize the cross-correlation between the various components to be measured. Since, the resultant force system is expected to be random in nature, a piezo-electric transducer is used.

1.3.3 Machine Tool Dynamics

The dynamic analysis of various machine tools have been consid-

ered and the stability analysis carried out [64,65], to achieve higher accuracy and productivity in manufacturing.

Peters [66] presented a method of representing the dynamic characteristics of a machine tool using the complex flexibility method. A computer program called DYNPAR was developed, which yields the natural frequencies and mode shapes from a set of response curves.

Tlusty, Lau, and Parthiban [67] compared the use of shock and harmonic forced excitations in establishing the stability of machine tools against chatter. Sexton, and Stone [68] studied the transient effects during variable speed cutting on a lathe and came to the conclusion that improvements in stability may be obtained using variable spindle speed.

Nigm [69] extended the work of Merritt [70] by accounting for the dynamics of the cutting process and simplified the graphical procedure presented by Merritt.

Kwiatkowski, and Bennett [71,72], recognizing the stochastic nature of the cutting forces, determined the receptances of machine tool stuctures by random signal analysis and also suggested correlation methods for system identification.

Peklenik, and Kwiatkowski [73] point out that the time dependent forces, temperatures, displacement, and wear vary by the law of chance. They also point out that the true system identification is not possible without the consideration of the random nature of the above mentioned variables. Continuing the investigation, Al Samari, and Kwiatkowski [74] treat the machine tool structure as basically excited by two dimensional random forces and evaluate the structure response characteristics towards a true system identification.

Opitz, and Weck [75] outline a method of system identification by means of stochastic signals and derive relations for the dynamic compliance of a machine tool by means of spectral density measurements.

Osman, and Sankar [76], treated the random force vibrations as a stationary, delta correlated process with a gaussian distribution and developed a short-time acceptance test based on the inverse of the standard deviation of the steady state translational dynamic response. Samaha and Sankar [77] extended the work of Osman and Sankar [76] by modelling the machine tool as a non-linear two degree of freedom system and developing a dynamic acceptance test based on the response of the machine tool both in the translational and rotational modes.

Sharan, Sankar, and Sankar [78] studied the free vibration of a lathe spindle using a finite element model and determined the effect of the bearing stiffness on the natural frequencies as well as mode shapes.

Burney, Pandit, and Wu [79] evaluated the joint dynamics of the cutting process and the machine tool structure by using a time series technique, by developing a mathematical model based on the relative displacement between the tool and the workpiece.

An extensive review of the state of the art in machine tool dynamics is given by Tlusty [84] and Ramamurthi, and Srinivasan [81]. The various methods of system identification in machine tool dynamics presented gives the limitations and advantages of each method. Such a review helps in choosing an appropriate method to obtain a stochastic characterization of the machine tool workpiece in BTA deep-hole machining.

1.3.4 BTA Deep-Hole Machining

Researchers in the area of BTA deep-hole machining are attempting to study the various aspects of the process, so that the machining process can be well understood and used efficiently.

Osman [82] presented the economic developments that have taken place in the BTA machining process and gave the application range and machining quality of the process.

Corney and Griffths [83] studied the cutting and burnishing operation due to the self guiding action of the BTA cutting tool, and came to the conclusion that main burnishing pressure occurs in front of the wear pads.

Griffths [80] measured the static component of torque and thrust in BTA deep-hole machining using a strain gauge dynamometer and obtained plots for the variation of thrust and torque with feed and diameter.

Osman and Latinovic [85,86,87] presented the design concept and analysis of multi-edge BTA deep-hole machining tools wherein the tool cutting edges are unsymmetrically located on the boring head. It was also shown that besides achieving higher material removal rate, the unsymmetrical multi-edge cutting tool provides similar performance to that of a single edge cutting tool. Latinovic, Blakely, and Osman [88] extended the work of Osman and Latinovic [85] to prove the feasibility of multi-edge cutting by developing a mathematical model for cutting forces. A non-linear objective function was developed and was minimized using the Hooke and Jeeves method, thus arriving at an optimal tool design.

Sakuma, Taguchi, and Katsuki [90] studied the effects of guide

pads on the burnishing action and accuracy of the machined hole in using a specially designed tool. The mechanism by which the machined hole becomes oversized is also discussed. This work was extended by Sakuma, Taguchi, and Katsuki [91], who studied the formation of polygonal holes and tried to correlate the frequency of oscillation of the boring bar with the number of lobes. This work was extended by the same authors [92] to study the self-guiding action.

Osman, Latinovic, and Greuner [93] investigated the influence of various additives to a base stock cutting oil aiming at developing an oil which gives a maximum cutting efficiency at a minimum wear rate of the tool and guide pads. Thus, it can be seen that the research carried out so far concerns itself with the influence of wear pads on the accuracy of the hole produced and the development of multi-edge cutting tools towards improving productivity. But, no research has been carried out in understanding the influence of the resultant force on the workpiece. Such an analysis will lead to the production of workpieces with minimum inaccuracy and a better understanding of the machining process.

1.4 Objective of the Present Investigation

The dimensional accuracy of a machined workpiece, the development of new tool materials, and the introduction of automatic control and feedback in machine tools require a complete understanding of the dynamics of the machine tool. Specifically, the analysis of the machine tool behaviour during the process of machining a workpiece determines the applicability of the particular process. Since, the BTA deep-hole machining process encompasses both a roughing and finishing operation, in a relatively inaccessible zone, the understanding of the effect of

the high magnitude forces on the machine tool behaviour is important as the accuracy of the hole generated on the workpiece produced should be as high as possible.

In view of the above, the major purposes of this investigation are fourfold. First, the characteristics of the cutting action taking place at the cutting edge is examined and equations are derived to compute the static and the periodic components of the cutting forces and the torque using the thin shear plane model. The periodic components of the cutting force represent a deterministic chatter thoery. In this investigation, the region of interest is the non-chatter zone. Secondly, since the resultant force system (an axial force and torque) consists of the cutting force, the oil-force, the burnishing force, and the friction, a completely theoretical approach to estimate the resultant force system would be difficult and impractical. Further, the random characteristics of the resultant force system can only be determined by performing machining experiments. Therefore a set of laboratory tests are performed to determine an appropriate stochastic model for the resultant force system. Thirdly, the influence of the resultant force system on the machine tool workpiece system is obtained through the derivation of an appropriate mathematical model. Finally, the solutions to these stochastic equations of motion give the tool tip motion, which in turn dictates the nature of the produced surface. Using, the description of the motion of the tool tip, a methodology of building a microprocessor based adaptive control unit is suggested.

In Chapter 2, expressions are derived to calculate the steady state and periodic components of the three components of the cutting force and torque by taking into account the difference in rake angles in

the two regions of the cutting tool, and the number of steps in the cutting tool.

Chapter 3 deals with the laboratory measurements of the axial force and torque signals. The experimental set up used for the measurement, including the design of the BTA dynamometer, is presented in detail. The static and dynamic calibration of the dynamometer are also explained. The frequency response curves of the machine tool-workpiece system are given and a method for obtaining the true values of the axial force and torque in the frequency range of interest are stated.

An analysis of the steady state and dynamic components of the axial force and torque are presented in Chapter 4. The recorded dynamic signals are fed into an FFT analyzer and the test for stationarity, power spectrum test and probability density function test are performed. A mathematical model for the dynamic fluctuations are obtained from which equations to determine the peak value of the axial force and the torque are derived.

Chapter 5 presents the mathematical modelling of the machine tool-workpiece system. All the components are identified and modelled separately and then combined to give the total system model. Based on the mathematical model of the resultant force and the Lagrange's equations, a set of mathematical equations which describe the system are derived.

The response analysis of the machine tool-workpiece assembly and the evaluation of the tool tip motion are described in Chapter 6. The responses of the machine tool workpiece system under the action of the axial force and torque are determined. These responses are then combined to obtain the tool tip motion, which in turn is described by a set of

design curves identified as the Maximum Deviation Curve, Minimum Deviation Curve and Average Curve.

Chapter 7 presents the details of a recommendation for setting up a microprocessor-based adaptive control unit for deep-hole machining system in which, the choice of the initial state is made based on the tool tip motion. The discussion of the results and conclusions drawn from the analysis are presented in Chapter 8 along with the recommendations for future work.

CHAPTER 2

TIME DOMAIN REPRESENTATION OF CUTTING FORCES IN THE BTA PROCESS

CHAPTER 2

TIME DOMAIN REPRESENTATION OF CUTTING FORCES IN THE BTA PROCESS

The BTA method basically utilizes a single edge cutting tool with an internal chip removal system. The basic machining process is described in Fig. 1.5. Also, the BTA tools have in common one cutting edge and two guide pads as seen in Fig. 1.4. The cutting edge geometry is important since it determines the model for metal cutting, the cutting force distribution, the chip formation, and the surface accuracy of the hole produced. Usually, the smaller the cutting tool diameter, the more significant the tool geometry becomes due to the diminished space available for chip removal. Figure 2.1 shows the geometry of a typical BTA boring head. The nose is so designed that it is offset from the axis of the head. In the vicinity of the hole center, a 30° negative rake angle is introduced to strengthen the cutting edge in that area. To obtain narrow chips, the cutting edge is divided into two or three steps depending upon the hole diameter and the material properties of the work [6]. A single step edge is used for tools not exceeding 9 mm in diameter, a two step edge for bores between 9 mm and 30 mm in diameter, and three steps for bores over 30 mm in diameter. Chip breakers are required to produce short chips of C-shape, which must be small enough to exit freely through the very restrictive chip mouth and throat. With poor chip forming materials a chip breaker with a small positive rake angle may be used. Table 2.1 summarizes the deep-hole machining operations and shows the optimal geometry of the chip breaker and chip forms in each operation [85].

Based on the above geometry and due to the fact that the velocity of cutting is perpendicular to the cutting edge, the deep-hole machining

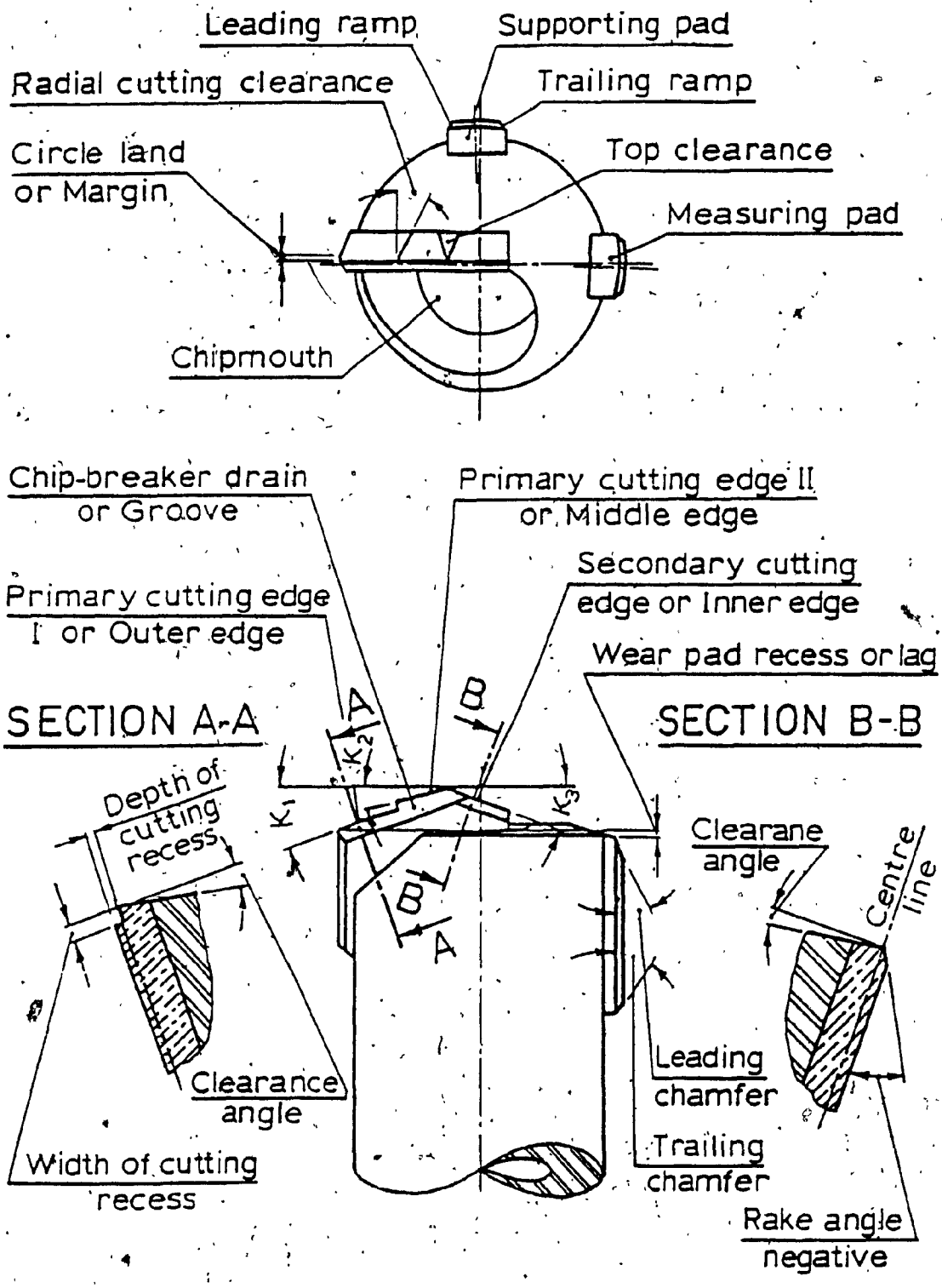

Fig. 2.1 : Tool Geometry of a Typical BTA Solid Boring Head

Table 2.1: Geometry of Chip Breaker and Chip Forms for Deep-Hole Machining

No.	TOOL		b / t / r	CHIP TYPE	SYMBOL	CHIP FORM
1	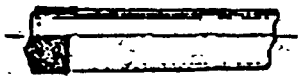	SOLID-GUN DRILL	–	CONTINUOUS		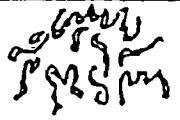
2	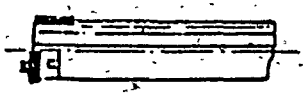	TREPANNING GUN-DRILL	–	CONTINUOUS		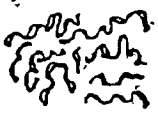
3	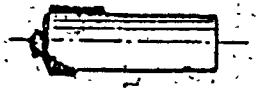	SOLID-BTA	b = 1,4 t = 0,4 r = 0,5	SHORT		
4	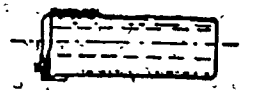	TREPANNING-BTA	b = 1,6 t = 0,4 r = 0,5	SHORT		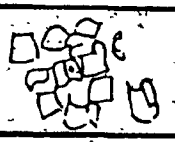
5	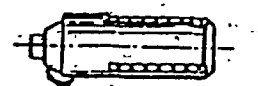	COUNTER BORING -BTA	b = 1,8 t = 0,8 r = 0,8	SHORT		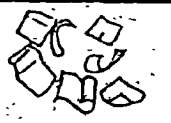
6	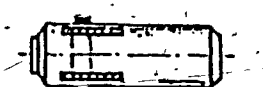	SKIVING	–	CURLY		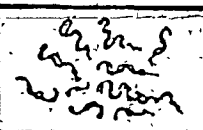
7	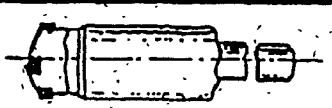	EJECTOR	b = 1,4 t = 0,4 r = 0,5	SHORT		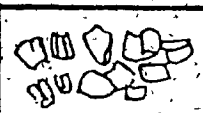

operation may be treated as an orthogonal machining operation. The resultant cutting force is commonly resolved into three components viz. the tangential or the power contributing component F_T parallel to the cutting velocity, the radial component F_R and the axial component F_a as shown in Fig. 2.2(a), [85].

To completely specify the cutting process the following quantities have to be specified:

(i) the magnitude of the resultant force R,

(ii) the direction cosines of the resultant R,

(iii) the position of application of the resultant force.

In order to avoid calculating the position of the resultant force R, an alternative approach is to move the resultant force to the axis of the boring bar-cutting tool system and specify the following quantities:

(i) the magnitudes of the tangential force F_T, the radial force F_R and the axial force F_a,

(ii) the magnitude of the torque,

(iii) the direction of application of torque.

This Chapter presents a method for evaluating the cutting forces and torque, without resorting to empirical equations, using the thin shear plane angle approach. The thin shear plane model is used due to the high relative cutting velocities in the BTA deep-hole machining process and also the presence of the chip breaker groove, under the action of which, small chips are produced. The advantages of such a force equation is that the BTA process can be better understood by obtaining an analytical expression to describe the process rather than a need for empirical testing.

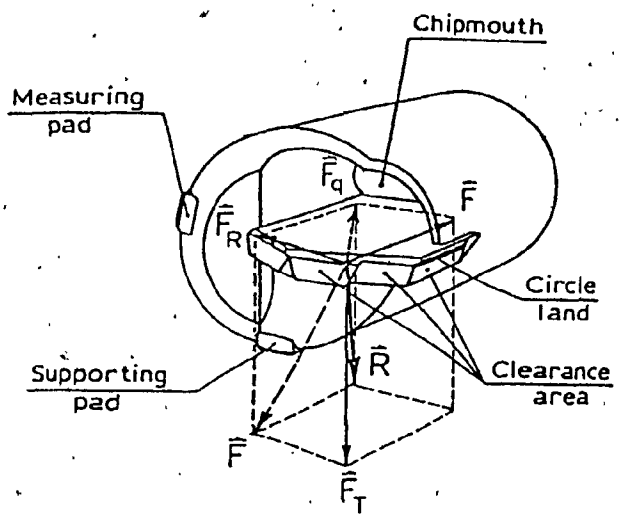

Fig. 2.2(a) Cutting Forces Acting on BTA Solid Boring Cutter

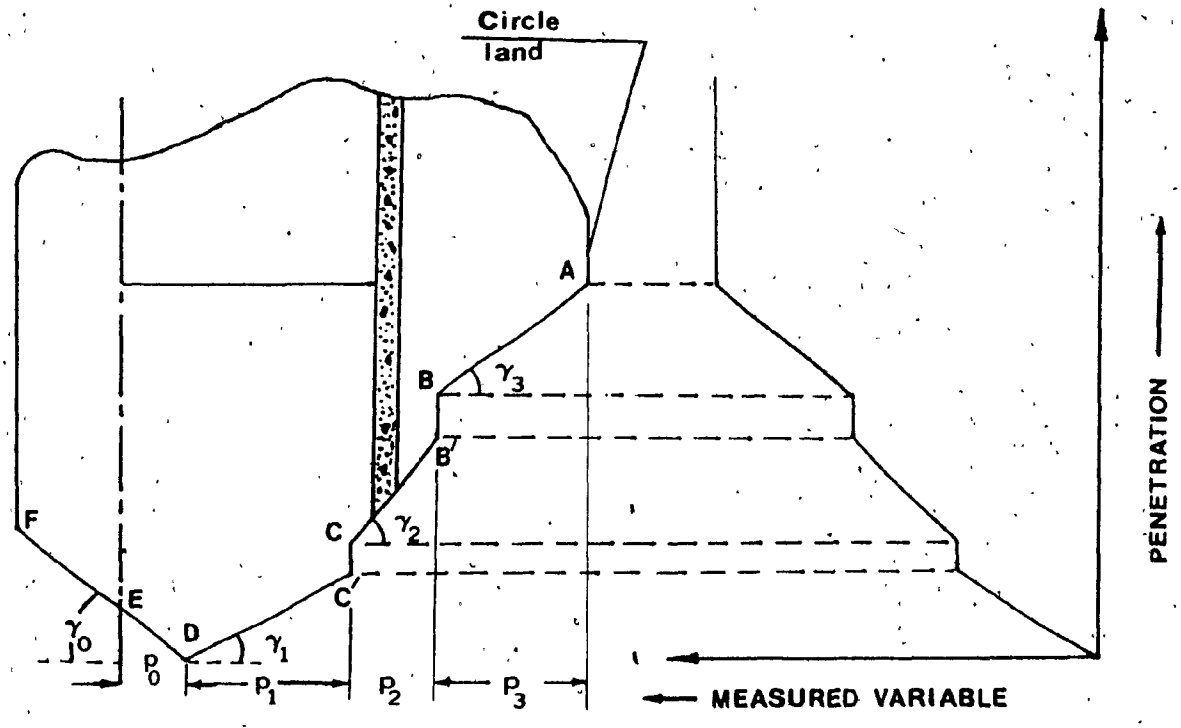

Fig. 2.2(b): Section of the BTA Cutting Profile

Fig. 2.2(c): Variation of Measured Variable with Penetration

2.1 Modelling of the Cutting Forces

Investigators in metal cutting have attempted to develop an analysis of the cutting process which gives a clear understanding of the mechanism involved and enables its prediction without a need for empirical testing. Knowledge of the nature and magnitude of the cutting force shows that the cutting force is dynamic [23,24] with some random fluctuations [41,42,43]. Just as the machined surface can be considered to be made up of macro and micro geometrical errors, the cutting forces can be considered to be made up of three components viz. the steady state component, the periodic component, the randomly varying component as shown in Fig. 2.3. So, to mathematically express the cutting force, each component should be modelled separately and combined to obtain the resultant force.

The modelling of the steady state cutting force equation requires evidence on the nature of the deformation zone. There have been two schools of thought regarding the nature of the deformation zone, one favouring the thin shear plane model [7,8] shown in Fig. 2.4(a), the other basing their analysis on the thick shear zone model [9,10] shown in Fig. 2.4(b). The available experimental evidence indicates that the thick shear zone models describe the cutting process fairly well at low speeds, but at higher speeds a thin shear plane model is found to be more appropriate. In the BTA deep-hole machining, not only is the cutting velocity quite high, but also a chip breaker groove is present in the tool. In view of such machining conditions, a thin shear plane model is preferred in the analysis presented here for the cutting forces and the torque.

2.2 Representation of the Steady State Forces

The force system represented in Fig. 2.2(a) shows that the resultant

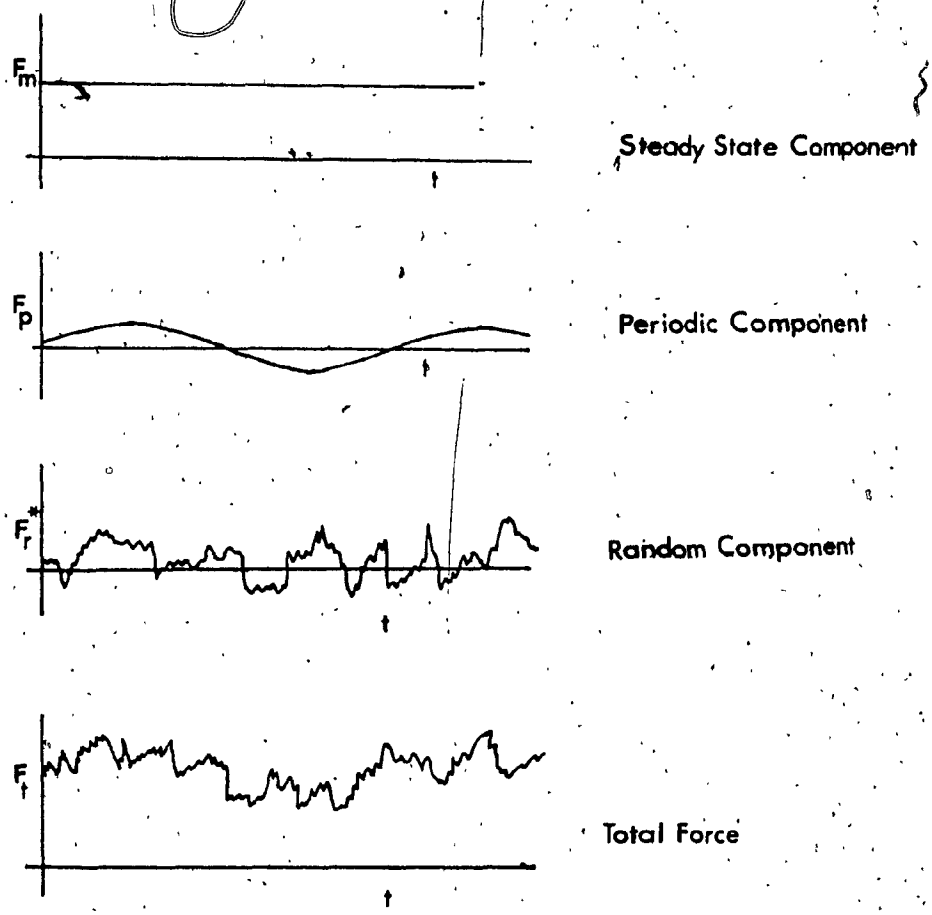

Fig. 2.3: Representation of the Cutting Force

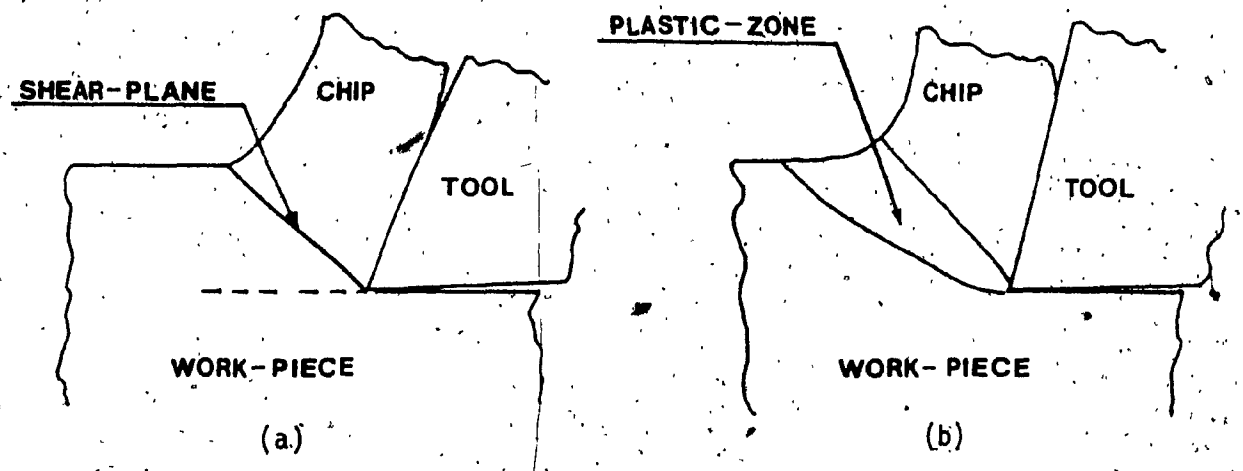

Fig. 2.4: Basic Models for Metal Cutting Analysis

force acting on the cutting edge is eccentric with respect to the axis of the cutting tool boring bar system. Therefore the complete force system in the deep-hole machining operation will be specified by the axial, tangential, radial force components and the point of application of the resultant force. An alternate procedure for specifying the force system is to shift the forces to the axis of the tool. But such a shift of the three forces leads to an introduction of a torque acting along the axis of the boring bar-cutting tool system. Therefore to specify the BTA deep-hole machining operation not only are the axial, radial and tangential forces to be evaluated, but also an expression for torque is to be obtained.

The BTA cutting tool shown in Fig. 2.2(b) has the following characteristics:

(i) The number of steps on the cutting edge is either 1,2 or 3.

(ii) The cutting region extends from point A to point E.

(iii) The rake angle in the region ED is usually $-\pi/6$ radians.

(iv) The rake angle in the region AD is usually 0°.

(v) The lengths p_0, p_1, p_2, and p_3 of the steps and the approach angles γ_0, γ_1, γ_2, and γ_3 for each part will be specified for each cutting tool.

(vi) The variation of the steady state component of the axial force, radial force, tangential force and the torque with the penetration of the tool into the workpiece is shown in Fig. 2.2(c), [61,90]. This is due to the geometry of the cutting tool. Initially point D comes into contact with the workpiece. For a given value of the feed, the force components or torque will increase until point C' starts cutting. Then, for a small

period of time, until point C contacts the job, the force and torque remain constant. Similarly, increases in force and torque will take place until all steps take part in the machining, after which time the values of the torque and forces do not change with time. The intermediate values of the forces and torque can be evaluated knowing the feed, the number of steps, and the maximum values of the forces and torque.

Thus, it may be assumed that the entire profile of the cutting edge is taking part in the machining operation. For the purpose of evaluating the total cutting force the entire cutting edge can be considered as being made up of small strips of thickness "dr" and then summing up the contributions due to these small steps the total force is obtained.

The force system on an incremental thickness of the cutting profile is shown in Fig. 2.5(a). Also, the cutting velocity at each incremental thickness of the cutting profile is at right angles to the cutting profile, and hence the machining is an orthogonal operation. The cutting force at each section can then be described by Fig. 2.5(b), consequently giving the following relations

$$(d\,F_{Tm})_r = A \cos(\beta_r - \alpha_r)\, dr \qquad (2.1)$$

$$(d\,F_{qm})_r = A \sin(\beta_r - \alpha_r)\, dr \qquad (2.2)$$

where

$$A = \tau f_m [\sin \phi_r \cos(\phi_r + \beta_r - \phi_r)]^{-1}$$

Assuming that the Bridgeman relationship is valid, the shear strength "τ" of the material could be expressed in terms of the shear strength "τ_0" at zero compressive strength as

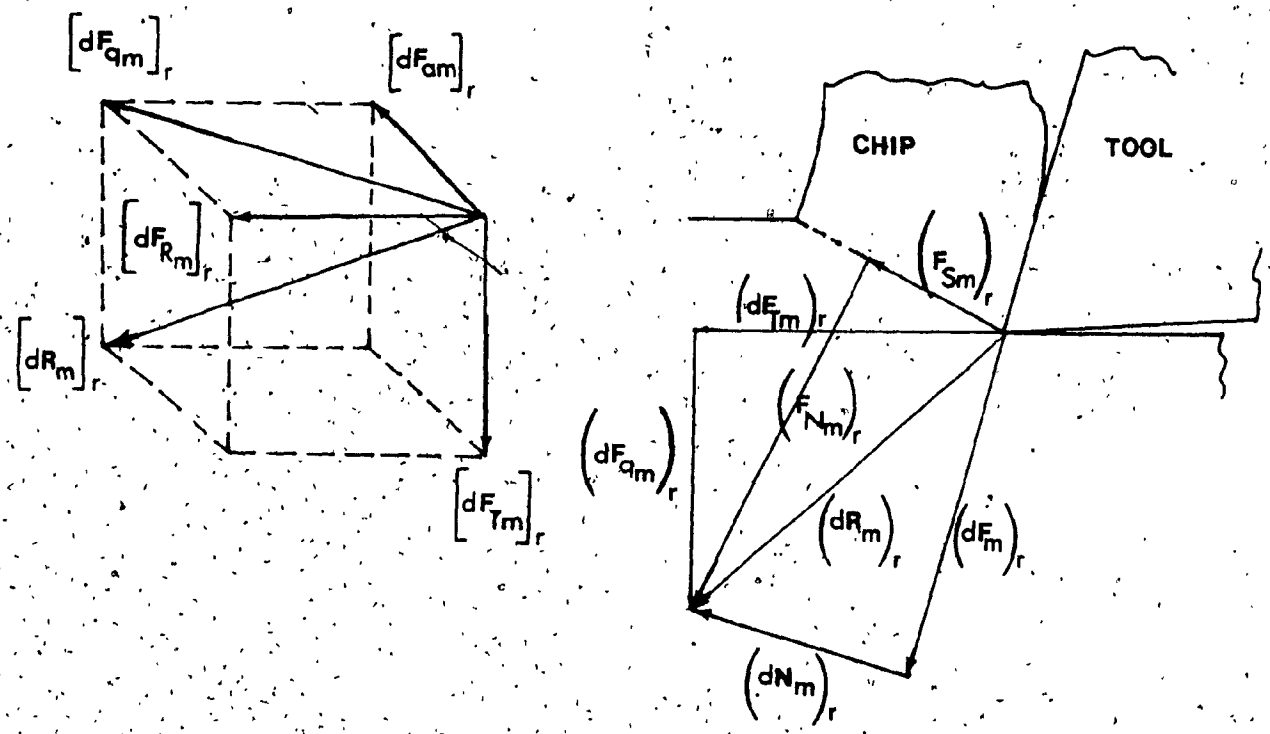

Fig. 2.5: Representation of Cutting Force at Each Section

$$\tau = \tau_0 \left[1 - k \tan (\phi_r + \beta_r - \alpha_r)\right]^{-1}$$

It is well known that the shear angle ϕ_r and the friction angle β_r depend upon the velocity of the machining V_c, the feed f_m, the chip compression factor λ, the rake angle α_r, cutting tool material, the workpiece material, and the medium of cutting. Mathematically they can be expressed by the following functional forms:

$$\phi_r = f^*[V_c, f_m, \lambda, \alpha_r]$$

$$\beta_r = g^*[V_c, f_m, \lambda, \alpha_r, \text{cutting tool material, workpiece material medium of cutting}]$$

The relationship between the shear angle, rake angle, and the chip compression factor can be obtained from the geometry of metal cutting [Fig. 2.5(b)]. This is given by

$$\tan \phi_r = \frac{\cos \alpha_r}{\lambda - \sin \alpha_r} \tag{2.3}$$

The value of the rake angle for a particular tool is specified. So, if the fluctuation of the chip compression factor as a function of the depth of cut and the velocity is determined, then the function f* can be given. The value of the chip compression factor varies gradually with an increase in feed and the cutting velocity, with the range of variation being 3 to 3.25 in the presence of cutting fluids [13]. Since, the BTA deep-hole machining operation takes place in the presence of high pressure cutting fluid, the value of chip compression factor is taken to have a constant value of 3.125.

Also, an equation relating the chip compression factor, feed, and the co-efficient of friction can be obtained [13,94], as

$$\mu = \frac{0.468}{\pi/2 - \alpha_r} f_m^{-0.23} \ell n\lambda \qquad (2.4)$$

Using equations (2.3) and (2.4) the functions f* and g* may be written in the form

$$\phi_r = \tan^{-1}\left[\frac{\cos \alpha_r}{3.125 - \sin \alpha_r}\right]$$

$$\beta_r = \tan^{-1}\left[\frac{0.468}{\pi/2 - \alpha_r}\right] f_m^{-0.23} \ell n\lambda$$

As stated previously, the rake angle in the region AD in Fig. 2.3(b) is different from that for region ED. Therefore, the force on each region has to be estimated separately and later summed up to obtain the total force.

2.2.1 Cutting Forces Corresponding to Region AD

In this region (Fig. 2.2(b)), the rake angle of the cutting tool is 0°. Therefore equations (2.1) and (2.2) reduce to

$$(d F_{Tm})_r = A^* \cos \beta_r \, dr$$

$$(d F_{qm})_r = A^* \sin \beta_r \, dr$$

where

$$A^* = \tau_0 f_m[\sin \phi_r \cos (\phi_r + \beta_r) \cdot (1 - k \tan (\phi_r + \beta_r)]^{-1}$$

Substituting the value of rake angle as 0° in equations (2.3) and (2.4), the expressions for $\tan \phi_r$ and μ in the region AD can be obtained, and are

$$\tan \phi_r = 0.32$$

$$\mu = 0.34\ f_m^{-0.23}$$

Using the expression for $\tan \phi_r$, μ, $(d F_{qm})_r$ and $(d F_{Tm})_r$ and performing certain mathematical transformations the following expressions are obtained.

$$(d F_{Tm})_r = \tau_0 \Psi (f_m,k)\, dr \qquad (2.5)$$

$$(d F_{qm})_r = \tau_0 \Psi^*(f_m,k)\, dr \qquad (2.6)$$

where

$$\Psi (f_m,k) = 3.445\ f_m B^* (k,f_m)$$

$$\Psi^*(f_m,k) = 1.1713\ f_m^{0.77} B^* (k,f_m)$$

$$B^*(k,f_m) = [(1 - 0.32k) + (0.34k - 0.1088)\ f_m^{-0.23}]^{-1}$$

Using equation (2.6) and the geometry of the cutting edge, the expression for radial and axial components of the cutting force in the region under consideration can be written as given below:

$$(d F_{Rm})_r = \Psi^* (f_m,k)\ \tau_0 \sin \gamma_r\, dr$$

$$(d F_{am})_r = \Psi^* (f_m,k)\ \tau_0 \cos \gamma_r\, dr$$

Therefore the total tangential, radial and axial forces are

$$F_{Tm} = \int_p^u \Psi (f_m,k)\ \tau_0\, dr$$

$$F_{Rm} = \Psi^* (f_m,k)\tau_0 \left[\int_{p_0}^{p_0+p_1} \sin \gamma_1\, dr + \ldots + \int_{p_0+p_1\ldots p_r}^{U} \sin \gamma_r\, dr\right]$$

$$F_{am} = \Psi^* (f_m,k)\tau_0\left[\int_{p_0}^{p_0+p_1} \cos\gamma_1\, dr + \ldots\ldots + \int_{p_0+p_1+\ldots p_r}^{U} \cos\gamma_r\, dr\right]$$

where

$$U = \begin{cases} p_0 + p_1 + p_2 \text{ , for a two step tool} \\ p_0 + p_1 + p_2 + p_3 \text{ , for a three step tool} \end{cases}$$

Rewriting,

$$F_{Tm} = \Psi (f_m,k)\ \tau_0\ [U - p] \qquad (2.7)$$

$$F_{Rm} = \Psi^*(f_m,k)\ \tau_0 \sum_{r=1}^{n} p_r \sin\gamma_r \qquad (2.8)$$

$$F_{am} = \Psi^*(f_m,k)\ \tau_0 \sum_{r=1}^{n} p_r \cos\gamma_r \qquad (2.9)$$

where

$$n = \begin{cases} 2, \text{ for a two step tool} \\ 3, \text{ for a three step tool} \end{cases}$$

As stated earlier, a complete specification of the BTA deep-hole machining process requires an expression for the torque acting on the cutting edge. The torque on a given section under consideration is given by

$$(d\ T_m)_r = r\ (d\ F_{Tm})_r$$

Substituting equation (2.5) into the above mentioned expression for torque, the following equation is obtained

$$(d\ T_m)_r = \Psi\ (f_m,k)\ \tau_0\ r\ dr$$

or

$$T_m = \int_{p_0}^{U} \Psi\ (f_m,k)\ \tau_0\ r\ dr$$

giving

$$T_m = \frac{\tau_o}{2} \Psi (f_m,k) [U^2 - p_o^2] \qquad (2.10)$$

2.2.2 Cutting Forces Corresponding to Region ED

In this region (Fig. 2.2(b)) the rake angle of the cutting tool is $-\pi/6$ radians. Therefore equations (2.1) and (2.2) reduce to

$$(d F_{Tm})_r = C^* \cos (\beta_r + \pi/6)\, dr$$

$$(d F_{qm})_r = C^* \sin (\beta_r + \pi/6)\, dr$$

where

$$C^* = \tau_o f_m \left[\sin \phi_r \cos (\phi_r + \beta_r + \pi/6)[1 - k \tan (\phi_r + \beta_r + \pi/6)]\right]^{-1}$$

Similarly equations (2.3) and (2.4) giving the expression for $\tan \phi_r$ and μ in the region ED become

$$\tan \phi_r = 0.24$$

$$\mu = 0.26\, f^{-0.23}$$

The above stated equations after certain mathematical transformations lead to

$$(d F_{Tm})_r = \Phi (f_m,k)\, \tau_o\, dr \qquad (2.11)$$

$$(d F_{qm})_r = \Phi^*(f_m,k)\, \tau_o\, dr \qquad (2.12)$$

where

$$\Phi (f_m,k) = D^*(k,f_m)(0.866 - 0.13\, f_m^{-0.23})$$

$$\Phi^*(f_m,k) = D^*(k,f_m)\, f_m\, (0.866 - 0.13\, f_m^{-0.23})(1 + 0.45\, f_m^{-0.23})$$

$$D^*(k,f_m) = \frac{4.4\ f_m}{[A(1 - 0.0624\ f_m^{-0.23}) + B(0.24 + 0.26\ f_m^{-0.23})]}$$

$$A = 0.866 - 0.5\ k$$

$$B = 0.5 + 0.866\ k$$

Using equation (2.12) and the geometry of the cutting profile, the expressions for the radial and axial force in the region under consideration are given by

$$(d\ F_{Rm})_r = -\Phi^*\ (f_m,k)\ \tau_0 \sin \gamma_0\ dr$$

$$(d\ F_{am})_r = \Phi^*\ (f_m,k)\ \tau_0 \cos \gamma_0\ dr$$

Therefore the total tangential, radial, and axial force in the region ED are

$$F_{Tm} = \Phi\ (f_m,k)\ \tau_0\ p_0 \qquad (2.13)$$

$$F_{Rm} = -\Phi^*\ (f_m,k)\ \tau_0\ p_0 \sin \gamma_0 \qquad (2.14)$$

$$F_{am} = \Phi^*\ (f_m,k)\ \tau_0\ p_0 \cos \gamma_0 \qquad (2.15)$$

The torque at any section of thickness "dr" at a distance r from the axis of the cutting tool in the region ED can be obtained from

$$(d\ T_m)_r = \Phi\ (f_m,k)\ \tau_0\ r\ dr$$

Integrating the above for the total torque in the region ED,

$$T_m = \frac{\tau_0}{2}\ p_0^2\ \Phi\ (f_m,k) \qquad (2.16)$$

2.3 Resultant Cutting Force System on the BTA Tool

The total force system on the cutting tool consists of a tangential component, an axial component, a radial component and a torque acting along the axis of the cutting tool. As explained earlier, the total tangential, axial, radial forces and the torque is obtained by summing the values of the above stated components in the regions AD and ED of the cutting tool. Performing this operation, the total tangential, radial, axial forces and the torque acting on the boring bar-cutting tool system are

$$F_{Tm} = [(U - p_o)\ \Psi\ (f_m,k) + p_o\ \Phi\ (f_m,k)]\ \tau_o \qquad (2.17)$$

$$F_{Rm} = [\Psi^*(f_m,k) \sum_{r=1}^{n} p_r \sin \gamma_r - \Phi^*(f_m,k)\ p_o \sin \gamma_o]\ \tau_o \qquad (2.18)$$

$$F_{am} = [\Psi^*(f_m,k) \sum_{r=1}^{n} p_r \cos \gamma_r + \Phi^*(f_m,k)\ p_o \cos \gamma_o]\ \tau_o \qquad (2.19)$$

$$T_m = [(U^2 - p_o^2)\ \Psi\ (f_m,k) + p_o^2\ \Phi\ (f_m,k)]\ \frac{\tau_o}{2} \qquad (2.20)$$

The variation of these quantities with feed and diameter have been plotted in Figs. 2.6(a),(b),(c),(d) and 2.7(a),(b),(c),(d). The diameters and dimensions of the various sections of the cutting tool have been obtained from the drawings supplied by a certain manufacturer. These values are tabulated in Table 2.2.

Also, a comparison has been made between the values predicted by the equations derived previously, with the values published [61] for the same tool diameter. These have been shown in Figs. 2.8(a) and 2.8(b). However, due to lack of sufficient data, two assumptions had to be made to enable a comparison. They are

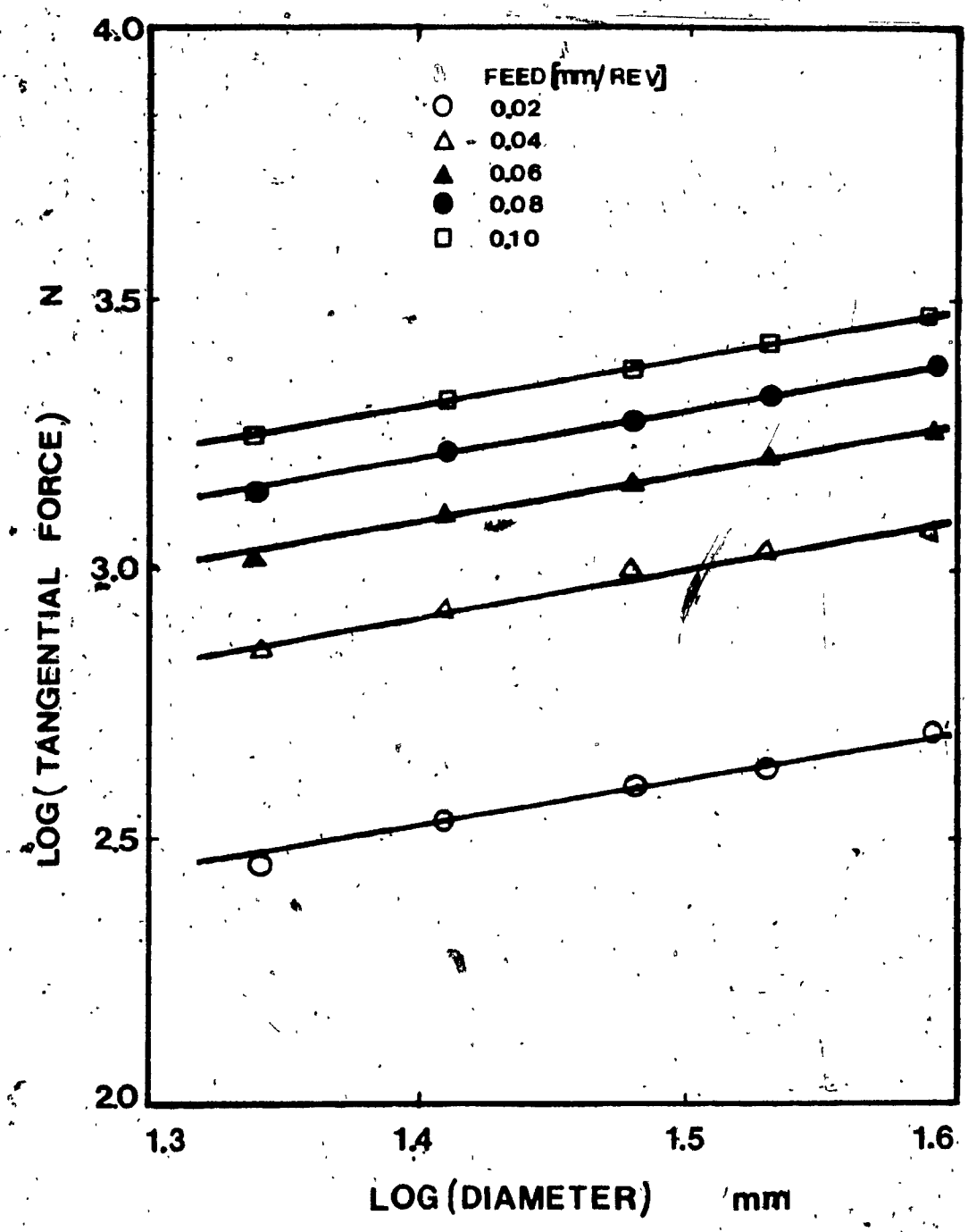

Fig. 2.6(a): Variation of Mean Tangential Force with Diameter

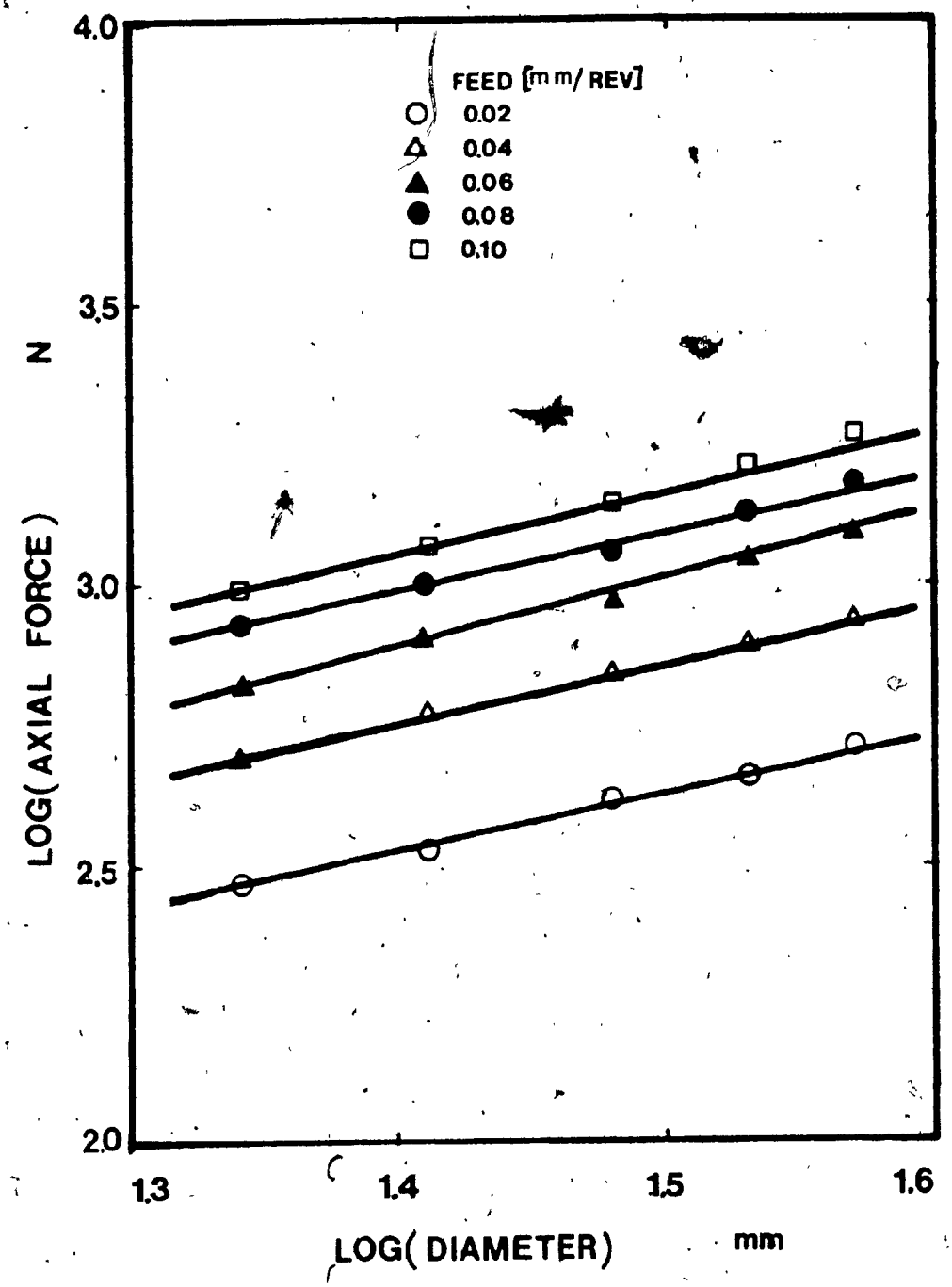

Fig. 2.6(b): Variation of Mean Axial Force with Diameter

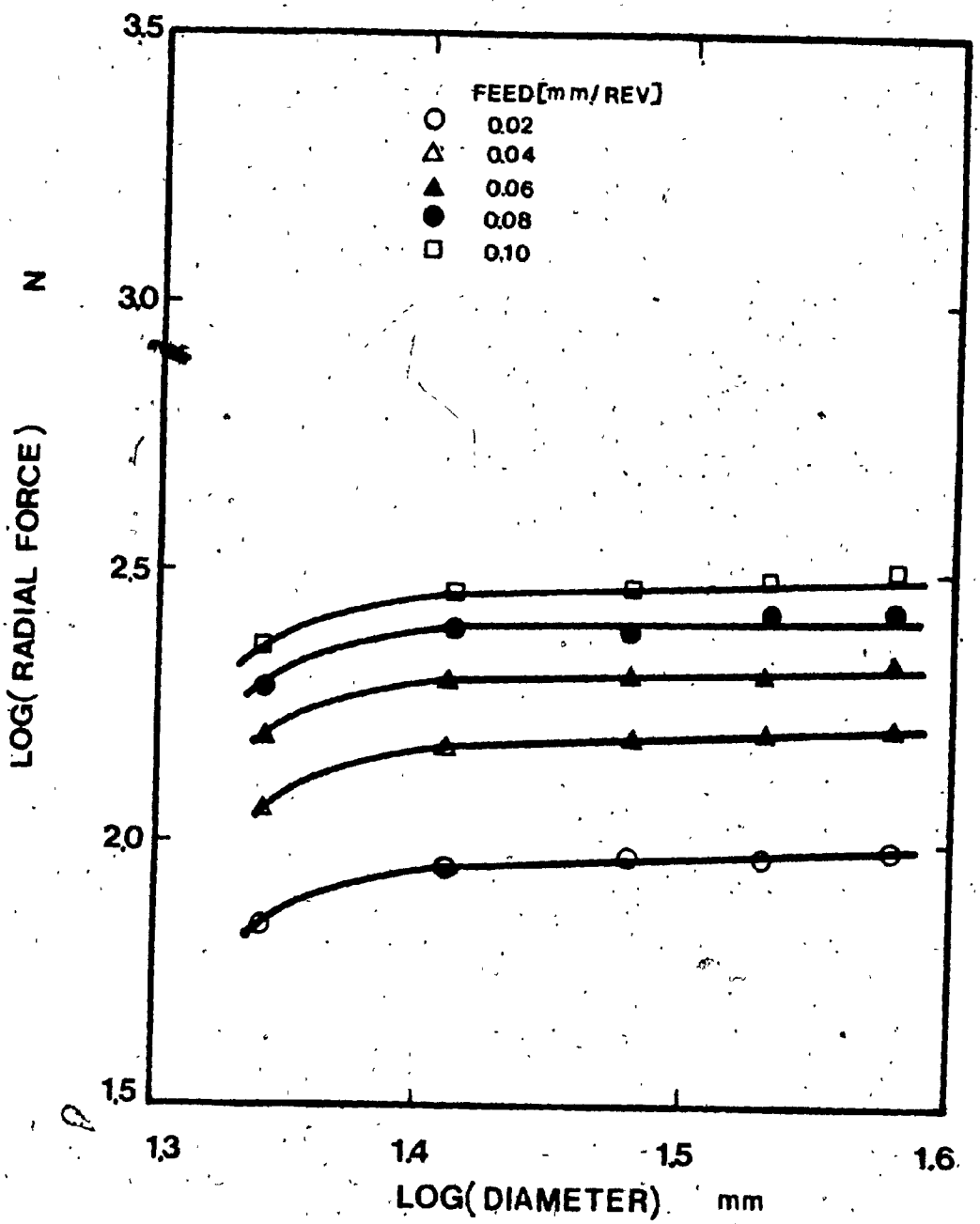

Fig. 2.6(c): Variation of Mean Radial Force with Diameter

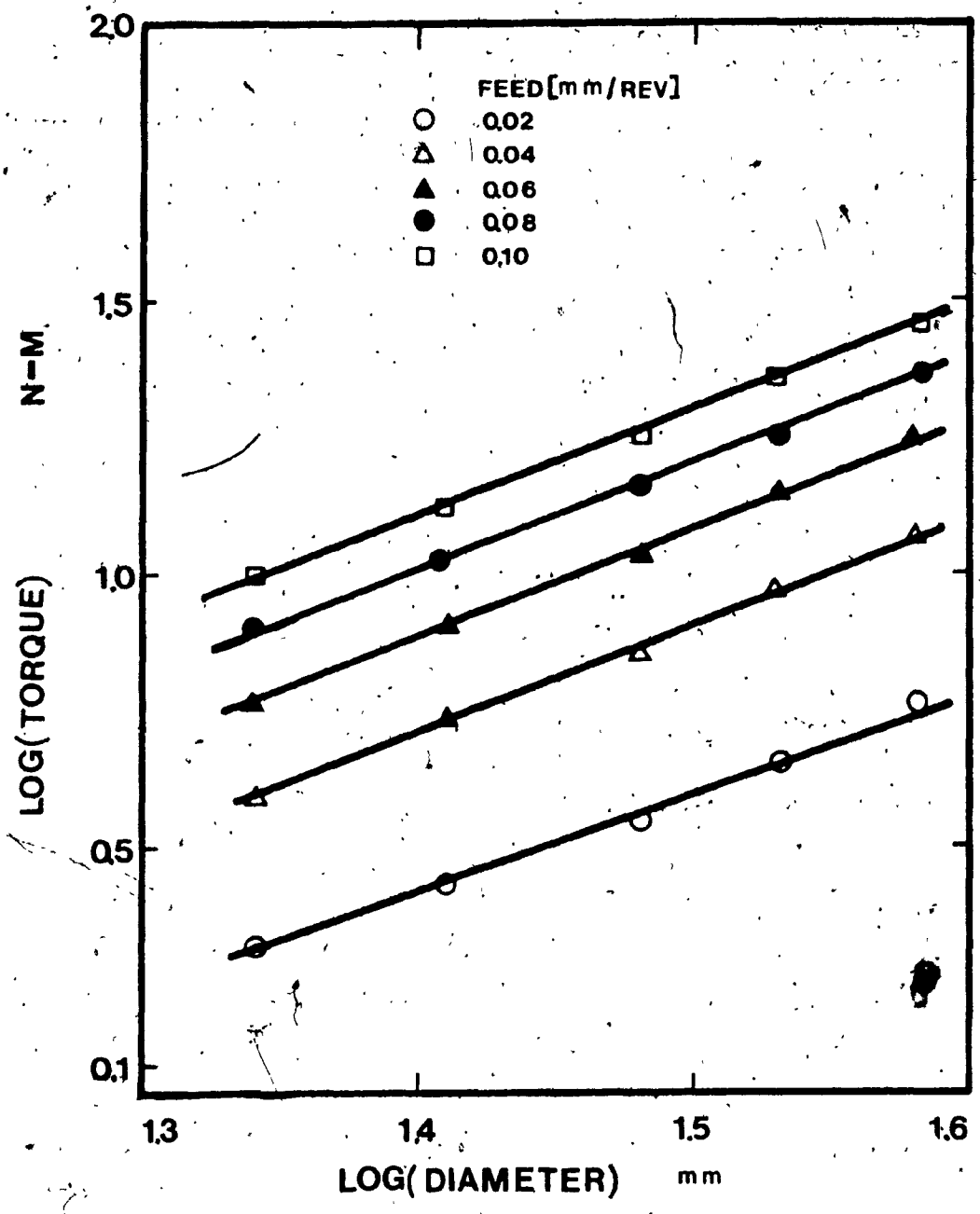

Fig. 2.6(d): Variation of Mean Torque with Diameter

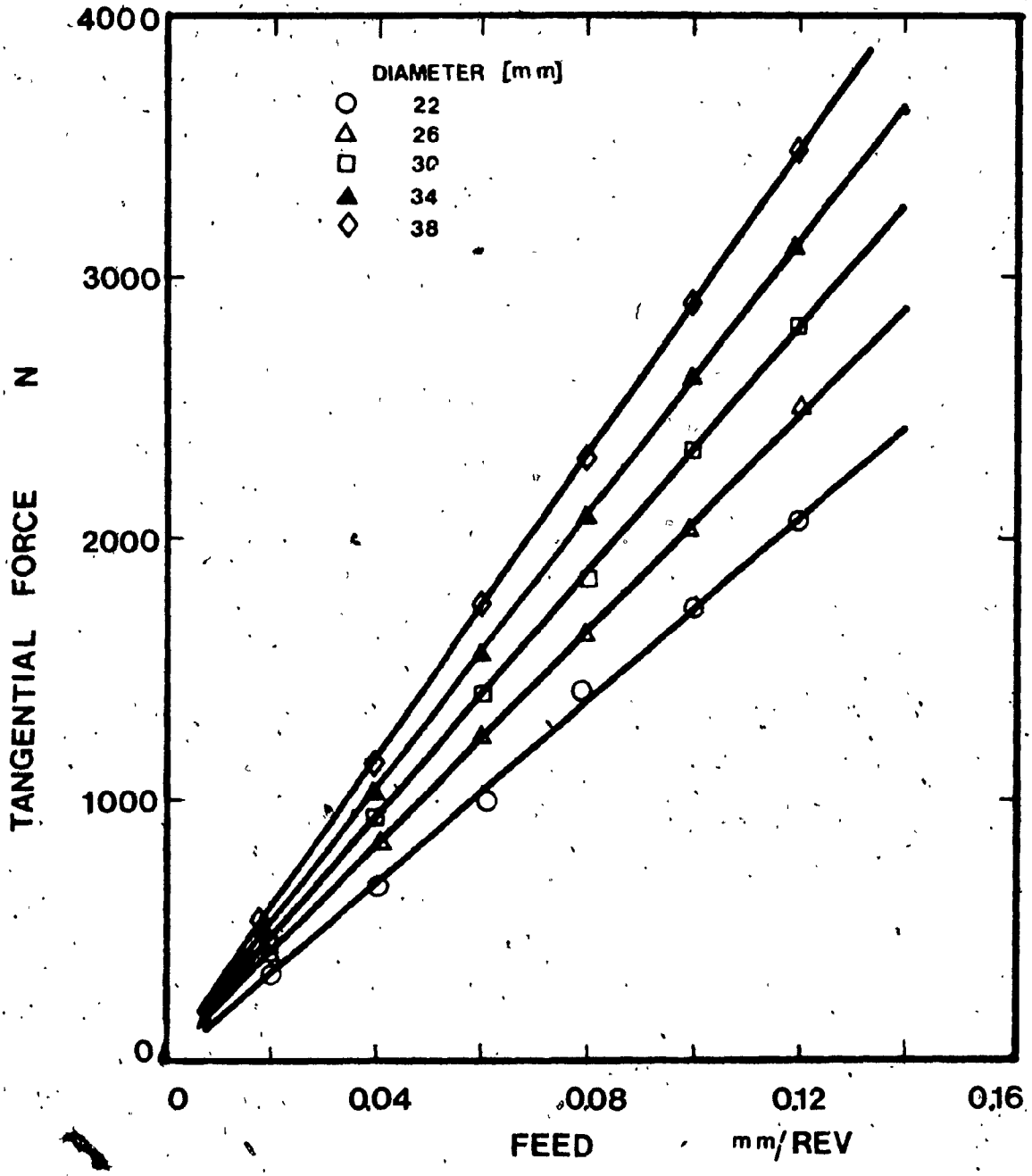

Fig. 2.7(a): Variation of Mean Tangential Force with Feed

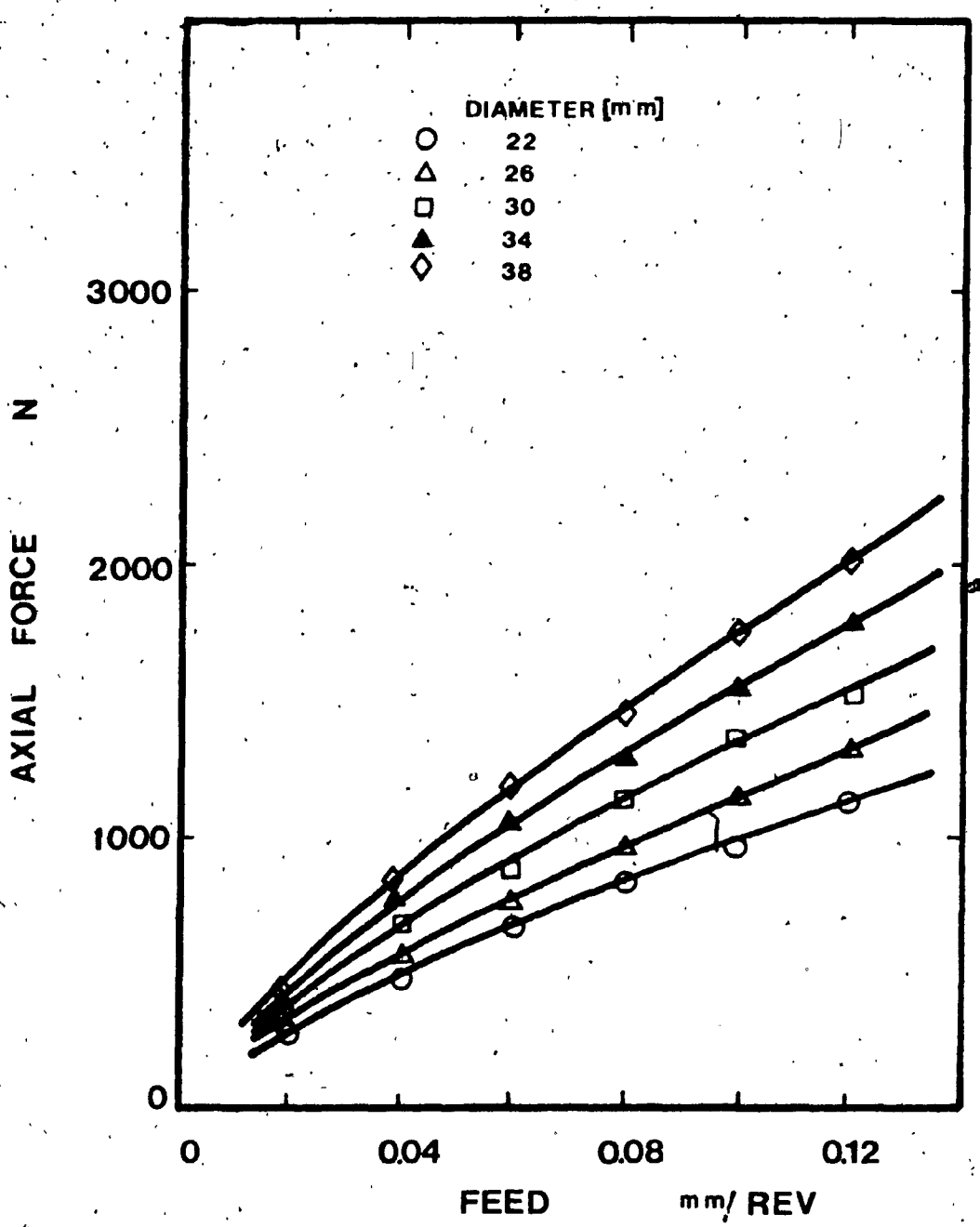

Fig. 2.7(b): Variation of Mean Axial Force with Feed

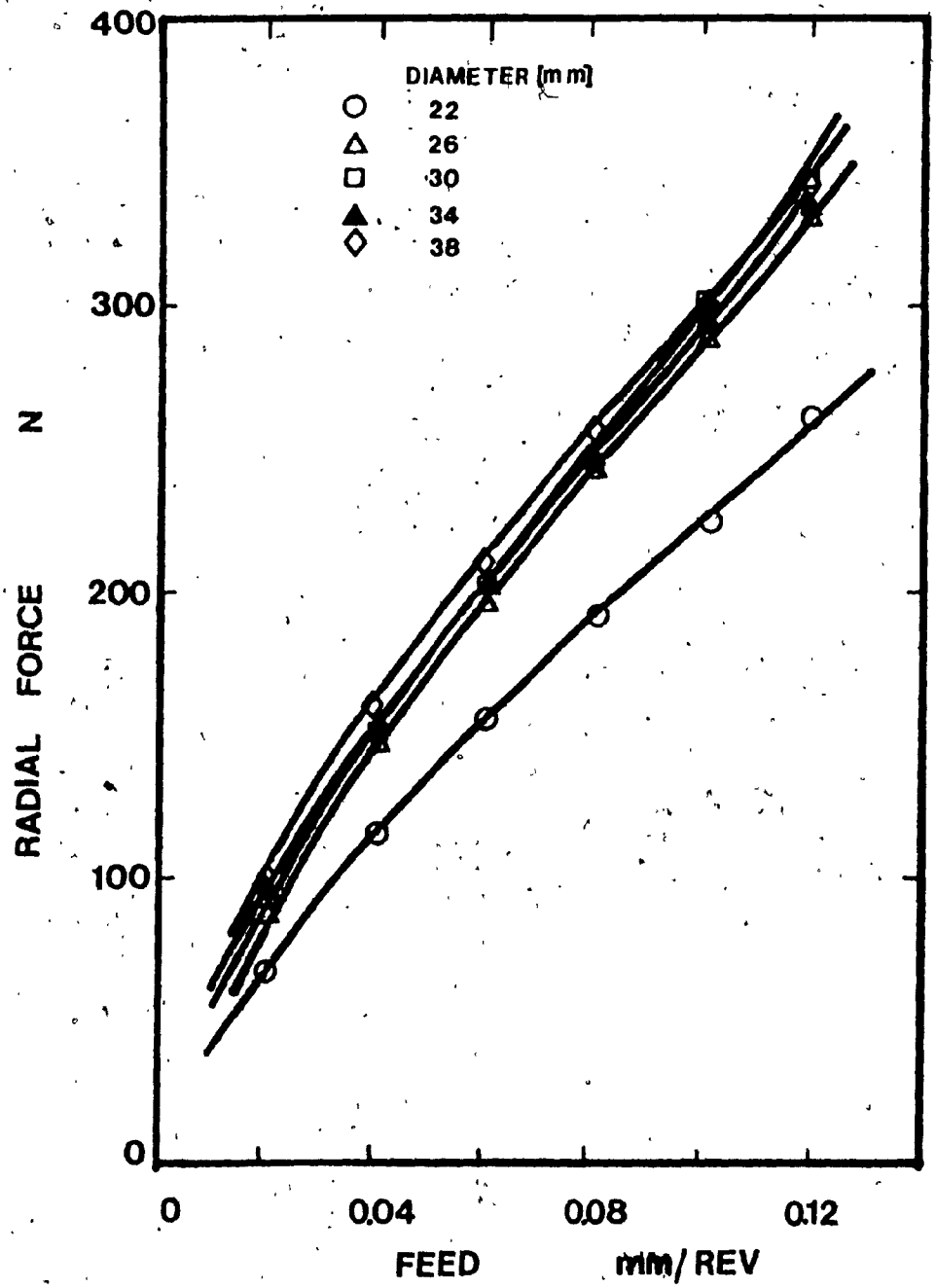

Fig. 2.7(c): Variation of Mean Radial Force with Feed

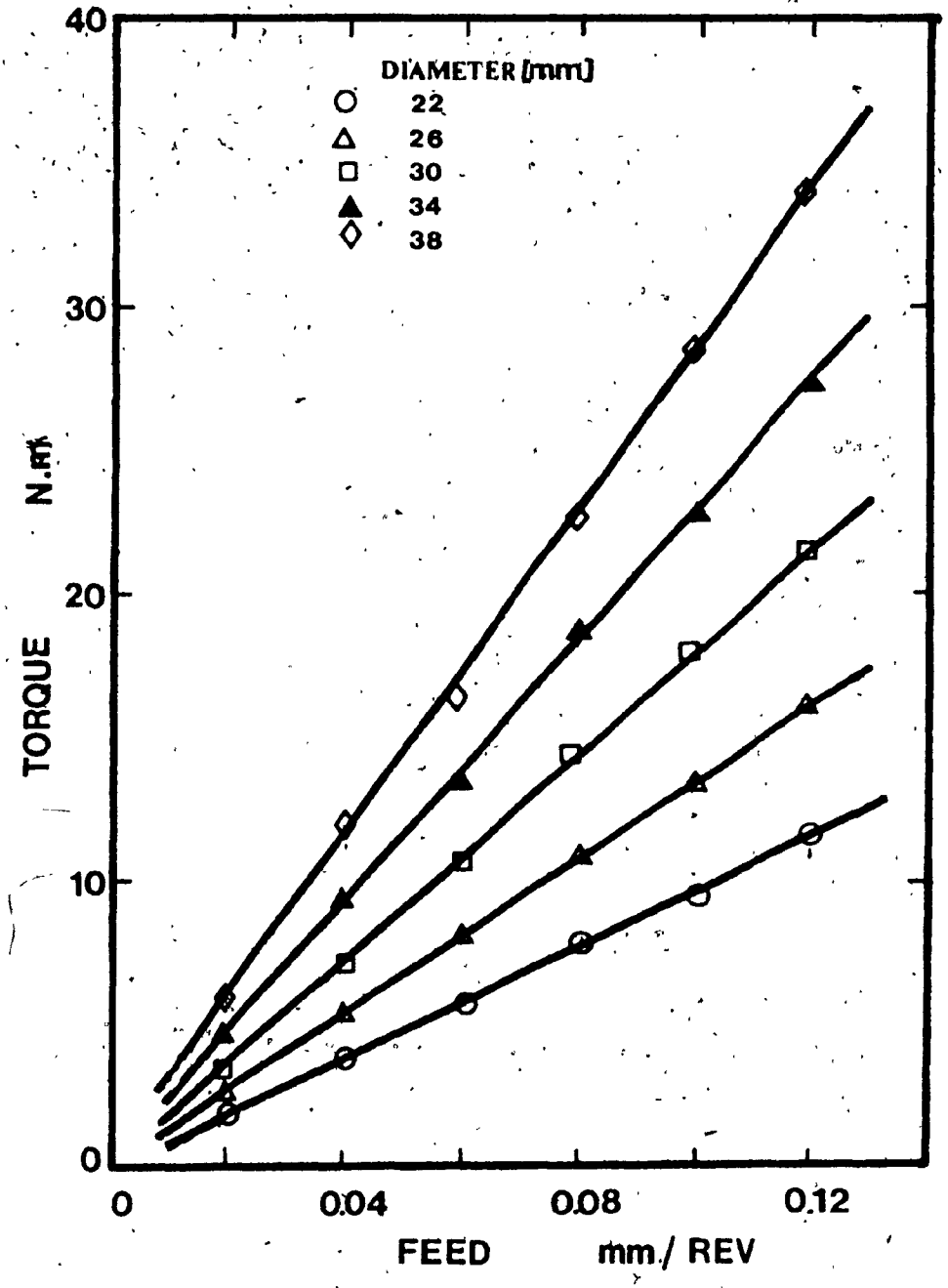

Fig. 2.7(d): Variation of Mean Torque with Feed

TABLE 2.2: Specification of Cutting Tools

Tool Diameter [in mm.]	No. of Steps	p_0	p_1	p_2 [in mm.]	γ_0	γ_1	γ_2 [in radians]
22	2	0.3	6.7	4.0	0.349	0.209	0.314
26	2	0.0	8.2	4.8	0.349	0.209	0.314
30	2	0.6	8.5	5.9	0.349	0.209	0.314
34	2	1.5	8.5	7.0	0.349	0.209	0.314
38	2	2.0	9.3	7.7	0.349	0.209	0.314

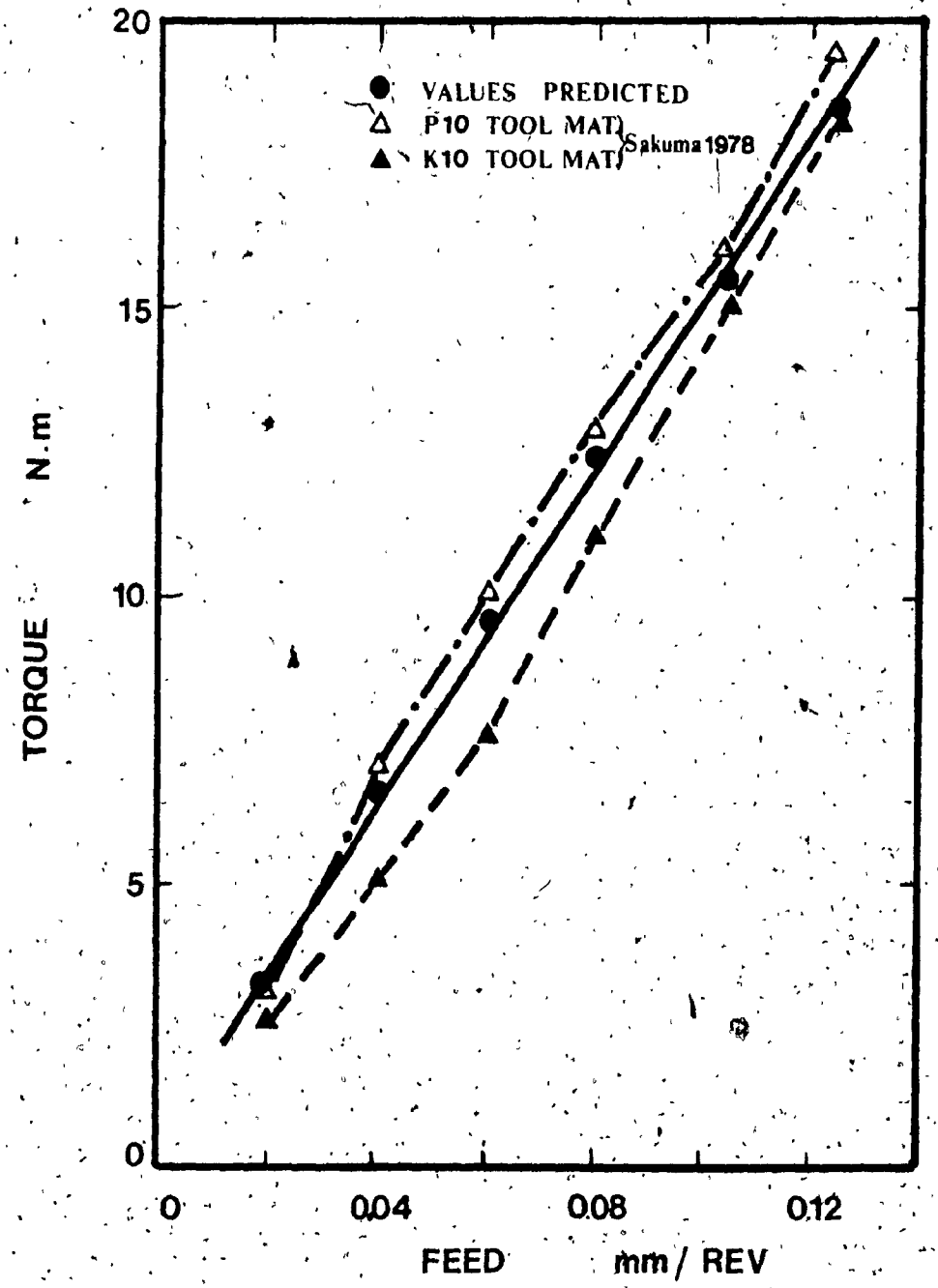

Fig. 2.8(a): Comparison of Predicted and Experimental Values of Torque

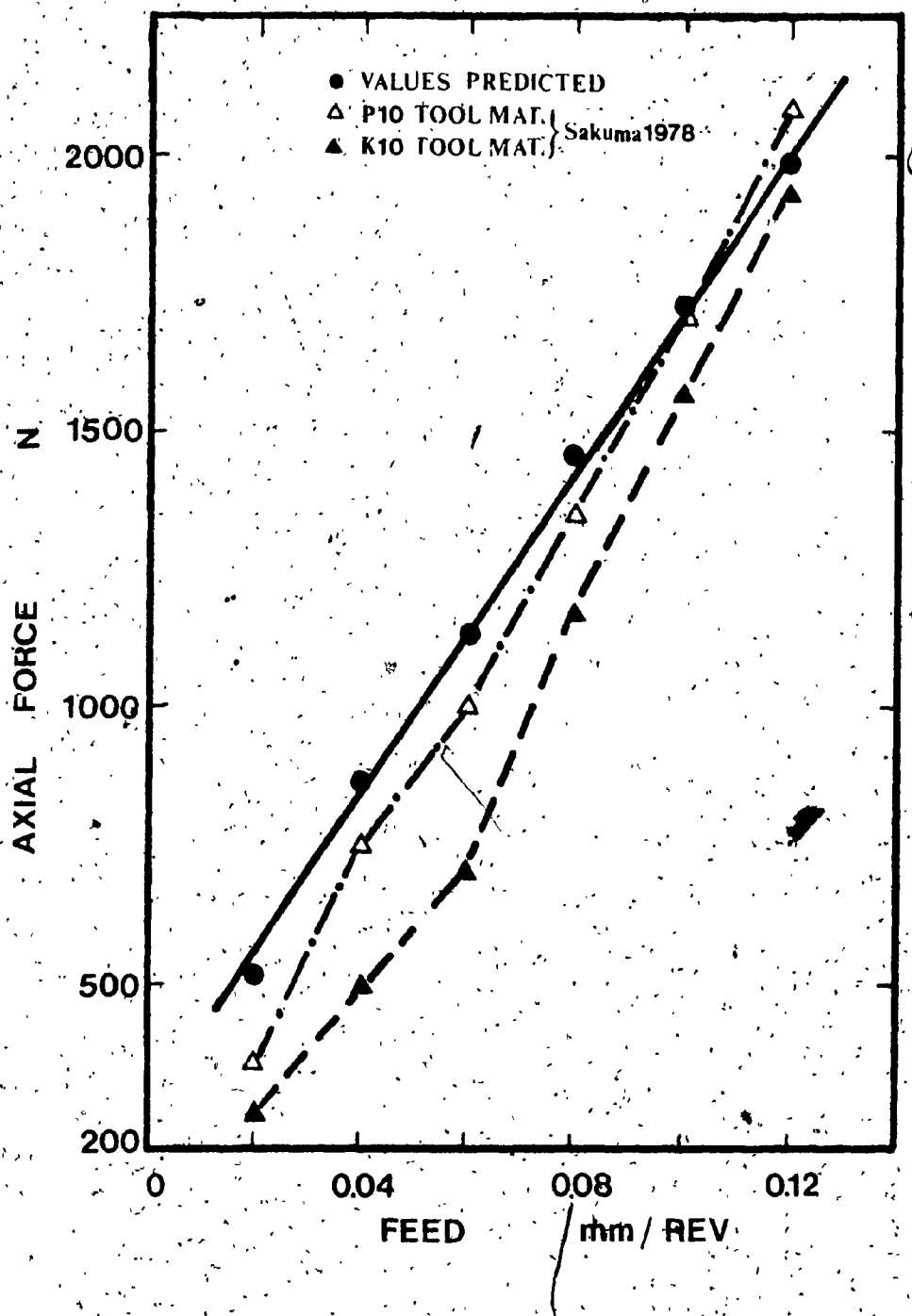

Fig. 2.8(b): Comparison of Predicted and Experimental Values of Axial Force

(i) The value of "k" for a JIS S55C steel was assumed as the same for the nearest AISI steel.

(ii) The values of p_0, p_1, and p_2 were not specified and so they were chosen from a standard table specified by a manufacturer of BTA tools.

2.4 Representation of the Periodic Cutting Forces

The most common form of self-induced vibration in machine tools is the regenerative chatter. This self-induced vibration occurs because most of the cutting operations involve overlapping cuts, and although a system may be basically stable, the forced vibration resulting from the machining of the wavy surface from the previous stroke or revolution of the workpiece or tool can amplify the vibration. Also, in the case of regenerative chatter, the tool vibrates in a direction normal to the mean cutting velocity.

In BTA machining operation the velocity of cutting is a linear function of the radius. Therefore the cutting profile is taken to be made up of infinite number of segments of thickness "dr" as described earlier. The dynamics of a thin section of width "dr" at a distance "r" from the axis of the cutting tool is shown in Fig. 2.9. In the case of regenerative chatter phenomenon, it is necessary to consider both the wave generation and wave removing phenomena as in Fig. 2.9.

The instantaneous value of the cutting force depends upon,

(i) the instantaneous value of the uncut chip thickness,

(ii) the work surface slope,

(iii) the instantaneous value of the rake angle,

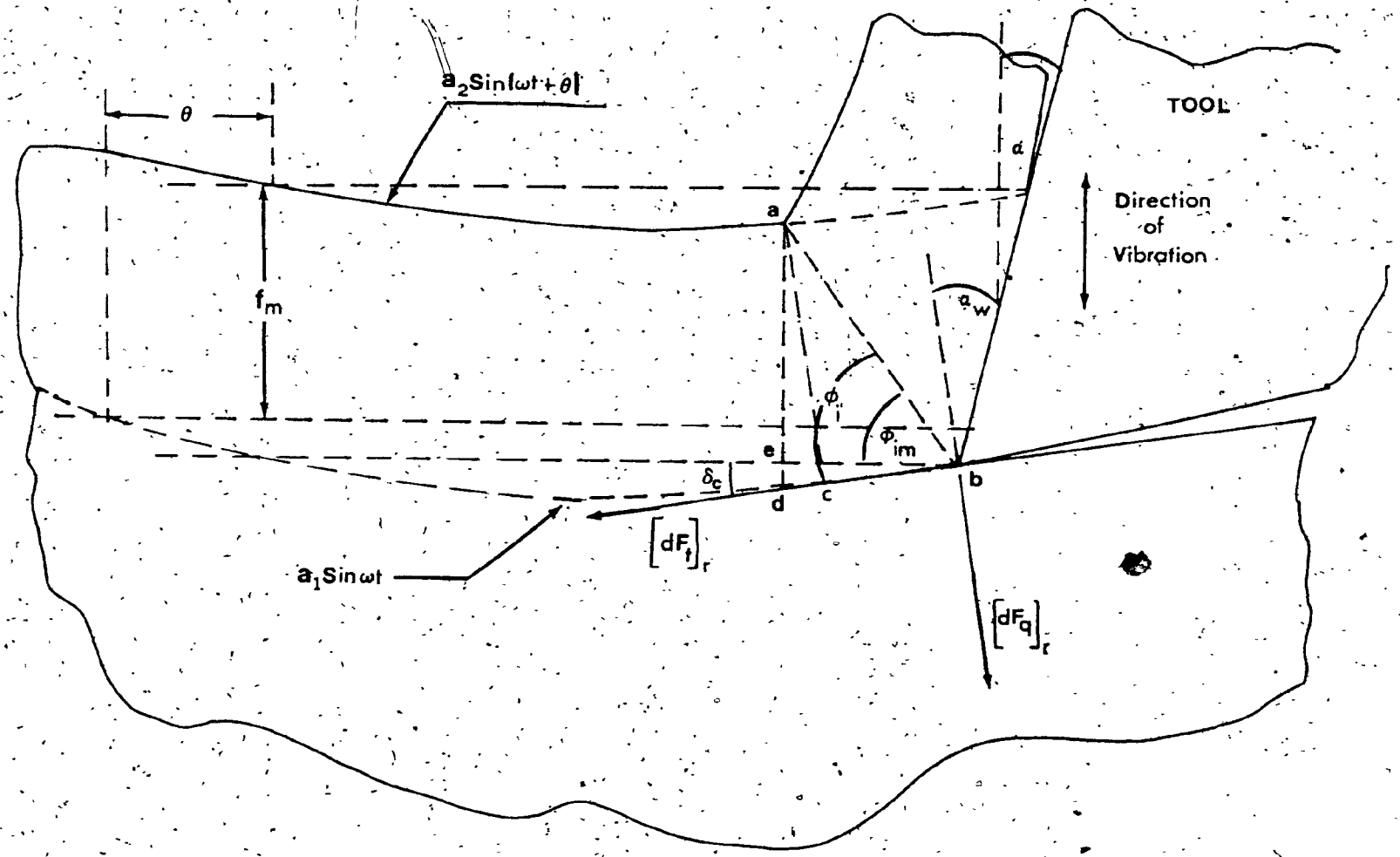

Fig. 2.9: Representation of the Dynamics of Machining at a Small Section on the Cutting Profile

(iv) the instantaneous value of the shear angle.

Thus to determine the instantaneous value of the cutting force, the variation of the above four quantities with time will have to be determined.

The instantaneous value of the uncut chip thickness is the chip thickness perpendicular to the direction of the cutting force. So, from Fig. 2.9, the chip thickness at a distance "r" from the axis of the cutting tool is given by ac. Making the approximation that the length "ac" is very nearly equal to "ad", the relation for the instantaneous chip thickness can be written as

$$f = (1 + \cot \phi_{im})[f_m + a_1 \sin \omega t - a_2 \sin (\omega t + \theta)] \qquad (2.21)$$

From Fig. 2.9, the equation relating the work surface slope δ_c and the velocity of cutting is

$$\delta_c = \frac{\text{Rate of change of uncut chip thickness}}{\text{velocity of cutting}}$$

Since, the wavelength and the amplitude at each cross-section is assumed to have the same value, the work surface slope at each section is assumed to take the value taken up by the section at a distance (d/4) from the axis of the cutting tool. But, the rate of change of uncut chip thickness is obtained by differentiating the equation for the instantaneous chip thickness. So,

$$\left.\begin{matrix}\text{Rate of change of uncut} \\ \text{chip thickness}\end{matrix}\right\} = \omega(1 + \delta_c \cot \phi_{im})[a_1 \cos \omega t - a_2 \cos (\omega t + \theta)]$$

Thus, substituting the expressions for the velocity of cutting and the rate of change of uncut chip thickness into the equation for the work surface slope, the following equation is obtained

$$\delta_c = \frac{120\omega\,[a_1 \cos \omega t - a_2 \cos (\omega t + \theta)]}{\pi dn + 120\omega\,[a_1 \cos \omega t - a_2 \cos (\omega t + \theta)] \cot \phi_{im}} \qquad (2.22)$$

From Fig. 2.9,

$$\alpha_w = \alpha + \delta_c \qquad (2.23)$$

So, the equation for the instantaneous value of the rake angle can be derived using equations (2.22) and (2.23).

$$\alpha_w = \alpha + \frac{120\omega\,[a_1 \cos \omega t - a_2 \cos (\omega t + \theta)]}{\pi dn + 120\omega\,[a_1 \cos \omega t - a_2 \cos (\omega t + \theta)] \cot \phi_{im}} \qquad (2.24)$$

A relation can be obtained from Fig. 2.9 between the instantaneous value of the shear angle measured relative to the mean cutting direction and the instantaneous value of shear angle.

$$\phi_i = \phi_{im} + \delta_c$$

But, the instantaneous value of the shear angle measured relative to the mean cutting direction is related to the average value of the shear angle by the following equation, where C could be evaluated by performing some experiments on regenerative chatter.[36].

$$\phi_{im} = \phi_r + C\,\delta_c$$

Thus, the relation between the instantaneous value of the shear angle and the average value of the shear angle is given by

$$\phi_i = \phi_r + (1 + C)\,\delta_c \qquad (2.25)$$

This is assumed to be valid at each section of the BTA tool. For small wavelengths of the worksurface the value of C approaches zero but when

the wavelength is large, it is given by

$$C = \frac{C_1}{1 + C_2 \frac{\omega f_m}{v_c}} \tag{2.26}$$

Also in the above equation the cutting velocity is taken as the velocity at a distance (d/4) from the axis of the cutting tool. Thus in the case of BTA deep-hole machining, the expression for C can be written as

$$C = \frac{C_1}{1 + \frac{120\ C_2 \omega f_m}{\pi dn}}$$

From equations (2.25) and (2.26) the relation between the instantaneous value of the shear angle and the average value of the shear angle can be expressed as

$$\phi_i = \phi_r + \left[1 + \frac{C_1}{1 + \frac{120\ C_2 \omega f_m}{\pi dn}}\right] \delta_c \tag{2.27}$$

Following a similar procedure as in the case of the derivation of the steady state cutting force equations, the contributions corresponding to each of the regions ED and AD are considered separately.

2.4.1 Cutting Forces in the Region AD

In this region (Fig. 2.2(b)) the tool rake angle is 0°. So, the working rake angle in this region is given by

$$\alpha_w = \delta_c$$

Assuming that Merchant's analysis is valid even under dynamic conditions, the cutting force dF_T and the thrust force dF_q at each section "dr" are given by

$$dF_T = G \cos (\beta_r - \alpha_w)\, dr$$

$$dF_q = G \sin (\beta_r - \alpha_w)\, dr$$

with

$$G = \tau_0 f \left[\sin \phi_i \cos (\phi_i + \beta_r - \alpha_w)[1 - k \tan (\phi_i + \beta_r - \alpha_w)]\right]^{-1}$$

Substituting the expressions for instantaneous value of shear angle, the working rake angle, and worksurface slope into the above expressions and performing certain transformations, the following expressions are obtained

$$dF_T = K_1^*(f,\delta_c)\, \tau_0\, dr$$

$$dF_q = K_2^*(f,\delta_c)\, \tau_0\, dr$$

where

$$K_1^*(f,\delta_c) = \frac{f[1 + \tan^2 (1 + C)\, \delta_c]}{(0.32A_1+B_1) + [0.88A_1+0.64B_1] \tan (1+C)\delta_c + (B_1-0.32A_1) \tan (1+C)\delta_c}$$

$$K_2^*(f,\delta_c) = \frac{f[0.32f^{-0.23} + \tan \delta_c][1 + \tan^2 (1 + C)\, \delta_c]}{[1+0.34f^{-0.23}\tan\delta_c][(0.32A_1+B_1) + (0.88A_1+0.64B_1) \tan (1+C)\delta_c + (B_1-0.32A_1) \tan^2 (1+C)\delta_c]}$$

with

$$A_1 = \frac{(1 - k \tan \delta_c) + 0.34f^{-0.23}(\tan\delta_c - k)}{(1 + 0.34f^{-0.23} \tan \delta_c)}$$

$$B_1 = \frac{(\tan \delta_c - k) - 0.34f^{-0.23}(k + 1)}{(1 + 0.34f^{-0.23} \tan \delta_c)}$$

Thus, the axial and radial components of the force at each section "dr"

are given by

$$dF_a = K_2^*(f,\delta_c)\ \tau_0 \cos\gamma_r\ dr$$

$$dF_R = K_2^*(f,\delta_c)\ \tau_0 \sin\gamma_r\ dr$$

Similarly the expression for torque is

$$dT = K_1^*(f,\delta_c)\ \tau_0\ r\ dr$$

Integrating the expressions for the incremental forces and torque in the region AD, the following equations are obtained

$$F_T = 1.1\ K_1^*(f,\delta_c)\ \tau_0\ [U - p_0] \qquad (2.28)$$

$$F_a = 1.1\ K_2^*(f,\delta_c)\ \tau_0 \sum_{r=1}^{n} p_r \cos\gamma_r \qquad (2.29)$$

$$F_R = 1.1\ K_2^*(f,\delta_c)\ \tau_0 \sum_{r=1}^{n} p_r \sin\gamma_r \qquad (2.30)$$

$$T = \frac{1.1\ K_1^*(f,\delta_c)}{2}\ \tau_0\ [U^2 - p_0^2] \qquad (2.31)$$

2.4.2 Cutting Forces in the Region ED

In this region (Fig. 2.2(b)) the tool rake angle is $-\pi/6$ radians and therefore the working rake angle is given by

$$\alpha_w = \delta_c - \pi/6$$

Using the above expression for the instantaneous rake angle the expressions for the incremental cutting and thrust force are obtained as

$$dF_T = L_1^*(f,\delta_c)\ \tau_0\ dr$$

$$dF_q = L_2^*(f,\delta_c)\,\tau_0\,dr$$

where

$$L_1^*(f,\delta_c) = \frac{f[1+\tan^2(1+C)(\delta_c-\pi/6)]}{[(0.32A^*+0.1B^*)+(0.88A^*+0.64B^*)\tan(1+C)(\delta_c-\pi/6)+(B^*-0.32A^*)\tan^2(1+C)(\delta_c-\pi/6)]}$$

$$L_2^*(f,\delta_c) = \frac{f[0.26f^{-0.23}-\tan^2(\delta_c-\pi/6)][1+\tan^2(1+C)(\delta_c-\pi/6)]}{[1+0.26f^{-0.23}\tan(\delta_c-\pi/6)][(0.32A^*+0.1B^*)+(0.88A^*+0.64B^*)\tan(1+C)(\delta_c-\pi/6)+(B^*-0.32A^*)\tan(1+C)(\delta_c-\pi/6)]}$$

with

$$A^* = 1 - k\left[\frac{0.26f^{-0.23}-\tan(\delta_c-\pi/6)}{1+0.26f^{-0.23}\tan(\delta_c-\pi/6)}\right]$$

$$B^* = -\left[k+\frac{0.26f^{-0.23}-\tan(\delta_c-\pi/6)}{1+0.26f^{-0.23}\tan(\delta_c-\pi/6)}\right]$$

Similarly, the expression for the incremental value of torque is,

$$dT = L_1^*(f,\delta_c)\,\tau_0\,r\,dr$$

Using the geometry of the cutting edge and integrating the expressions for the incremental forces and torque, the total forces and torque in the region ED are obtained.

$$F_T = 1.1\,L_1^*(f,\delta_c)\,\tau_0\,p_0 \qquad (2.32)$$

$$F_a = 1.1\ L_2^*(f,\delta_c)\ \tau_0\ p_0 \cos \gamma_0 \tag{2.33}$$

$$F_R = -1.1\ L_2^*(f,\delta_c)\ \tau_0\ p_0 \sin \gamma_0 \tag{2.34}$$

$$T = \frac{1.1}{2}\ L_1^*(f,\delta_c)\ \tau_0\ p_0^2 \tag{2.35}$$

2.5 Resultant Periodic Cutting Force System on BTA Tool

Similar to the steady state force equations, the total tangential, axial, radial forces and the torque is obtained by summing the values of the above stated components in the regions AD and ED of the cutting tool. Performing this operation the total tangential, radial, axial forces and torque acting on the cutting tool are,

$$F_T = 1.1\ \tau_0[(U - p_0)\ K_1^*(f,\delta_c) + p_0\ L_1^*(f,\delta_c)] \tag{2.36}$$

$$F_R = 1.1\ \tau_0\ [K_2^*(f,\delta_c) \sum_{r=1}^{n} p_r \sin \gamma_r - p_0\ L_2^*(f,\delta_c) \sin \gamma_0] \tag{2.37}$$

$$F_a = 1.1\ \tau_0\ [K_2^*(f,\delta_c) \sum_{r=1}^{n} p_r \cos \gamma_r + p_0\ L_2^*(f,\delta_c) \cos \gamma_0] \tag{2.38}$$

$$T = 0.55\ \tau_0\ [(U^2 - p_0^2)\ K_1^*(f,\delta_c) + p_0^2\ L_1^*(f,\delta_c)]. \tag{2.39}$$

Thus equations (2.36), (2.37), (2.38), (2.39) represent the periodically varying dynamic cutting forces in the BTA deep-hole machining operation. But the resultant force system on a new BTA cutting tool consists of an axial force and torque, as the radial and tangential forces are balanced by the reactions at the wear pads. Also, with the increase in the number of holes bored, the cutting profile as well as the wear pads deteriorate. This creates a certain imbalance of forces along the radial

and tangential directions. So, the resultant force system consists of three force components and a torque. Under such conditions, the cutting force equations represented by equations (2.36), (2.37), (2.38) and (2.39) coupled with the properties of the randomly varying component can be used to evaluate, not only the response but also the regions of stability and instability during the machining operation.

2.6 Conclusions

The equations for the prediction of the cutting forces and torque based on a thin shear plane model is developed by summing the forces due to each step. It is found that the steady state cutting forces and torque are independent of the velocity of cutting. Also the analytical expressions derived do not depend upon whether the boring bar or workpiece is rotating or both are counter-rotating. Besides, accounting for the fact that the cutting force is dependent upon the workpiece material, it eliminates the need for empirical testing. Further, the predicted results of the steady state cutting force have been compared with earlier literature, and show a fairly good agreement. Lastly, such a theoretical treatment of the cutting forces enables the determination of the percentage of the cutting forces in the total force.

The equations for the periodic forces enable the determination of the effects of displacement, velocity, and acceleration of the tool tip upon the cutting force. Also, these equations can be used to predict not only the machine tool response, but also the regions of stability and instability in the machining operation as the tool gets worn out and under conditions of chatter.

In this investigation, the region of working is the non-chatter

zone. Since, the resultant force system consists of an axial force and torque, with each one consisting of four components, namely the oil force, friction force, the burnishing force, and the cutting force, the usage of a completely theoretical approach to obtain a model for the mean values of the axial force and torque is difficult. Further, the randomly varying characteristics of the resultant force system can only be determined by performing a series of experiments. Therefore a set of experiments are performed to obtain a mathematical model of the resultant force system as described in the next Chapter.

CHAPTER 3

EXPERIMENTAL MEASUREMENT OF THE TORQUE AND THE AXIAL FORCE IN BTA DRILLING

CHAPTER 3

EXPERIMENTAL MEASUREMENT OF THE TORQUE AND THE AXIAL FORCE IN BTA DRILLING

3.1 Importance of the Measurement of Forces

The knowledge of the actual cutting forces in machining is of paramount importance to both designers and users of machine tools due to several reasons. The major factors are (i) the estimation of the power requirements of a machine tool, (ii) the estimation of the tool forces that must be supported by the machine tool frame, components, bearings, jigs and fixtures, and (iii) the determination of the characteristics of new work and tool materials.

The magnitude of the cutting forces may be estimated by different experimental methods. They are (i) by indirect power measurements, (ii) by calorimetric methods and (iii) by suitable development of tool force dynamometers. But, for research purposes, direct measurements by dynamometers have won a general acceptance and since then, many research workers in the field of metal cutting have tackled the problem of constructing dynamometers to measure accurately the force signals using different types of transducers. The transducers normally employed are, piezo-electric transducers, potentiometric transducers, low voltage differential transformers, capacitive transducers, strain gauge transducers, photocells, and permanent magnets. The measurement of forces in machining corresponds to the analytical problem of determining all the components of a general force and moment vector in a chosen coordinate system. As it is impossible to measure the cutting forces at their actual

point of generation, the reactions have to be measured in an appropriately defined plane distance from the cutting edge. Therefore, a satisfactory measuring system is essential through which one can obtain accurately the characteristic values, independent of the point of application of the force and/or the moments.

In order to obtain such precise measurements, the measuring system should satisfy the following requirements [95]:

a) the original rigidities should be maintained as far as possible;
b) the dynamic characteristics should be similar to the original set up;
c) the mounting of the tool or workpiece should remain as close as possible to those of the original set up;
d) the frequency response should be as large as possible;
e) any cross talk or interference between the components of the force and moments should be a minimum;
f) sensitivities of the transducers should be unaffected by time; temperature and the location of mounting of tool and workpiece;
g) the capacity to measure small variations of force and/or moments accurately;
h) the adjustments of zero points, sensitivities, and measuring ranges should be non-critical.

These measuring systems consist of three basic parts [96]:

i) A detector transducer stage for detecting the physical variable. Here, in the present case, it is the force due to machining. At this stage the transducer converts the magnitudes of the cutting force into an electric signal.

ii) An intermediate stage for conditioning the signal by magnification, filtration and stabilization.

iii) A final read out stage for reading, recording or monitoring the output signal.

A schematic arrangement of such a measuring device is shown in Fig. 3.1.

3.2 The Experimental Set Up

The experimental set up for measuring both the static and dynamic torque and axial force in deep-hole machining consists of the following sub-systems:

a) The deep-hole drilling machine.

b) The dynamometer capable of holding the two component load washer.

c) Two charge amplifiers.

d) An XYZ compensator.

e) A magnetic tape recorder.

f) A Fast Fourier Transform analyser

g) A cathode ray oscilloscope.

h) Two digital voltmeters.

and are described in the following sections.

The deep-hole drilling machine is a 30HP Schaerer HPD 631 Lathe converted into a deep-hole machining system. It is equipped with a wide range of feeds and speeds that can be used in all the three working methods, namely, the rotating cutting tool-stationary workpiece, rotating workpiece-stationary cutting tool, and counter-rotation. The charge amplifier is used for converting the electrical charge from the piezo-electric transducer of the dynamometer into a proportional voltage. The function of the compensator is to cancel out the undesirable mutual interference of

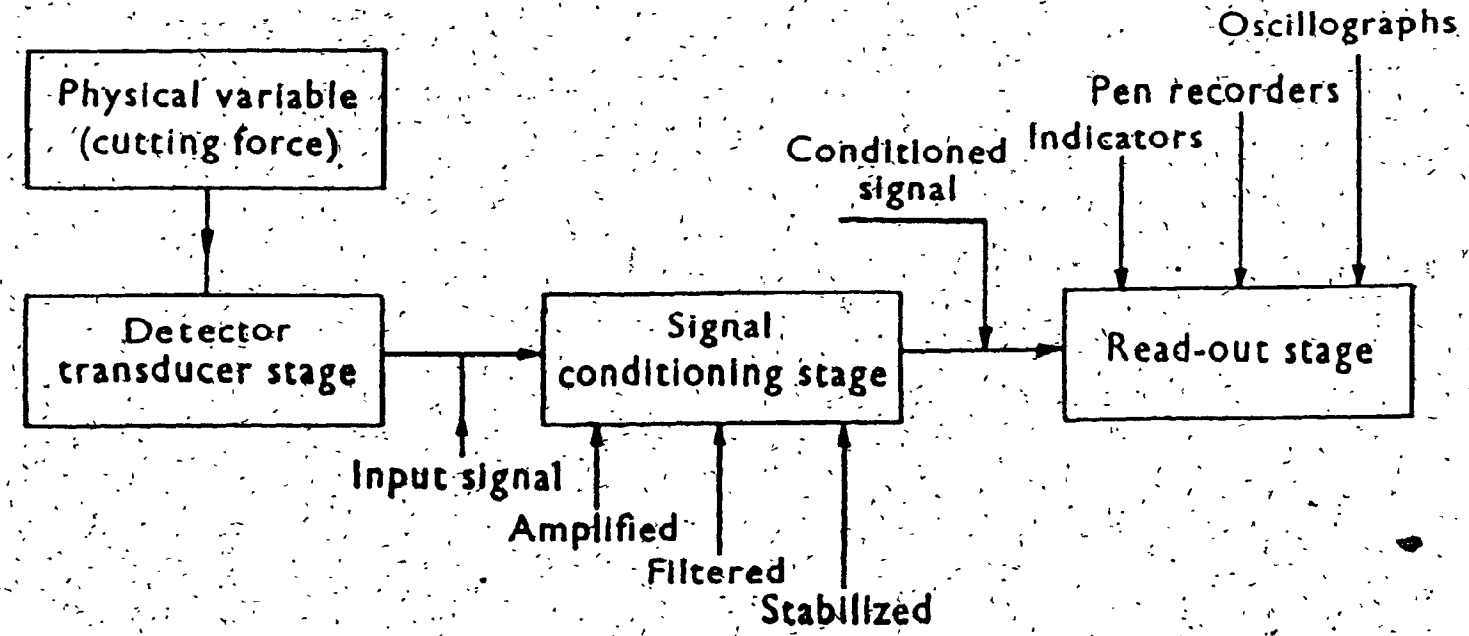

Figure 3.1: Schematic Arrangement for the Measurement of Cutting Forces

the two independent measuring channels. The two operational amplifiers (one charge amplifier is not active) are fed with the two measured signals from the charge amplifiers. Any desired portion of the output voltage of any one channel may be tapped through a voltage divider and fed as a compensation signal to the input of the other channels. When this is done for both the components, the outputs from the compensator are the actual measured values of the forces. Figure 3.2 shows the functional schematic diagram of the compensator.

The force signal is stored on a magnetic tape and in order to relate the measured variable to the generalized force, the dynamometer must be calibrated statically. The dynamometer should be so designed that it measures only the force fluctuations, and not the vibrations of the tool due to any possible resonance with the machine tool, over as wide a range of frequencies as possible. This requires that the natural frequency of the dynamometer be exactly known. A dynamic test of the dynamometer-workpiece-machine tool system is carried out to determine this useful frequency band, in which the dynamometer can be used for obtaining reliable measurements.

3.3 The BTA Dynamometer

The dynamometer shown in Fig. 3.3 is designed to measure the resultant force system in any deep-hole machining operation. It is held in the chuck and has been so designed that it can be used only when the workpiece is stationary and the cutting tool is rotating.

The dynamometer employed is a simple unit that was designed and manufactured using only commercially available components, so that such a unit can be readily produced and repaired. So, from a mechanical design

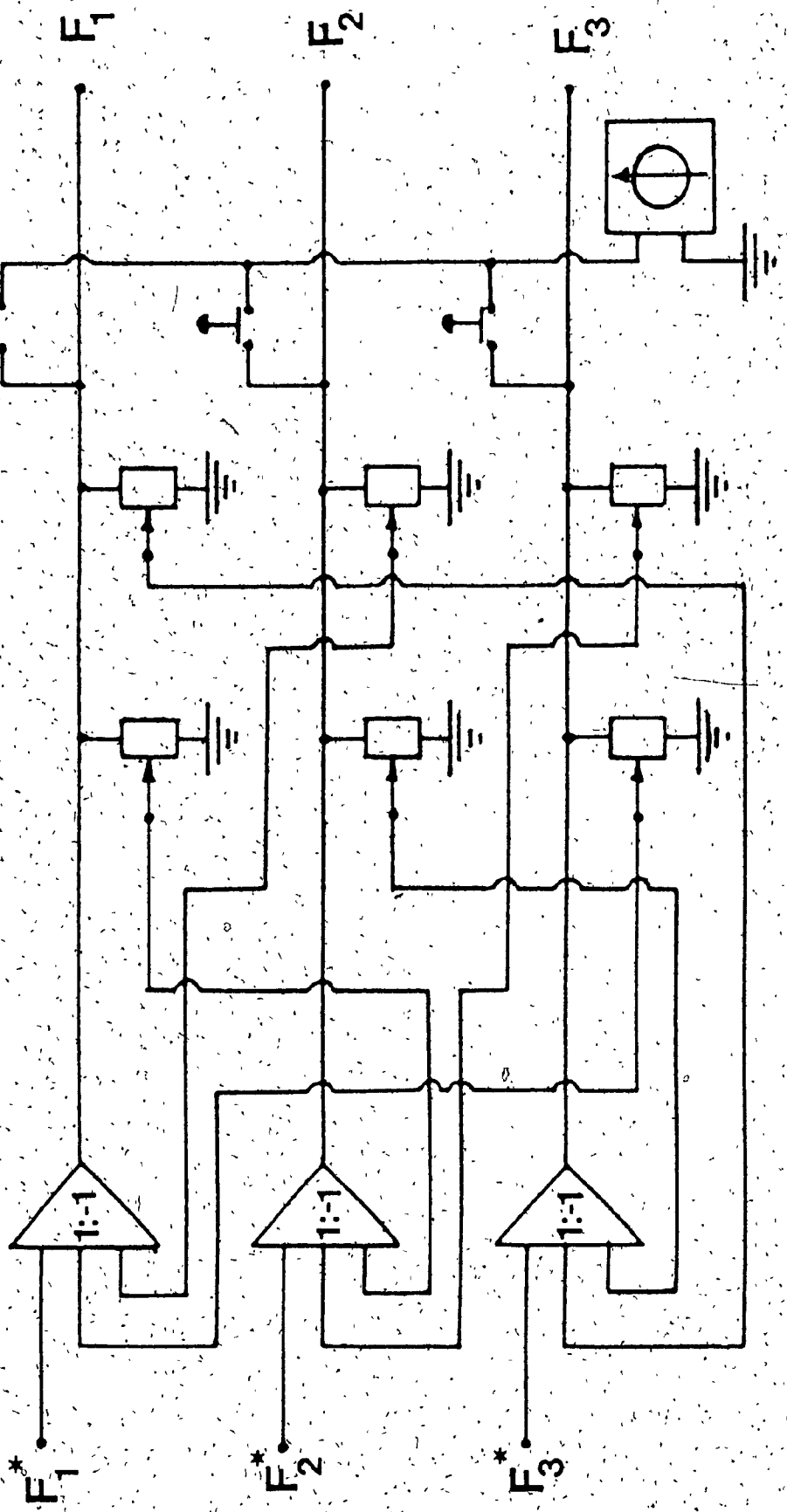

Figure 3.2: Functional Schematic Diagram of a Compensator

Figure 3.3: BTA Dynamometer

point of view the dynamometer consists of four components:

(i) A piezo-electric load washer.

(ii) Ten bolts to preload the load washer.

(iii) Chuck jaw

(iv) Pressure head jaw.

The chuck jaw, and the pressure head jaw, made out of mild steel, are two main components of the dynamometer. The chuck jaw is to be held in the chuck of the deep-hole drilling unit where as the pressure head jaw holds the workpiece, which in turn is clamped on to the pressure head. Also, the jaws hold the piezo-electric load washer. Ten bolts used for preloading the load-washer pass through the holes provided on the chuck jaw and the pressure head jaw. These preloading bolts fix the load washer between the two chucks and give the load washer proper pre-load and avoid the possibility of any separation during the operation of the dynamometer [97].

The dynamometer can accommodate two types of load washers, namely, Kistler Z-11758 and Z-9065 types. Since, only the Z-9065 type load washer was used in the test, a knowledge of the characteristics of this type of load washer is necessary. These are listed in Table 3.1 [98].

3.4. Static Calibration of the Dynamometer

The purpose of static calibration is to establish a relation between the measured output of the dynamometer and the actual value of the force and/or moment to be measured. In spite of the fact that the piezoelectric transducers are generally used to sense dynamic quantities, the static calibration is possible because of the high insulation resistance of the load washer, and by the high input impedance provided by the charge

TABLE 3.1: Characteristics of Z9065 Piezoelectric Load Washer

Property	Generalized Force	Units	Numerical Value
Measuring Range	Axial Force	KN	± 20
	Torque	N-m	± 200
Resolution	Axial Force	N	0.02
	Torque	N-cm	0.02
Sensitivity	Axial Force	pc/N	-1.8
	Torque	pc/N-cm	-1.6
Overload	Axial Force	KN	144
	Shear Force	KN	± 12
	Bending Moment	N-m	± 200
Cross Talk	Axial Force ↔ Torque	N-cm/N	≤ ±0.02
	Torque ↔ Axial Force	N/N-cm	≤ ± 0.01
Stiffness	Axial direction	KN- m	≈6.5
	Torsional direction	N-m/m-rad	≈500
Resonant Frequency	-	KHz	≈ 40
Weight	-	gm	150
Temperature Error	Axial Force	N/°C	+30
	Torque	N-cm/°C	-5

amplifier. Thus, for any value of the load, less than the maximum value, in both the axial and torque direction, the time duration of the signal is sufficiently large enough to permit the reading on a digital voltmeter. So, in the present case a static calibration is performed for both the channels of observation.

3.4.1 Static Calibration Along the Axial Direction

The static calibration of the dynamometer is carried out by applying a known load of different magnitudes, measuring the output of the dynamometer, and establishing a graphical relation between the measured quantities and the applied forces.

In the case of the static calibration of the dynamometer along the axial direction the known load was applied using a vertical loading machine as shown in Fig. 3.4. A schematic diagram of the dynamometer and instrumentation used along with it is presented in Fig. 3.5.

During the measurement, the charge amplifiers were set to "long", so that the time constant of the system becomes large, and the rate of decay of charge during the static measurement is reduced. This minimizes considerably the error introduced in the static calibration. The load was increased from zero to a value of 13.4 kN and readings from the digital voltmeter were recorded. The output from the torque channel was also recorded to estimate the cross coupling between the channels. Similar readings of the digital voltmeter were taken during the unloading cycle. The latter is performed to estimate the hysteresis present in the system. It was observed that the difference in the readings obtained during loading and unloading were small, which implies that the system exhibits practically no hysteresis properties.

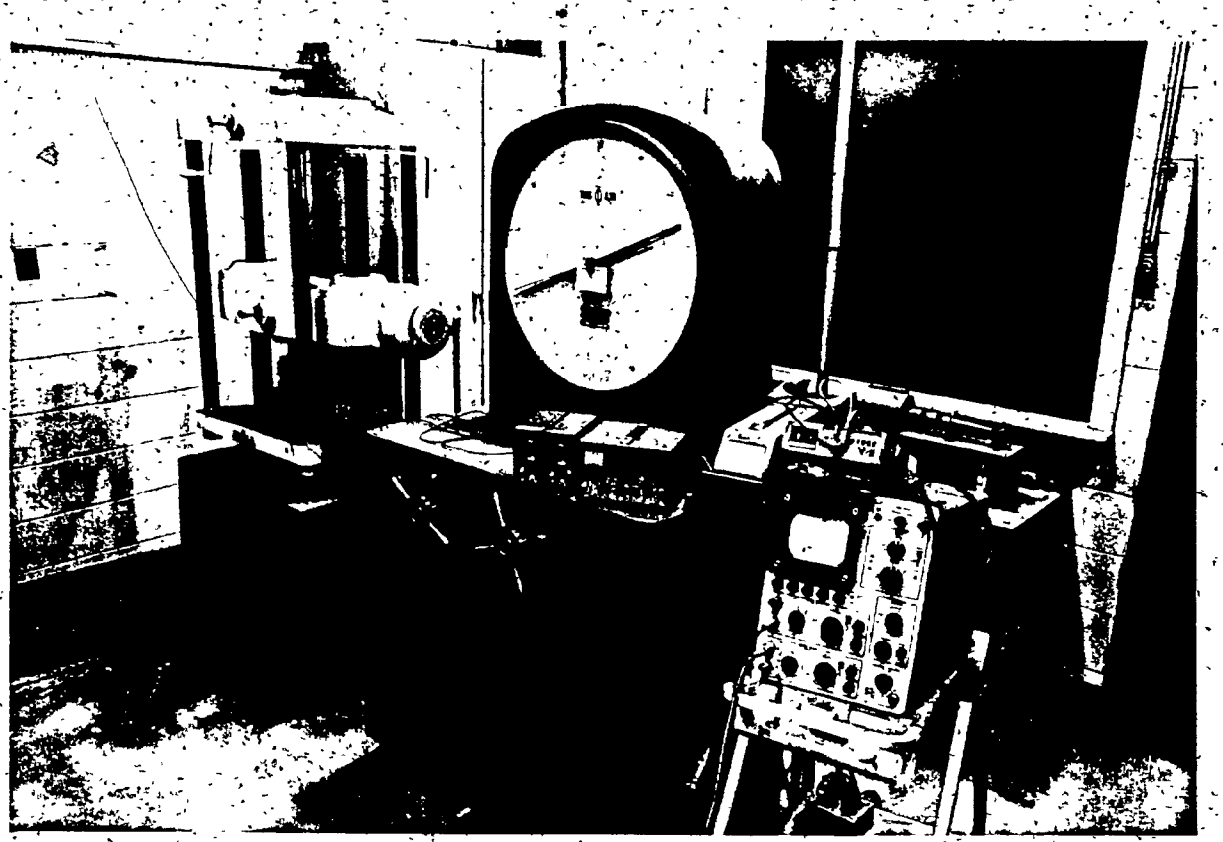

Figure 3.4: Pictorial View of Equipment used for Static Calibration along the Axial Direction

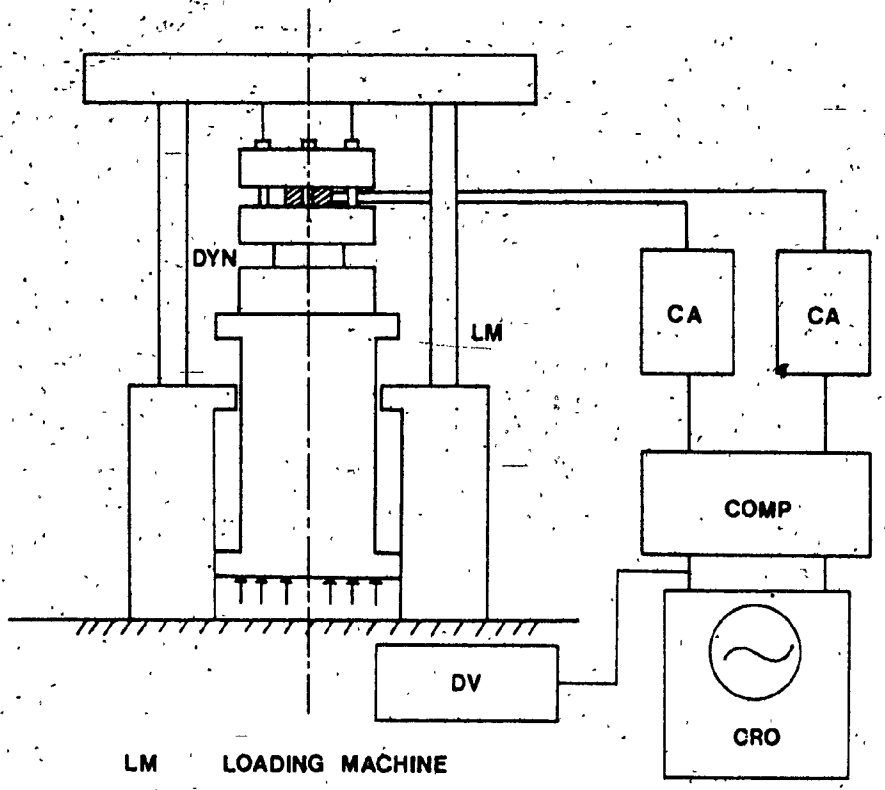

LM	LOADING MACHINE
DYN	DYNAMOMETER
CA	CHARGE AMPLIFIER
COMP	COMPENSATOR
DV	DIGITAL VOLTMETER
CRO	CATHODE RAY OSCILLOSCOPE

Figure 3.5: Schematic Diagram of the Dynamometer and Instrumentation used for Static Calibration along the Axial Direction.

Based on the obtained readings of the digital voltmeter a calibration curve of the charge developed by the piezo-electric load washer with the axial force is established and is shown in Fig. 3.6. The charge developed on the load washer is calculated using the equation

$$Q = CV \tag{3.1}$$

where

Q represents the charge developed by the piezo-electric load washer

V denotes the reading of the digital voltmeter

C represents the gain set on the charge amplifier.

3.4.2 Static Calibration in the Torque Direction

The static calibration of the dynamometer along the torque direction is carried out by applying a pure torque of known value. The dynamometer is held in the chuck of the lathe and to the pressure head jaw of the dynamometer is attached a bar, whose length is much greater than the distance between its supports. Dead weights are introduced at the free end of this bar. So, the resultant torque introduced equals the moment arm times the load. The entire set up is shown in Fig. 3.7. A schematic diagram of the dynamometer and the instrumentation used is described in Fig. 3.8. Similar to the calibration procedure described in the previous sub-section, the charge amplifiers were set to "long" so that the error introduced in static calibration is a minimum. The compensator was adjusted with 80% of the maximum torque, using the nomogram provided [99].

The load was increased gradually from zero to about 470 N and the readings from the digital voltmeter are noted. The output from the axial

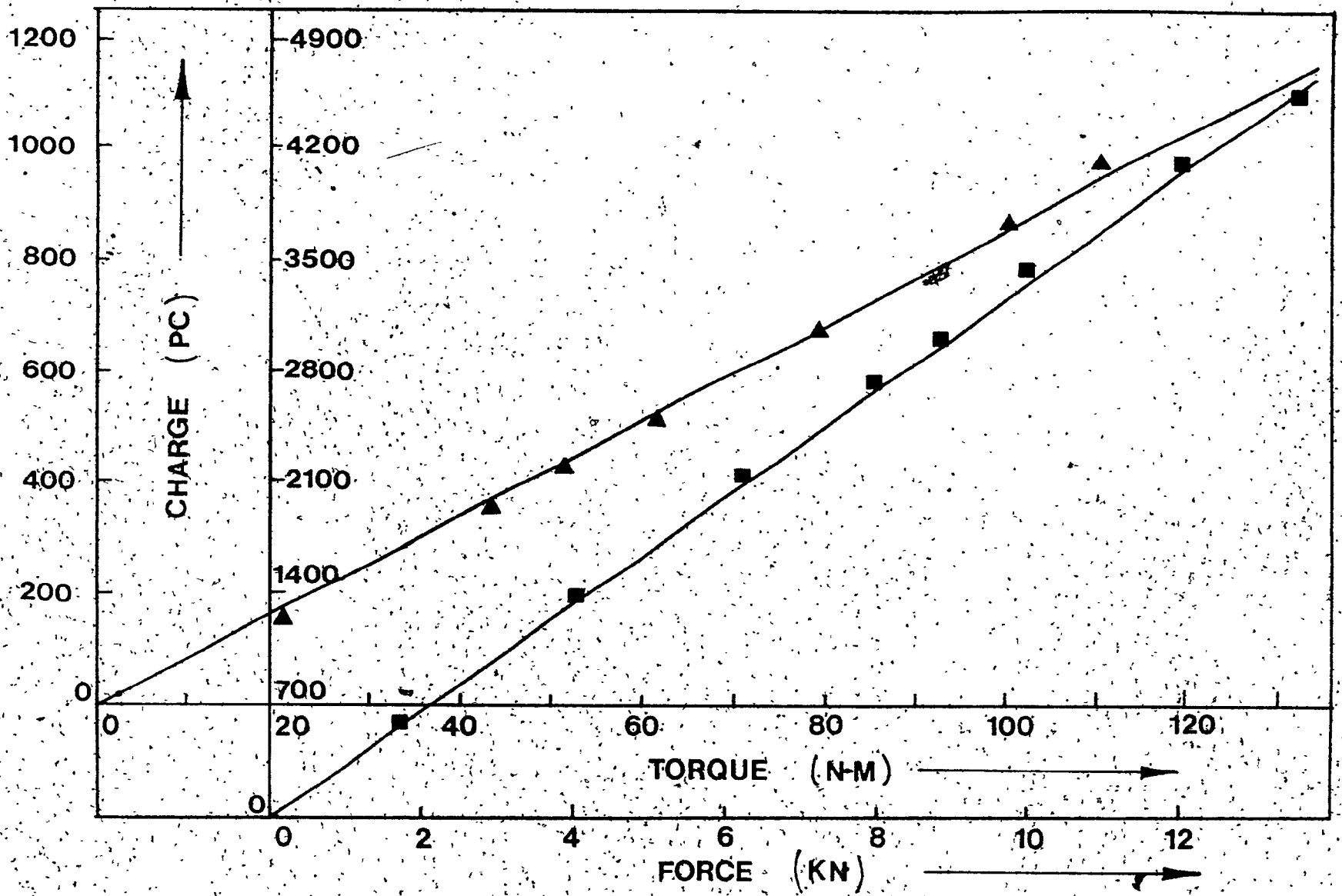

Figure 3.6: Static Calibration Curves

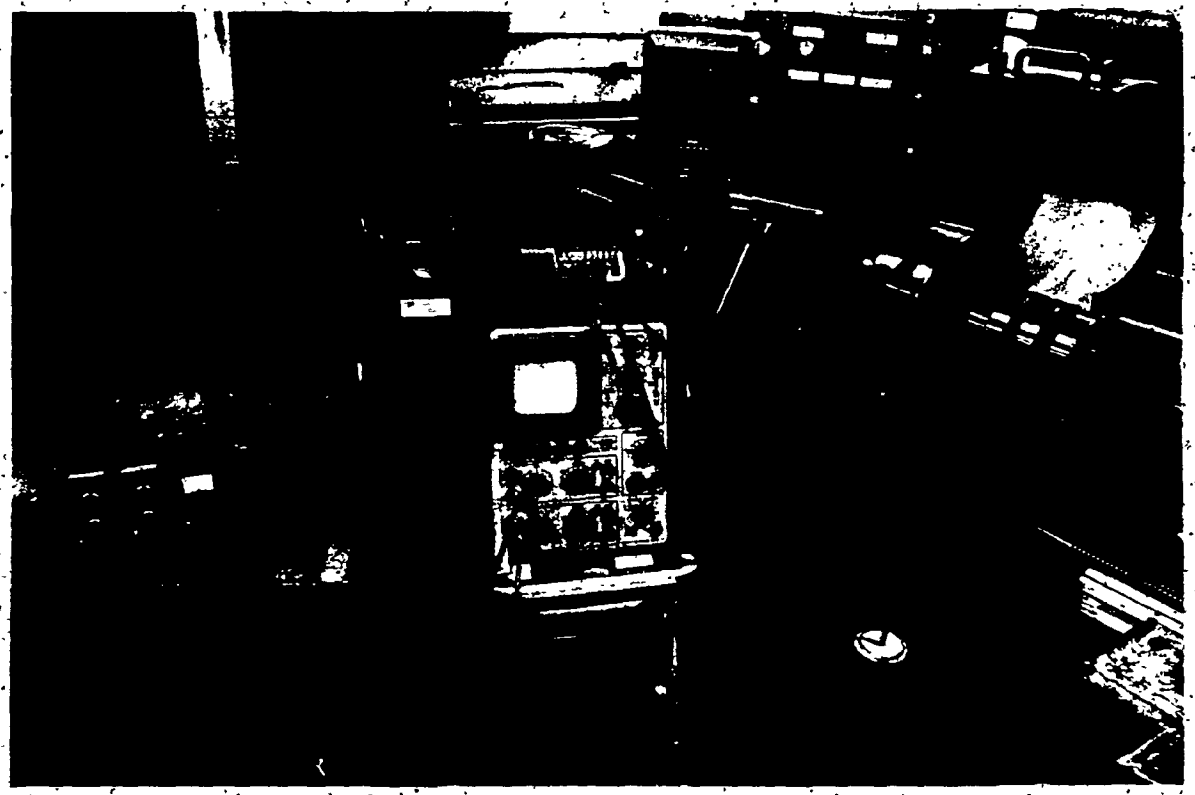

Figure 3.7: Pictorial View of Equipment used for Static Calibration in the Torque Direction

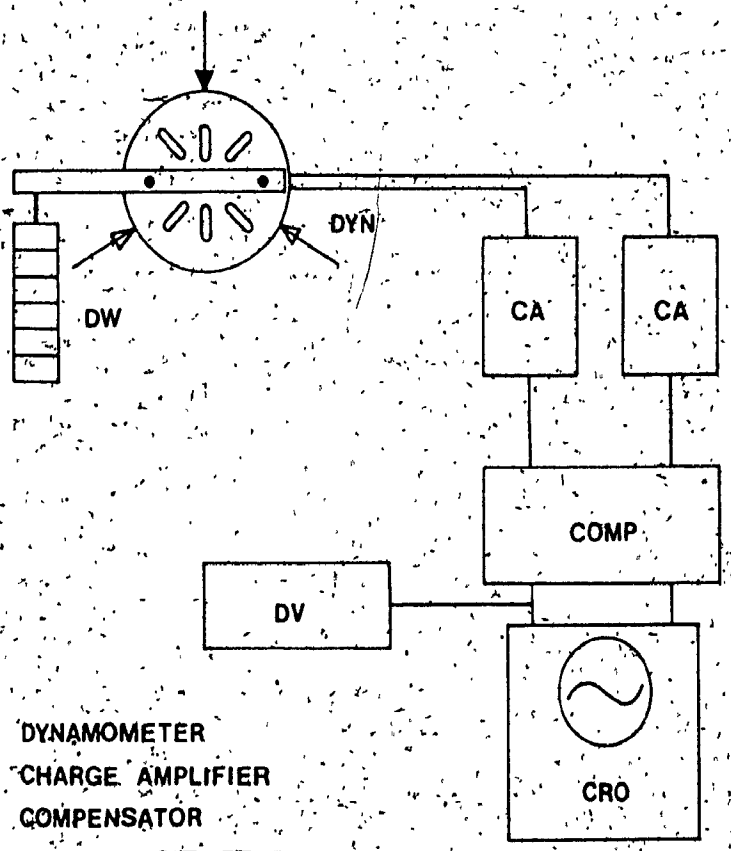

DYN DYNAMOMETER
CA CHARGE AMPLIFIER
COMP COMPENSATOR
DV DIGITAL VOLTMETER
CRO CATHODE RAY OSCILLOSCOPE

Figure 3.8: Schematic Diagram of the Dynamometer and Instrumentation used for Static Calibration in the Torque Direction

force channel is also recorded to estimate the influence of the torque on the axial force. Similar readings of the digital voltmeter were taken during an unloading sequence. It is observed that the readings taken during loading and unloading are very close indicating practically no hysteresis present in the system.

Based on the obtained readings of the digital voltmeter a calibration curve for the charge developed by the load washer and the applied torque is established and is given in Fig. 3.6. The charge developed is calculated using equation (3.1).

3.4.3 Correlation Between the Measured Values and the True Values

The static calibration of the dynamometer enables the determination of a relation between the charge developed and the magnitude of the axial force and torque. Since, in this case a two component dynamometer is used, the relation between the measured values of the axial force and torque obtained from the calibration chart (Fig. 3.6), and the true values of the axial force and torque can be presented as

$$\begin{bmatrix} F_{am}^{*} \\ T_{m}^{*} \end{bmatrix} = \begin{bmatrix} 1 & k_1 \\ k_2 & 1 \end{bmatrix} \begin{bmatrix} F_{am} \\ T_{m} \end{bmatrix} \tag{3.2}$$

where

F_{am}^{*} represents the measured value of the mean axial force

T_{m}^{*} represents the measured value of the mean torque

F_{am} represents the true value of the mean axial force

T_{m} represents the true value of the mean torque

k_1, k_2 cross correlation coefficients

In this case, $k_1 = k_2 = 0.02$. Using equation (3.2) a relation between the true values of the axial force and torque and their respective measured values is obtained as

$$\begin{bmatrix} F_{am} \\ T_m \end{bmatrix} = \begin{bmatrix} 1.0004 & -0.02 \\ -0.02 & 1.0004 \end{bmatrix} \begin{bmatrix} F_{am}^* \\ T_m^* \end{bmatrix} \qquad (3.3)$$

and is employed in further calculations.

3.5 Dynamic Calibration of the Dynamometer

The dynamic calibration of the dynamometer is essential for two reasons:

(i) To determine the resonant frequencies of the dynamometer so as to make sure that the dominant frequencies of the resultant force system are not in the neighbourhood of the dynamometer resonant frequencies.

(ii) To determine the frequency response of the dynamometer-work-piece-machine tool system, so as to determine the range of frequency of the resultant force system which can be measured without signal distortion.

The resonant frequencies of the dynamometer along the axial force and torque directions, are found out using the impact method. A steel ball of about 0.01m diameter is dropped onto the dynamometer along both the axial force and torque directions. The output signals are recorded on an oscilloscope screen. The natural frequencies along the axial and torsional directions are determined to be 4 kHz and 2.8 kHz respectively. The dominant frequencies of the resultant force system are expected to be

well within these values of the natural frequencies and hence, test measurements will be valid.

The frequency response of the machine tool-workpiece system is determined in order to find out the frequency band in which the ratio of output to input remains unity. This frequency band determines the range of frequencies of the resultant force system, which can be measured without the introduction of any signal distortion due to the system dynamics or near resonance response.

The experimental set up used for the determination of the frequency response of the system, when the input load is applied along the axial direction, is shown in Fig. 3.9. This experiment is first performed with the workpiece fixed to the dynamometer. Next, the workpiece is removed and the load is directly applied on to the dynamometer. This is carried out because, in an actual drilling operation, as the depth of the hole increases, the cutting tool will approach close to the dynamometer. This will lead to a continuous change in the frequency response of the system. So, to determine the upper and lower bounds of the frequency response characteristics, the experiment is repeated with and without the workpiece. Here, the dynamometer is held in the chuck of the deep-hole drilling machine and the workpiece is clamped onto it. Further, a steady rest supports the workpiece, in order to simulate the effect of the pressure head. The free end of the workpiece is attached to an electro-dynamic shaker. The force with which the shaker excites the system is measured by a piezo-electric crystal introduced in between the shaker and the workpiece. A frequency sweep is carried out at a fixed load, and the magnitude of the ratio of the output of the dynamometer

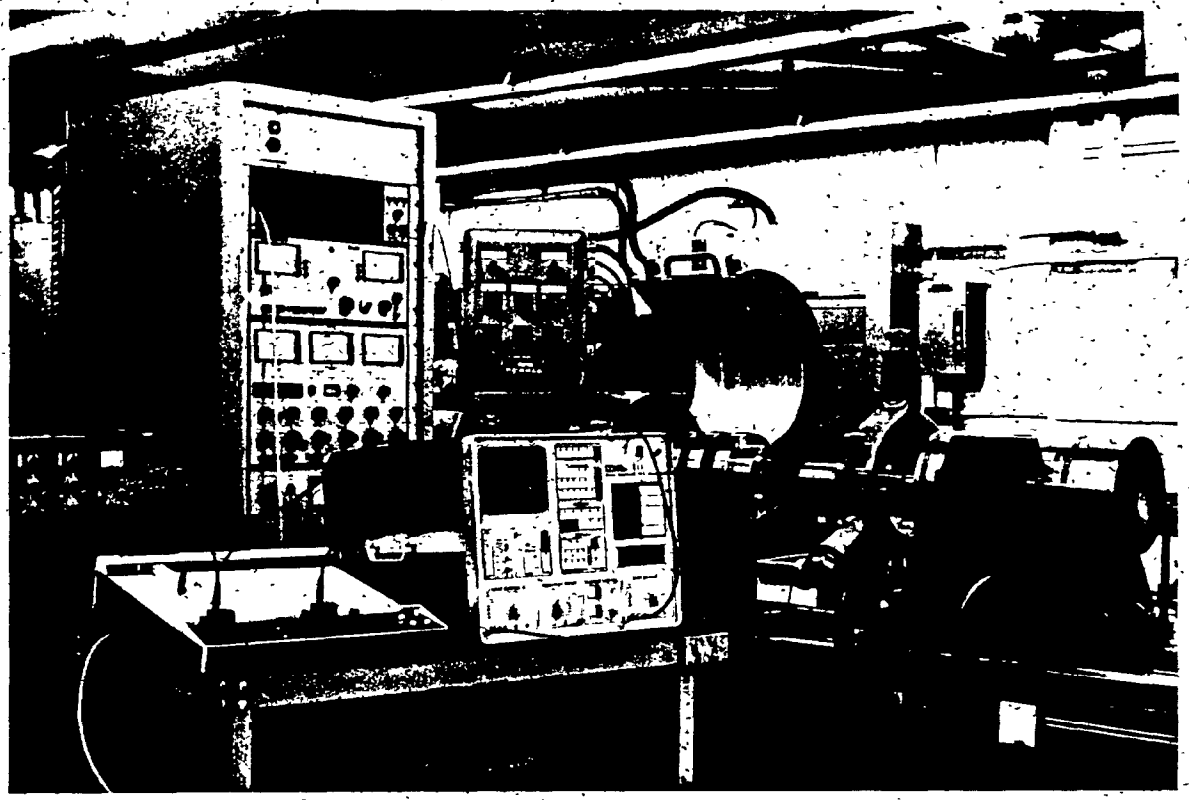

Figure 3.9: Pictorial View of Set Up used to Determine the Frequency Response of the Machine Tool-Dynamometer Workpiece System along the Axial Direction

to the force applied by the shaker, in frequency range 0 to 2 kHz, is determined. The schematic diagram of the instrumentation used for this experiment is indicated in Fig. 3.10. Here, since forces that are being measured are dynamic, the charge amplifier is set to "short". The plots of the direct and cross correlation terms obtained with and without the workpiece are shown in Figs. 3.11, 3.12, 3.13, and 3.14 respectively. As seen from the direct correlation plots, the ratio of the output to input is unity in the frequency range 0-800 Hz without the workpiece and 0-700 Hz in the presence of the workpiece. The cross correlation plots show that the ratio of the output to input has a constant value of 0.02 in the frequency range 0-650 Hz without the workpiece and 0-500 Hz with the workpiece. The decrease in frequency can be attributed to the reduction in mass.

The frequency response of the machine tool-dynamometer-workpiece system when the input force is along the torque direction is carried out using the experimental set up shown in Fig. 3.15. Here also, the experiment was initially performed with the workpiece clamped to the dynamometer and later on repeated without the workpiece. The schematic diagram of the instrumentation used for this experiment is similar to Fig. 3.10. A similar experiment, to the one described previously, is carried out and the plots of the direct and cross correlation terms with and without the workpiece are obtained. These are shown in Figs. 3.16, 3.17, 3.18 and 3.19. As can be seen from the direction correlation plots, the ratio of the output to input is unity in the frequency range 0-350 Hz for the cases with and without the workpiece. Similarly the cross-correlation plots show that the ratio of the output to input has a constant value of 0.02 in the frequency range 0-350 Hz. So, it can be concluded that

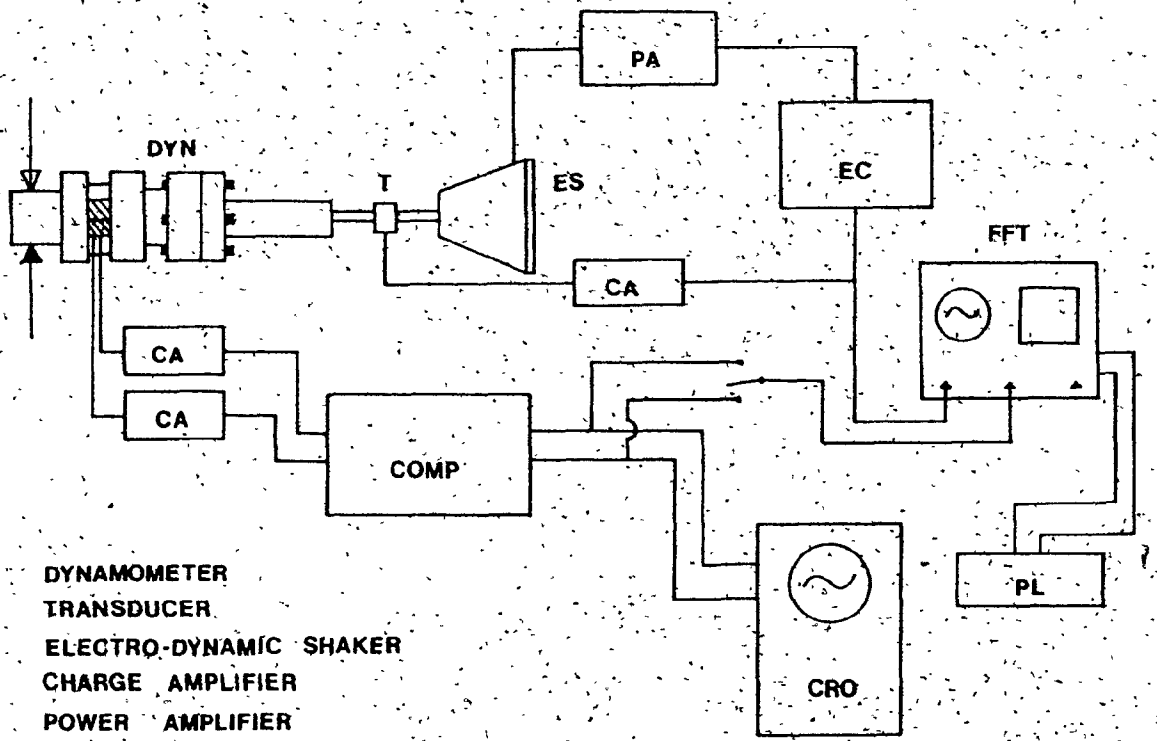

DYN	DYNAMOMETER
T	TRANSDUCER
ES	ELECTRO-DYNAMIC SHAKER
CA	CHARGE AMPLIFIER
PA	POWER AMPLIFIER
EC	EXCITOR CONTROL
FFT	FAST FOURIER TRANSFORM ANALYSER
CRO	CATHODE RAY OSCILLOSCOPE
PL	X-Y PLOTTER
COMP	COMPENSATOR

Figure 3.10: Schematic Diagram of the Instrumentation Used to Determine the Frequency Response of the Machine Tool Workpiece System Along the Axial Force Direction

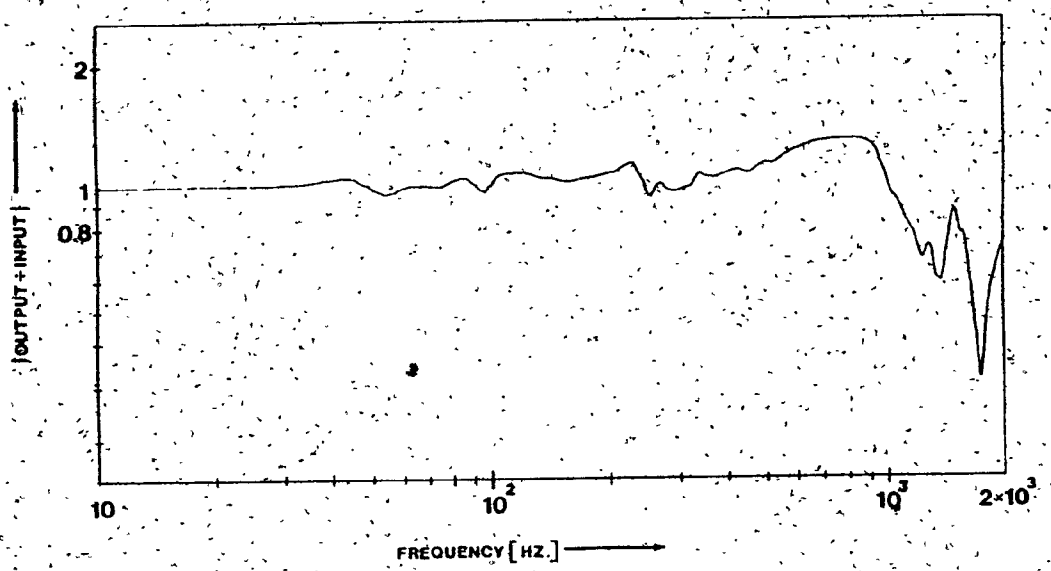

Figure 3.11: Plot of the Direct Correlation, with the Workpiece, when the Input is along the Axial Force Direction

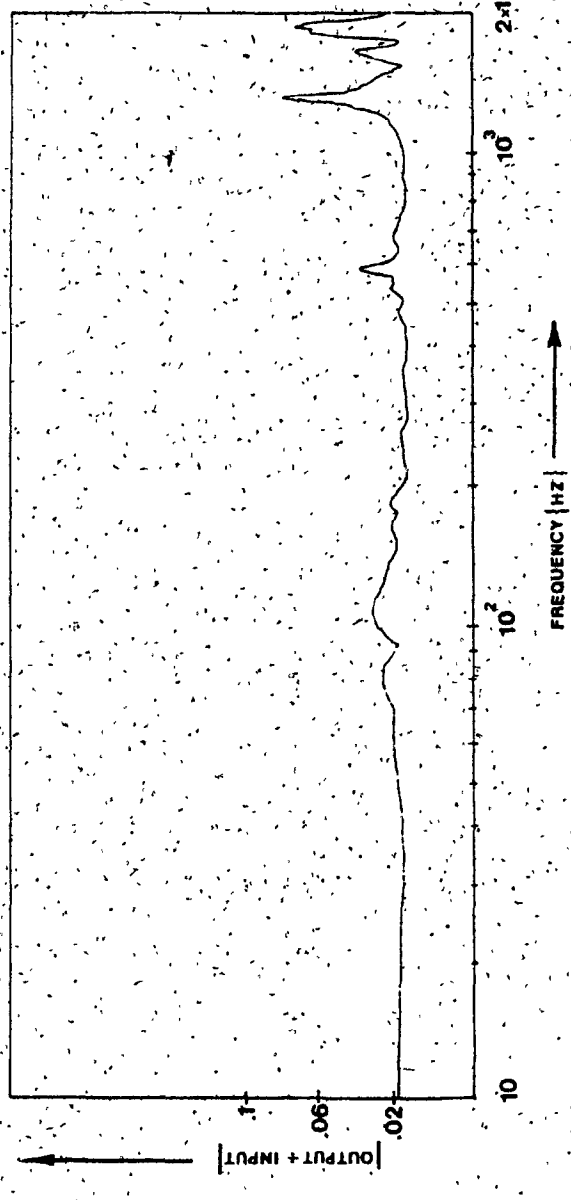

Figure 3.12: Plot of the Cross Correlation, with the Workpiece, when the Input is along the Axial Force Direction

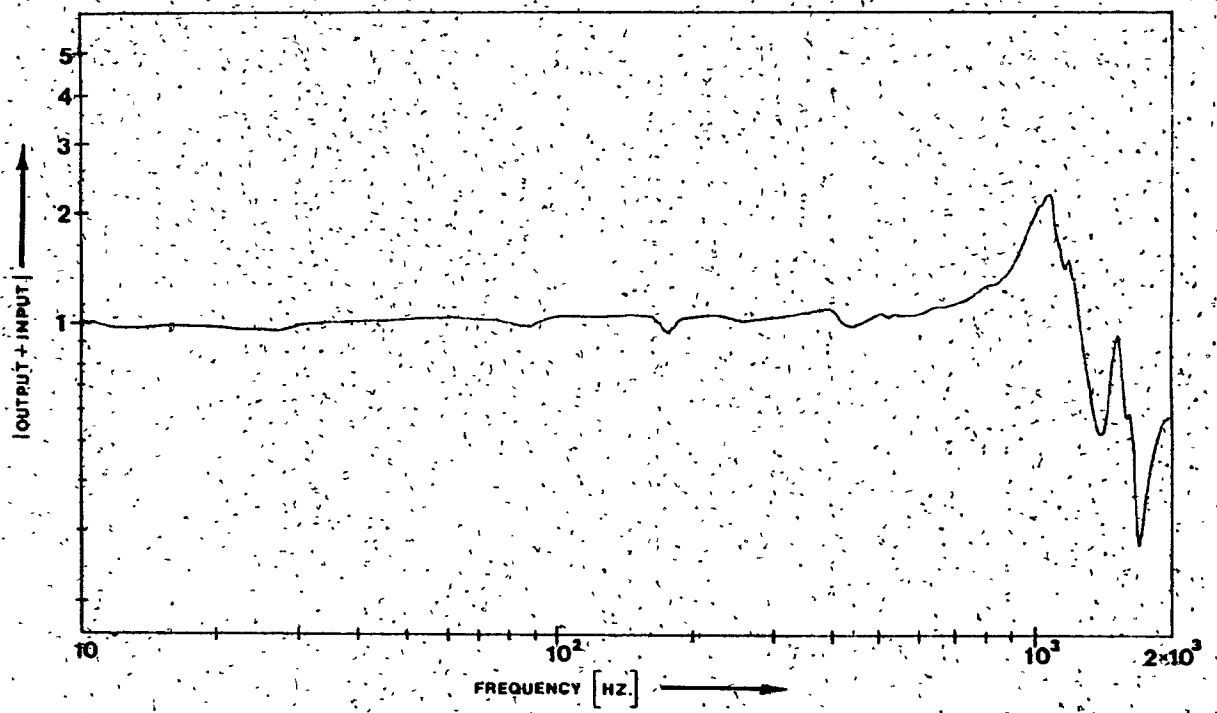

Figure 3.13: Plot of the Direct Correlation, without the Workpiece, when the Input is along the Axial Force Direction

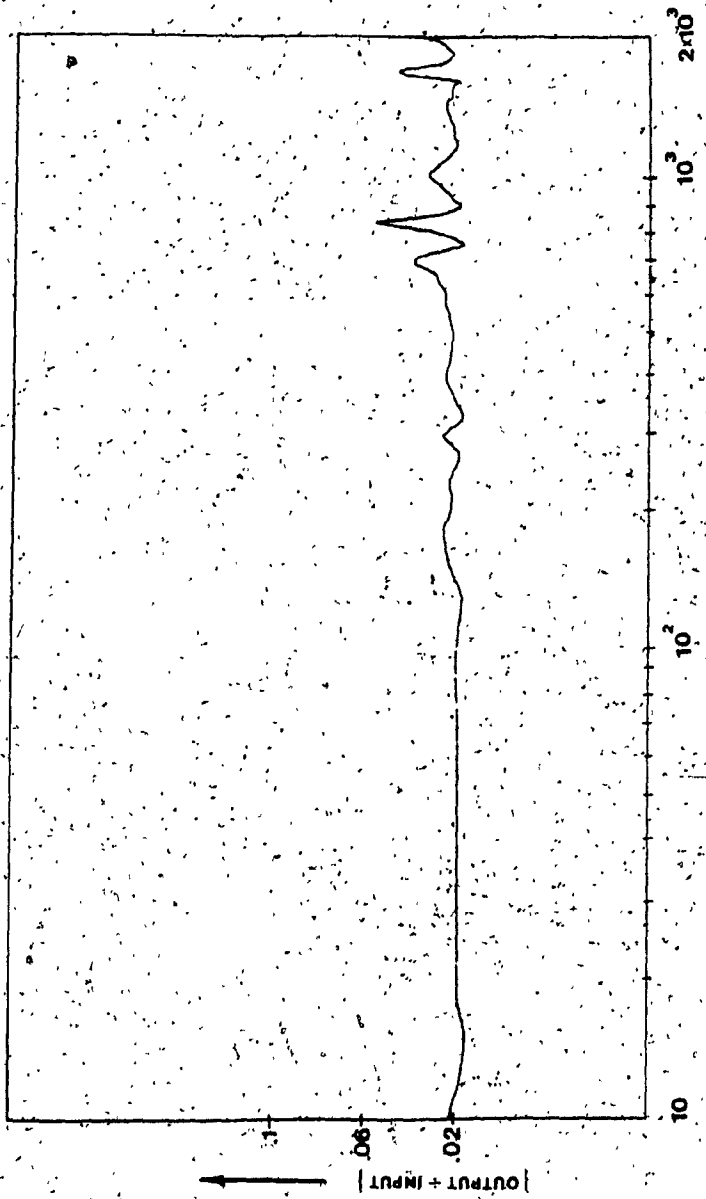

Figure 3.14: Plot of the Cross Correlation, without the Workpiece, when the Input is along the Axial Force Direction

Figure 3.15: Pictorial View of Set Up used to Determine the Frequency Response of the Machine Tool-Dynanometer-Workpiece in the Torque Direction

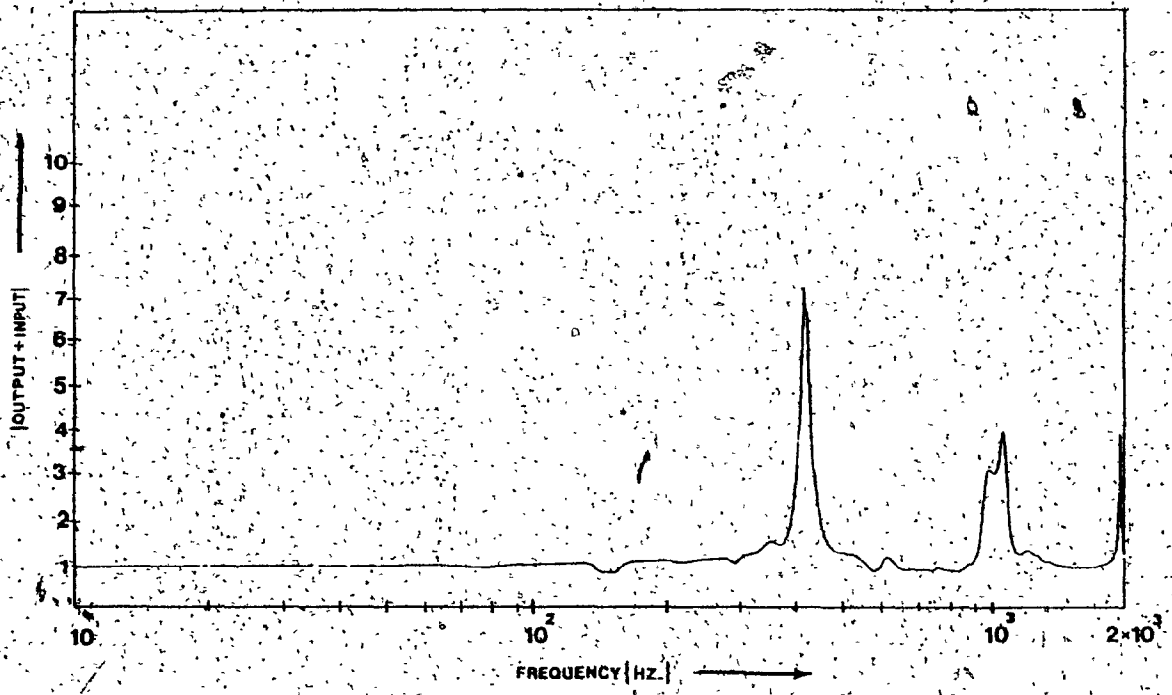

Figure 3.16: Plot of the Direct Correlation with the Workpiece, when the Input is along the Torque Direction

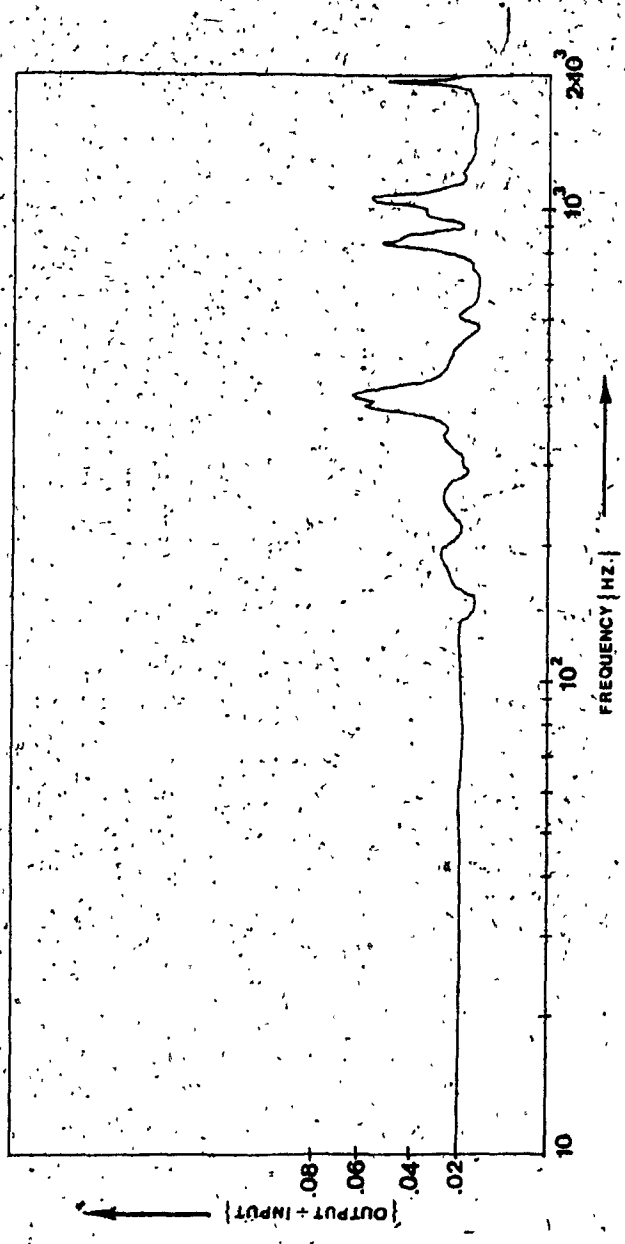

Figure 3.17: Plot of the Cross Correlation, with the Workpiece, when the Input is along the Torque Direction

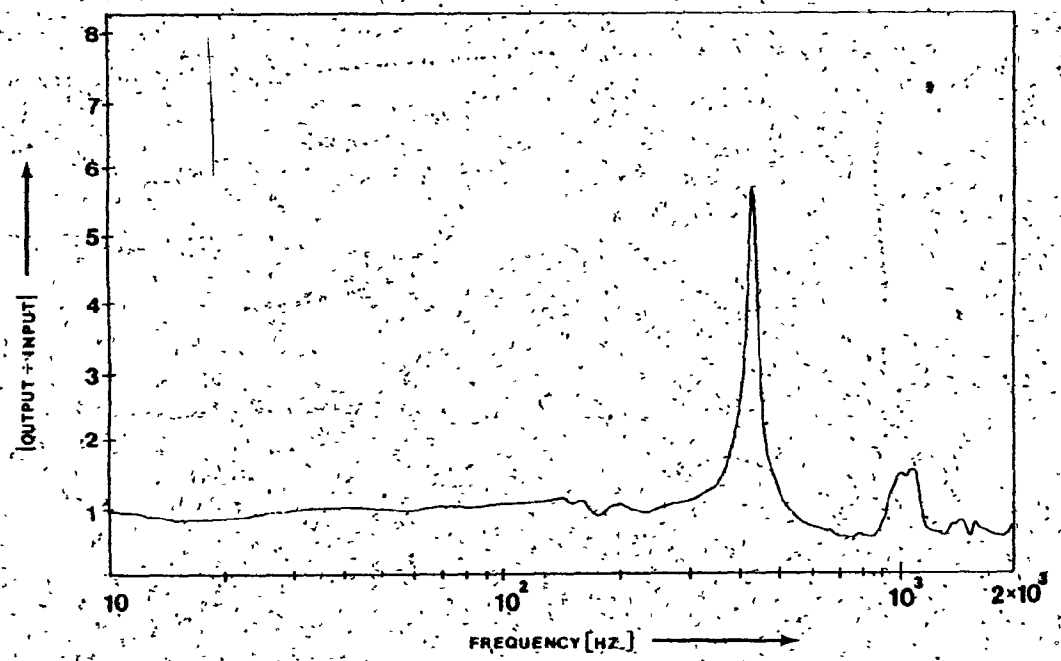

Figure 3.18: Plot of the Direct Correlation, without the Workpiece, when the Input is along the Torque Direction

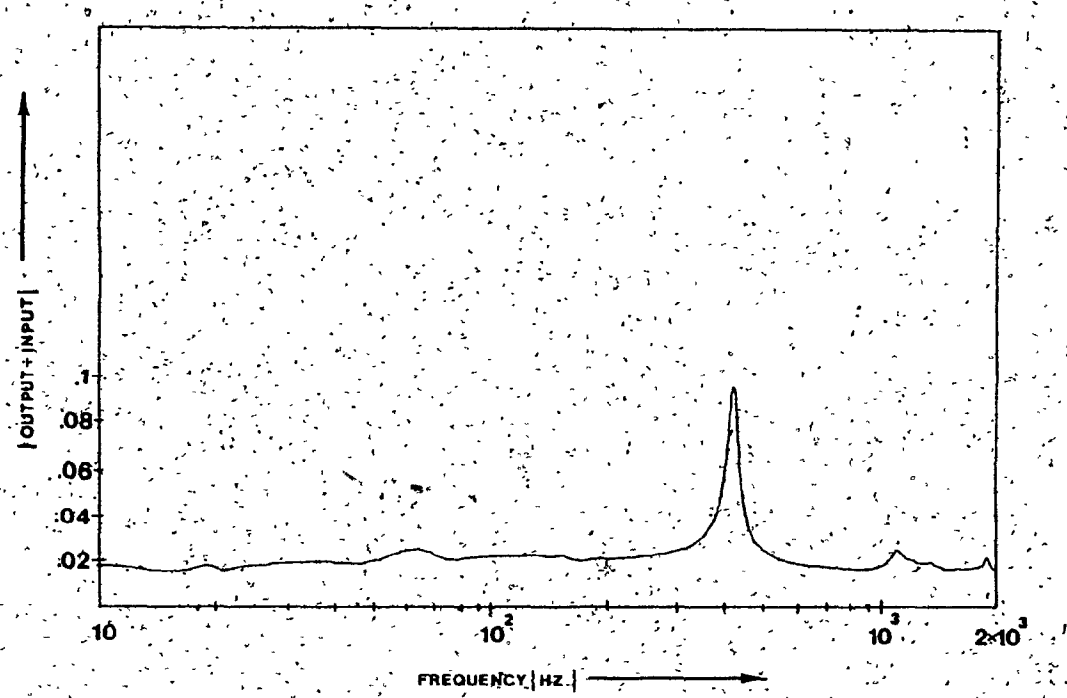

Figure 3.19: Plot of the Cross Correlation, without the Workpiece, when the Input is along the Torque Direction

the reduction in mass does not have a significant influence on the useable frequency range, in this case.

3.6 Correlation Between the True Signals and the Measured Signals

The response of a cutting force dynamometer is often complicated due to fluctuating errors or distortions, which arise when the dynamometer moves during dynamic cutting or due to the dynamic behaviour of the machine tool. Such dynamic errors can be corrected using a suitable data modification programme [100], by using a time series technique [101], or by obtaining the frequency response by transient loading [102]. Here, in this investigation, the dynamic errors are corrected by evaluating the transfer function of the machine tool workpiece system assembly by exciting the system at various frequencies.

As seen from the various transfer function plots, the transfer function value remains a constant until about 350 Hz after which non-linearities are introduced into the system due to influence of nearness of the system to resonance. Therefore, the reliable measurable range of frequency of the resultant force system is only 0-350 Hz. In this frequency range, the cross-correlation between the axial force and torque is 0.02. Therefore, the following relation can be written between the measured values and the true values of the resultant force system

$$\begin{bmatrix} F_a^* \\ T^* \end{bmatrix} = \begin{bmatrix} 1 & 0.02 \\ 0.02 & 1 \end{bmatrix} \begin{bmatrix} F_a \\ T \end{bmatrix} \qquad (3.4)$$

from which the following relation can be established between the true values and the measured values of the resultant force system

$$\begin{bmatrix} F_a \\ T \end{bmatrix} = \begin{bmatrix} 1.0004 & -0.02 \\ -0.02 & 1.0004 \end{bmatrix} \begin{bmatrix} F_a^* \\ T^* \end{bmatrix} \qquad (3.5)$$

3.7 Reliability and Accuracy of Measurements

The accuracy of measurements of the dynamic variation of the axial force, the torque, and the steady state component will be high when the quantities mentioned above are measured separately. The steady state component is measured by setting the time constant on the charge amplifiers to "long" which in turn, changes the time constant of the measuring system to a high value. After the steady state component has been measured, the charge amplifiers are set to the reset position. Then, after setting the transducer sensitivity range to a more sensitive value, the time constant is switched to the "short" position. This enables the filtering out of the very small frequency signals [steady state component of the measured signals]. Then the amplifiers are switched to the operational mode again. This has the effect of shifting the steady state value of the signal to zero and thus enabling the recording of small variations of the signal with a greater degree of accuracy. A line diagram showing the effect of resetting the charge amplifier is shown in Fig. 3.20.

3.8 Measurement of Axial Force and Torque

The equipment used for the measurement of the axial force and torque is divided into two groups. One group consists of the deep-hole drilling machine, the test piece, the dynamometer, and the cutting tool boring bar system. The second group consists of the electronic instrumentation necessary to measure and record the dynamic signals which are the charge

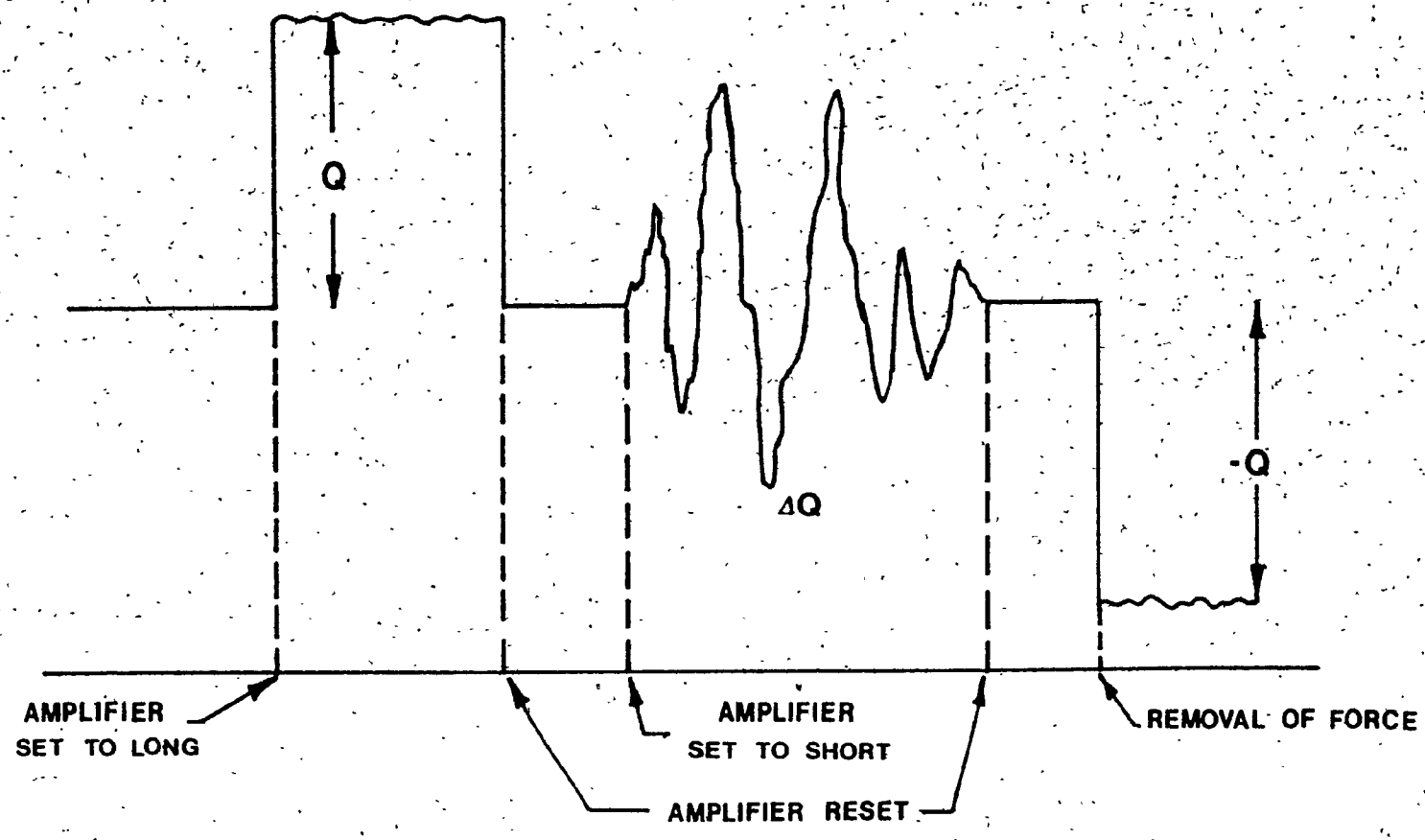

Figure 3.20: Line Diagram Showing the Effect of Resetting the Charge Amplifier

amplifiers, the XYZ compensator, the magnetic tape recorder, the oscilloscope, and the digitial voltmeters. The experimental set up used for this purpose is shown in Figs. 3.21 and 3.22. Also, the schematic diagram of the instrumentation used in the measurement is shown in Fig. 3.23.

The material used for the experiment is AISI 1020 steel. Since, the effect of feed and diameter on the cutting force is to be determined, the static and dynamic components of the axial force and torque are recorded for four different values of feeds for each of the four diameters of the cutting tool used. The cutting tools used in the experiment are new. This is done so as to eliminate the influence of the wear of the cutting tool on the measured signals.

3.9 Conclusions

The methodology for the experimental measurement of the axial force and torque is presented in order to obtain a mathematical model. An appropriate BTA dynamometer is designed which has a high natural frequency, so that the dynamic fluctuations of the resultant force system can be measured accurately. A frequency response measurement of the dynamometer-machine tool-workpiece system reveals that the dynamic fluctuations of the resultant force system can be measured without distortion up to 350 Hz. A transfer function approach is used to correct the measured signals and to obtain true signals. Also, the experimental set up has been described in detail. The analysis of the results obtained from these experiments are discussed in the next chapter.

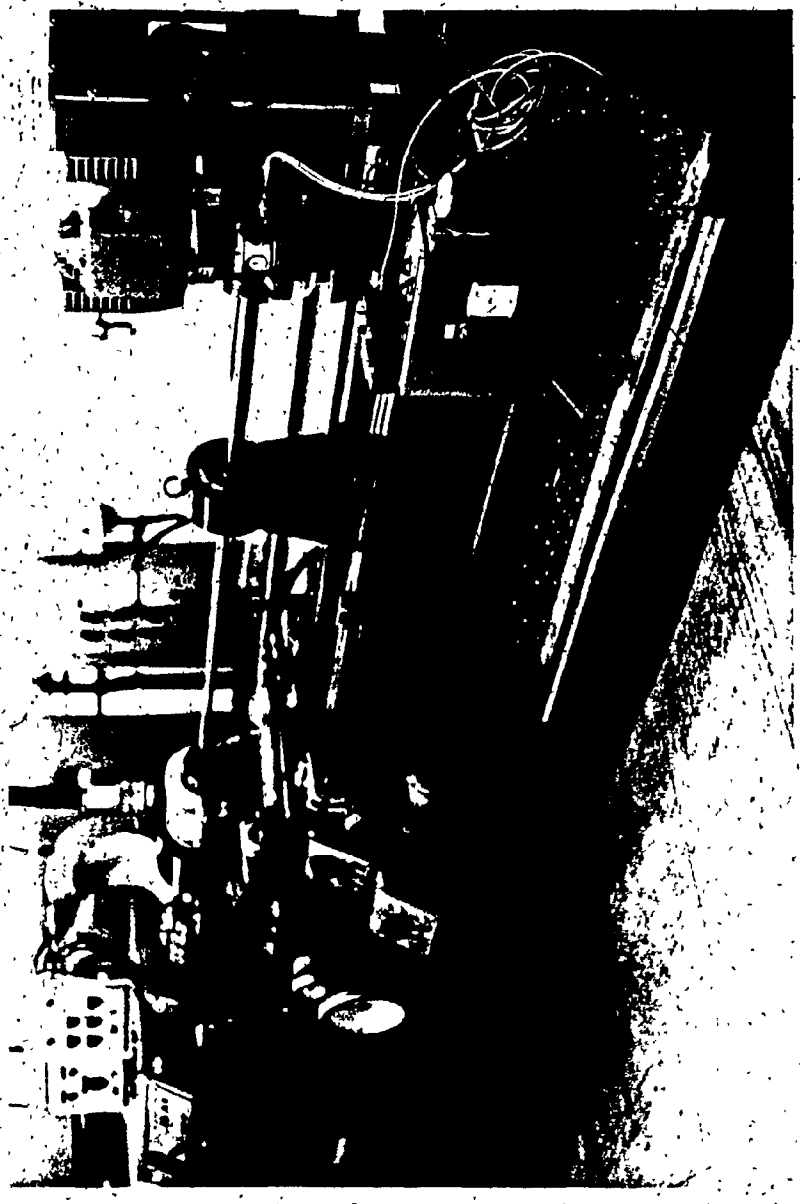

Figure 3.21. Pictorial View of the Experimental Set Up Showing the Machine Tool

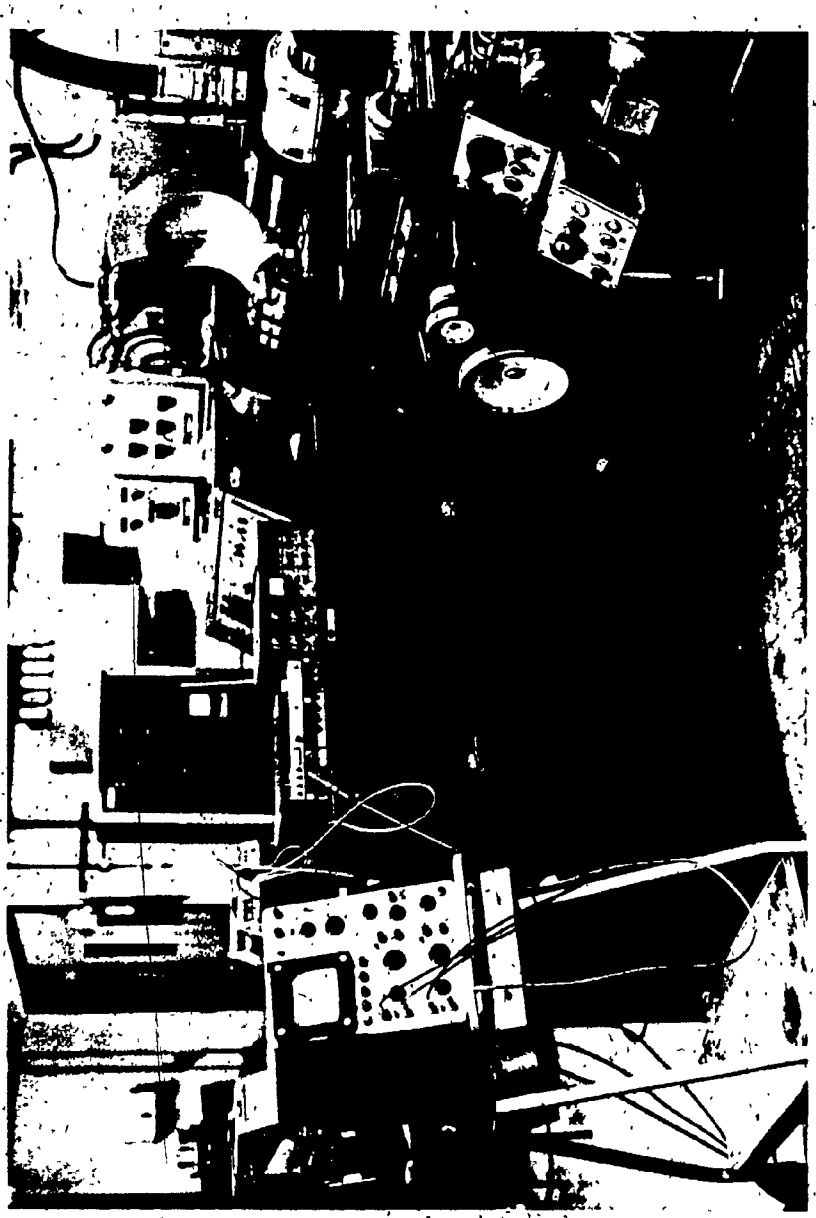

Figure 3.22: Pictorial View of the Experimental Set Up Showing the Instrumentation

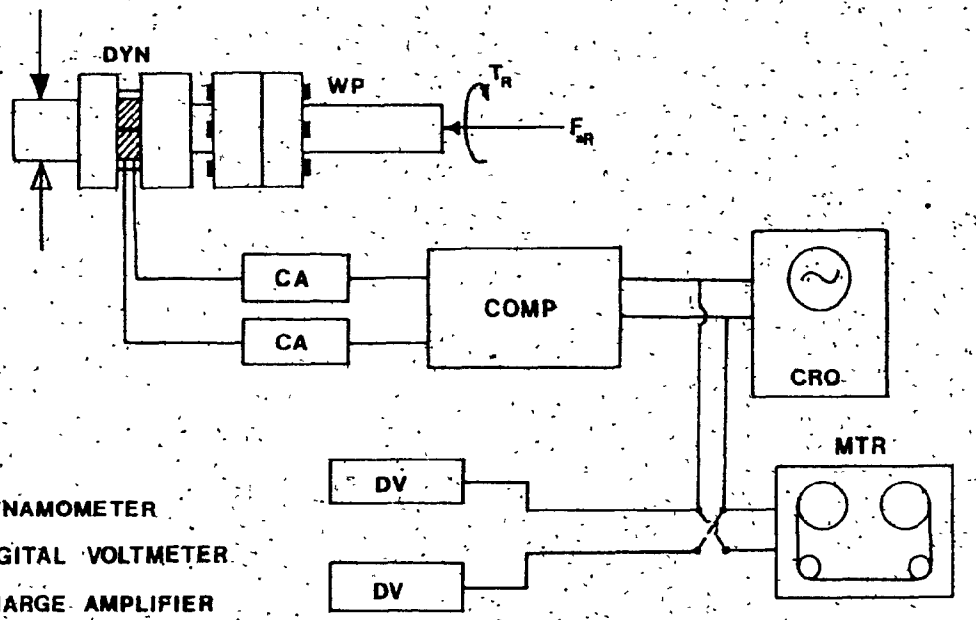

DYN DYNAMOMETER
DV DIGITAL VOLTMETER
CA CHARGE AMPLIFIER
CRO CATHODE RAY OSCILLOSCOPE
WP WORK PIECE
COMP COMPENSATOR
MTR MAGNETIC TAPE RECORDER

Figure 3.23: Schematic Diagram of the Instrumentation Used to Measure the Resultant Force System

CHAPTER 4

STOCHASTIC REPRESENTATION OF THE AXIAL FORCE AND TORQUE

CHAPTER 4

STOCHASTIC REPRESENTATION OF THE AXIAL FORCE AND TORQUE

Experimental investigations carried out for obtaining the static and dynamic components of the axial force and torque were described in the previous chapter. The static components were recorded using digital voltmeters/oscilloscope, and based on these measured values, the true values are obtained. The dynamic components of the axial force and torque are to be evaluated to determine their stochastic properties. For this purpose, a stationarity test, a power spectral density analysis, and a probability density analysis of the measured signals are performed and are described in this chapter. From these results, the relation between the peak value of the axial force, torque and the feed and diameter can be obtained for appropriate mathematical modelling and analysis.

4.1 Analysis of the Steady State Components

The piezoelectric load washer used in the BTA dynamometer generally measures only the dynamic fluctuations. But, if the charge amplifiers are set to "long", and the transducer sensitivity set to a high value, then the static components can be measured with a high degree of accuracy. The values of these steady state components are measured for each of the four cutting tool diameters with four different values of feed. Experimentally measured values are listed in Table 4.1. Based on these measured values, the true values of the axial force and torque are obtained using equation (3.4). These true values, along with the average for each drilling condition are given in Table 4.2. Then, their variations with feed and diameter are plotted in Figs. 4.1, 4.3, and 4.4 respectively. The lines drawn through these experimental values exhibit

Table 4.1: Measured Values of the Mean Axial Force and Torque

Diameter [mm]	Feed [mm/rev]	Torque [N·m]			Axial Force [N]		
19.050	0.104	11.79	12.71	11.68	1605.32	1622.76	1603.69
	0.113	13.90	13.20	13.40	1792.60	1778.90	1782.12
	0.117	14.37	14.63	14.32	1827.30	1835.60	1831.36
	0.123	15.52	15.08	15.24	1916.00	1906.20	1907.35
22.225	0.117	21.48	20.98	21.35	2335.90	2327.10	2333.18
	0.123	22.50	23.02	22.82	2418.00	2429.20	2426.60
	0.134	26.00	25.40	25.28	2703.30	2695.20	2687.10
	0.140	27.32	27.66	27.25	2837.20	2845.20	2834.15
25.400	0.113	25.10	24.63	25.84	2606.21	2598.82	2621.64
	0.123	28.30	28.07	28.59	2809.06	2801.56	2811.85
	0.130	30.68	30.78	30.70	3003.10	3005.56	3005.56
	0.138	32.59	33.11	32.88	3098.46	3110.50	3099.05
28.575	0.111	28.31	28.37	28.85	2803.41	2799.02	2806.63
	0.117	30.74	31.11	30.45	3031.82	3037.65	3027.16
	0.123	33.00	33.36	32.42	3133.33	3142.46	3119.40
	0.130	34.63	35.45	34.47	3320.92	3337.01	3317.55

Table 4.2: True Values of the Mean Axial Force and Torque

Diameter [mm]	Feed [mm/rev]	Torque [N·m]			Mean	Axial Force [N]			Mean
19.050	0.104	11.51	12.43	11.40	11.78	1375.12	1374.16	1375.69	1374.99
	0.113	13.60	12.90	13.10	13.20	1520.60	1520.90	1520.12	1520.54
	0.117	14.06	14.32	14.01	14.13	1546.10	1549.20	1551.16	1548.82
	0.123	15.20	14.76	14.92	14.96	1612.00	1611.00	1608.95	1610.65
22.225	0.117	21.10	20.60	20.97	20.89	1913.90	1915.10	1913.78	1914.26
	0.123	22.10	22.62	22.42	22.38	1976.00	1976.80	1978.20	1977.00
	0.134	25.56	24.96	24.84	25.12	2192.10	2196.00	2190.30	2192.80
	0.140	26.86	27.20	26.79	26.95	2300.00	2301.20	2298.35	2299.85
25.400	0.113	24.68	24.21	25.42	24.77	2112.61	2114.62	2113.24	2113.49
	0.123	27.85	27.62	28.14	27.87	2252.06	2249.16	2249.05	2250.09
	0.130	30.20	30.30	30.22	30.24	2399.10	2399.56	2401.16	2399.94
	0.138	32.10	32.62	32.39	32.37	2456.46	2458.10	2451.25	2455.27
28.575	0.111	27.86	27.92	28.40	28.06	2246.21	2240.62	2238.63	2241.82
	0.117	30.26	30.62	29.96	30.28	2426.62	2425.25	2427.96	2426.61
	0.123	32.51	32.86	31.92	32.43	2483.13	2485.26	2481.00	2483.13
	0.130	34.10	34.92	33.94	34.32	2638.92	2638.61	2638.75	2638.76

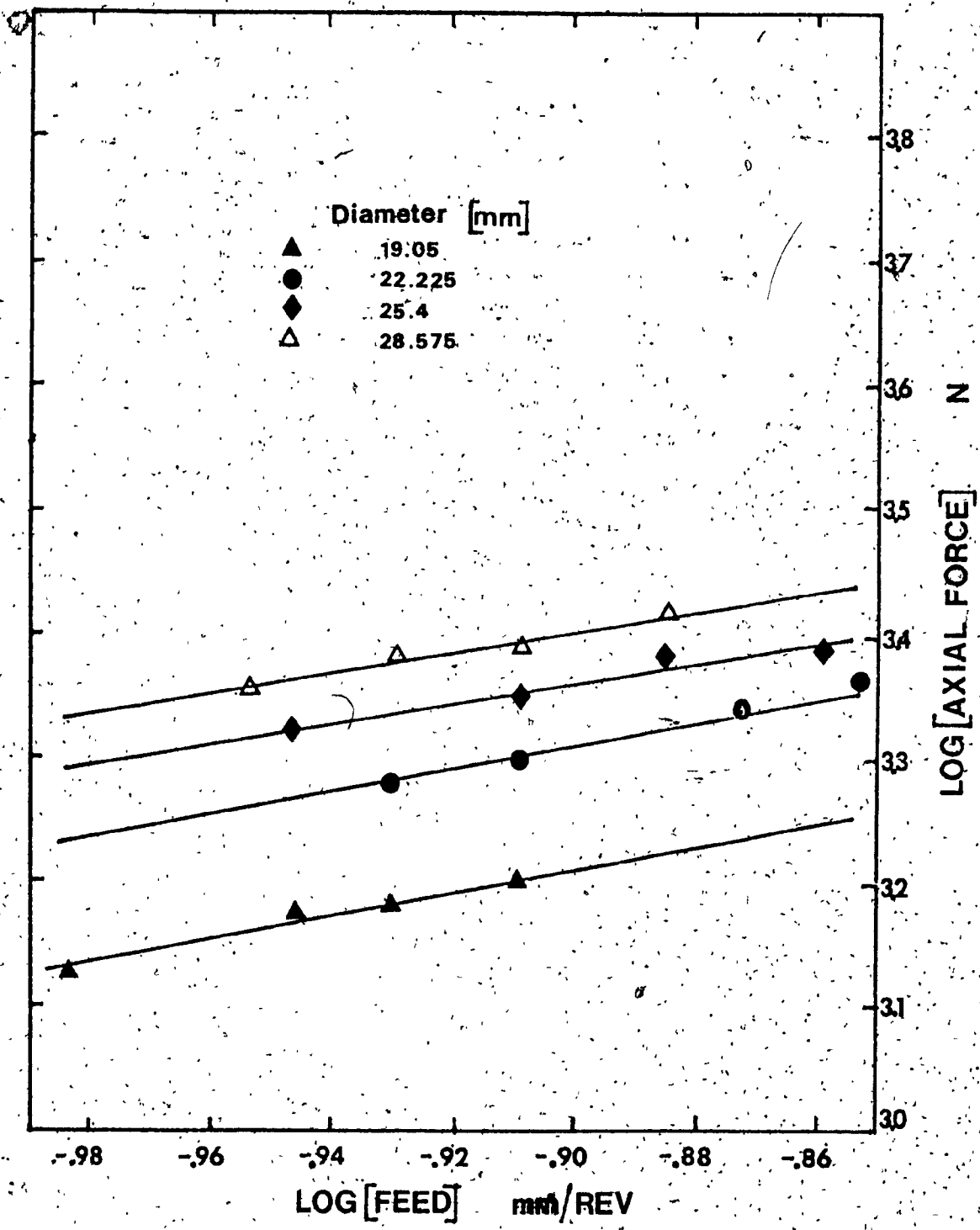

Fig. 4.1: Variation of Axial Force with Feed

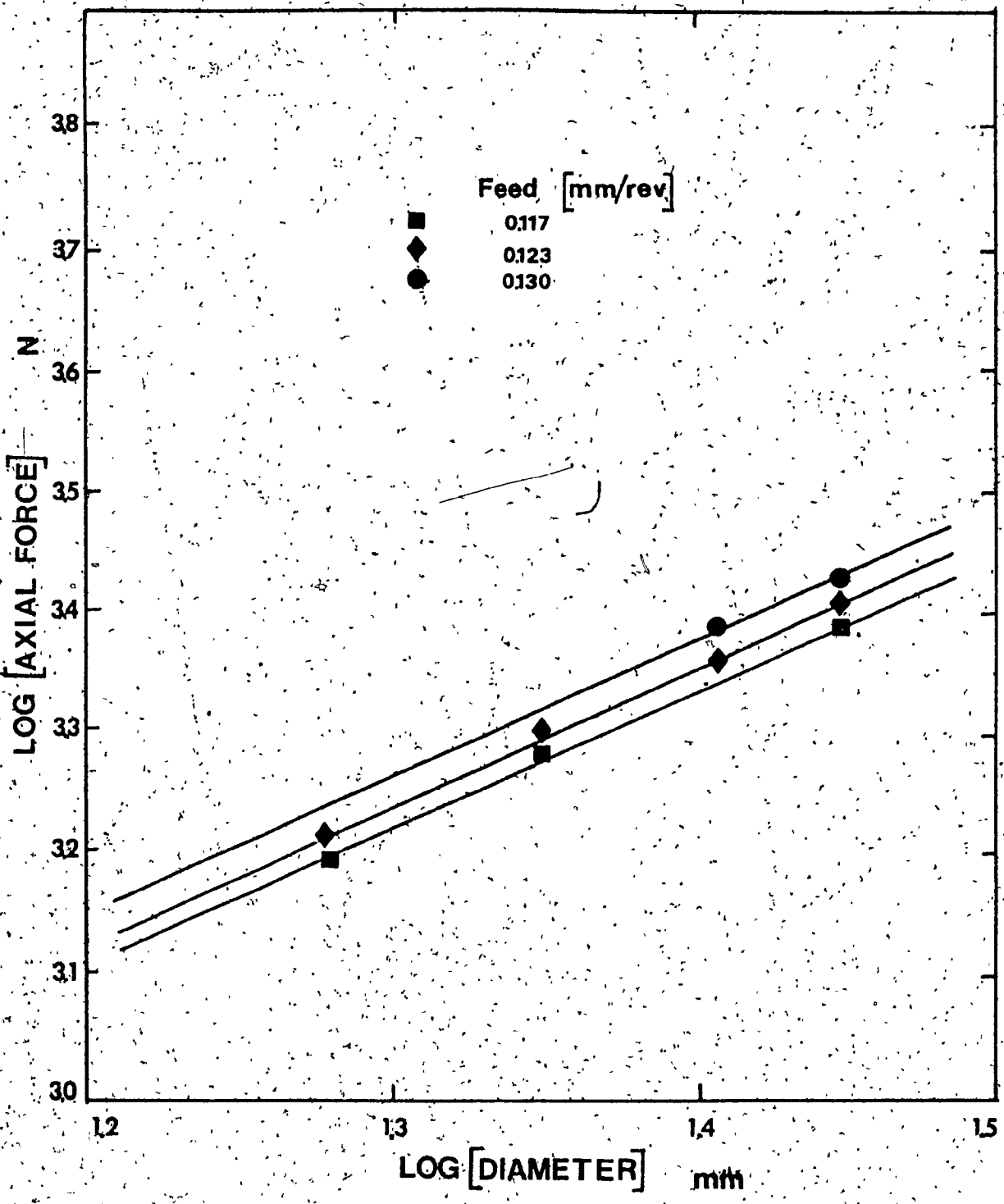

Fig. 4.2: Variation of Axial Force with Diameter

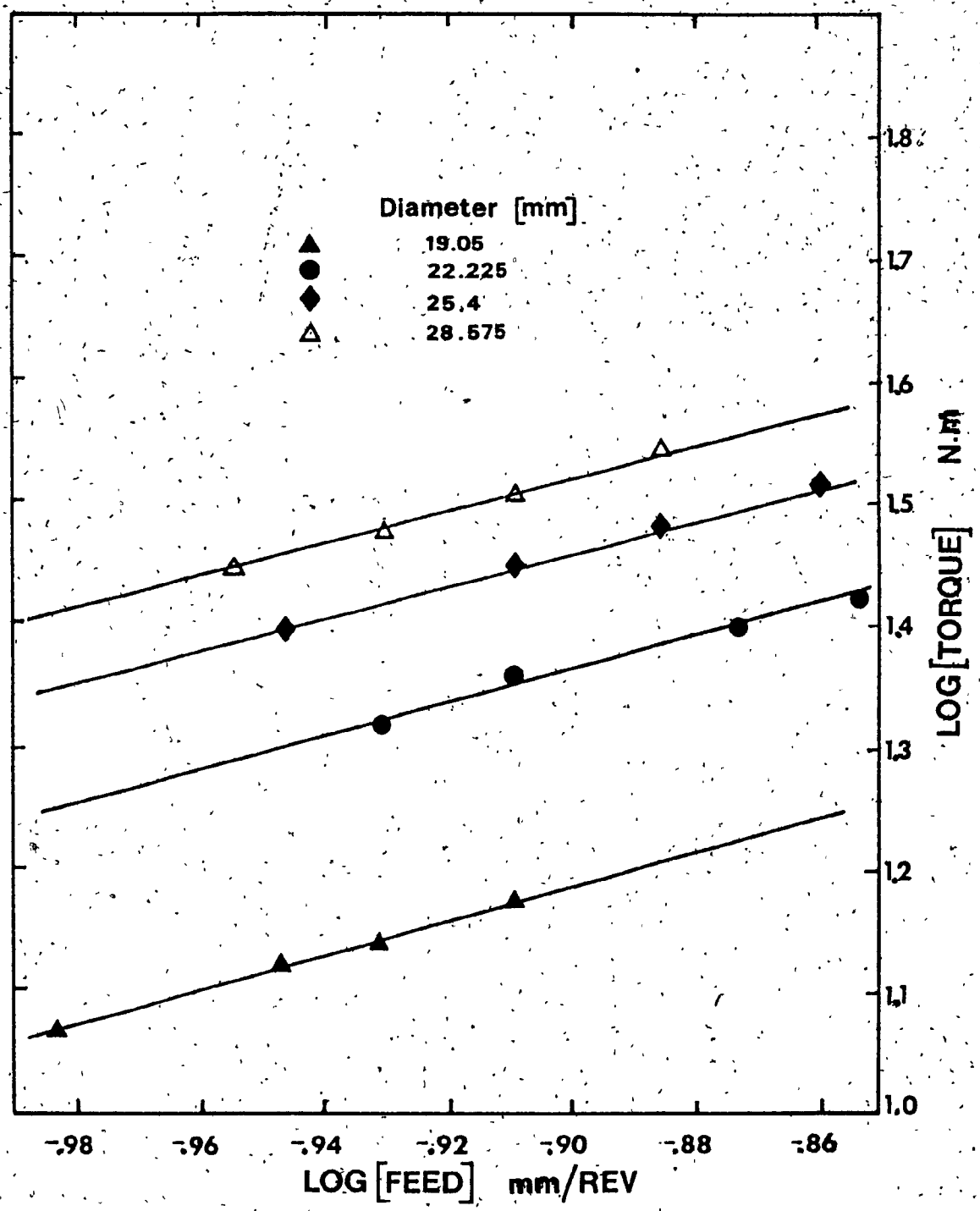

Fig: 4.3: Variation of Torque with Feed

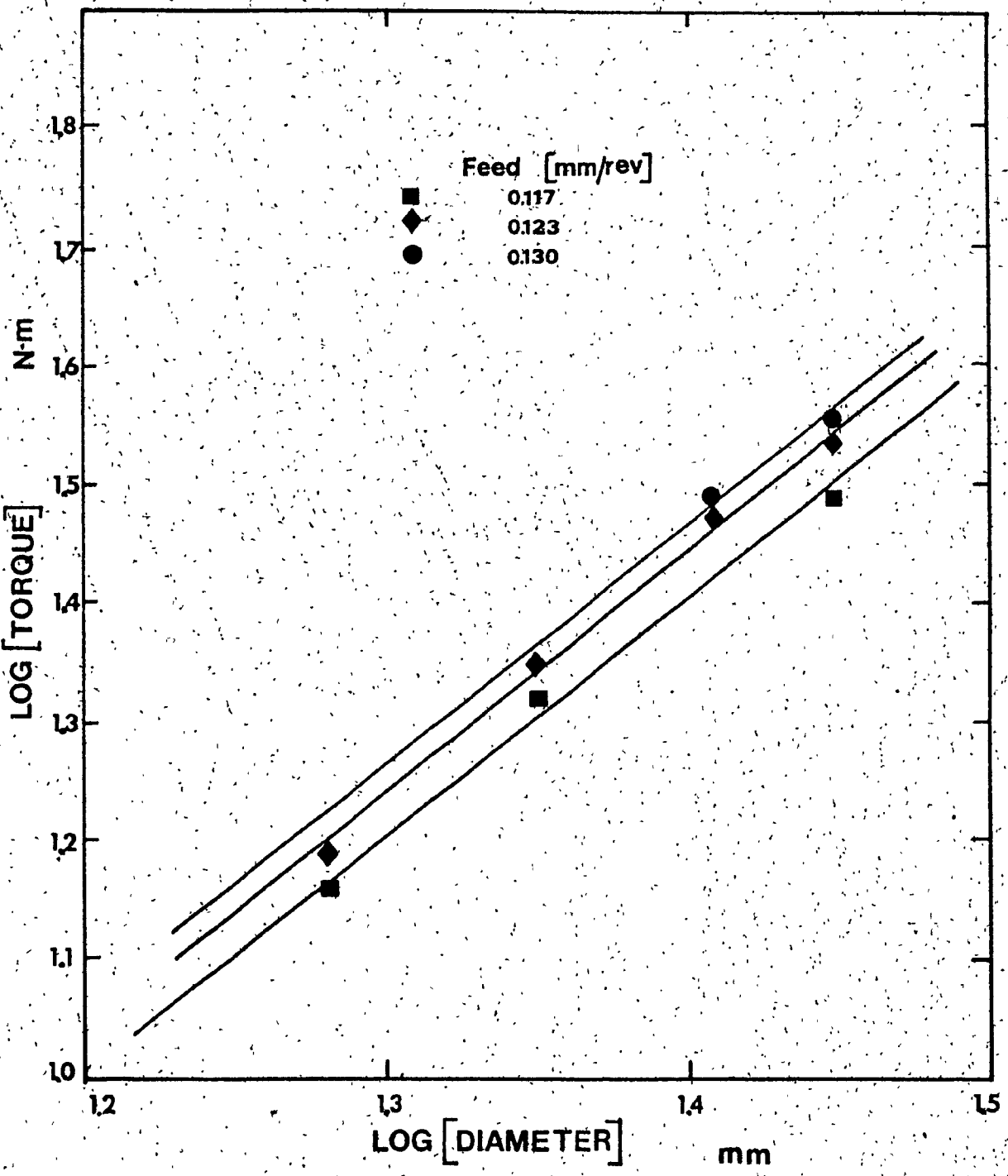

Fig. 4.4: Variation of Torque with Diameter

slopes of 0.982, 1.144, 1.429, and 2.02 respectively. Therefore, based on Figs. 4.1, 4.2, 4.3, and 4.4, the empirical equations for estimating the axial force and torque in BTA deep-hole machining valid for AISI 1020 material employing the BTA Heller cutting tool can then be written as.

$$F_{aR} = 430\, f_m^{0.982}\, d^{1.144} \tag{4.1}$$

$$T_R = 0.820\, f_m^{1.429}\, d^{2.02} \tag{4.2}$$

where

F_{aR} is the resultant mean axial force in Newtons

T_R is the resultant mean torque in Newton-metres

f_m is the mean value of feed in mm./rev.

d is the diameter of the cutting tool in mm.

These empirical relationships cannot be directly validated using the previously published data since, no other investigation has concerned itself with AISI 1020 material. But, for the sake of completion, the above empirical equations are grouped with previously published data [80] and are listed in Table 4.3. As seen from equations (4.1) and (4.2) the axial force and torque are essentially nonlinear functions of the feed. This is probably due to the burnishing effect taking place between the wear pads and the drilled hole.

4.2 Analysis of the Dynamic Components

To establish a valid stochastic model for the system behaviour in a machining process, it is necessary that a complete statistical description of the resultant force system be obtained. The following analysis [103, 104] was carried out on the recorded data using a Nicolet FFT

Table 4.3: Torque and Thrust Equation in the BTA Heller Process

Investigator	Material	Torque/Axial Force
Griffths	EN8	$T_R = 0.713 f_m^{0.95} d^{1.81}$ $F_{aR} = 1912 f_m^{1.06} d^{0.78}$
Weber	C60	$T_R = f_m \, 10^{0.026d + 1.863}$ $F_{aR} = 33300 f_m V d^{-1.0} 10^{0.026d - 0.137}$
Present Investigator	AISI 1020	$T_R = 0.820 f_m^{1.429} d^{2.02}$ $F_{aR} = 430 f_m^{0.982} d^{1.144}$

analyzer as represented schematically in Fig. 4.5.

4.2.1 Test for Stationarity

Any random process is said to be strongly stationary if all its possible moments of the probability distributions are independent of a time translation and the process is considered weakly stationary if the first two moments, namely the mean values and the covariance functions are independent of the time shift. Since, it is easier to deal with signals in the frequency domain, the entire signal is divided into many intervals and the power spectral densities for each of the time intervals compared. These tests are repeated for each of the 32 signals and these results are shown in Figs. 4.6 and 4.7. On the basis of the analysis and since, the power spectral density curves of the axial force and torque signals have similar trend and characteristics, they can be taken to be represented by a weakly ergodic process in the mathematical model.

4.2.2 Spectral Density Analysis

One of the most important single descriptive characteristic of random data is its power spectra, which defines the frequency composition of the signal. Further, a dynamic response analysis of the machine tool workpiece system requires that the statistics of the axial force and torque be mathematically modelled, for which the spectral density of the resultant force system is needed.

To obtain the spectral decomposition of the axial force and torque fluctuations, the recorded signals were fed to a FFT analyzer. The number of data points were chosen to be 512 and the frequency range was chosen as 0-1 kHz. The reasons for the above mentioned choices are:

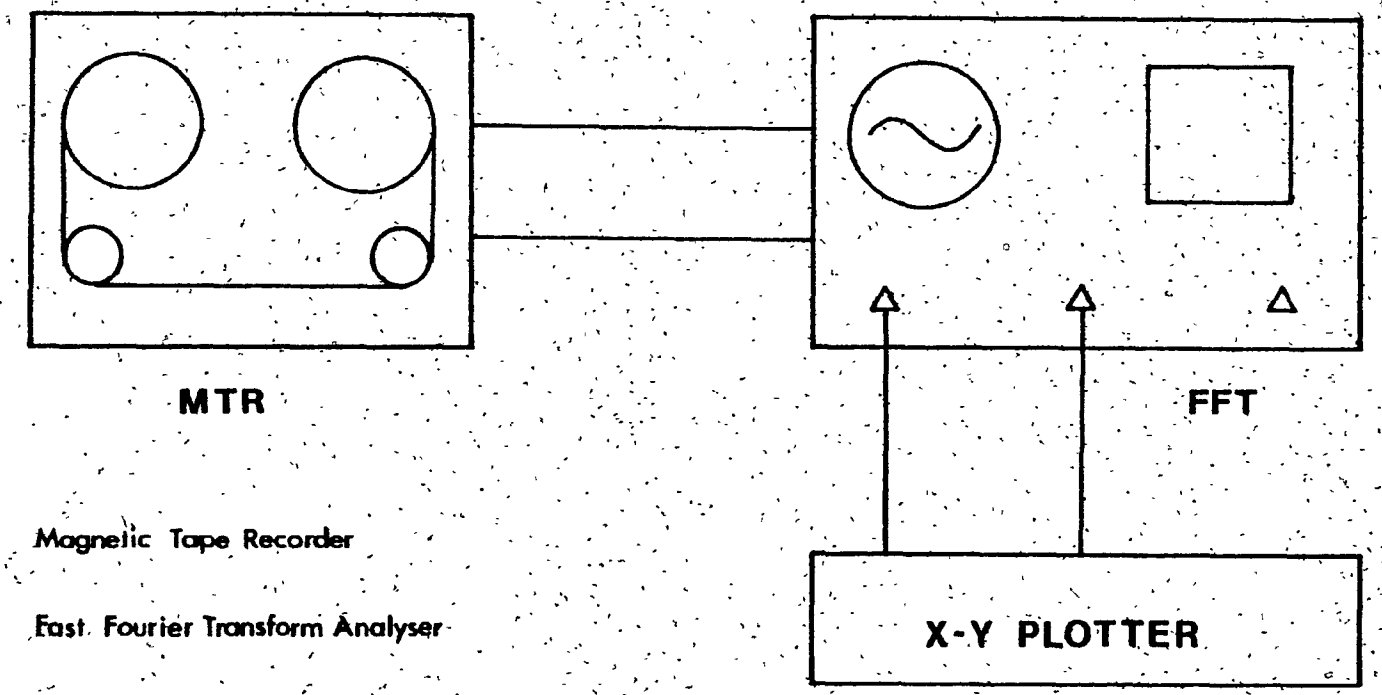

MTR : Magnetic Tape Recorder

FFT : Fast Fourier Transform Analyser

Fig. 4.5: Schematic Representation of Set-Up Used to Analyze Recorded Data

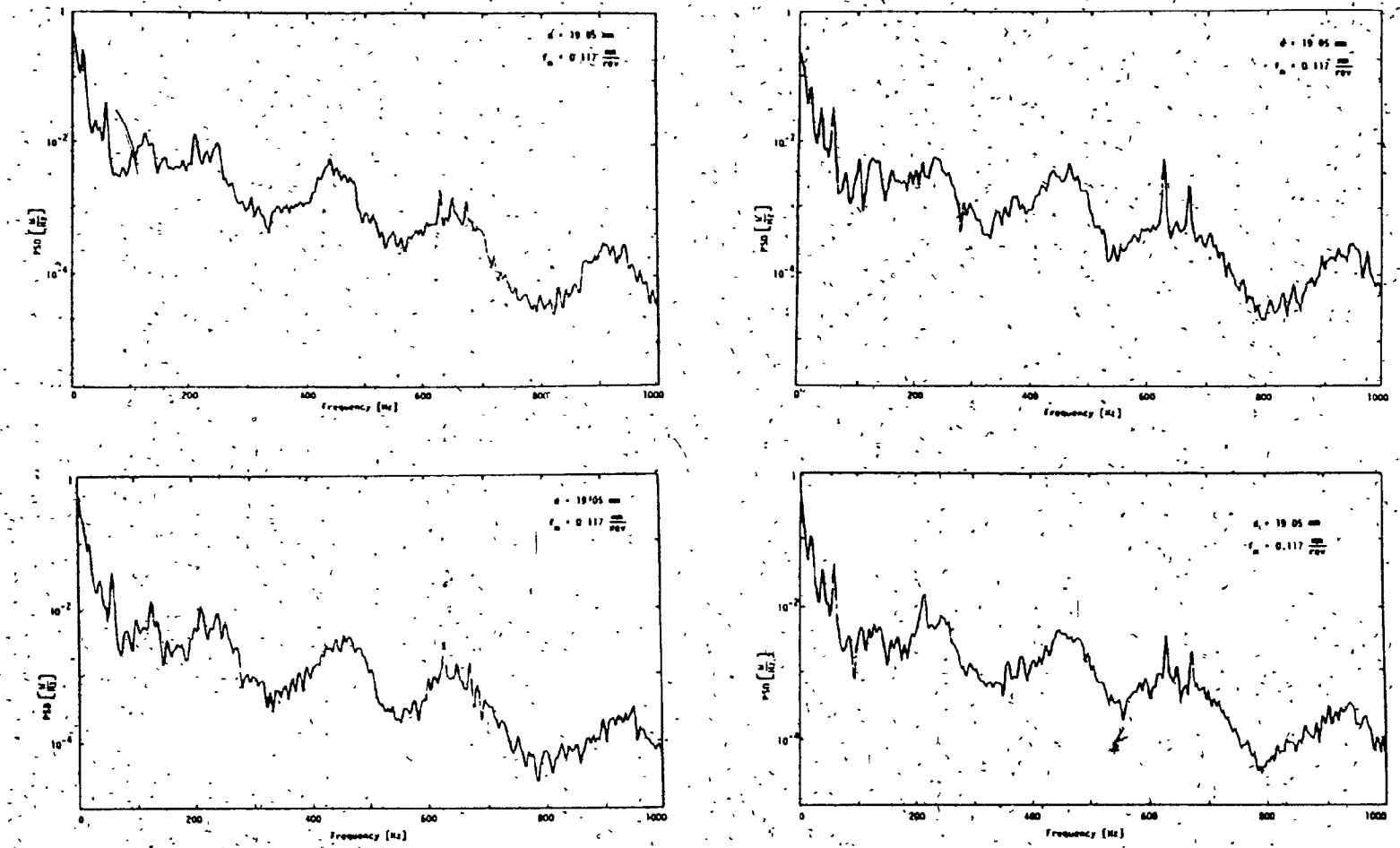

Fig. 4.6 : Test for Stationarity – Measured Axial Force

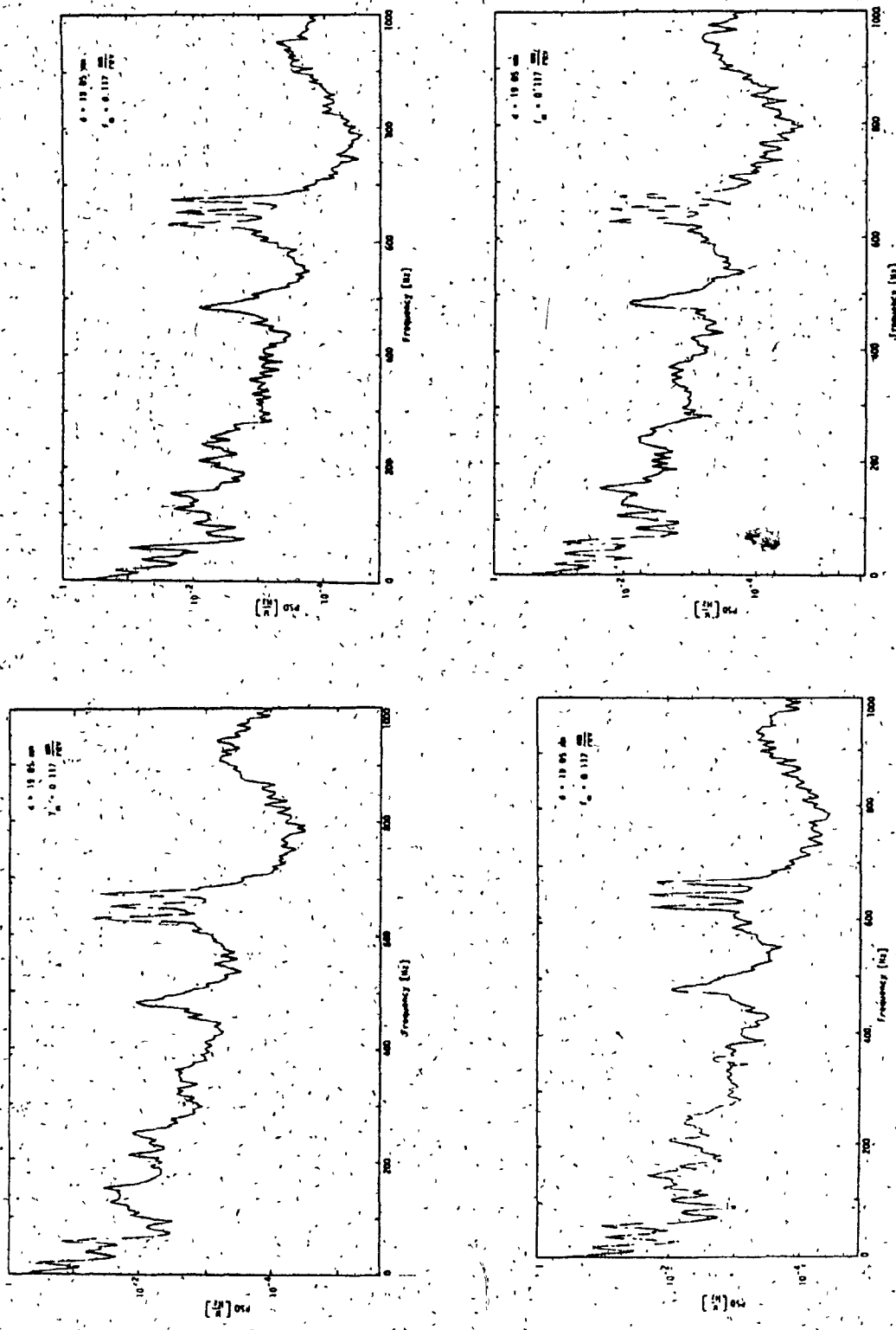

Fig. 4.7: Test for Stationarity - Measured Torque

a) The ratio of the output to input of the dynamometer-workpiece system is unity till about 350 Hz, and a plot of the power spectrum till 1000 Hz will give the error made in neglecting the power content above 350 Hz.

b) Since, the frequency range was chosen to be 0-1000 Hz, the time window was 0.4 seconds long. This coupled with the fact that the recorded axial force and torque signals were about 3 minutes long made the choice of 512 data points ideal.

The power spectrum and the auto-correlation function, which is the inverse Fourier Transform of the power spectrum, for the stationary process, for each of the 32 signals were plotted and are shown in Figs. 4.8, 4.9, 4.10, and 4.11. The spectral density plots show that the power content of the signal is significant in the range of 0-350 Hz and the error made in neglecting the power content of the signal beyond 350 Hz is small. Thus, the power spectrum could be idealized as a band limited white noise, with the upper and lower bound of frequency being 350 Hz and 0 Hz respectively. But, since the domain of interest is essentially 0 to 350 Hz, the power spectrum can be considered as an ideal white noise since this does not affect the model characteristics. This is confirmed by the auto-correlation plots where $R(0)$ has a very large value as compared to $R(\tau)$ when $\tau \neq 0$. Thus, the stochastic representation of the force and torque signals can be written as

$$< F_a(t)\, F_a(t+\tau) > = 2D_1\delta(\tau) \qquad (4.3)$$

$$< T(t)\, T(t+\tau) > = 2D_2\delta(\tau) \qquad (4.4)$$

where

D_1 is the intensity co-efficient for the axial force signal

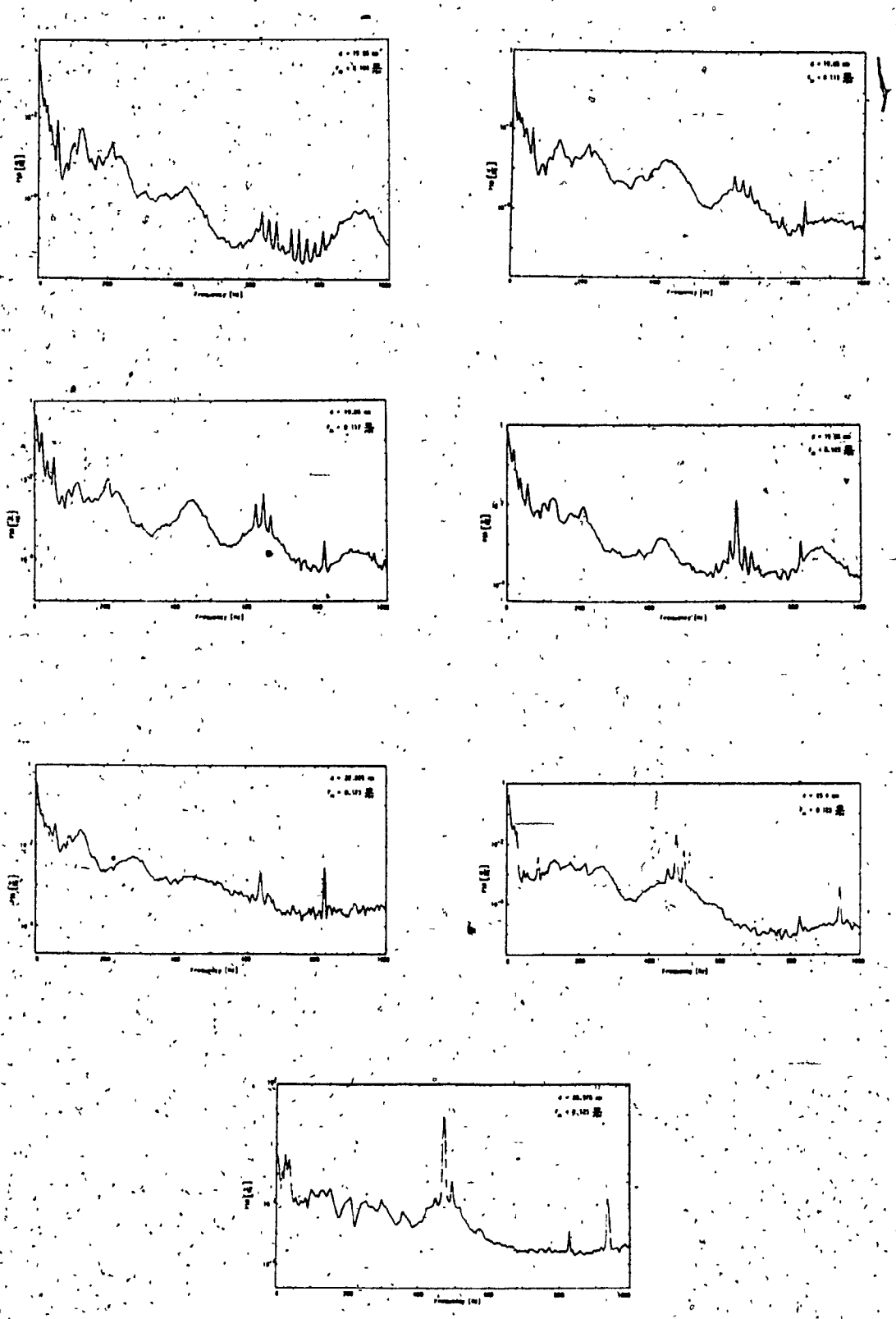

Fig. 4.8: Power Spectrum of the Measured Axial Force

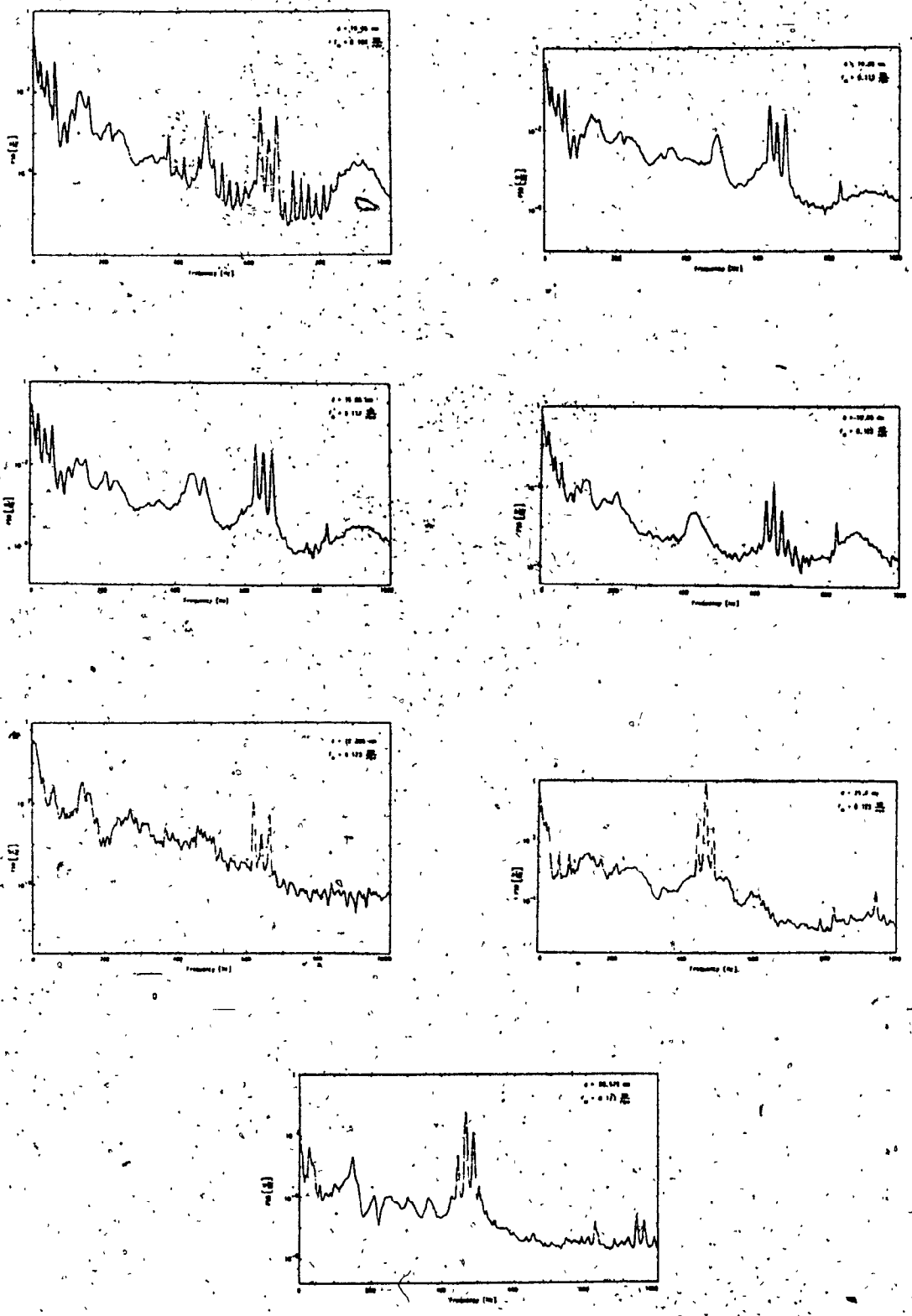

Fig. 4.9: Power Spectrum of the Measured Torque

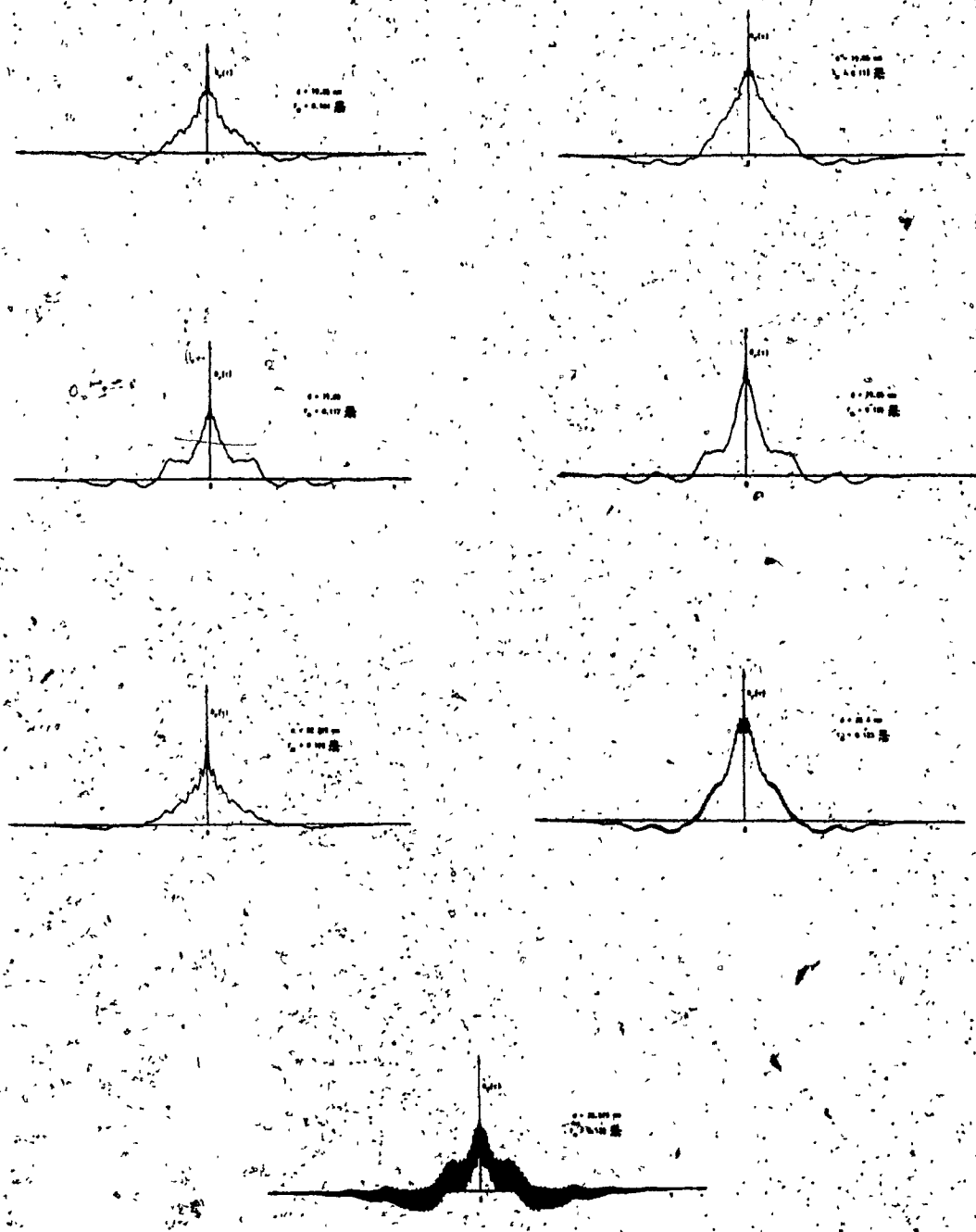

Fig. 4.10: Autocorrelogram of the Measured Axial Force

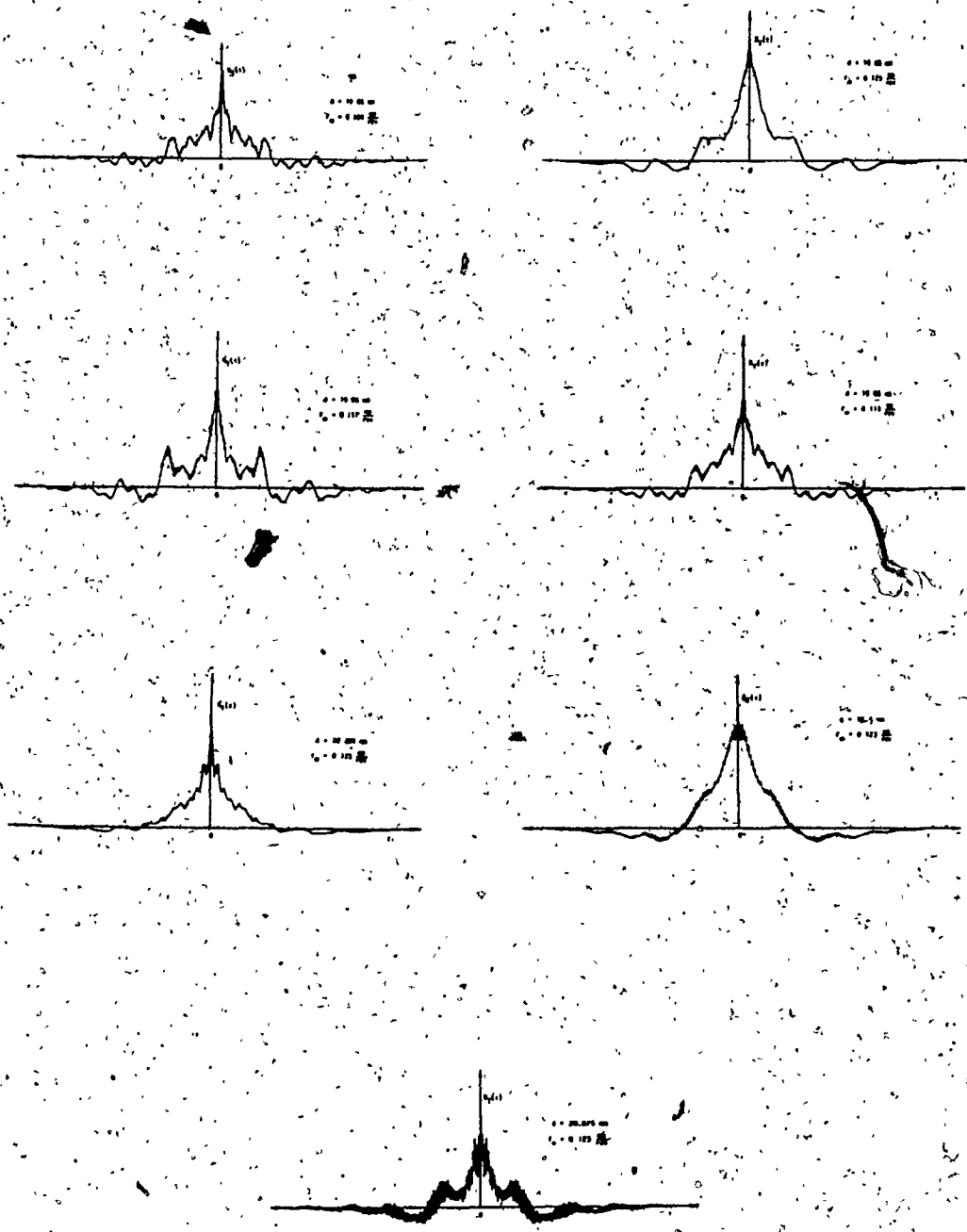

Fig. 4.11: Autocorrelogram of the Measured Torque

D_2 is the intensity co-efficient for the torque signal represents the random fluctuations of the axial force and torque signals. The values of D_1 and D_2 as seen from Figs. 4.8 and 4.9 are approximately 0.05 W/Hz.

4.2.3 Probability Characteristics

A probability density analysis is performed to obtain further information on the stochastic character of the process involved. Although it can be assumed that most natural random phenomena are normally or gaussian distributed, a probability density analysis is required to verify the validity of such a statement and also to obtain values of the peak axial force and torque.

The signals were fed to the FFT analyzer and the probability density plots for each of the 32 signals are obtained using 512 points and a frequency range of 0-1000 Hz. A sample of these results are shown in Figs. 4.12 and 4.13. They indicate a gaussian or normal distribution justifying the general expectations for such metal removal random processes. Since, the true values of the axial force and torque have a linear relationship with the measured values in the range of interest, the true axial force and torque functions will also be normally distributed.

4.3 Peak Values of Axial Force and Torque

The description of the peak values of the resultant force system provides an expression for the upper bound of the forces arising due to machining. These expressions give the most probable value of the maximum force which can result in BTA machining. Such a description, of the peak axial force and torque is useful as design equations and in the

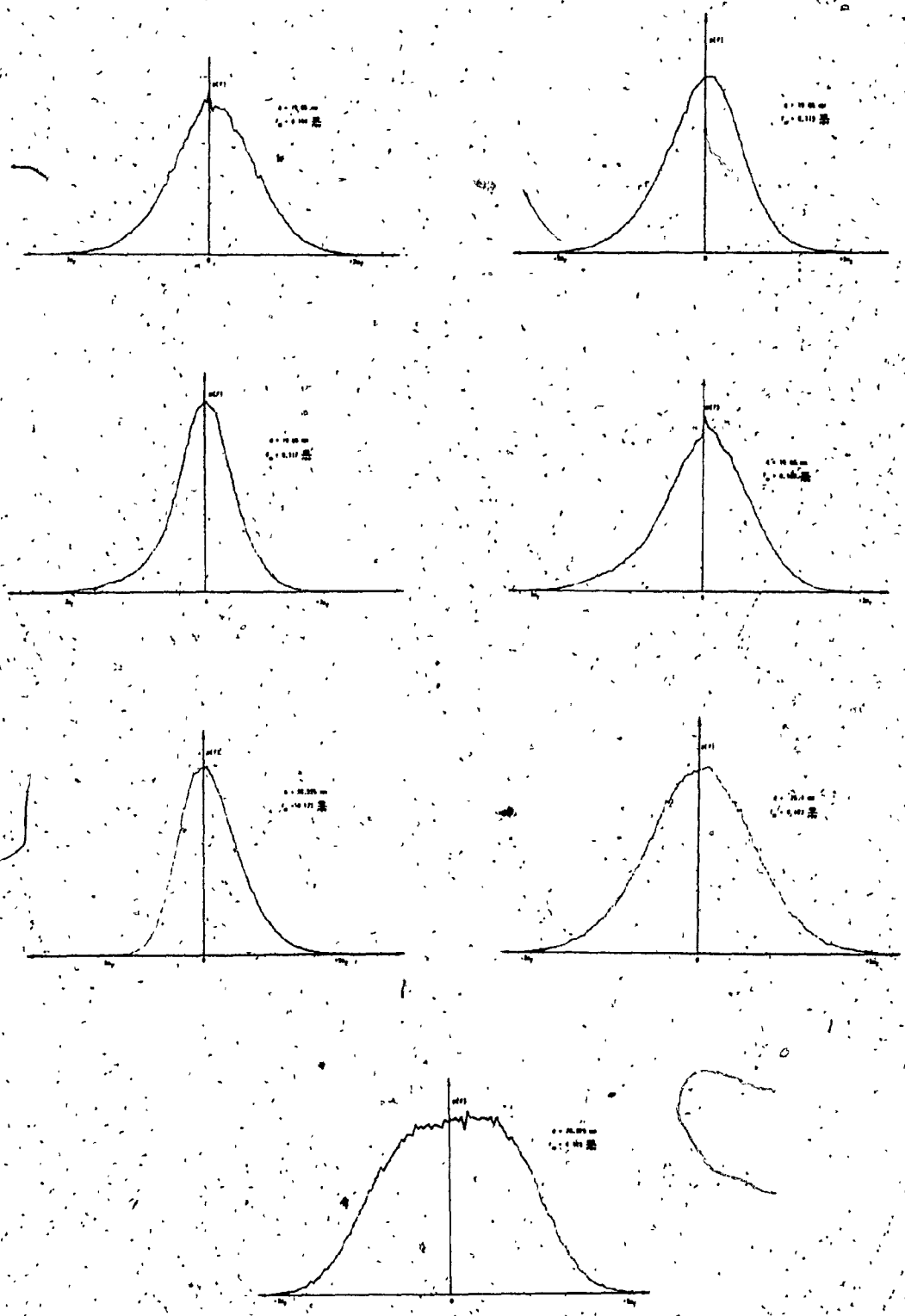

Fig. 4.12: Probability Density Function of the Measured Axial Force

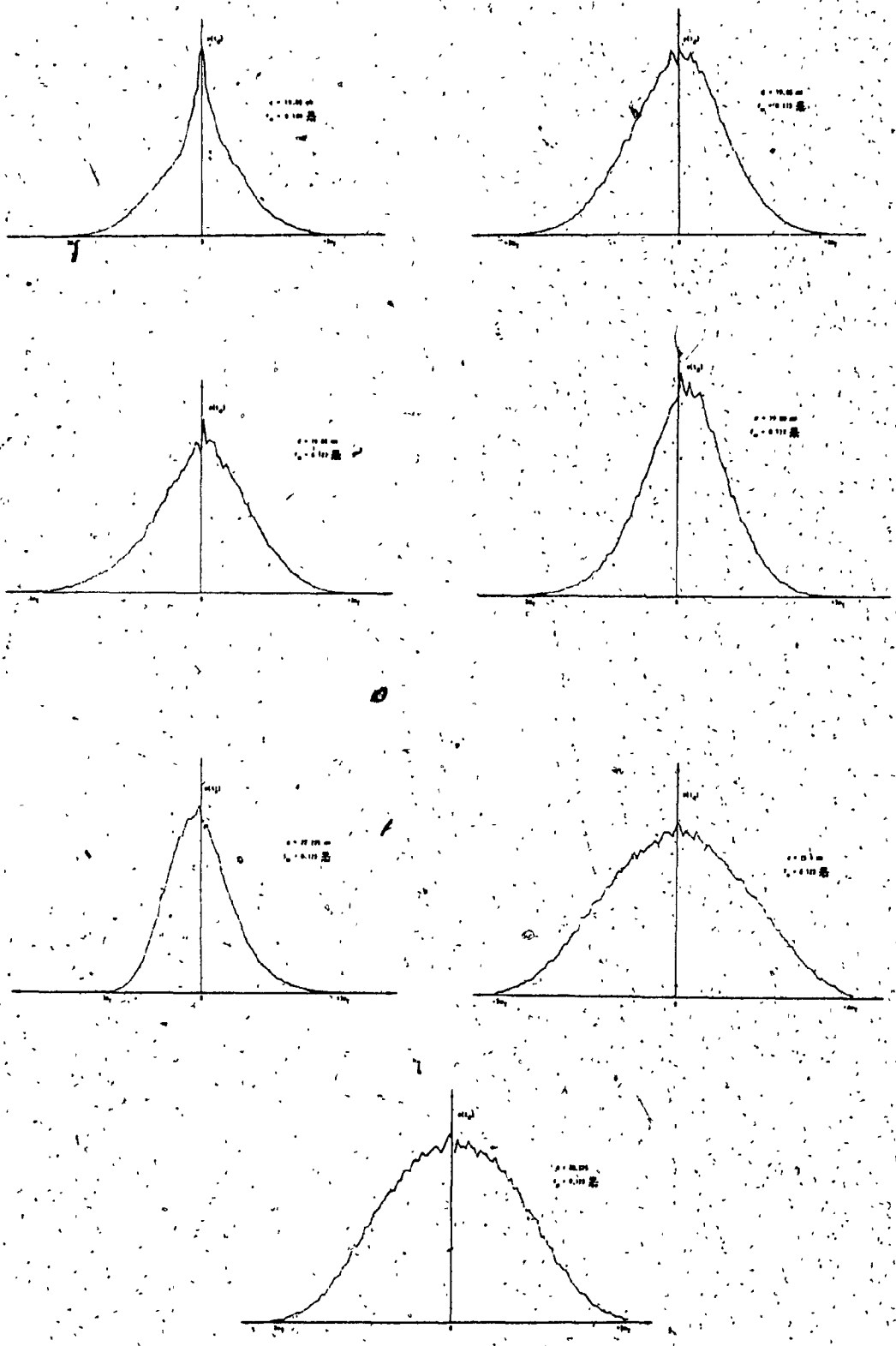

Fig. 4.13: Probability Denisty Function of the Measured Torque

reliability analysis of machine elements. These peak values can be obtained from the mean values of the axial force and torque and the variance of their dynamic fluctuations.

The measured as well as true values of the axial force and torque have now been established as a stationary wide band process with a gaussian distribution. Therefore the following relations are valid between the mean and peak values, with 99.87% degree of confidence.

$$F_{ap} = F_{aR} + 3\sigma_F \tag{4.5}$$

$$T_p = T_R + 3\sigma_T \tag{4.6}$$

The values of $3\sigma_F$ and $3\sigma_T$ can be determined from the probability density plots for each of the measurements performed. Based on these measured values, the true values of $3\sigma_F$ and $3\sigma_T$ are obtained using equations (3.4). These peak deviations of the axial force and torque are given in Table 4.4. Based on the true values of $3\sigma_F$ and $3\sigma_T$, the true values of the peak axial force and torque are determined using equations (4.5) and (4.6) and these are tabulated in Table 4.5.

To describe mathematically the peak values of axial force and torque, the variations of these quantities with the mean axial force, mean torque, feed and diameter are to be determined. These are shown in Figs. 4.14, 4.15, 4.16, 4.17, 4.18, and 4.19. As seen from Figs. 4.14 and 4.15, the variation of mean axial force with peak axial force, and mean torque with peak torque are linear, but have different slopes for different diameters of the cutting tool. Any general mathematical model to describe the peak values of axial force and torque will be inaccurate and not sufficiently valid. Therefore, this is done through empirical equations for estimating the peak values of axial force and torque in

Table 4.4: Measured and True Values of Peak Deviations of Axial Force and Torque

Diameter [mm]	Feed [mm/rev]	Peak Fluctuation of Torque [N·m]		Peak Fluctuation of Axial Force [N]	
		Measured Value	True Value	Measured Value	True Value
19.05	0.104	7.76	7.76	292	137
	0.113	8.52	8.51	447	277
	0.117	8.17	8.16	429	266
	0.123	8.17	8.16	494	331
22.225	0.117	7.42	7.41	389	251
	0.123	6.12	6.11	381	233
	0.134	5.82	5.81	307	191
	0.140	5.59	5.58	324	212
25.4	0.113	9.82	9.81	569	373
	0.123	9.96	9.95	530	331
	0.130	9.82	9.81	483	287
	0.138	9.96	9.95	548	349
28.575	0.111	9.96	9.95	530	331
	0.117	8.33	8.32	483	317
	0.123	9.60	9.59	530	338
	0.130	9.14	9.13	548	365

Table 4.5: Mean and Peak Values of Axial Force and Torque

Diameter [mm]	Feed [mm/rev]	True Value of Torque [N·m]		True Value of Axial Force [N]	
		Mean	Peak	Mean	Peak
19.05	0.104	11.78	19.54	1374.99	1511.99
	0.113	13.20	21.71	1520.54	1797.54
	0.117	14.13	22.29	1548.82	1814.82
	0.123	14.96	23.12	1610.65	1941.65
22.225	0.117	20.89	28.30	1914.26	2165.26
	0.123	22.38	28.49	1977.00	2210.00
	0.134	25.12	30.93	2192.80	2383.80
	0.140	26.95	32.53	2299.85	2511.85
25.4	0.113	24.77	34.58	2113.49	2486.49
	0.123	27.87	37.82	2250.09	2581.09
	0.130	30.24	40.05	2399.94	2686.94
	0.138	32.37	42.32	2455.27	2804.27
28.575	0.111	28.06	38.01	2241.82	2572.82
	0.117	30.28	38.60	2426.61	2743.61
	0.123	32.43	42.02	2483.13	2821.13
	0.130	34.32	43.45	2683.76	3003.76

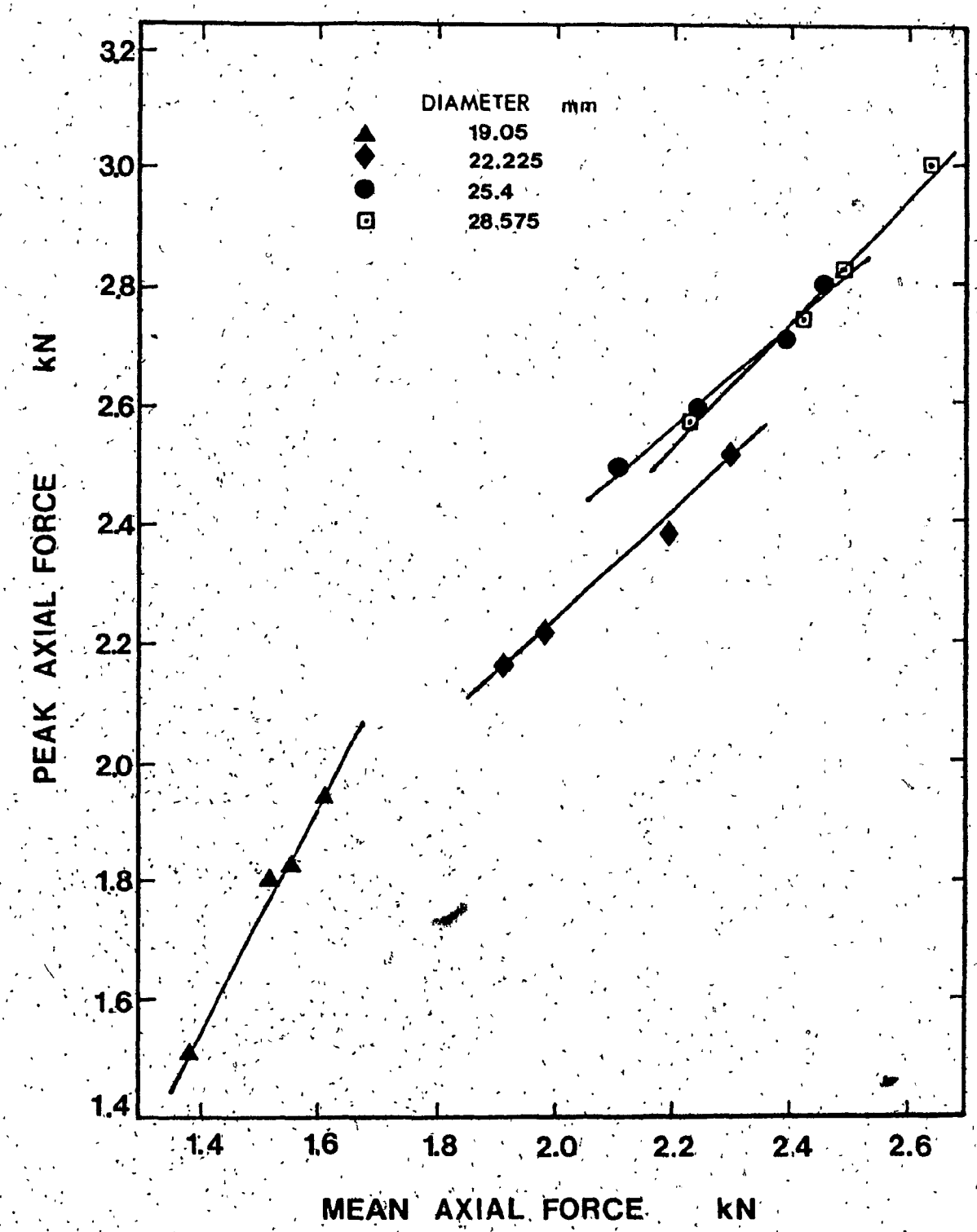

Fig. 4.14: Variation of Peak Axial Force with Mean Axial Force

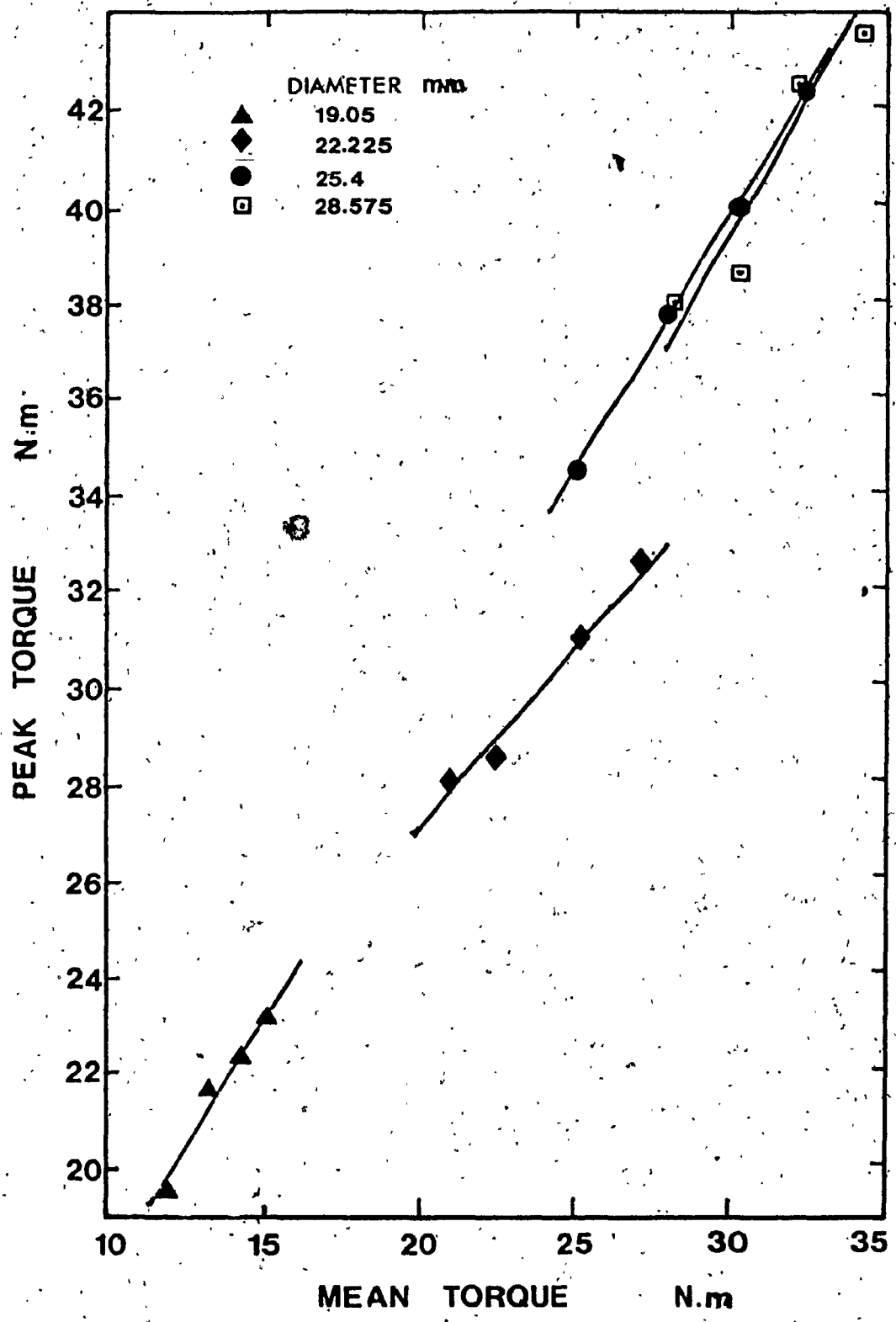

Fig. 4.15: Variation of Peak Torque with Mean Torque

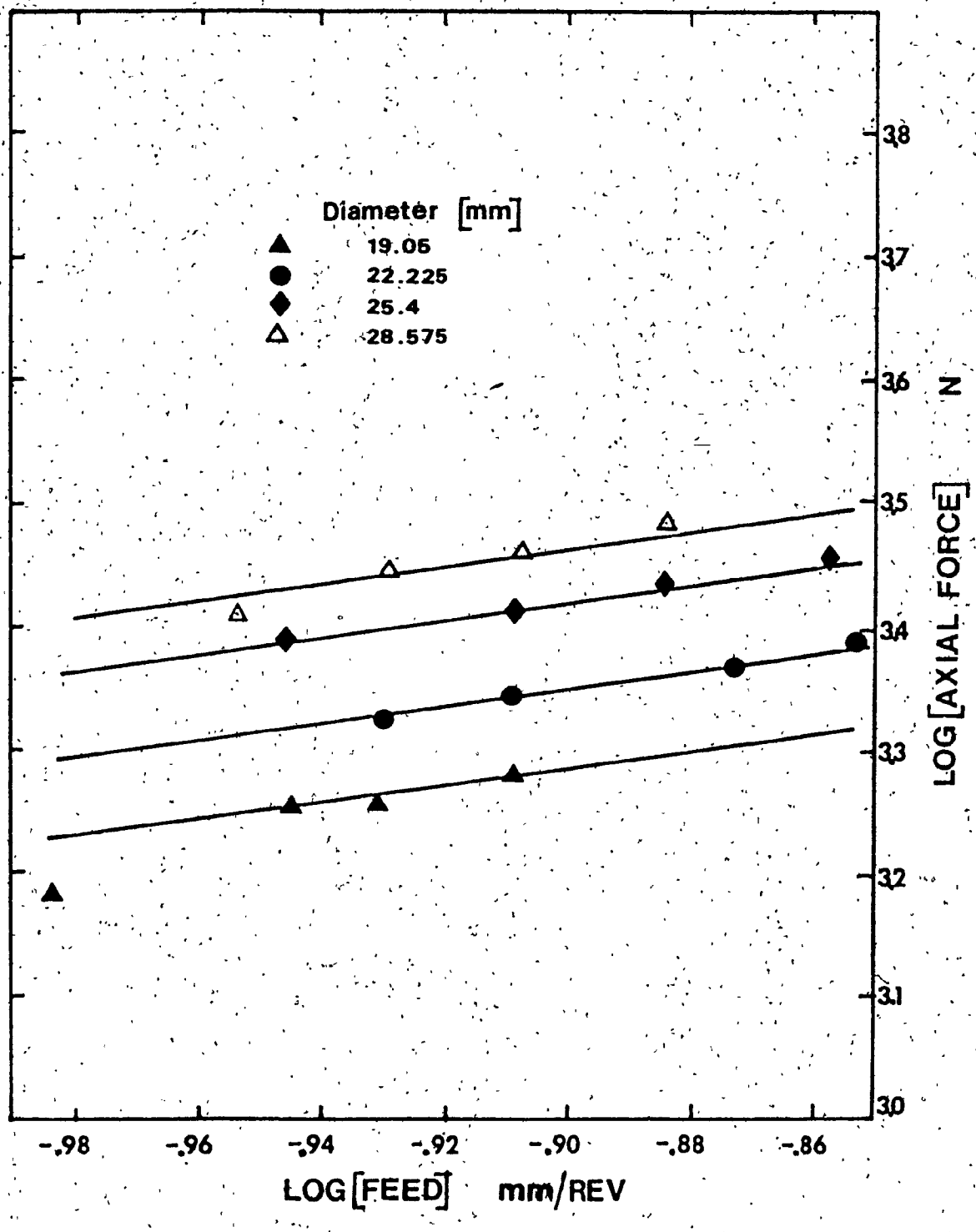

Fig. 4.16: Variation of Peak Axial Force with Feed

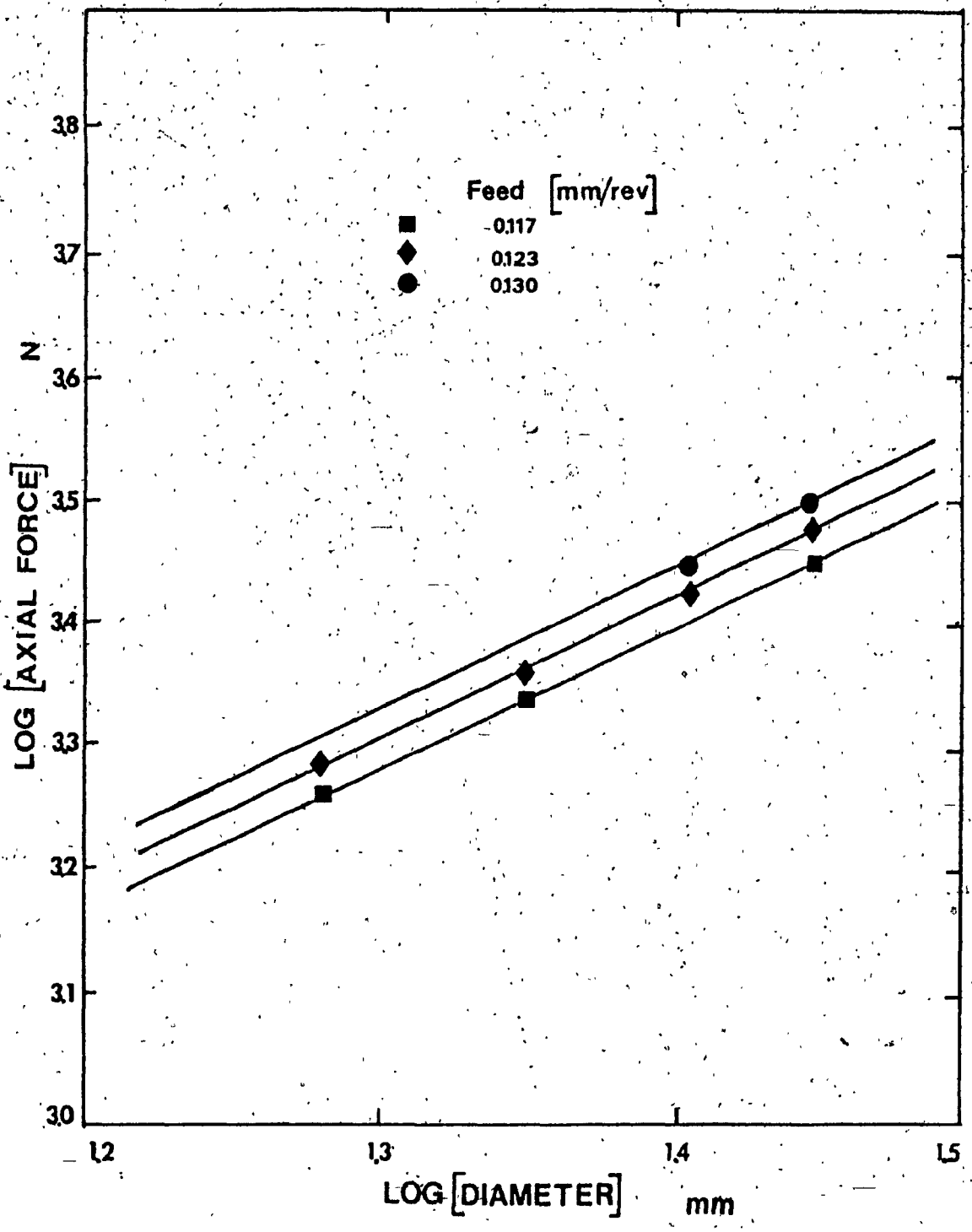

Fig. 4.17: Variation of Peak Axial Force with Diameter

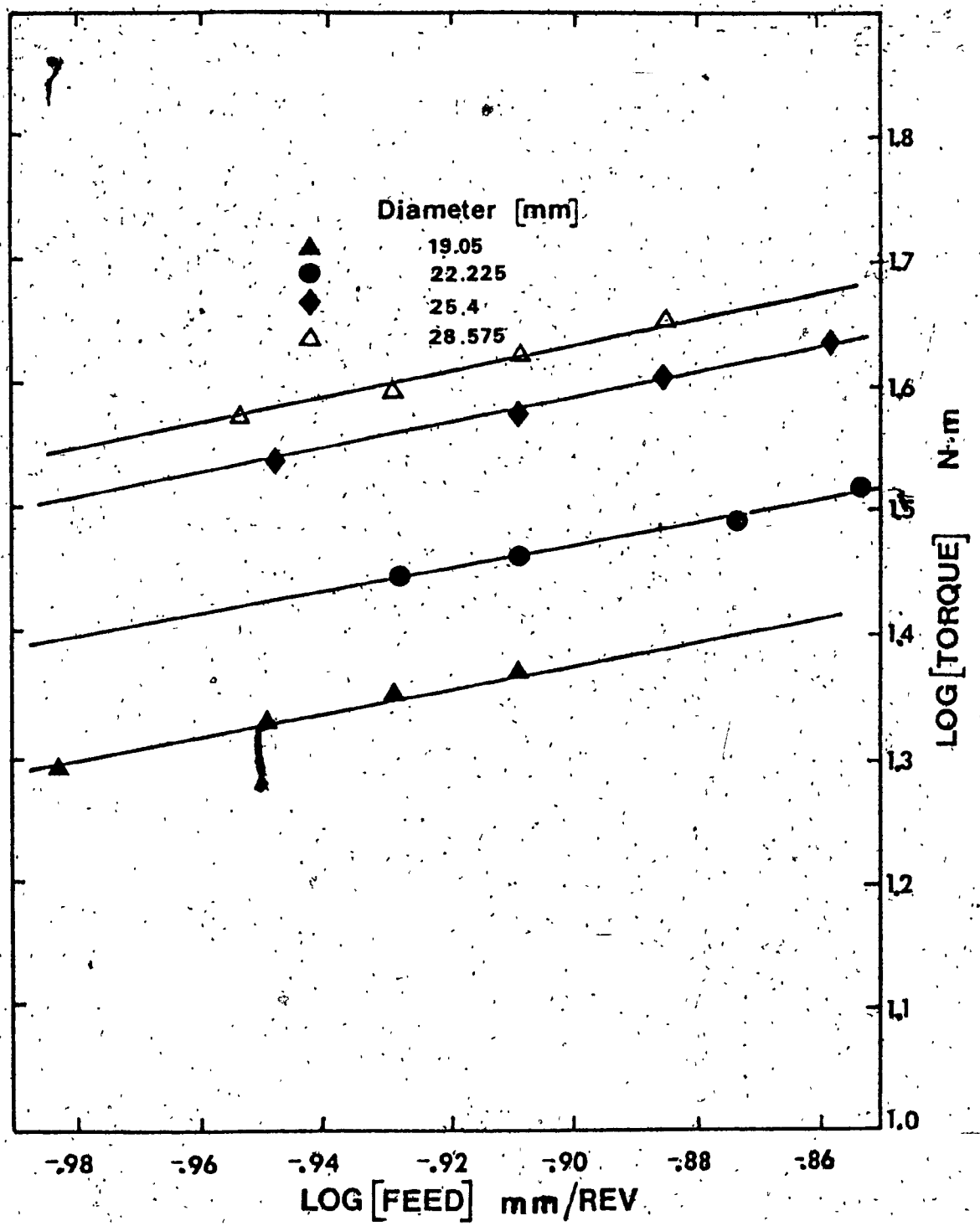

Fig. 4.18: Variation of Peak Torque with Feed

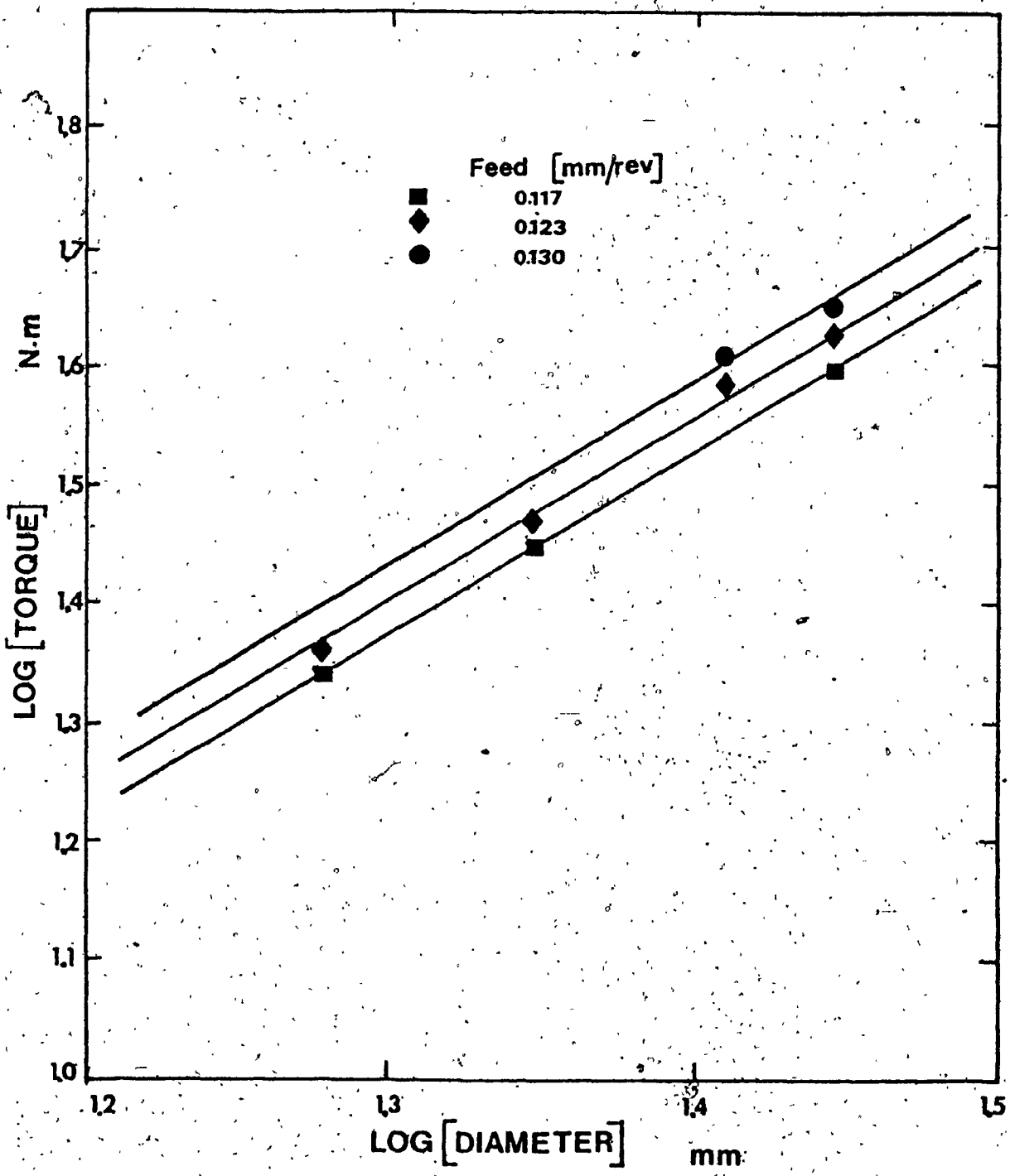

Fig. 4.19: Variation of Peak Torque with Diameter

BTA deep hole machining with AISI 1020 using a BTA Heller cutting tool and are established using figures 4.16 to 4.19. They are

$$F_{ap} = 267\ f_m^{0.679}\ d^{1.15} \tag{4.7}$$

$$T_p = 1.88\ f_m^{0.929}\ d^{1.516} \tag{4.8}$$

where

F_{ap} is the peak axial force in Newtons

T_p is the peak torque in Newton-metre

d is the diameter of the cutting tool in mm.

f_m is the mean value of feed

The above empirical equations cannot be compared with known results as there are no previously published data using conditions adopted in this investigation.

4.4 Conclusion

The analysis of the axial force and torque experimental data reveals that the torque and axial force are stochastic in nature. The fluctuations in the axial force and torque can be approximated by a weakly stationary wide band process with a gaussian distribution. Also, the expressions for the steady state axial force and torque point out that the true steady state axial force and torque vary nonlinearly with the feed for BTA deep-hole machining of AISI 1020 steel using a BTA Heller tool. Based on these equations and the peak fluctuations from the normal distribution curves, equations for the peak values of the axial force and torque have been derived. Such a mathematical description of the resultant force system coupled with a mathematical model of the

machine tool is needed to establish the stochastic characterization of the behaviour of the machine tool-workpiece system and is carried out in the subsequent chapter.

CHAPTER 5

THE MATHEMATICAL MODEL OF THE MACHINE TOOL WORKPIECE SYSTEM

CHAPTER 5

THE MATHEAMTICAL MODEL OF THE MACHINE TOOL-WORKPIECE SYSTEM

The improvement of the dimensional accuracy and geometric features of the machined workpiece, the development of new materials which are difficult to machine, and the introduction of automatic control and feedback adjustments in machining have greatly increased the role of understanding the dynamic processes taking place in a machine tool. The problem concerning the dynamic aspects in machine tool design can be reduced to three main types [105].

a) Selection of the parameters of a drive.

b) Analysis of the machine tool behaviour upon travel of the components without cutting action.

c) Analysis of the machine tool behaviour in the process of machining a workpiece.

The indices reflecting the dynamic performance of a machine tool are generally given in terms of the following quantities [105]

a) Margin or degree of stability.

b) Deviations of the parameters of a system upon external action.

c) Speed of response of a system.

The total dynamic system representing a machine tool constitutes the aggregate of the elastic system-the machine-fixture-tool-workpiece complex-and the kinematics occuring in the moveable joints or associations of the components of the elastic system like cutting, friction, electrodynamic, and hydrodynamic processes. In the machine tool operation, deformation of the elastic system occurs under the action of

cutting forces, friction forces, and forces developed by the motor. The effect of these factors on the elastic system can be represented as shown in Fig. 5.1. Such a representation is valid for the case in which the deformation of the elastic system does not lead to variations in the magnitude of the forces, their orientation or the character of the load application. But in practice this is not true, since the forces acting on the elastic system change with the variations in deformation of the elastic system. Thus the system configuration shown in Fig. 5.1 has to be modified as illustrated in Fig. 5.2. So, as seen from Fig. 5.2, the dynamical system of the machine tool is a complex multiply connected closed loop system. In many applications, it is convenient to replace such a complex process by a simplified system. Since, in this investigation, the effect of cutting forces on the dynamics of the machine tool is of primary interest, the elastic system, the friction process, and the process in the motor are replaced by an equivalent elastic system as shown in Fig. 5.3.

In this Chapter, a step by step three-dimensional modelling procedure of the equivalent elastic system of the deep-hole machining system is presented using discrete stiffness elements and dampers. Such a modelling scheme can be employed to evaluate the stability of the machine tool under operating conditions, to study the effect of the bearing stiffness on the performance of the machine tool, for the development of the system transfer function which is needed for both the active control of the cutting tool-boring bar and in the development of an adaptive control system for the unit, and predicting accurately the motion of the cutting tool tip. To reduce the complexity of the model, a simplified physical model of the deep-hole machining system

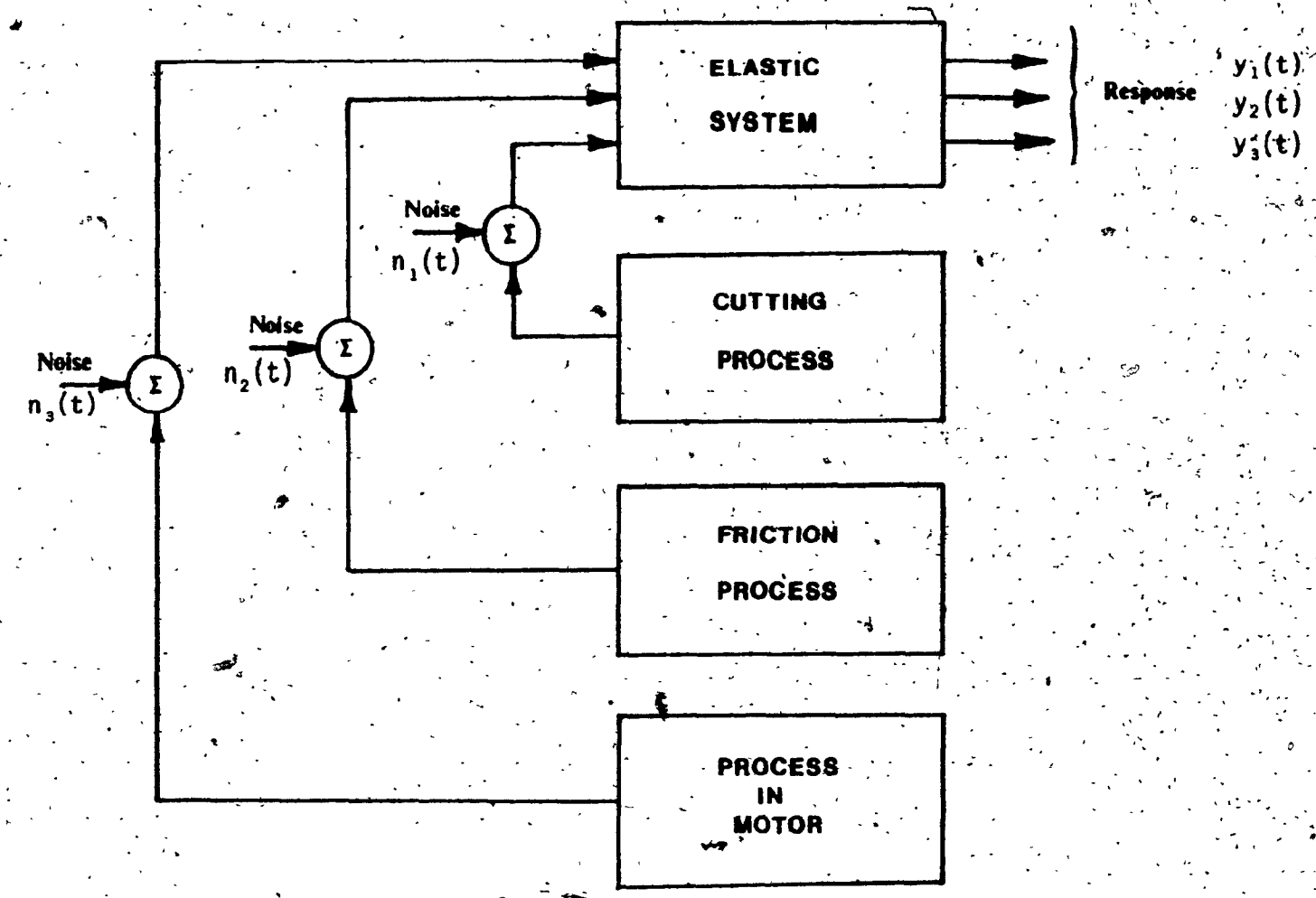

Fig. 5.1: An Open Loop Representation of the Dynamic System of a Machine Tool

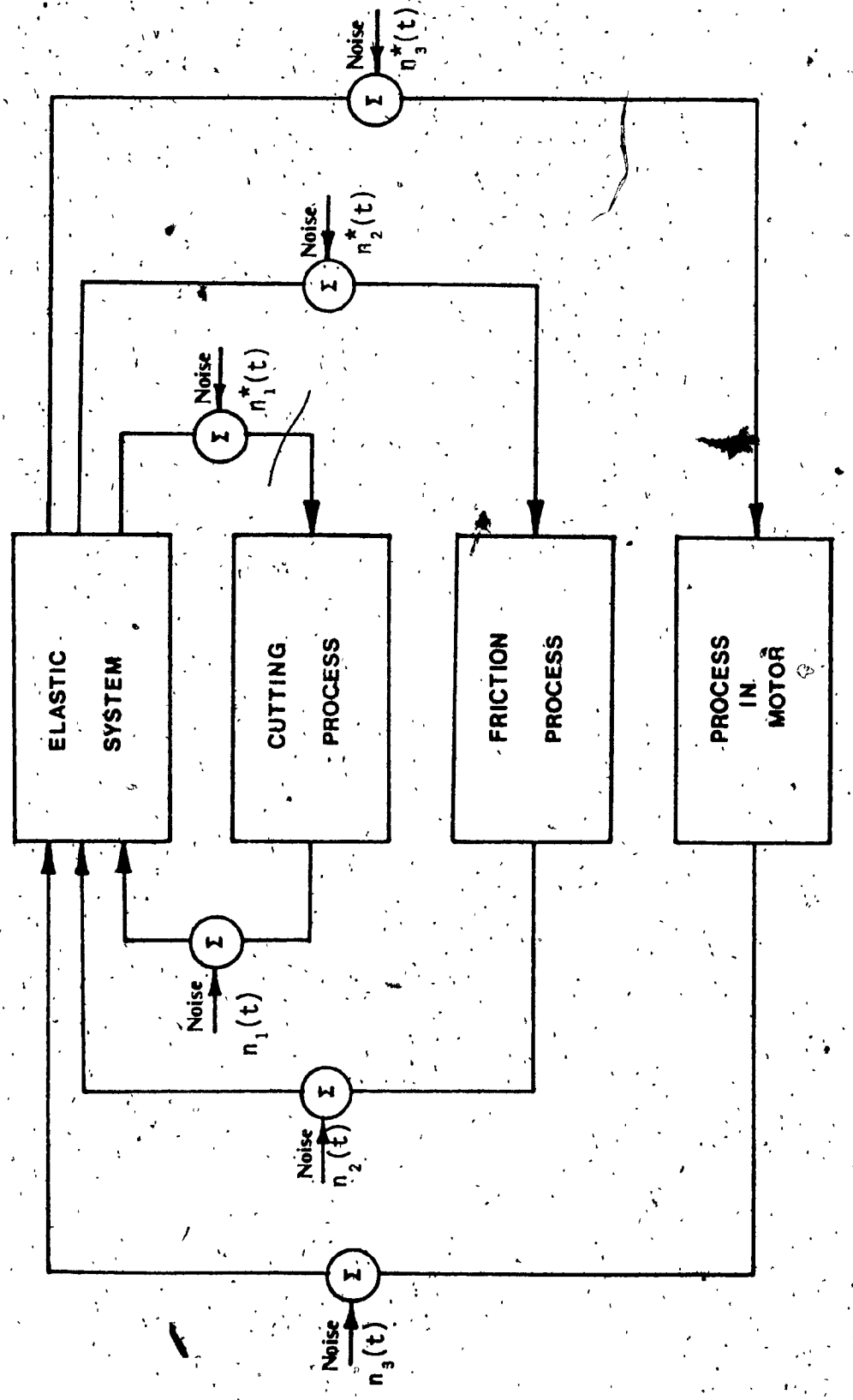

Fig. 5.2: A Closed Loop Representation of the Dynamic System of a Machine Tool

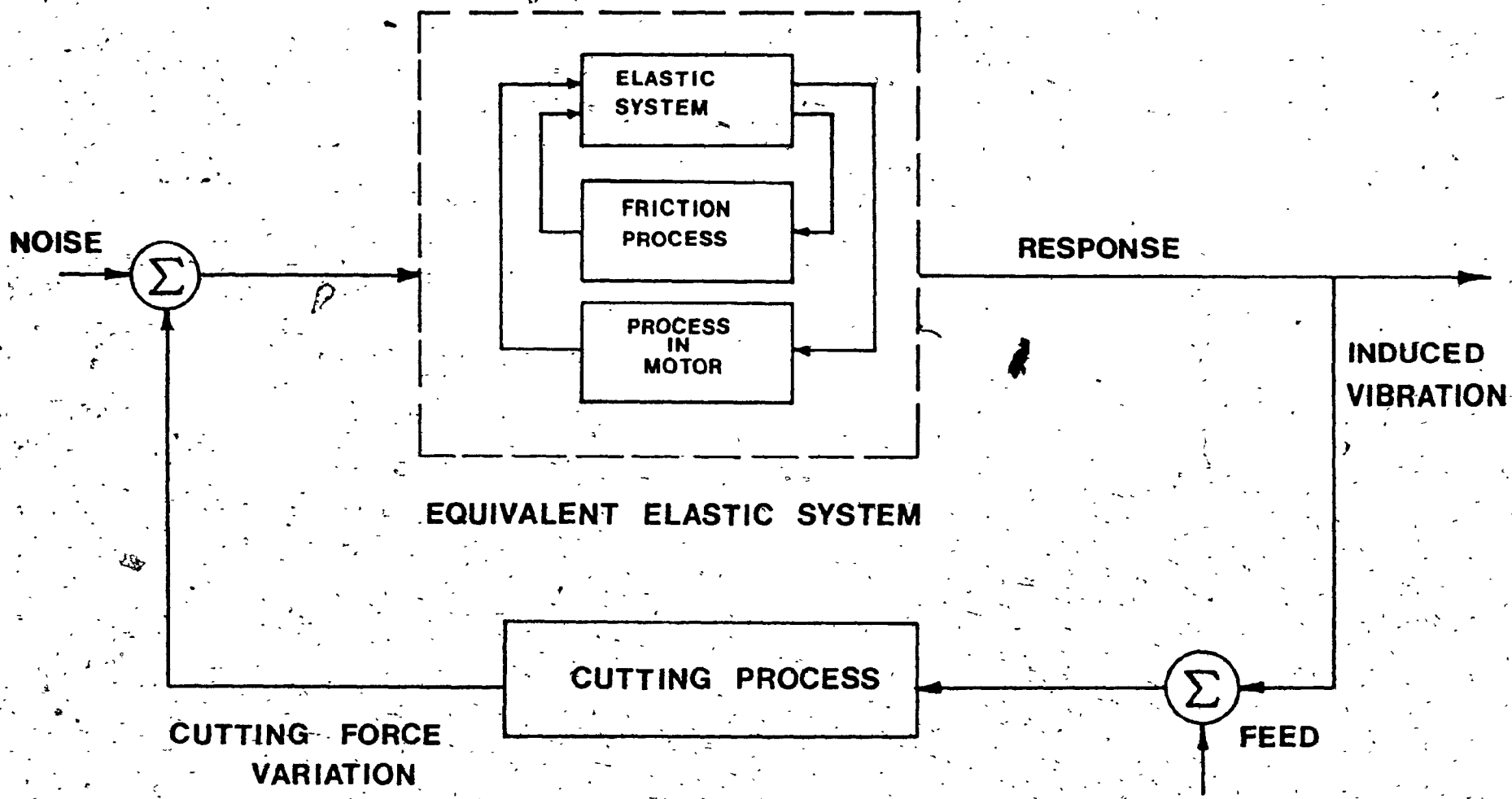

Fig. 5.3: A Simplified Closed Loop Representation of the Dynamic System of the Machine Tool

is developed based on appropriate assumptions and the stochastic differential equations have been derived using the assumed modes method [106,107]. This mathematical model can also be used to predict the true motion of the tool tip.

5.1 Description of the Deep-Hole Machining System

The deep-hole machining system considered consists of five major components namely,

a) The Lathe.

b) The Oil Pressure Head.

c) The Rest.

d) The Drive Unit.

e) The Boring-Bar Cutting Tool Assembly.

The function of each of these components are described below.

The Lathe: The lathe is a SCHAERER HPD631 with a center to center distance of 4 m. The spindle height is 0.45 m and the total weight of the machine is 4950 kg. The lathe bed is made up of one piece of cast iron cast with the ground ways. The attachment of the lathe to the foundation is by six foundation bolts distributed into three sections along the length of the machine. The power source of the lathe is a 30 HP AC motor, which drives a multispeed gear box through a set of V belts. The lubrication, for the head stock which houses the gear box, is provided by an internal oil circulating system. The spindle is supported on two high accuracy roller bearings mounted on a cast iron structure which forms the head stock frame. The head stock is fixed onto the lathe bed by a number of bolts.

The Oil Pressure Head: The oil pressure head is the hub of the system. Its purpose is fourfold and these are:

a) Introduction of the coolant to the tool.

b) Seals against workpiece face to contain the coolant.

c) Guides the tool into the work.

d) Seals the outside diameter of the boring bar at the end opposite to the tool to contain the coolant.

The Rest: The function of the rest in the machining process is to provide support to the 180 cm long boring bar. The rest consists of two parts, the pedastal and the bearing. The pedestal is made up of mild steel and has V-grooves milled into its base to provide guidance when moving on the lathe bed-ways. The rest always moves along with the boring bar. Hence, there is no relative longitudinal motion between the boring bar and the rest. The bearing consists of two parts: a tapered bushing of phenolic material and two ball bearings on either side of the phenolic material. The boring bar is attached to the inner bore of the phenolic material which has the same diameter as the outer diameter of the boring bar. To rigidly clamp the boring bar on the phenolic material, nuts are used to push the latter on the tapered bore.

The Drive Unit: The drive unit is an accessory to the deep-hole machining system. The location of the drive unit on the machine is at the end opposite to that of the head stock assembly. The unit basically replaces the tail-stock of a lathe. It is mounted on the carriage which moves longitudinally along the bed of the machine powered for this travel by the feed screw. This provides a combination of high speeds and feeds needed for the long boring bars to drill into the workpiece. The drive unit consists of a 20 HP motor, a timing belt assembly, a

spindle housing and an oil mist lubrication system. The electric motor is supported by the spindle housing. This housing serves two functions and these are (a) it acts as a base for the motor; (b) supports the bearings. The spindle is made of tool steel, precision ground and rotates on three bearings. One of the ball bearings is located at the timing belt sheave and the other two ball bearings are at the other end. Lubrication to these three ball bearings is by a continuous oil mist.

The Boring-Bar-Cutting Tool Assembly: The hollow boring bar to which the tool is fixed is made of alloy steel, centerless ground and engineered to strict BTA thread and clearance standard. Standard boring bars vary from 0.0127 m to 0.6096 m in diameter. The cutting tool consists of a hollow steel body with an inserted carbide cutting edge and carbide bearing strips or wear pads. The cutting edge and wear pads are brazed to the steel body, then ground cylindrically to form the tool diameter. The diameter of the body must be slightly smaller than that of the tool to allow passage of the coolant around the tool. The two carbide wear pads are located at 180° opposed to the cutting plane and 90° to the cutting edge.

5.2 Working Methods in BTA Systems

There are three methods of working in BTA deep-hole machining systems. They are, stationary tool-rotating workpiece, rotating tool-stationary workpiece, rotating tool-rotating workpiece, and are briefly described below.

Stationary tool-rotating workpiece system

This is shown in Fig. 5.4(a) and is the most common method for drilling long symmetrical workpieces where the difference between the

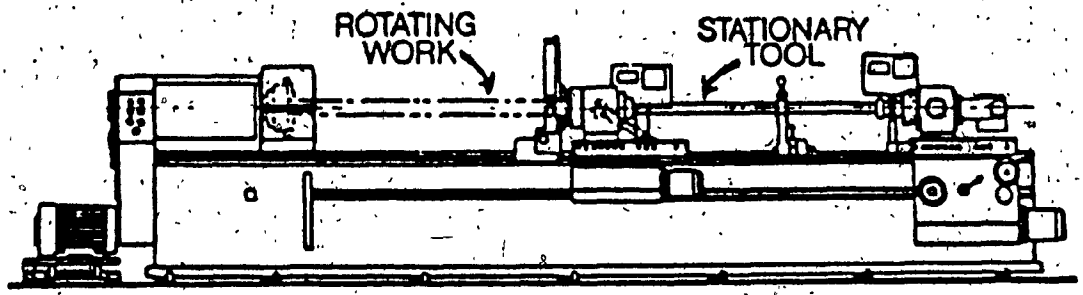

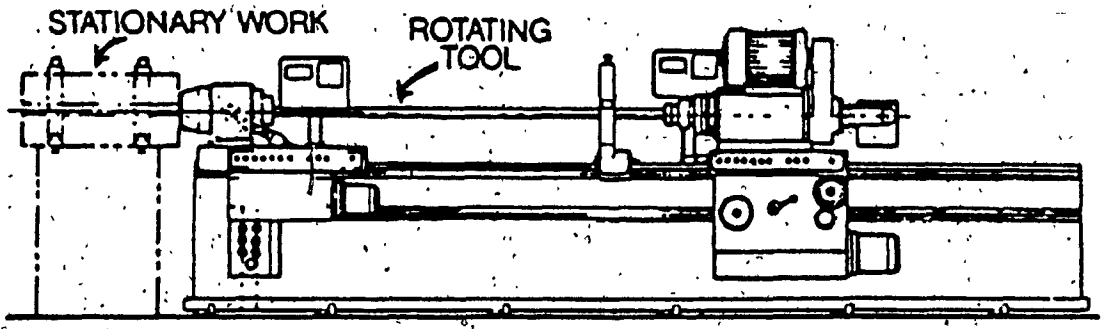

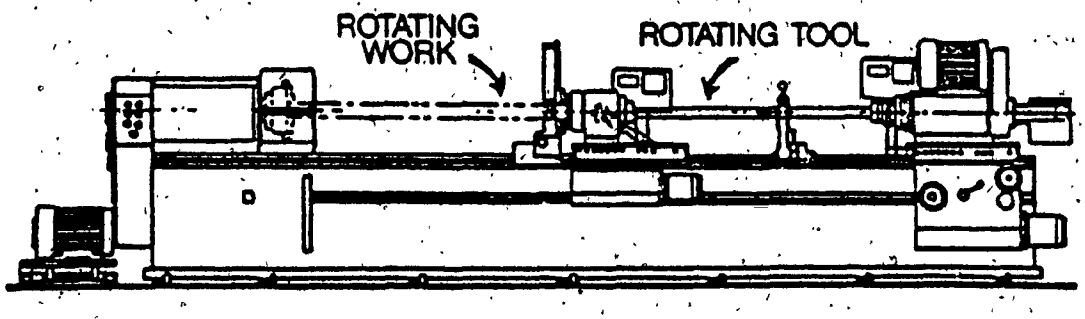

Fig. 5.4: Working Methods in BTA Deep-Hole Machining Operation

outer diameter of the work and the diameter of the hole being produced is not large. Extremely straight holes can be expected.

Rotating tool-stationary workpiece system

Workpieces of any shape can be drilled using this method and is shown in Fig. 5.4(b). This can be used to drill workpieces on or off the machine bed. Straightness and accuracy are not as good compared with the previous method.

Rotating tool-rotating workpiece system

This working method, also called the counter-rotating system, is used whenever straightness requirements are critical and the workpiece can be rotated, as this gives the best accuracy of the holes as compared to the other two working methods. This is shown in Fig. 5.4(c) and is used for materials such as aluminum alloys which require very high surface speeds not obtainable with a single rotating spindle or head stock.

5.3 Modelling of System Components

This section presents a discrete modelling of the deep-hole machining system described earlier, using springs, masses and dampers. The model of the entire system is obtained by combining the model of each of the components of the system obtained separately. Such a description of the system can be used not only in performing a complete dynamic analysis for response but also in the design of an appropriate control system. The deep-hole machining system can be divided into three separate sub-systems for the purpose of modelling and are:

a) The boring bar-cutting tool system.

b) The lathe assembly.

c) The interaction between the cutting tool and workpiece.

5.3.1 Boring Bar-Cutting Tool Assembly

The cutting tool is screwed on and clamped rigidly on to the boring bar, which is a hollow pipe to enable the chips together with the coolant oil under pressure to flow back to the sump via the filters. The boring bar is always filled with the oil chip heterogeneous mixture. The boring bar-cutting tool assembly is modelled as a hollow pipe with a constant velocity fluid flow and is shown in Fig. 5.5 based on the following assumptions:

a) The mass density of the fluid-chip heterogeneous mixture is assumed to be the same as that of the oil, as the exact mass density cannot be determined due to the random nature of chip flow.

b) The change in diameter between the cutting tool and the boring bar is small and is neglected.

c) The change in velocity of the fluid-chip mixture as it flows through the boring bar is neglected.

d) The structural damping of the boring bar-cutting tool system can be reduced to an equivalent viscous damping per unit length which is denoted by C_b for the transverse vibration and C_{Tb} for the torsional vibration.

5.3.2 Lathe Assembly

The lathe assembly consists of the following components:

a) The lathe-dynamometer workpiece.

b) The oil pressure head.

c) The rest.

d) The Drive Unit.

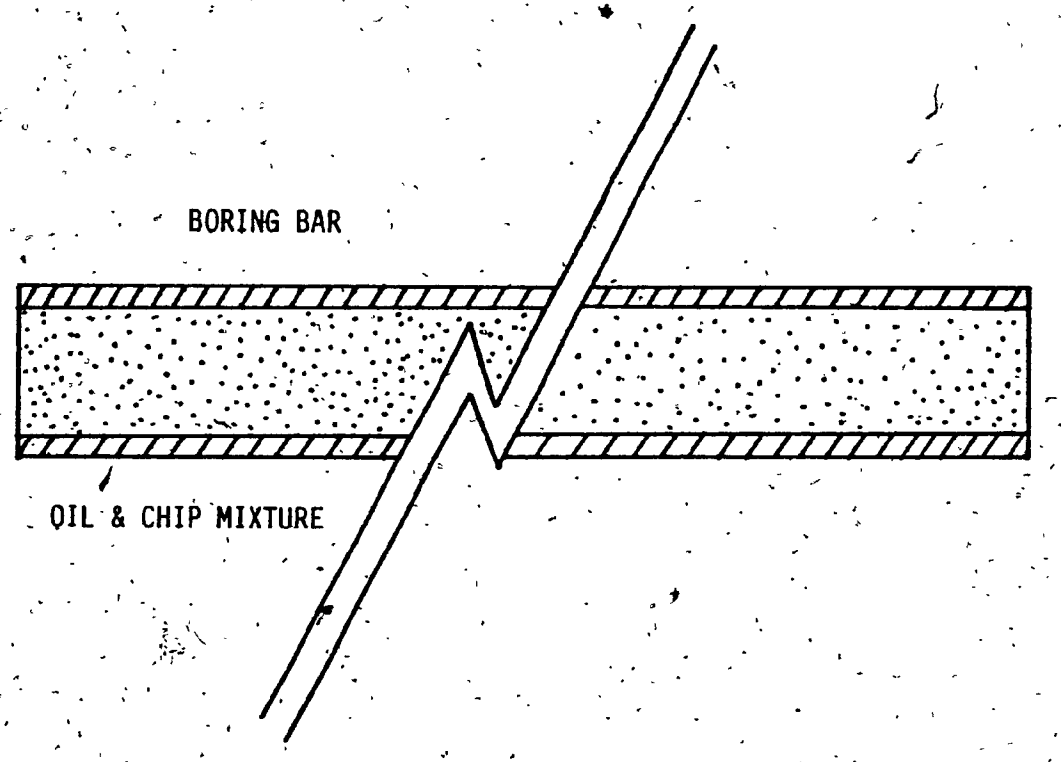

Fig. 5.5: Model of Boring Bar

Each of the above is modelled separately and later combined to represent the model of the entire system.

5.3.2.1 The Lathe-Dynamometer-Workpiece Assembly

This sub-system consists of three components, the lathe, dynamometer, and the workpiece. These three components are grouped together because the workpiece is clamped to the dynamometer which in turn is held in the chuck.

The model is based on the following assumptions:

a) The lathe bed is taken to have three degrees of freedom, with the foundation bolts assembly represented by cubic springs $K_1(Z,\theta,\Phi)$, $K_2(Z,\theta,\Phi)$....$K_6(Z,\theta,\Phi)$ and equivalent viscous dampers $C_1, C_2, \ldots C_6$[108].

b) The lathe bed, along with the motor and gear box assembly is represented by a single mass M_B having moments of inertia I_{Bx} and I_{By} about the x and y axis respectively.

c) The variation in diameter of the chuck, dynamometer and the spindle is neglected. Hence the spindle shaft, chuck, dynamometer, and workpiece can be represented by a shaft of uniform diameter.

d) The spindle unit rests on the lathe bed. The entire gear assembly of the spindle unit can be represented by a mass M_G and moment of inertia I_{Gx} and be located on the spindle shaft.

e) The two bearings supporting the spindle shaft are represented by linear and torsional springs K_{B_1}, K_{B_2}, K_{T_1}, and K_{T_2} respectively, with equivalent viscous damping C_{B_1}, and C_{B_2} along the radial direction.

f) The overhang beyond bearing 1 is small and can be neglected.

Based on these assumptions the model of the lathe-dynamometer-workpiece

system is constructed and is shown in Fig. 5.6.

5.3.2.2 The Oil Pressure Head

The model representing the oil pressure head is shown in Fig. 5.7 and is based on the following assumptions:

a) The pedestal of the pressure head is represented by a mass M_P and a moment of inertia I_{Px} about the x axis.

b) The stiffness of the pedestal is represented by non-linear springs $K_{P_1}(Z_L,\theta_L)$ and $K_{P_2}(Z_L,\theta_L)$ [73] and the structural damping by equivalent viscous dampers C_{P_1} and C_{P_2}.

c) The pedestal is taken to have two degrees of freedom to account not only for the motion along the Z axis but also for the possible rocking due to the effect of tolerances and clearances between the bed and the carriage on which the pressure head rests.

d) The stiffness of the oil pressure head bearings is represented by K_{TP} and K_{P_3} along the torsional and transverse directions. The damping along the transverse direction is represented by an equivalent viscous damper C_{P_3}.

5.3.2.3 The Rest

The model of the rest shown in Fig. 5.8 has been arrived at making use of the following assumptions:

a) The pedestal of the rest is considered to possess two degrees of freedom. This is due to the fact that the pedestal has not only a tendency to show displacements in the vertical direction, but also a rocking action about its axis due to the clearances and tolerances between the lathe bed guides and the guideways provided in the rest.

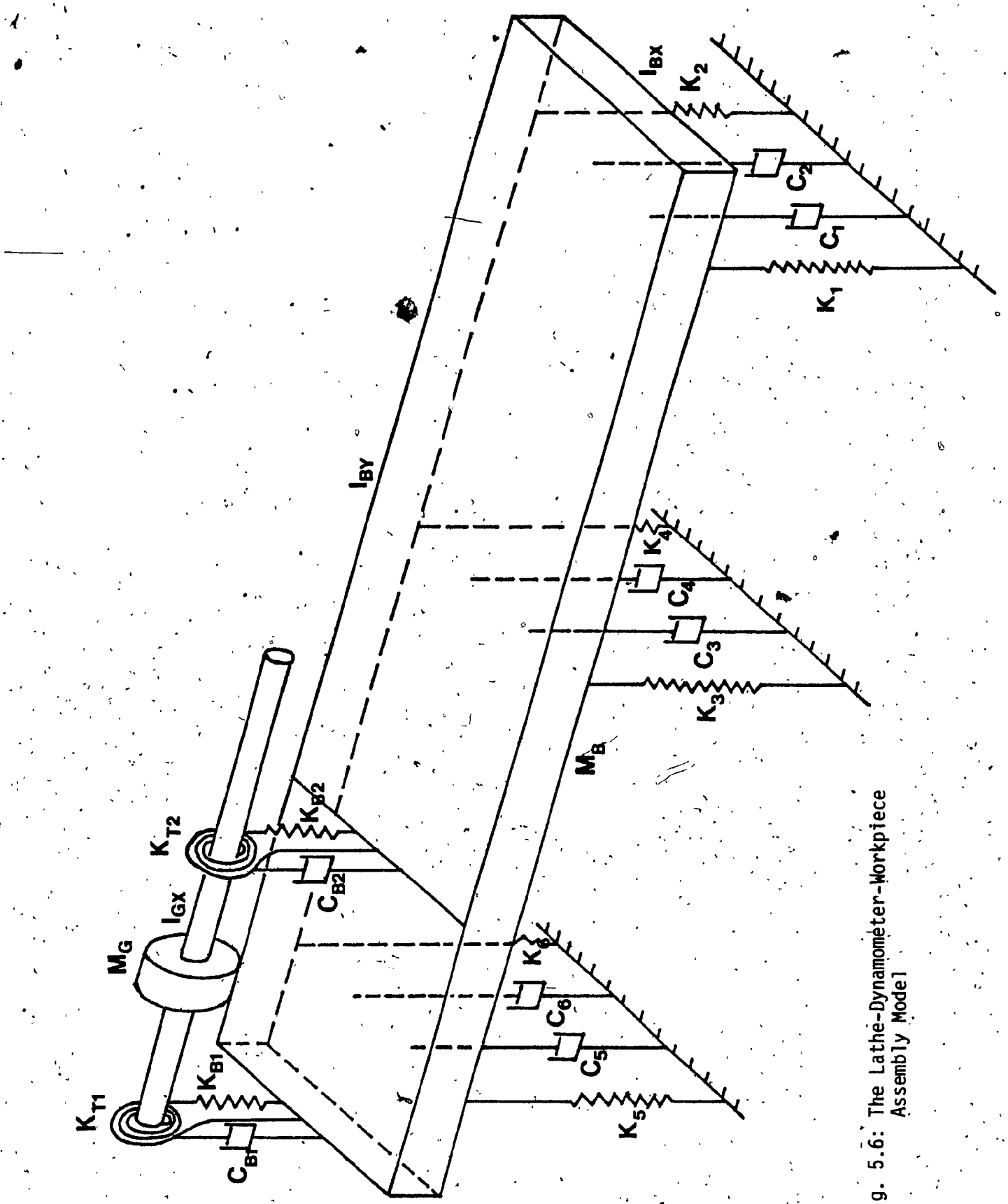

Fig. 5.6: The Lathe-Dynamometer-Workpiece Assembly Model

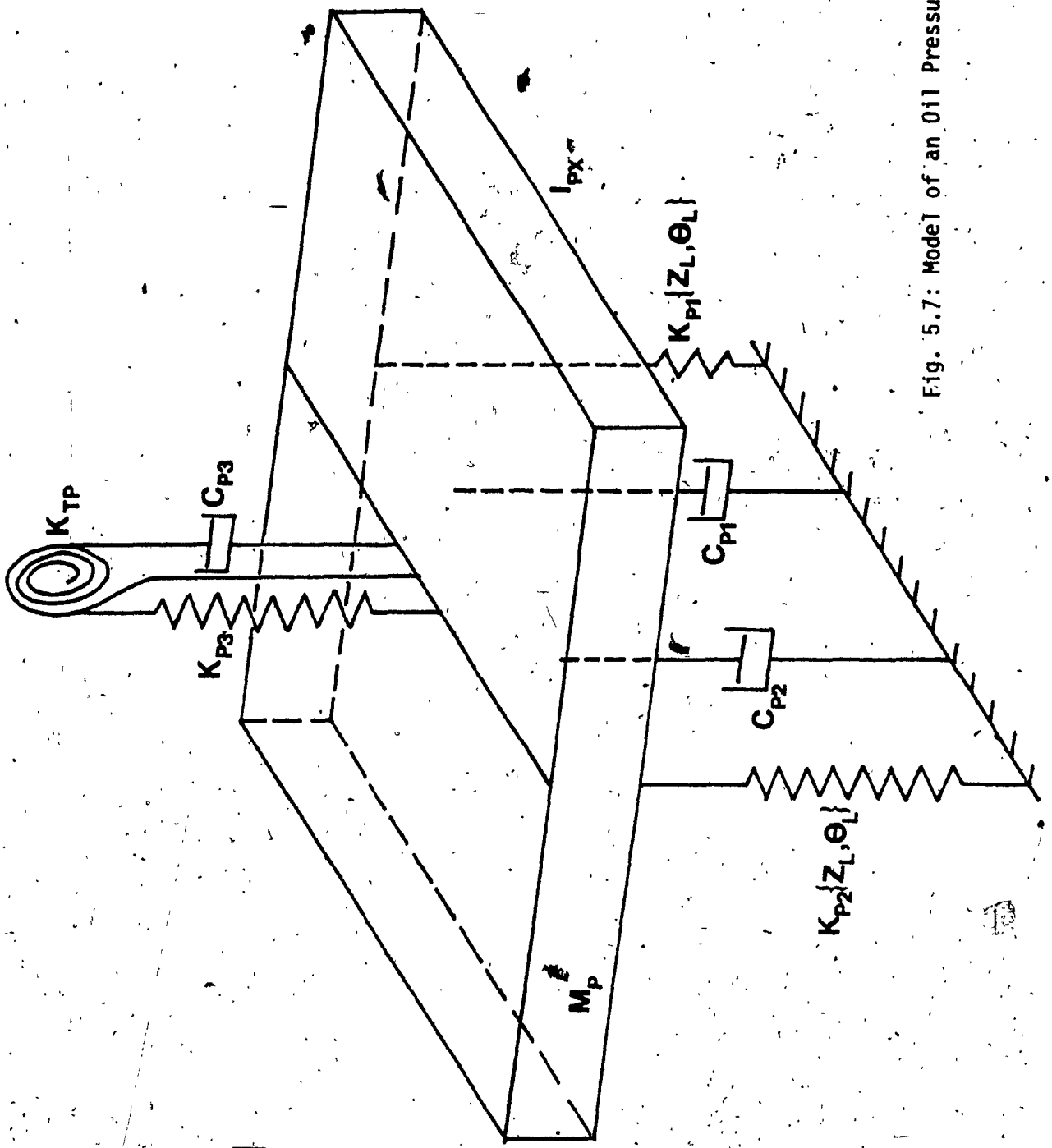

Fig. 5.7: Model of an Oil Pressure Head

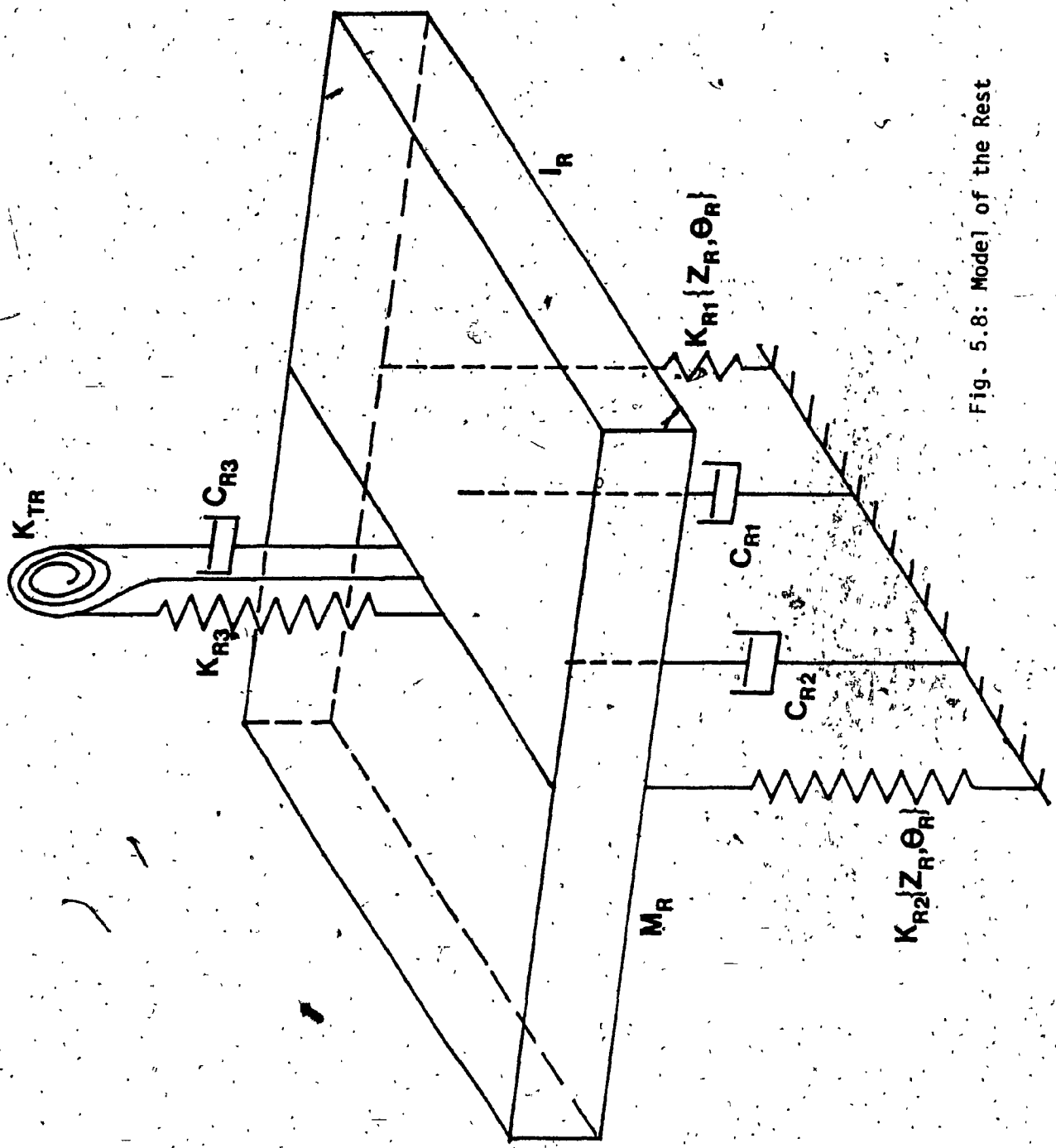

Fig. 5.8: Model of the Rest

b) The mass of the pedestal is represented by a mass M_P and a moment of inertia I_R about its axis.

c) The pedestal stiffness can be represented by non-linear springs $K_{R_1}(Z_R,\theta_R)$ and $K_{R_2}(Z_R,\theta_R)$ and the total damping of the structure and the contribution due to friction damping between the guide and guide-ways are represented by equivalent viscous dampers C_{R_1} and C_{R_2}.

d) The stiffness of the bearing in the rest is accounted for in the torsional direction by K_{TR} and in the transverse direction by K_{R_3}. The damping in the bearing along the transverse direction is represented by C_{R_3}.

e) The torsional damping of the bearing is small and is neglected.

5.3.2.4 The Drive Unit

The model representing the drive unit is shown in Fig. 5.9 and it is developed under the following assumptions.

a) The drive unit pedestal along with the motor is represented by a mass M_D and a moment of inertia I_{Dx} about the axis.

b) The pedestal is taken to have two degrees of freedom in view of the clearance and tolerance between the lathe bed guide and guideways.

c) The stiffness of the pedestal is represented by non-linear springs $K_{D_1}(Z_D,\theta_D)$ and $K_{D_2}(Z_D,\theta_D)$ and the total damping by equivalent viscous dampers C_{D_1} and C_{D_2}.

d) The spindle of the drive unit is represented by a beam of uniform diameter of mass per unit length M_D.

e) The overhang of the spindle to accommodate the sheave for the timing belt is negligible.

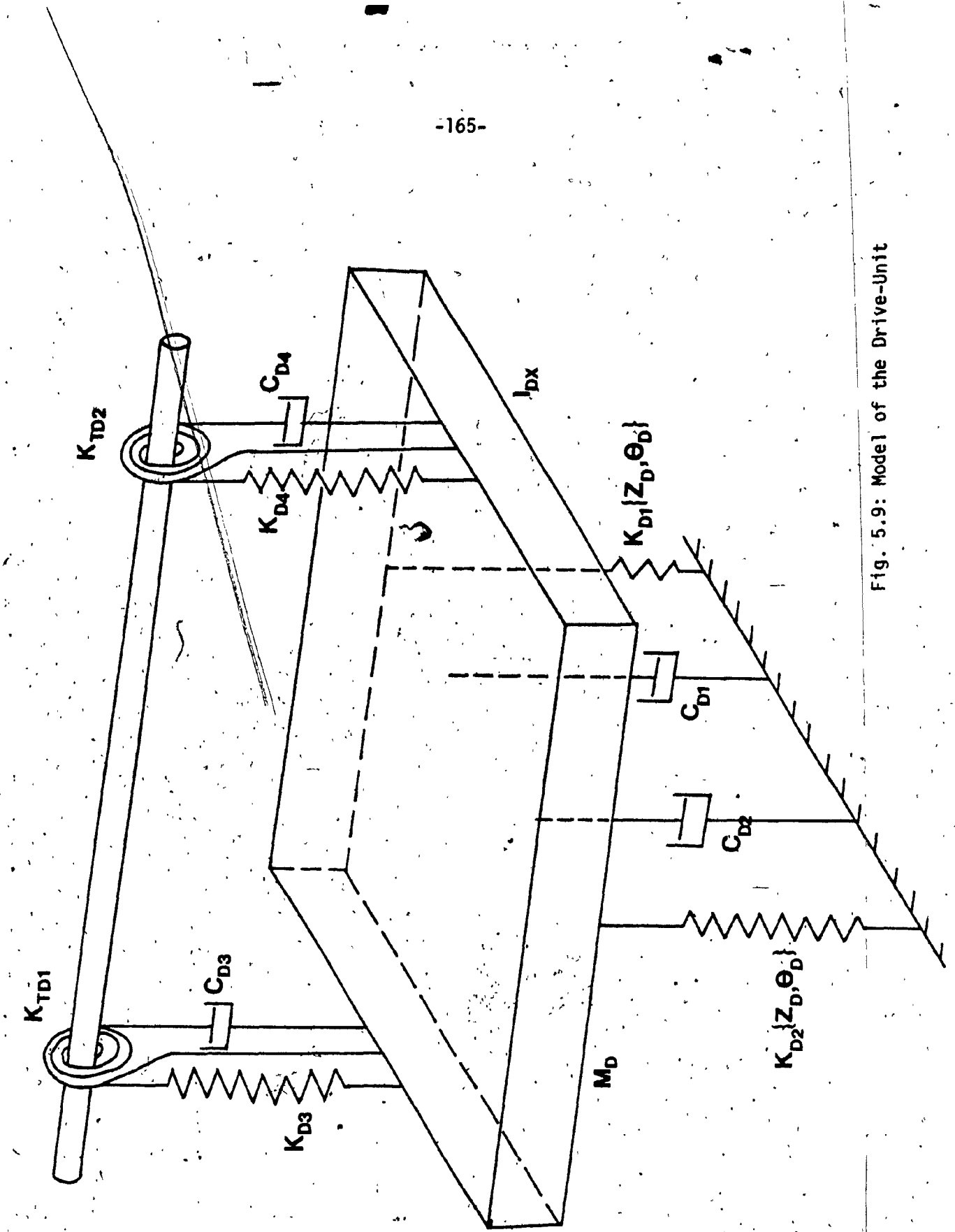

Fig. 5.9: Model of the Drive-Unit

f) The bearings supporting the spindle of the drive unit are assumed to have a torsional stiffness K_{TD_1} and K_{TD_2} and a stiffness along the transverse direction represented by K_{D_3}, and K_{D_4}.

g) The torsional damping of the bearings are small and can be neglected. Also the damping along the transverse direction is represented by equivalent viscous dampers C_{D_3} and C_{D_4}.

5.3.3 Interaction Between the Workpiece and the Cutting Tool

In-BTA machining process the interaction between the cutting tool and the workpiece takes place in two different regions, namely the cutting edge and the wear pads. The frictional force generated due to machining process actually exhibits a non-linear damping characteristic depending upon certain machining parameters. But, here the damping due to friction has been represented by an equivalent viscous damper [109] C_{eq} oriented at an angle θ and located at a distance "Z_o" from the axis. The interaction between the wear pads and the workpiece takes place in an oil medium. This interaction, known as the burnishing action, is a very complicated mechanism and not only does it affect the forces but also affects the roundness and surface finish of the bored hole [80,85, 110]. Here, this burnishing action in the oil medium can be represented by a spring and damper at each wear pad. The stiffness represents the stiffness of the partial bearing (approximation of the interaction) at each of the wear pads. The interaction is assumed to be different at each of the pads and also have components of different magnitudes along the radial and tangential direction due to the shape of the tool and the magnitude of the cutting forces. Thus, the total burnishing action at the pads can be represented by K_{TW_1}, C_{TW_1}, K_{TW_2}, and C_{TW_2} at each of

two pads oriented at an angle of θ_1 and θ_2 with repsect to radius as shown in Fig. 5.10.

5.4 The Overall System Model

The overall system model illustrated in Fig. 5.11 is obtained by assembling the models of each of the three sub-systems. This physical model has to be further simplified depending upon the dynamic aspect of the machine tool that is to be analyzed. Since, the primary interest in this investigation is to determine the influence of the machining process on the machine tool-workpiece, a simpler model based on the following assumptions is proposed.

a) The force system on the cutting tool is taken equal and opposite to that acting on the workpiece. By this assumption, the stiffness of the cutting tool along the radial direction becomes infinite.

b) All the bearings are considered to possess infinite stiffness and a very small amount of damping.

c) The interaction between the pressure head and the boring bar is negligible compared to the interaction between the rest and the boring bar.

d) In the case of a rotating boring bar-stationary workpiece the gears of the spindle are locked and hence the section of the shaft to the left of the gear represented by a mass M_G and moment of inertia I_G does not play any significant role. This locking is assumed to have the same end conditions as that of a fixed beam.

e) The conditions for the interaction between the workpiece and the pressure head, the boring bar and the drive unit are similar to that

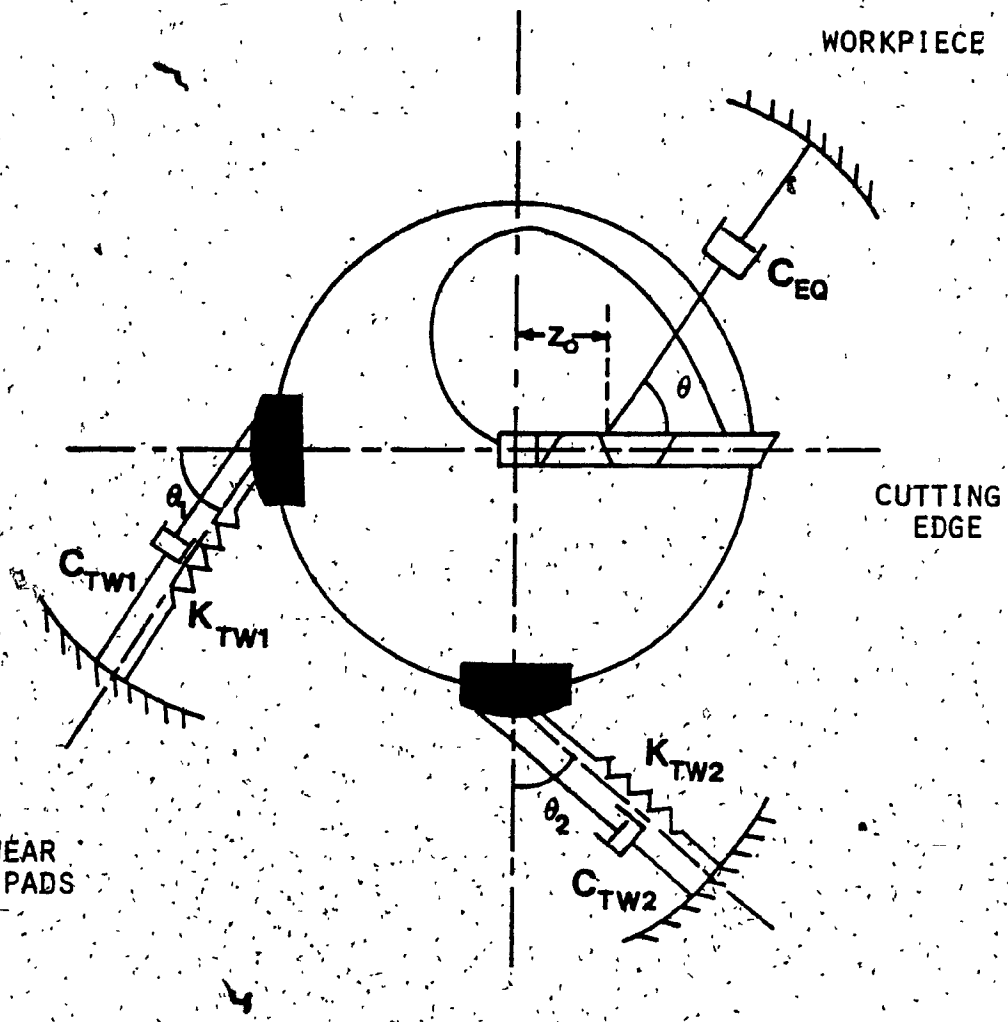

Fig. 5.10: Model of Interaction Between Cutting Tool and Workpiece

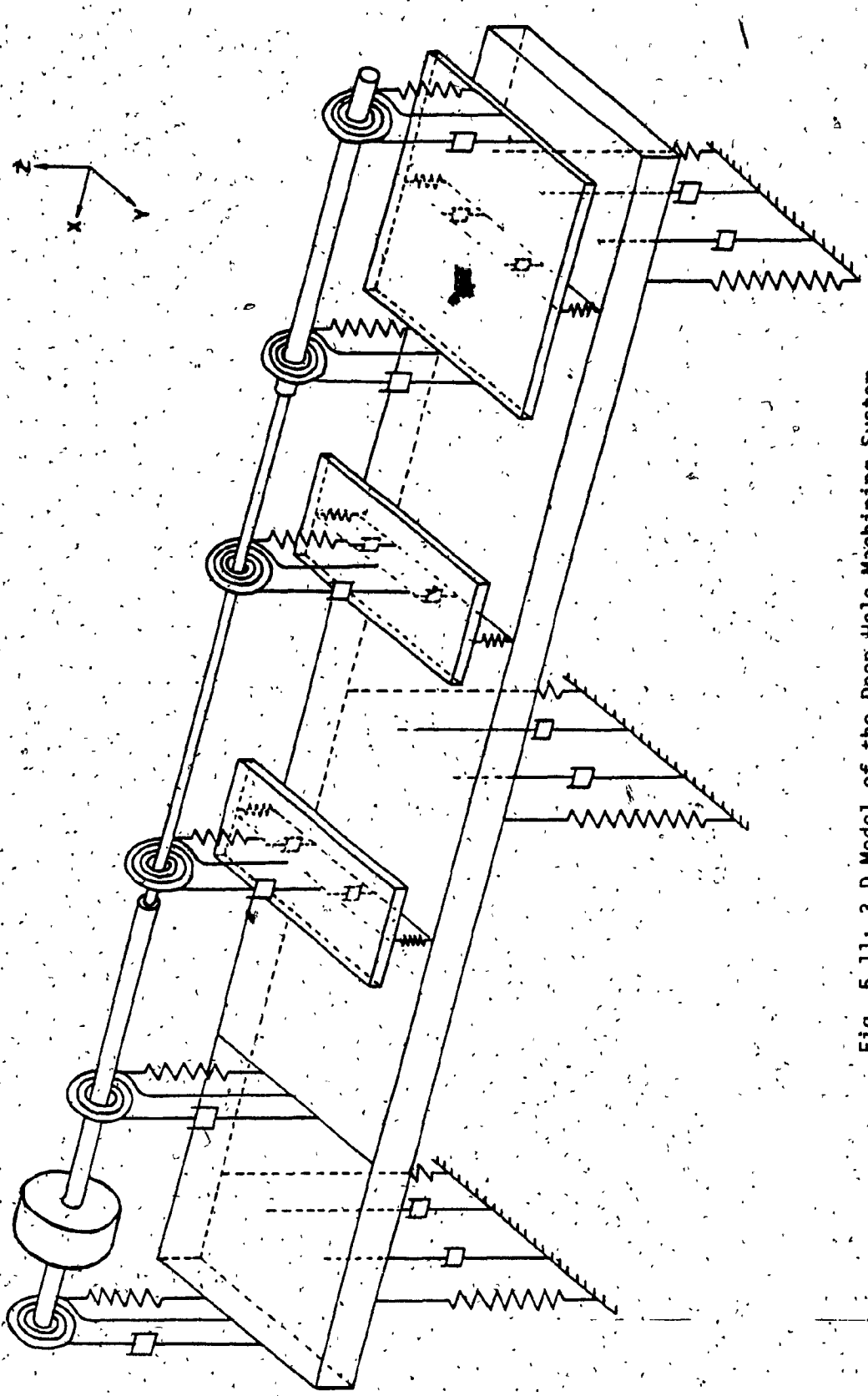

Fig. 5.11: 3-D Model of the Deep-Hole Machining System

of a fixed beam, but in the case of the torsional vibrations, the interaction between the work and the pressure head is taken to be similar to that of a free end of a beam.

f) The bearings in the spindle [in the case of a rotating workpiece-stationary bar and a counter-rotating case] and the rest behave like simple supports.

g) The translational displacements and rocking of the lathe bed are small, because of high rigidity.

h) The transmission of vibration between the boring bar and the spindle is small and can be neglected due to the large inertia of the lathe bed.

In view of these assumptions, the models of the spindle workpiece system for (a) rotating workpiece, (b) stationary workpiece are reduced to that shown in Figs. 5.12(a) and 5.12(b) respectively. The model of the boring bar-drive unit system is described in Fig. 5.12(c).

5.5 The BTA Force System

The cutting forces acting on the cutting edge are balanced at the pads resulting in a burnishing action. The resultant force system based on the major axis of the cutting tool consists of 26 major force components and can be identified as shown in Fig. 5.13. These forces can be classified into four groups [80], which are, Oil Forces, Cutting Forces, Burnishing Forces, Friction Forces and are briefly explained below.

Oil Forces: Since the oil is under pressure, it exerts axial force O_a. In addition, when the boring bar is rotating about its axis, the oil is

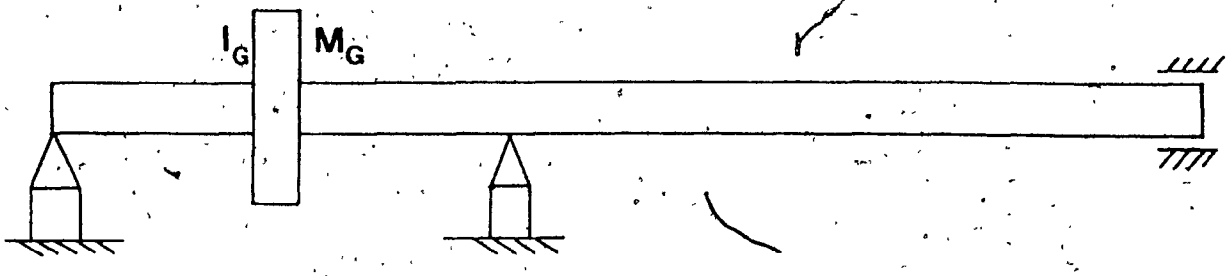

a) Model of Spindle-Workpiece (Rotating)

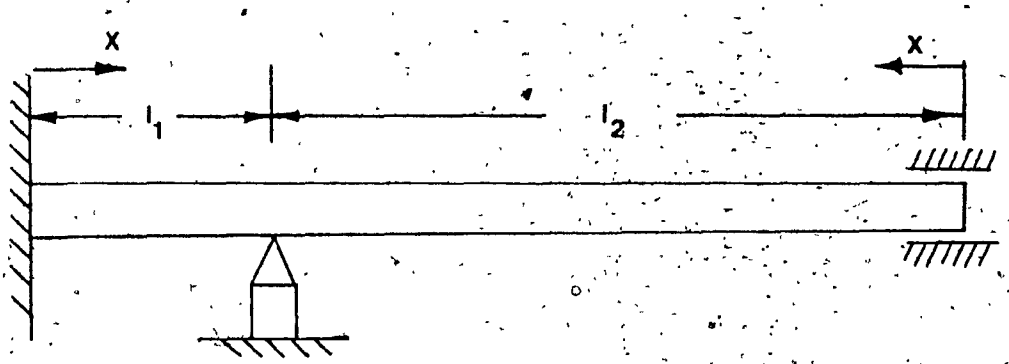

b) Model of Spindle-Workpiece (Fixed)

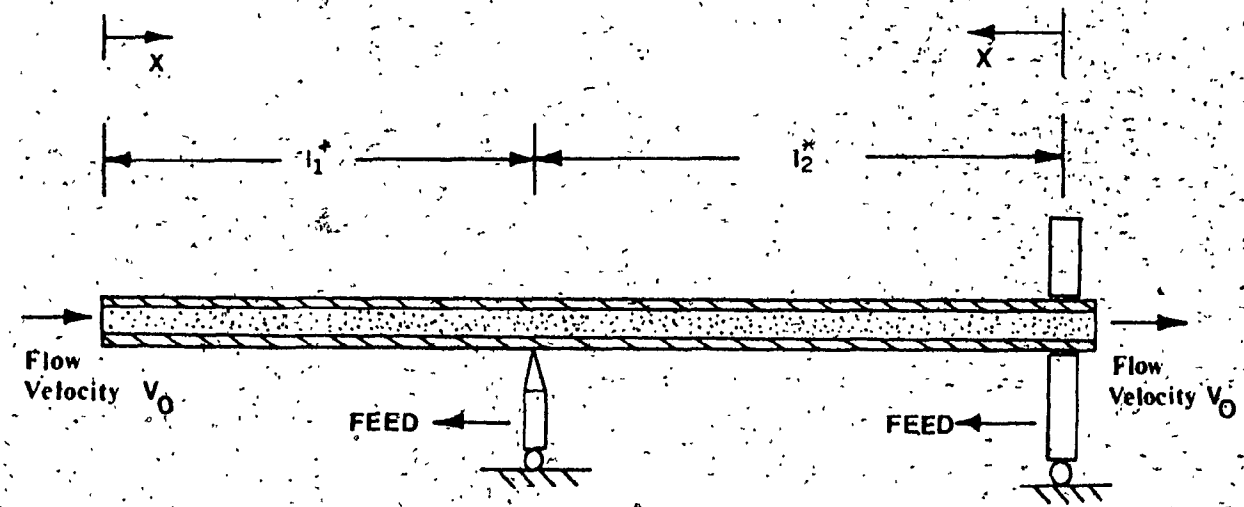

c) Model of the Cutting Tool Boring Bar System

Fig. 5.12: Simplified Model of the Machine Tool

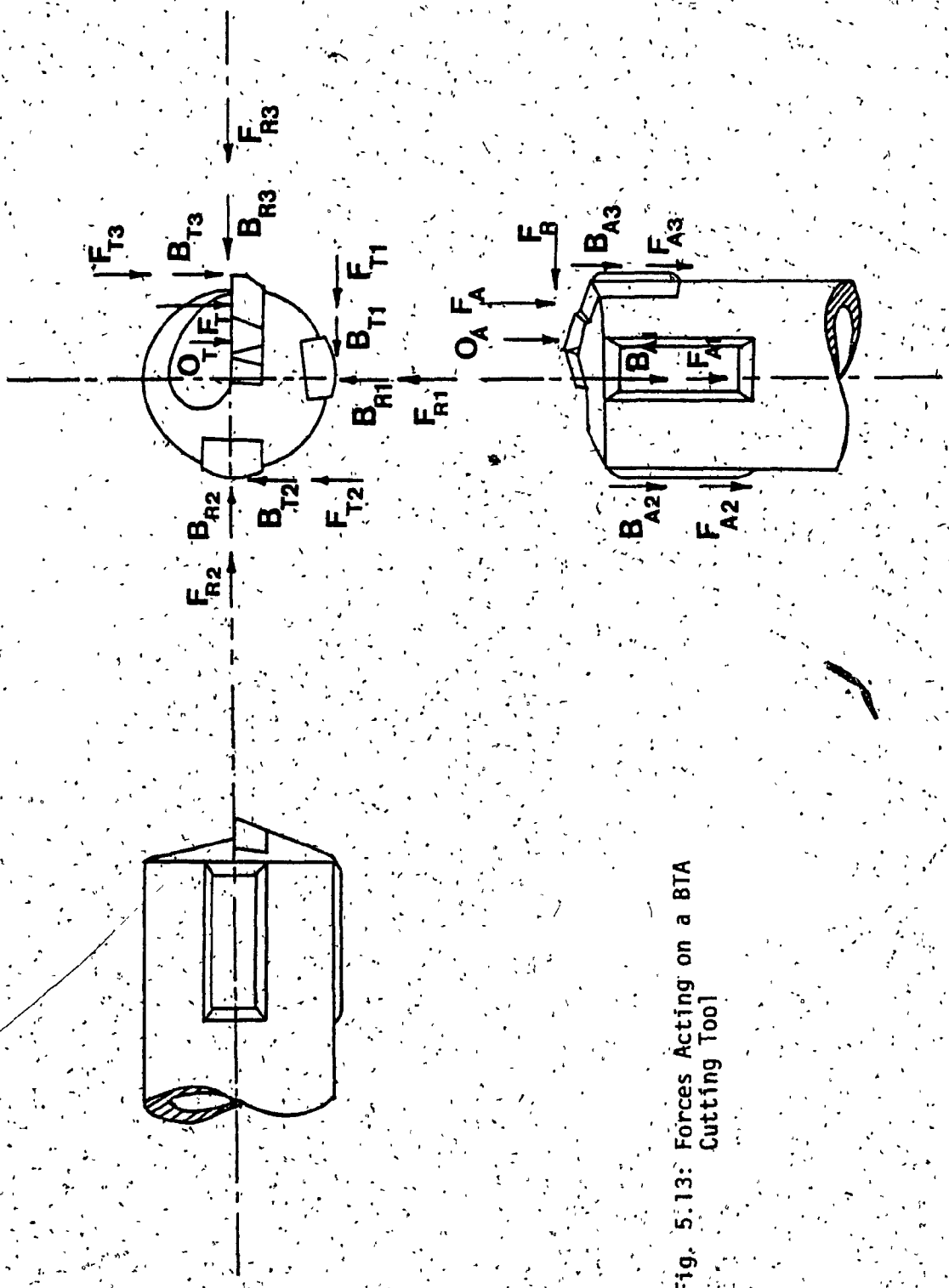

Fig. 5.13: Forces Acting on a BTA Cutting Tool

paddled, giving rise to a tangential force O_T acting at a distance "h_o" from the axis of the boring bar.

Cutting Forces: Metal removal occurs at the cutting edge resulting in the cutting forces F_a, F_T and F_R. These forces act at a distance "h" from the axis of the cutting tool. This force system can be replaced by the three forces F_a, F_R and F_T acting at the center of the tool along with a torque [111].

Burnishing Forces: Burnishing occurs at the front of the pads and can be represented by forces B_{T_1}, B_{a_1}, and B_{R_1} at the 90° pad and forces B_{T_2}, B_{a_2}, and B_{R_2} at the 180° pad. It is also possible that some burnishing accompanies the metal removal as the ridge is truncated by a high negative rake cutting edge. This is represented by B_{T_3}, B_{R_3}, and B_{a_3}.

Friction Forces: The wear pads rub against the bore wall in an oil medium and help to provide the self guiding reaction forces. This rubbing action results in frictional forces, F_{T_1}, F_{a_1}, and F_{R_1} at the 90° pad and forces F_{T_2}, F_{a_2}, and F_{R_2} at the 180° pad. These forces will act over the portions of each pad which are not involved in burnishing. It is also likely that some frictional force will be present as the ridge is truncated yielding frictional forces F_{T_3}, F_{a_3}, and F_{R_3}.

A further set of forces can also be identified which are the out-of-balance forces caused by the asymmetrical BTA cutting tool as it rotates. But these out of balance forces have been shown to be small [80] and can be neglected.

On the basis of the force system that has been identified it is possible to derive the resultant force system acting both on the

workpiece and on the cutting tool-boring bar system. In this manner, the resultant axial force and torque acting on the cutting tool are given by

$$F_{aR} = O_a + F_a + \sum_{i=1}^{3} (B_{ai} + F_{ai})$$

$$T_R = O_T h_o + T + \sum_{i=1}^{3} \frac{d}{2} (B_{Ti} + F_{Ti})$$

It was previously shown [112] that the resultant axial force and torque are stochastic in nature and that the dynamic fluctuations form an appropriate wide band process with a gaussian probability density distribution. These characteristics will be used to describe the complete forcing function on the machine tool-workpiece system.

5.6 Free Lateral Vibration of the Cutting Tool-Boring Bar System

The model of the cutting tool-boring bar system shown in Fig. 5.12 (c) has two distinct regions in view of three distinct support conditions. Therefore, the mode shapes in the two regions will be difficult. These can be represented by the equations [113].

$$\Phi_1(x) = A_1 \cosh\beta x + B_1 \sinh\beta x + C_1 \cos\beta x + D_1 \sin\beta x \qquad (5.1)$$

$$\Phi_2(x) = A_2 \cosh\beta x + B_2 \sinh\beta x + C_2 \cos\beta x + D_2 \sin\beta x \qquad (5.2)$$

because $\Phi_1(x)$ and $\Phi_2(x)$ have to satisfy the condition that their respective fourth derivatives are equal to a constant multiplied by the functions. The constants A_1, B_1, C_1, D_1, A_2, B_2, C_2, and D_2 are evaluated using the following boundary conditions

$$\Phi_1(0,t) = \Phi_2''(0,t) = 0$$

$$\Phi_1'(0,t) = \Phi_2'''(0,t) = 0$$

$$\Phi_1(\ell_1^*,t) = \Phi_2(\ell_2^*,t) = 0$$

$$\Phi_1'(\ell_1^*,t) = \Phi_2'(\ell_2^*,t)$$

$$\Phi_1''(\ell_1^*,t) = \Phi_2''(\ell_2^*,t)$$

Substituting the boundary conditions into equations (5.1) and (5.2) and solving for the constants the equations representing the mode shapes can be written as

$$\Phi_{1r}(x) = \left[\cosh p_r \frac{x}{\ell_1^*} - \cos p_r \frac{x}{\ell_1^*}\right] - h_r \left[\sinh p_r \frac{x}{\ell_1^*} - \sin p_r \frac{x}{\ell_1^*}\right]$$

$$\Phi_{2r}(x) = \left[\cosh p_r^* \frac{x}{\ell_2^*} + \cos p_r^* \frac{x}{\ell_2^*}\right] - h_r^* \left[\sinh p_r^* \frac{x}{\ell_2^*} + \sin p_r^* \frac{x}{\ell_2^*}\right]$$

Here the values of the constants p_r, p_r^*, h_r, and h_r^* are determined from the frequency equation

$$\left[(\cosh\beta\ell_1^* \cos\beta\ell_1^* - 1)(\cos\beta\ell_2^* \sinh\beta\ell_2^* + \sin\beta\ell_2^* \cosh\beta\ell_2^*)\right] -$$

$$\left[(\cosh\beta\ell_1^* \cos\beta\ell_1^* - 1)(\cos\beta\ell_1^* \sinh\beta\ell_1^* - \cosh\beta\ell_1^* \sin\beta\ell_1^*)\right] = 0$$

The values of p_r, p_r^*, h_r and h_r^* are tabulated in Table 5.1 for the first five modes of vibration and different values of (ℓ_1^*/ℓ_2^*). In the case of BTA deep-hole machining, the ratio of ℓ_2^* to ℓ_1^* is unity as the rest is placed in the middle of the boring bar. Based on this the natural frequencies of the system for the first five modes of vibration are given by the equation

Table 5.1: Constants for Mode Shapes

ℓ_2^*/ℓ_1^*	Mode No.	p_r	p_r^*	h_r	h_r^*
1	1	3.92660	3.92660	1.00077740	1.00077718
	2	7.06858	7.06858	1.00000140	1.00000146
	3	10.21020	10.21020	1.00000000	1.00000001
	4	13.35180	13.35180	1.00000000	1.00000000
	5	16.49340	16.49340	1.00000000	1.00000000
2	1	1.10770	2.21540	2.71477753	0.94755934
	2	3.21054	6.42108	1.07786816	0.92781475
	3	6.27941	12.55820	0.99624393	1.00377023
	4	9.42494	18.84988	1.00016136	0.99983867
	5	12.56636	25.13272	0.99999303	1.00000697
3	1	0.69045	2.07135	4.34655945	1.45928344
	2	1.80362	5.41086	1.69098657	0.73537417
	3	3.17990	9.53970	1.08327118	0.92314868
	4	4.70357	14.11071	0.98251458	1.01846565
	5	6.28131	18.84393	0.996258110	1.00375595

$$\omega_r = \left[\frac{p_r + p_r^*}{\ell_1^* + \ell_2^*}\right]^2 \left[\frac{EIg}{\gamma S}\right]^{\frac{1}{2}}$$

where

$$I = \frac{\pi}{64} d^4 \quad \text{and} \quad S = \frac{\pi}{4} d^2$$

In the above mentioned calculation, the following values represent the properties of the boring bar

$$E = 2 \times 10^{11} \text{ N/m}^2$$

$$\gamma = 76036 \text{ N/m}^3$$

$$2\ell = (\ell_1^* + \ell_2^*) = 1.8288 \text{ m}$$

The results obtained are tabulated in Table 5.2 for various diameters of cutting tools. Also, the first two mode shapes for the boring bar vibration are presented in Fig. 5.14(a). As can be seen from the figure, the number of nodes in the first mode of vibration is one and in the second mode it is three. More nodes appear in the region between the pinned and free end due to the nature of the boundary conditions.

5.7 Free Lateral Vibration of the Spindle-Workpiece Assembly

The model of the spindle-workpiece assembly for the case of a stationary workpiece was presented in Fig. 5.12(b) for a free vibration analysis, it must be recognized that the spindle-workpiece assembly has two distinct regions with distinct mode shapes in the two regions. Taking the mode shapes in terms of the equations

$$\Psi_1(x) = A_1^* \cosh\beta x + B_1^* \sinh\beta x + C_1^* \cos\beta x + D_1^* \sin\beta x \qquad (5.3)$$

$$\Psi_2(x) = A_2^* \cosh\beta x + B_2^* \sinh\beta x + C_2^* \cos\beta x + D_2^* \sin\beta x \qquad (5.4)$$

Table 5.2: Natural Frequencies of the Boring Bar $(\ell_2^*/\ell_1^*) = 1$

Diameter of Cutting Tool (mm)	Mode	Natural Frequency (Hz)
19.05	1	453.76
	2	1470.47
	3	3068.02
	4	5246.50
	5	8005.91
22.225	1	529.38
	2	1715.54
	3	3579.36
	4	6120.92
	5	9340.23
25.4	1	605.00
	2	1960.62
	3	4090.70
	4	6995.34
	5	10674.55
28.575	1	680.64
	2	2205.70
	3	4601.32
	4	7869.75
	5	12008.86
31.75	1	756.26
	2	2450.77
	3	5113.38
	4	8744.17
	5	13343.18

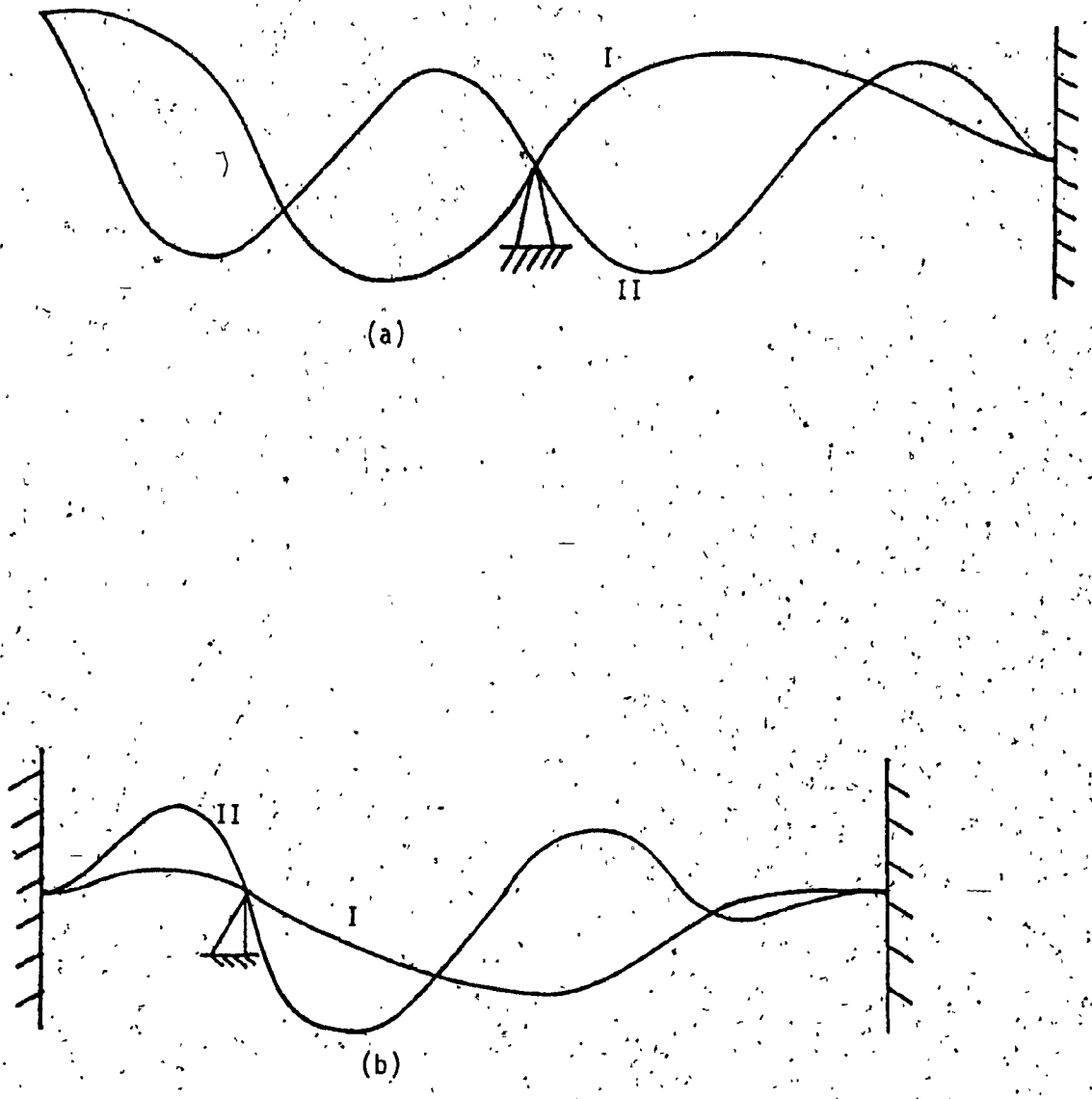

Fig. 5.14: Mode Shapes for the First Two Modes of Vibration
(a) Cutting Boring Bar Assembly
(b) Spindle-Workpiece Assembly

the constants A_1^*, A_2^*, B_1^*, B_2^*, C_1^*, C_2^*, D_1^*, D_2^* can be evaluated based on the set of boundary conditions, and are

$$\Psi_1(0,t) = \Psi_2(0,t) = 0$$

$$\Psi_1'(0,t) = \Psi_2'(0,t) = 0$$

$$\Psi_1(\ell_1,t) = \Psi_2(\ell_2,t) = 0$$

$$\Psi_1'(\ell_1,t) = \Psi_2'(\ell_2,t)$$

$$\Psi_1''(\ell_1,t) = \Psi_2''(\ell_2,t)$$

Substituting the boundary conditions into equations (5.3) and (5.4) and solving for the constants, the equations representing the mode shapes in the two regions of the workpiece-assembly can be written as

$$\Psi_{1r}(x) = \left(\cosh q_r \frac{x}{\ell_1} - \cos q_r \frac{x}{\ell_1}\right) - u_r \left(\sinh q_r \frac{x}{\ell_1} - \sin q_r \frac{x}{\ell_1}\right)$$

$$\Psi_{2r}(x) = \left(\cosh q_r^* \frac{x}{\ell_2} - \cos q_r^* \frac{x}{\ell_2}\right) - u_r^* \left(\sinh q_r^* \frac{x}{\ell_2} - \sin q_r^* \frac{x}{\ell_2}\right)$$

where the constants q_r, q_r^*, u_r and u_r^* are obtained from the frequency equation

$$\left[(\cosh\beta\ell_1 \cos\beta\ell_1 - 1)(\cosh\beta\ell_2 \sin\beta\ell_2 - \cos\beta\ell_2 \sinh\beta\ell_2)\right]$$

$$= \left[(\cosh\beta\ell_2 \cos\beta\ell_2 - 1)(\cos\beta\ell_1 \sinh\beta\ell_1 - \cosh\beta\ell_1 \sin\beta\ell_1)\right]$$

The values of q_r, q_r^*, u_r, and u_r^* are tabulated in Table 5.3 for the first five modes of vibrations for a ratio of (ℓ_2/ℓ_1) equal to 3 as is the case for the system under consideration. Also, the natural frequencies for the first five modes of the spindle-workpiece assembly are determined using

Table 5.3: Constants for Mode Shapes of Spindle Workpiece Assembly

ℓ_2/ℓ_1	Mode No.	q_r	q_r^*	u_r	u_r^*
3	1	1.81382	5.44146	1.6820986	0.9878791
	2	3.17978	9.53934	1.0832927	1.0001265
	3	4.70357	14.11071	0.9825146	1.0000014
	4	6.281307	18.84392	0.9962581	1.0000000
	5	7.854370	23.56311	1.0007773	1.0000000

$$\omega_r = \left[\frac{q_r + q_r^*}{\ell_1 + \ell_2}\right]^2 \left[\frac{EIg}{\gamma S}\right]^{\frac{1}{2}}$$

where

$$I = \frac{\pi}{64} d_S^4 \quad \text{and} \quad S = \frac{\pi}{4} d_S^2.$$

The values of ω_r are presented in Table 5.4. In these calculations the properties of the spindle-workpiece assembly are measured and taken as

$$E = 2 \times 10^{11} \text{ N/m}^2$$

$$\gamma = 76036 \text{ N/m}^3$$

$$(\ell_1 + \ell_2) = 1.2192 \text{ m}$$

$$d_S = 0.1016 \text{ m}$$

Also, the first two mode shapes for the spindle-workpiece assembly are shown in Fig. 5.14(b). As seen from the figure, there are no nodes in the first mode of vibration due to identical boundary conditions in both the regions of the spindle workpiece system. In the second mode two nodes are present in the region between the workpiece and the pressure head because the length in this region is three times that between the gear and the bearing.

5.8 Forced Vibration Analysis of the Cutting Tool-Boring Bar System

The cutting tool boring bar system is acted upon by a resultant axial force and torque. In view of the symmetric cross-section of the system and also due to the fact that the cross-section is circular, the effect of axial force and torque can be considered separately [114].

The mathematical descriptions of the static and dynamic components

Table 5.4: Natural Frequencies of Spindle-Workpiece Assembly

ℓ_2/ℓ_1	Mode No.	Natural Frequency [Hz]
3	1	4646.98
	2	14281.59
	3	31249.10
	4	55729.15
	5	87137.49

of the axial force have already been established [112] wherein it is shown that the dynamic fluctuations can be represented by a Gaussian, wide band (band limited) stationary process. Thus, the equations of motion arising due to the influence of the axial force on the cutting tool-boring bar assembly can be derived from the Lagrange's equation namely

$$\frac{d}{dt}\left(\frac{\partial T}{\partial \dot{\xi}_i}\right) - \frac{\partial T}{\partial \xi_i} + \frac{\partial V}{\partial \xi_i} + \frac{\partial D}{\partial \dot{\xi}_i} = Q_i \tag{5.5}$$

The kinetic energy T of the system is

$$T = \frac{1}{2}\int_0^{\ell} m_b \dot{r}_1^2\, dx + \frac{1}{2}\int_0^{\ell} m_b \dot{r}_2^2\, dx + \frac{1}{2}\int_0^{\ell} I_x \omega_0^2\, dx + \frac{1}{2}\int_0^{\ell} I_x \omega_0^2\, dx$$

$$+ \frac{1}{2}\int_0^{\ell} \mu_c \left[\nu_o^2 + \left(\frac{\omega_o d_i}{4}\right)^2 + (\dot{r}_1 + \nu_o r_1')^2\right] dx$$

$$+ \frac{1}{2}\mu_c \int_0^{\ell} \left[\nu_o^2 + \left(\frac{\omega_o d_i}{4}\right)^2 + (\dot{r}_2 + \nu_o r_2')^2\right] dx$$

$$+ \frac{1}{2}\left[I_t \int_0^{\ell} \left\{\left[\frac{d}{dt}\left(\frac{dr_1}{dx}\right)\right]^2 + \omega_p^2\right\} dx + \int_0^{\ell} \left\{\left[\frac{d}{dt}\left(\frac{dr_2}{dx}\right)\right]^2 + \omega_p^2\right\} dx\right]$$

where the last term represents the kinetic energy due to precession [115] and since the rest is in the midpoint, $\ell_1^* = \ell_2^* = \ell$. The potential energy V stored in the system is

$$V = \frac{1}{2} EI\left[\int_0^{\ell} \left(\frac{\partial^2 r_1}{\partial x^2}\right)^2 dx + \int_0^{\ell} \left(\frac{\partial^2 r_2}{\partial x^2}\right)^2 dx\right]$$

$$- \frac{1}{2} F_a\left[\int_0^{\ell} \left(\frac{\partial r_1}{\partial x}\right)^2 dx + \int_0^{\ell} \left(\frac{\partial r_2}{\partial x}\right)^2 dx\right]$$

$$D = \frac{C_b}{2}\left[\int_0^{\ell}\left(\frac{\partial r_1}{\partial t}\right)^2 dx + \int_0^{\ell}\left(\frac{\partial r_2}{\partial t}\right)^2 dx\right]$$

Substituting the expressions for T, V, and D into the Lagrange's equation, using the assumed modes method by which

$$r_1(x,t) = \sum_{j=1}^{n} \phi_{1j}(x)\, \xi_j(t)$$

$$r_2(x,t) = \sum_{j=1}^{n} \phi_{2j}(x)\, \xi_j(t)$$

and performing certain mathematical transformations using the orthogonality relation [106] the equations representing the influence of the axial force on the cutting tool-boring bar system can be obtained in the form

$$[M][\ddot{X}] + [C][\dot{X}] + [\{K\} + \{F(t)\}][X] = 0 \qquad (5.6)$$

where

$$[M] = \begin{bmatrix} 2\ell(m_b + \mu_c) + I_t(M_{11} + M_{11}^*) & I_t(M_{12} + M_{12}^*) & \cdots & I_t(M_{1n} + M_{1n}^*) \\ I_t(M_{21} + M_{21}^*) & 2\ell(m_b + \mu_c) + I_t(M_{22} + M_{22}^*) & \cdots & I_t(M_{2n} + M_{2n}^*) \\ \vdots & \vdots & & \vdots \\ I_t(M_{n1} + M_{n1}^*) & \cdots & & 2\ell(m_b + \mu_c) + I_t(M_{nn} + M_{nn}^*) \end{bmatrix}$$

$$[C] = \begin{bmatrix} 2\ell C_b & 1 & 1 & 1 \\ 1 & 2\ell C_b & 1 & 1 \\ & & & \\ 1 & 1 & & 2\ell C_b \end{bmatrix}$$

$$[K] = \begin{bmatrix} EI(p_r^{*4} + p_r^4)/\ell^3 & -\frac{\mu}{c}v_o^2(M_{12} + M_{12}^*) & -\frac{\mu}{c}v_o^2(M_{1n} + M_{1n}^*) \\ -\frac{\mu}{c}v_o^2(M_{11} + M_{11}^*) & & \\ -\frac{\mu}{c}v_o^2(M_{21} + M_{21}^*) & EI(p_r^{*4} + p_r^4)/\ell^3 & -\frac{\mu}{c}v_o^2(M_{2n} + M_{2n}^*) \\ & -\frac{\mu}{c}v_o^2(M_{22} + M_{22}^*) & \\ & & EI(p_r^{*4} + p_r^4)/\ell^3 \\ -\frac{\mu}{c}v_o^2(M_{n1} + M_{n1}^*) & & -\frac{\mu}{c}v_o^2(M_{nn} + M_{nn}^*) \end{bmatrix}$$

$$[F(t)] = \begin{bmatrix} -\frac{I_t}{I_x\omega_o^2}F_a^2 & -F_a(M_{12} + M_{12}^*) & -F_a(M_{1n} + M_{1n}^*) \\ -(M_{11} + M_{11}^*)F_a & & \\ -F_a(M_{21} + M_{21}^*) & -\frac{I_t F_a^2}{I_x\omega_o^2} & -F_a(M_{2n} + M_{2n}^*) \\ & -(M_{22} + M_{22}^*)F_a & \\ & & -\frac{I_t}{I_x\omega_o^2}F_a^2 \\ -F_a(M_{n1} + M_{n1}^*) & -F_a(M_{n2} + M_{n2}^*) & -(M_{nn} + M_{nn}^*)F_a \end{bmatrix}$$

and

$$[X]^T = [\xi_1\ \xi_2\ \xi_3 \ldots\ldots \xi_n]$$

Further,

$$\int_0^{\ell} \Phi'_{1i}(x)\ \phi'_{1j}(x)\ dx = M_{ij}$$

$$\int_0^{\ell} \Phi'_{2i}(x)\ \Phi'_{2j}(x)\ dx = M_{ij}^*$$

Only the fundamental mode of vibration is considered because the cutting forces can be measured without distortion only up to about 350 Hz and the power spectral density is comparitively small beyond about 350 Hz leading to the fact that the boring bar-cutting tool assembly will be vibrating predominantly in the fundamental mode. Therefore equation (5.6) can be simplified as

$$\ddot{\xi} + C_b^*\dot{\xi} + K^*\,[1 - Y^*F_a - Z^*F_a\,]\xi = 0 \qquad (5.7)$$

where

$$C_b^* = \frac{2\ell C_b}{2\ell(m_b + \mu_c) + I_t(M_{11} + M_{11}^*)}$$

$$K^* = \frac{(EI(p_r^4 + p_r^{*4})/\ell^3) - \mu_c v_o^2(M_{11} + M_{11}^*)}{2(m_b + \mu_c) + I_t(M_{11} + M_{11}^*)}$$

$$Y^* = \frac{I_t}{I_x^2\omega_o^2[\{EI(p_r^4 + p_r^{*4})/\ell^3\} - \mu_c v_o^2(M_{11} + M_{11}^*)]}$$

$$Z^* = \frac{M_{11} + M_{11}^*}{\left\{EI(p_r^4 + p_r^{*4})/\ell^3\right\} - \mu_c v_o^2 (M_{11} + M_{11}^*)}$$

The influence of torque, whose dynamic fluctuations have been represented by a wide band gaussian distributed stationary process, on the boring bar-cutting tool assembly is found in a manner similar to that for the treatment of the axial force. During the torsional mode of oscillation, the rest exerts no influence and hence the system behaves like a simple cantilever beam under the action of a torque. Thus, the boundary conditions are

$$\theta(0,t) = 0$$

$$JG \left.\frac{\partial\theta}{\partial x}\right|_{x=2\ell} = T(t).$$

The deep-hole machining operation takes place in an oil medium and the oil film between the surface of the hole and the pad is assumed to be a thin film. As can be seen in Fig. 5.15, which shows the variation of co-efficient of kinetic friction with velocity, the slope of the f-v curve is negative in the thin film zone. So, a phenomenon of stick slip takes place. Now, the mathematical model representing the influence of the torsion on the boring bar cutting tool system can be derived using the Lagrange's equation given by equation (5.5). In this case,

$$T = \frac{1}{2}\left[\int_0^{2\ell} I_x(\omega + \dot{\theta})^2 \, dx + \int_0^{2\ell} \mu_c \left\{\left[(\omega + \dot{\theta})\frac{D_i}{4}\right]^2 + v_o^2\right\}\right] dx$$

$$V = \frac{1}{2}\int_0^{2\ell} GJ \left(\frac{\partial\theta}{\partial x}\right)^2 dx$$

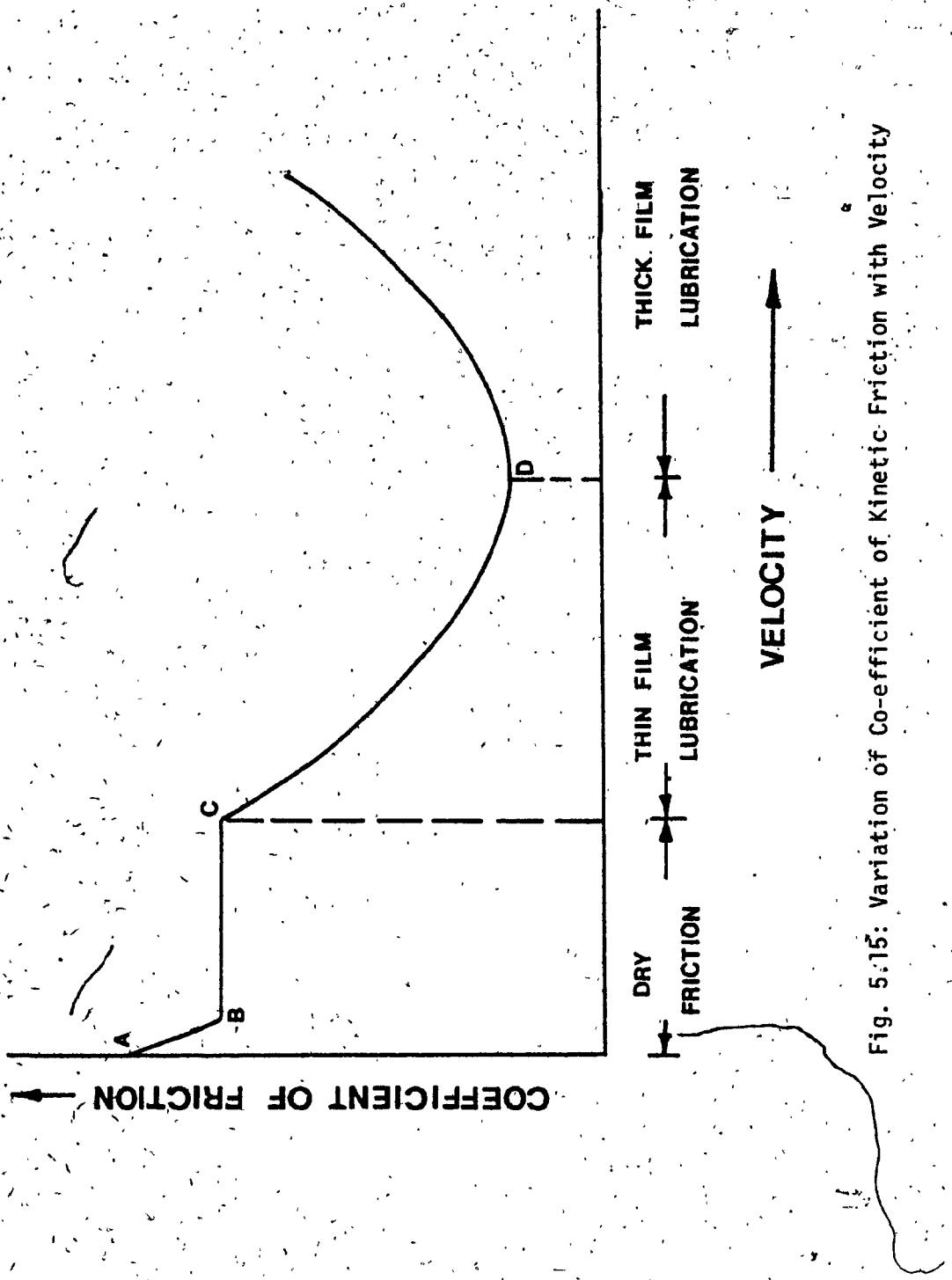

Fig. 5.15: Variation of Co-efficient of Kinetic Friction with Velocity

and

$$D = \frac{1}{2}\left[\int_0^{2\ell} C_T\dot{\theta}^2 dx + \int_0^{2\ell}\int_0^{\dot{\theta}} \Phi(\omega+\dot{\theta})\, dx d\dot{\theta}\right]$$

Expanding $\Phi(\omega+\dot{\theta})$ as a Taylor's series about ω and taking only the first two terms, the expression for D can be re-written as

$$D = \frac{1}{2}\left[\int_0^{2\ell}\left\{C_T\dot{\theta}^2 + \frac{\Phi'(\omega)\dot{\theta}^2}{2\ell} + \frac{\Phi(\omega)\dot{\theta}}{\ell}\right\} dx\right]$$

Substituting the expression for T, V, and D into the Lagrange's equation and using the assumed modes method by which

$$\theta(x,t) = \sum_{j=1}^{n} \pi_j(x)\, \eta_j(t)$$

where

$$\pi_j(x) = \sin(2j-1)\frac{\pi x}{4\ell}$$

and performing certain mathematical transformations using the orthogonality relationships, the equation representing the action of torque on the fundamental mode of vibration is obtained in the form,

$$\ddot{\eta} + C_T^*\dot{\eta} + K_T^*\eta + N = T(t) \qquad (5.8)$$

Here

$$C_T^* = \frac{(C_T + \Phi'(\omega)/2\ell)}{(I_X + \mu_c d_i^2/16)}$$

$$K_T^* = \frac{X_{11} JG}{(I_X + \mu_c d_i^2/16)\ell}$$

$$N = \frac{\Phi(\omega)}{2\ell^2[I_x + \mu_c d_i^2/16]}$$

Thus, equations (5.7) and (5.8) describe the dynamic behaviour of the cutting-tool boring bar system for the case when the cutting tool is rotating. The solutions to these stochastic differential equations will lead to the determination of the response of the system under the action of the stochastically varying resultant force system.

5.9 Forced Vibration Analysis of the Spindle-Workpice Assembly

The resultant force system on the spindle-workpice assembly will be equal and opposite to the force on the cutting tool with influence of the interaction neglected. In view of the symmetric cross-section of the shaft representing the spindle-workpiece assembly and due to the fact that the cross-section is circular the effect of axial force and torque can be considered separately, to set up the equations of motion.

The response of the spindle-workpiece assembly under the action of the axial force can be found from the Lagrange's equation with

$$T = \frac{1}{2} m_s \left[\int_0^{\ell_1} \left(\frac{\partial r_1}{\partial t} \right)^2 dx + \int_0^{\ell_2} \left(\frac{\partial r_2}{\partial t} \right)^2 dx \right]$$

$$V = \frac{1}{2} \left[EI \left\{ \int_0^{\ell} \left(\frac{\partial^2 r_1}{\partial x^2} \right)^2 dx + \int_0^{\ell_2} \left(\frac{\partial^2 r_2}{\partial x^2} \right)^2 dx \right\} - F_a \left\{ \int_0^{\ell_1} \left(\frac{\partial r_1}{\partial x} \right)^2 dx + \int_0^{\ell_2} \left(\frac{\partial r_2}{\partial x} \right)^2 dx \right\} \right]$$

and,

$$D = \frac{1}{2} C_S \left[\int_0^{\ell} \left(\frac{\partial r_1}{\partial t} \right)^2 dx + \int_0^{\ell_2} \left(\frac{\partial r_2}{\partial t} \right)^2 dx \right]$$

Substituting the expressions for T, V, and D into the Lagrange's equation and using the assumed modes method by which

$$r_1(x,t) = \sum_{j=1}^{n} \Psi_{1j}(x)\, \zeta_j(t)$$

$$r_2(x,t) = \sum_{j=1}^{n} \Psi_{2j}(x)\, \zeta_j(t)$$

and performing certain mathematical transformations using the orthogonality relation, the equation representing the influence of the axial force are obtained as

$$[M][\ddot{Y}] + [C][\dot{Y}] + [\{K\} + \{F(t)\}][Y] = 0 \qquad (5.9)$$

$$[M] = \begin{bmatrix} m_S(\ell_1+\ell_2) & 0 & 0 & 0 & 0 \\ 0 & m_S(\ell_1+\ell_2) & 0 & 0 & 0 \\ & & & & \\ 0 & & & & m_S(\ell_1+\ell_2) \end{bmatrix}$$

$$[C] = \begin{bmatrix} C_S(\ell_1+\ell_2) & 0 & 0 & & 0 \\ 0 & C_S(\ell_1+\ell_2) & 0 & & 0 \\ & & & & \\ 0 & & & & C_S(\ell_1+\ell_2) \end{bmatrix}$$

$$[K] = \begin{bmatrix} EI\left[\frac{q_r^4}{\ell_1^3} + \frac{q_r^{*4}}{\ell_2^3}\right] & 0 & 0 & 0 & 0 \\ 0 & EI\left[\frac{q_r^4}{\ell_1^3} + \frac{q_r^{*4}}{\ell_2^3}\right] & 0 & & 0 \\ & & & & \\ 0 & & & & EI\left[\frac{q_r^4}{\ell_1^3} + \frac{q_r^{*4}}{\ell_2^3}\right] \end{bmatrix}$$

$$[F(t)] = \begin{bmatrix} -F_a(P_{11} + P_{11}^*) & -F_a(P_{12} + P_{12}^*) & & -F_a(P_{1n} + P_{1n}^*) \\ -F_a(P_{21} + P_{21}^*) & -F_a(P_{22} + P_{22}^*) & & -F_a(P_{2n} + P_{2n}^*) \\ & & & \\ -F_a(P_{n1} + P_{n1}^*) & & & -F_a(P_{nn} + P_{nn}^*) \end{bmatrix}$$

and

$$[Y]^T = [\zeta_1 \; \zeta_2 \; \cdots \; \zeta_n]$$

Further,

$$\int_0^{\ell} \Psi'_{1j}(x) \, \Psi'_{1k}(x) \, dx = P_{jk}$$

$$\int_0^{\ell} \Psi'_{2j}(x) \, \Psi'_{2k}(x) \, dx = P_{jk}^*$$

Only the fundamental mode of vibration is considered because the first natural frequency of the spindle-workpiece assembly is much higher than the frequency of the cutting forces and thus it can be expected that the

system vibration would only correspond to the fundamental mode of vibration. Therefore equation (5.9) gets reduced to

$$\ddot{\zeta} + C_S^* \dot{\zeta} + K_1^* (1 - K_2^* F_a)\zeta = 0 \qquad (5.10)$$

where

$$C_S^* = C_S/m_S$$

$$K_1^* = \frac{EI\left[\frac{q_r^4}{\ell_1^3} + \frac{q_r^{*4}}{\ell_2^3}\right]}{m_S(\ell_1 + \ell_2)}$$

$$K_2^* \quad \frac{(P_{11} + P_{I1}^*)}{EI\left[\frac{q_r^4}{\ell_1^3} + \frac{q_r^{*4}}{\ell_2^3}\right]}$$

Similarly, the response of the system under the action of the torque can be determined. In this case,

$$T = \frac{1}{2}\int_0^{\ell_1+\ell_2} I_x^* \dot{\theta}_S^2 \, dx$$

$$V = \frac{1}{2}\int_0^{\ell_1+\ell_2} G^* J^* \left(\frac{\partial \theta_S}{\partial x}\right)^2 dx$$

and

$$D = \frac{1}{2}\left[\int_0^{\ell_1+\ell_2} \left\{ C_{ST} \dot{\theta}_S^2 + \frac{\Phi'(\omega)}{2\ell} \dot{\theta}_S^2 + \frac{\Phi(\omega)}{\ell} \dot{\theta}_S \right\} dx\right]$$

Substituting the expressions for T, V, and D into equation (5.5) and

again assuming the modes as

$$\theta_S(x,t) = \sum_{j=1}^{n} \alpha_j^*(x)\, \theta_S(t) ,$$

with

$$\alpha_j^*(x) = \sin (2j-1) \frac{\pi x}{2(\ell_1 + \ell_2)}$$

and performing certain mathematical transformations using the orthogonality relationships the equation representing the influence of torque on the fundamental mode of vibration is obtained as

$$\ddot{\theta}_S + C_{ST}^* \dot{\theta}_S + K_{ST}^* \theta + N^* = T(t) \qquad (5.11)$$

Here

$$C_{ST}^* = \frac{C_{ST} + \Phi'(\omega)/\ell_1+\ell_2}{I_X^*}$$

$$K_{ST}^* = \frac{G^* K_{11}^* J^*}{I_X^* K_1}$$

$$N^* = \frac{2\Phi(\omega)}{(\ell_1 + \ell_2)^2 I_X^*}$$

Thus, equations (5.10) and (5.11) describe the dynamic behaviour of the spindle-workpiece system for the case when the spindle is held stationary. The solutions to these stochastic differential equations will give the response of the system.

5.10 Conclusion

A three-dimensional representation of a deep-hole machining system is presented by modelling each of the components separately and combining them. A model of the interaction between the workpiece and the cutting tool has also been included. Such a scheme can be used to determine the response of any part of the machining system under consideration.

The resultant force due to machining consists of an axial force and torque, whose dynamic fluctuations can be represented by a stationary wide band process having a gaussian distribution. Since the vibration of the lathe bed due to resultant force system is very small, the entire machine tool has been modelled as comprising of the spindle-workpiece system and the cutting tool boring bar system. The spindle-workpiece system and the cutting tool boring bar system have circular cross-sections, so the influence of the torque and the axial force on each of the two systems can be considered separately. Using the Lagrange's equations and the assumed modes method, four stochastic differential equations are derived which describe the machine tool workpiece system for the case of a stationary workpiece rotating boring bar system. These can be used to predict the response of the system and the true motion of the tool tip as described in the next chapter.

CHAPTER 6

STOCHASTIC RESPONSE ANALYSIS AND PREDICTION OF TOOL TIP MOTION

CHAPTER 6

STOCHASTIC RESPONSE ANALYSIS AND PREDICTION OF TOOL TIP MOTION

In deep hole or gun drilling, proper guiding action is obtained due to the fact that the cutting forces are balanced by the reaction forces at the pads. This guiding action is stabilized in a manner that holes with good accuracy in size, cylindricity, and roundness are produced. Although, accurate holes can be produced in deep hole drilling, the problem of deviation of the machined hole from the required surface arises mainly due to the long slender boring bar holding the cutting tool. Such a deviation of the machined hole from the ideal surface leads to a lobing phenomenon and to the production of holes which are not smooth. Since, the tool tip motion directly dictates the actual surface produced on the workpiece, it is necessary to know completely the tool dynamic response under various operating conditions.

The phenomenon of lobing has been studied for drilling operation [89], and it has been shown that [86] this phenomenon is different in BTA deep hole machining, wherein the number of lobes formed depends upon the frequency of flexural vibrations. This particular study does not consider the influence of the random fluctuations of the resultant force system and the parametric effect of the axial force on the tool response.

This chapter of the investigation presents two methods of deriving the tool tip motion, which is one of the major influencing factors that dictate the lobing, as well as the macro and the micro geometrical errors of the drilled surface. The tool tip motion in turn depends solely upon the response of the cutting tool-boring bar assembly system and the

spindle-workpiece assembly. It may be noted, that the response of the cutting tool-boring bar assembly, and the spindle-workpiece assembly can be obtained from the four stochastic differential equations governing these system dynamics, derived in Chapter 5. These differential equations give the necessary input-output relationships between the resultant force system (which has been mathematically modelled in Chapter 4) and the two subsystems of the machine tool namely, the spindle-workpiece assembly and the cutting tool-boring bar assembly, and are now rewritten for easy representation as follows:

$$\ddot{\xi} + C_b\dot{\xi} + K^*[1 - Y^*F_a - Z^*F_a^2]\xi = 0 \tag{6.1}$$

$$\ddot{\eta} + C_T^*\dot{\eta} + K_T^*\eta + N = T(t) \tag{6.2}$$

$$\ddot{\zeta} + C_S^*\dot{\zeta} + K_1^*[1 - K_2^*F_a] = 0 \tag{6.3}$$

$$\ddot{\theta}_S + C_{ST}^*\dot{\theta} + K_{ST}^*\theta_S + N^* = T(t) \tag{6.4}$$

where

$$C_b^* = \frac{2\ell C_b}{2\ell(m_b + \mu_c) + I_t(M_{11} + M_{11}^*)}$$

$$K^* = \frac{[EI(p_r^4 + p_r^{*4})/\ell^3] - \mu_c\nu_o^2(M_{11} + M_{11}^*)}{2(m_b + \mu)\ell + I_t(M_{11} + M_{11}^*)}$$

$$Y^* = \frac{I_t}{I_x^2\omega_o^2[\{EI(p_r^4 + p_r^{*4})/\ell^3\} - \mu_c\nu_o^2(M_{11} + M_{11}^*)]}$$

$$Z^* = \frac{M_{11} + M_{11}^*}{[EI(p_r^4 + p_r^{*4})/\ell^3] - \mu_c\nu_o^2(M_{11} + M_{11}^*)}$$

$$C_T^* = \frac{(C_T + \phi'(\omega)/2\ell)}{[I_X + \mu d_1^2/16]}$$

$$K_T^* = \frac{X_{11}JG}{(I_X + \mu d_1^2/16)\ell}$$

$$N = \frac{\Phi(\omega)}{2\ell^2[I_X + \mu d_1^2/16]}$$

$$C_S^* = C_S/m_S$$

$$K_1^* = \frac{EI\left[\frac{q_r^4}{\ell_1^3} + \frac{q_r^{*4}}{\ell_2^3}\right]}{m_S(\ell_1 + \ell_2)}$$

$$K_2^* = \frac{P_{11} + P_{11}^*}{EI\left[\frac{q_r^4}{\ell_1^3} + \frac{q_r^{*4}}{\ell_2^3}\right]}$$

$$C_{ST}^* = \frac{[C_{ST} + \phi'(\omega)/\ell_1 + \ell_2]}{I_X^*}$$

$$K_{ST}^* = \frac{G^*X_{11}^*J^*}{I_X^*(\ell_1 + \ell_2)}$$

and

$$N^* = \frac{2\Phi(\omega)}{I_X^*(\ell_1 + \ell_2)^2}$$

Further,

F_a is the resultant axial force

$T(t)$ is the resultant torque

2ℓ is the length of the cutting tool boring bar system

$\ell_1 + \ell_2$ is the length of the spindle-workpiece system

$\Phi(\omega)$ is the function describing the variation of co-efficient of friction with the angular velocity

E is the Young's modulus of steel.

Equations (6.2) and (6.4) are non-parametric, non-homogeoneous differential equations of motion. The solutions to such equations have been presented in detail [121,122,123], and the same technique has been used to solve equations (6.2), and (6.4). But, equations (6.1) and (6.3) are known as parametric type of stochastic differential equations [117], solutions to these equations can be obtained using two techniques namely the averaging technique [118,119,120], and another technique which is a slight modification of the method used for the analysis of non-linear systems subjected to classical wideband or white random excitation [123]. Combining the solutions to equations (6.1), (6.2), (6.3) and (6.4), and using certain vector properties, the true motion of the cutting tool tip can be obtained in the case of a rotating cutting tool and a stationary workpiece system. Only the rotating cutting tool-stationary workpiece has been considered because this was the working system used in all the laboratory tests for the measurement and stochastic modelling of the resultant force system. Such a statistical solution for the true tool motion gives a sound mathematical basis for evaluating the possible variation in roundness at various depths

under various machining conditions. Since, these solutions explicitly depend upon time, the roundness error at any position, for a given machining condition, can take any value between the minimum error and maximum error depending upon the value of the probability density function for the response. This is later confirmed by actually measuring the roundness of the machined hole at various depths, for different machining conditions. The measurements reveal that no definite pattern exists for the roundness error variation with the depth of hole and feed.

6.1 Response due to the Axial Force on the Cutting Tool-Boring Bar System

The effect of the axial force on the cutting tool-boring bar system can be determined by solving equation (6.1), for which a mathematical model for the axial force has to be established. It was shown in Chapter 4 that the resultant axial force is stochastic in nature with a mean value which is a function of the feed and diameter, and dynamic fluctuations which are stationary, delta correlated with a gaussian probability density function. A mathematical model has been presented in Chapter 4 and is restated here for convenience.

$$\langle F_a(t) \rangle = F_{am}$$

$$\langle F_a(t)\ F_a(t+\tau) \rangle = 2D_1\delta(\tau)$$

where

D_1 is the intensity co-efficient

$\langle\ \rangle$ represents the time averaging of the signal

Defining, for easy representation,

$$F_\xi(t) = Y^* F_a + Z^* F_a^2$$

$$\gamma_b^2 = \frac{[EI(p_r^4 + p_r^{*4}/\ell^3)] - \mu_c \nu_o^2 (M_{11} + M_{11}^*)}{2(m_b + \mu_c)\ell + I_t(M_{11} + M_{11}^*)}$$

equation (6.1) can be rewritten as

$$\ddot{\xi} + C_b^* \dot{\xi} + \gamma_b^2 [1 - F_\xi(t)]\xi = 0 \qquad (6.5)$$

The solution to equation (6.5) is obtained on the basis of the following assumptions:

a) The intensity of fluctuation of $F_\xi(t)$ is small, that is, it does not lead to a large change in amplitude during one period. This is because, in a parametric system such as the one under consideration, only controlled frequency changes occur [119]. Such controlled frequency changes on quasi-harmonic systems leads to the condition that the intensity of fluctuation is generally small.

b) Since, the system is taken as a quasi-harmonic system, the response is taken to differ from a sinusoidal function because of a slowly varying but constantly accumulating deviation of amplitude and phase, similar to the one given in Krylov-Bogoliubov-Mitropol'skii method [106]. These accumulations are small for one or first several periods, but after a large number of periods of oscillations, the amplitude and phase will have changed considerably. Thus, after a sufficient period of time the response can be represented by a new sinusoidal function.

c) The time derivatives of amplitude and phase are small, due

to the fact that they contain components that are large but slowly varying in addition to small components that are rapidly varying. In view of the above assumptions, the solution to equation (6.5) can be written in the form

$$\xi = A(t) \cos[\gamma_b t + \phi(t)]$$

$$\dot{\xi} = -\gamma_b A(t) \sin[\gamma_b t + \phi(t)]$$

Squaring and adding the above equations, the following expressions for amplitude and phase are obtained

$$A(t) = [\xi^2 + (\dot{\xi}/\gamma_b)^2]^{\frac{1}{2}} \tag{6.6}$$

$$\phi(t) = \text{Arc tan}(\dot{\xi}/\gamma_b\xi) - \gamma_b t \tag{6.7}$$

Differentiating equations (6.6) and (6.7) and combining with (6.1)

$$\frac{\dot{A}(t)}{A(t)} = \gamma_b F_\xi(t) \sin[\gamma_b t + \phi(t)] \cos[\gamma_b t + \phi(t)] + C_b^* \sin^2[\gamma_b t + \phi(t)]$$

$$\dot{\phi}(t) = C_b^* \sin[\gamma_b t + \phi(t)] \cos[\gamma_b t + \phi(t)] - \gamma_b F_\xi(t) \cos[\gamma_b t + \phi(t)]$$

Discarding the terms containing the sine and cosine of a double angle, since the total effect of these periodic terms during a period is zero [120], the above equations can be rewritten as

$$\dot{u} = \xi_1 + m_1 + \frac{C_b^*}{2}$$

$$\dot{\phi}(t) = m_2 + \xi_2$$

where

$$u = \ell n A$$

$$\xi = \gamma_b F_\xi(t) \sin[\gamma_b t + \phi(t)] \cos[\gamma_b t + \phi(t)] - m_1$$

$$\xi_2 = -\gamma_b F_\xi(t) \cos^2[\gamma_b t + \phi(t)] - m_2$$

$$m_1 = \langle F_\xi(t) \sin[\gamma_b t + \phi(t)] \cos[\gamma_b t + \phi(t)] \rangle \gamma_b$$

$$m_2 = \langle F_\xi(t) \cos^2[\gamma_b t + \phi(t)] \rangle \gamma_b .$$

The values of m_1 and m_2 are evaluated using the equation [118]

$$\langle G[x(t), F_\xi(t)] \rangle = \langle G[x, F_\xi(t)] \rangle + \varepsilon \int_{-\infty}^{0} \langle \frac{\partial G}{\partial \phi} , H_\tau(\phi) \rangle \, d\tau$$

$$- \varepsilon \int_{-\infty}^{0} \langle \frac{\partial G}{\partial \phi} \rangle \langle H_\tau(\phi) \rangle \, d\tau \qquad (6.8)$$

where

$$G[x(t), F_\xi(t)] = \begin{cases} \frac{\gamma_b}{2} F_\xi(t) \sin[2\gamma_b t + 2\phi(t)] \\ \qquad \text{For the evaluation of } m_1 \\ \frac{\gamma_b}{2} F_\xi(t) \cos[2\gamma_b t + 2\phi(t)] \\ \qquad \text{For the evaluation of } m_2 \end{cases}$$

and

$$H_\tau(\phi) = \frac{-\gamma_b}{\varepsilon} F_\xi(t+\tau) \cos^2[\gamma_b t + \gamma_b \tau + \phi(t)]$$

Substituting the expressions for $G[x(t), F_\xi(t)]$ and $H_\tau(\phi)$ into equation (6.8) and performing the integration, the following expressions for m_1 and m_2 are obtained:

$$m_1 = \frac{\gamma_b^2}{8} \left[\{Y^* F_{am} + Z^*(\sigma_{Fa}^2 + F_{am}^2)\} \ \delta(2\gamma_b) - \chi(2\gamma_b) \right]$$

$$m_2 = \frac{\gamma_b}{2} \left[Y^* F_{am} + Z^*(\sigma_{Fa}^2 + F_{am}^2) \right]$$

where

$$\delta(2\gamma_b) = \begin{cases} \infty & \text{when the applied frequency is } 2\gamma_b \\ 0 & \text{elsewhere} \end{cases}$$

and

$$\chi(2\gamma_b) = \int_{-\infty}^{\infty} \langle F_\xi(t)\ F_\xi(t+\tau)\rangle \cos 2\gamma_b\tau\ d\tau$$

Since, the amplitude of vibration of the cutting tool-boring bar system is a function of ξ_1, and the phase angle between the applied axial force and the response ξ is a function of ξ_2, the correlation of the processes ξ_1 and ξ_2 have to be obtained. Substituting the expressions for ξ_1 and ξ_2, and dropping the oscillatory terms [120], the correlation expressions for the processes ξ_1, and ξ_2 are obtained as

$$\int_{-\infty}^{\infty} \langle \xi_1(t)\xi_1(t+\tau)\rangle d\tau = \frac{\gamma_b^2}{8}\chi(2\gamma_b) = \frac{1}{2\lambda_1}$$

$$\int_{-\infty}^{\infty} \langle \xi_2(t)\xi_2(t+\tau)\rangle d\tau = \frac{\gamma_b^2}{8}\left[\chi(0) + \chi(2\gamma_b)\right] = \frac{1}{2\lambda_2}$$

where λ_1 and λ_2 are the evaluated constants for easy representation in the analysis.

If the system is observed for a period of time which is much longer than the correlation time of the function $F_\xi(t)$, the variation of amplitude and phase can be represented as a Markov process [120]. Therefore the equation to compute the probability density function for the logarithm of the amplitude can be written as [118]

$$\frac{\partial p(u,t)}{\partial t} = -\frac{\partial}{\partial u}\left[\{M(u) + \frac{1}{4}K'(u)\}\ p(u,t)\right] + \frac{1}{2}\frac{\partial^2}{\partial u^2}\left[K(u)p(u,t)\right] \quad (6.9)$$

where

$$M(u) = \varepsilon\langle\nabla u\rangle$$

$$K(u) = 2\varepsilon^2\left[\int_{-\infty}^{0}\langle\nabla u\ \nabla_\tau u\rangle d\tau - \int_{-\infty}^{\infty}\langle\nabla(u)\rangle\langle\nabla_\tau(u)\rangle d\tau\right]$$

$$K'(u) = 4\varepsilon^2\left[\int_{-\infty}^{0}\left\langle\frac{\partial\nabla(u)}{\partial u}\ \nabla_\tau(u)\right\rangle d\tau - \int_{-\infty}^{0}\left\langle\frac{\partial\nabla(u)}{\partial u}\right\rangle\langle\nabla_\tau(u)\rangle d\tau\right]$$

For the case of the cutting tool-boring bar system

$$\nabla(u) = \frac{1}{\varepsilon}\left[\left(m_1 + \frac{C_b^*}{2}\right) + \varepsilon_1\right]$$

Substituting the expression for $\nabla(u)$ into (6.9) gives the following partial differential equation in probability density for the logarithm of the amplitude of the response

$$\frac{\partial p}{\partial t} = \left(m_1 + \frac{C_b^*}{2}\right)\frac{\partial p}{\partial u} + \frac{1}{4\lambda_1}\frac{\partial^2 p}{\partial u^2}$$

The solution of the above equation for the initial condition

$$p(u,o) = \delta(u)$$

is [118]

$$p(u,t) = \sqrt{\frac{\lambda_1}{\pi t}}\ e^{-\lambda_1[u + (m_1 + C_b^*/2)t]^2/t} \qquad (6.10)$$

Rewriting equation (6.10) in terms of the amplitude of vibration and evaluating the first and the second moments, the following relations [116] are obtained:

$$E[A] = e^{t[(1/\lambda_1) - 2(m_1 + C_b^*/2)]} = A_{bm} \tag{6.11}$$

$$E[A^2] = e^{t[9/4\lambda_1) - 3(m_1 + C_b^*/2)]} = A^2_{bMSV} \tag{6.12}$$

where

A_{bm} represents the mean amplitude of vibration of the cutting tool-boring bar system

A_{bMSV} represents the deviation of the amplitude of vibration of the cutting tool-boring bar system from the mean.

The complete statistical description of the response of the cuttting tool-boring assembly can be obtained only after the statistical description of the phase is derived. This is performed in the same manner used for the amplitude of vibration. Similar to the partial differential equation in the probability density for the logarithm of the amplitude of response, the partial differential equation in the probability density for phase is obtained from equation (6.9). Substituting

$$\nabla(u) = \frac{1}{\varepsilon}\,[m_2 + \xi_2]$$

into equation (6.9) the following partial differential equation in probability density function for phase is obtained.

$$\frac{\partial p_\phi}{\partial t} = m_2\,\frac{\partial p_\phi}{\partial u} + \frac{1}{4\lambda_2}\,\frac{\partial^2 p_\phi}{\partial \phi^2}$$

The solution to the above equation for an initial condition

$$p_\phi(\phi,0) = \delta(\phi)$$

is

$$p_{\phi}(\phi,t) = \sqrt{\frac{\lambda_2}{\pi t}}\; e^{-\lambda_2[\phi + m_2 t]^2/t}$$

Similar to the method used for amplitude, the first and second moments of the phase are obtained so that a complete statistical description of the response can be derived.

They are

$$E[\phi] = \phi_{bm} = \int_0^{2\pi} \phi p_{\phi}(\phi,t)d\phi$$

$$= \sqrt{\frac{\lambda_2}{\pi t}}\left[\frac{t}{2\lambda_2} Z_1(t) + \frac{m_2 t^{3/2}}{[8\lambda_2]^{\frac{1}{2}}}\; Z_2(t)\right] \tag{6.13}$$

$$E[\phi^2] = \phi^2_{MSV} = \int_0^{2\pi} \phi^2 p_{\phi}(\phi,t)d\phi$$

$$= \sqrt{\frac{\lambda_2}{\pi t}}\left[\sum_{m=0}^{\infty} (-1)^m \left(\frac{\lambda_2}{t}\right)^m \frac{1}{(2m+3)m!}\left\{(2\pi + m_2 t)^{2m+3} - (m_2 t)^{2m+3}\right\}\right.$$

$$\left. - \frac{m_2 t^2}{\lambda_2} Z_1(t) + m_2{}^2 t^2 \sqrt{\frac{\pi t}{8\lambda_2}}\; Z_2(t)\right] \tag{6.14}$$

where

$$Z_1(t) = e^{-\lambda_2 m_2{}^2 t^2} - e^{-\lambda_2[2\pi + m_2 t]^2/t}$$

$$Z_2(t) = e^{-2\lambda_2 m_2{}^2 t^2} - e^{-2\lambda_2[2\pi + m_2 t]^2/t}$$

Also

ϕ_{bm} represents the mean phase between the applied axial force and the response of the system

ϕ_{MSV} represents the deviation from the mean of the phase between the applied force and response of the system.

Equations (6.11) to (6.14) describe the mean and mean square value of the response amplitude and phase due to the action of the axial force on the cutting tool-boring bar system. Since, the response of the system is a function of only the amplitude and phase, the mean and mean square value of the response can be derived as explained later on in the Chapter. Thus, a statistical description of the response of the cutting tool-boring bar system has been obtained in terms of the amplitude and phase functions using the averaging technique.

6.2 Response due to Torque on the Cutting Tool-Boring Bar System

The result of torque acting on the cutting tool-boring bar system can be determined by solving equation (6.2). The right hand side of equation (6.2) is the torque acting on the system, for which a mathematical model has been obtained in Chapter 4. Similar to the resultant axial force, the resultant torque consists of a mean torque which is a nonlinear function of feed and diameter, and dynamic fluctuations which can be represented by a stationary wide band process with a gaussian density function [112]. The resultant torque is represented by

$$\langle T(t) \rangle = T_m$$

$$\langle T(t)T(t+\tau) \rangle = 2D_2\delta(\tau)$$

where

D_2 is the intensity co-efficient

$\langle\ \rangle$ temporal average of the torque signal

Prior to determination of the solution to equation (6.2), namely,

$$\ddot{\eta} + C_T^* \dot{\eta} + K_T^* \eta + N = T(t)$$

a stability criterion can be obtained based on the expression for the equivalent torsional damping C_T^*. In BTA deep-hole machining the metal removal takes place in an oil medium. So, a layer of oil exists in the small gap between the wear pads and machined hole. Since this gap between the workpiece and the wear pad is small, the lubrication may be assumed to be a thin film lubrication. Further, the slope of the curve representing the variation of co-efficient of friction with velocity is always negative in the thin film zone. Since,

$$C_T^* = \frac{\left(C_T + \Phi'(\omega)/2\ell\right)}{\left(I_x + \mu_c d_i^2/16\right)}$$

the torsional vibrations will be stable only when

$$\frac{\Phi'(\omega)}{2\ell} \leq C_T$$

and this inequality defines a stability criterion for the torsional oscillations of the cutting tool-boring bar assembly.

Since, the system has been modelled as a linear system in Chapter 5, the response of the system due to the mean and the oscillating component of the torque can be considered separately. Therefore, rewriting for convenience,

$$-N + T(t) = T_{em} + T_t$$

where

$T_{em} = T_m - N$ represents the mean value of torque

T_t represents the dynamically varying component of the torque

the response of the system due to the effective mean value of torque T_{em} can be determined by setting $\dot{\eta}$ and $\ddot{\eta}$ both equal to zero. Thus

$$\eta_s = \frac{T_{em}}{K_T^*} = \frac{(T_m - N)(I_x + \mu d_c^2/16)\ell}{X_{11} GJ}$$

where

η_s represents the static twist of the cutting tool-boring bar system due to the mean torque.

To obtain the response of the system due to the dynamically varying component of the torque, a mathematical model for T_t has to be obtained. Combining the mathematical model for T(t) and the definition of T_t, the following description is obtained for T_t.

$$\langle T_t \rangle = 0$$

$$\langle T_t(t) T_t(t+\tau) \rangle = 2D_2 \delta(\tau)$$

Since, the autocorrelation of the torque is a delta function, the system response describes a Markov process in the phase space and the Fokker-Planck approach can be used to obtain the system response [122]. Since the system is represented by a second order equation, and the dynamically varying component of torque by a stationary random process, the Fokker-Planck equation [122,123] for the system is given by

$$\sum_{i=1}^{2} \frac{\partial}{\partial x_i} [A_i(\tilde{y}) p(\tilde{y})] - \frac{1}{2} \sum_{j=1}^{2} \sum_{l=1}^{2} \frac{\partial^2}{\partial y_i \partial y_j} [B_{ij}(\tilde{y}) p(\tilde{y})] = 0$$

Here, the co-efficients are defined as

$$A_1 = \lim_{\delta t \to 0} \frac{1}{\delta t} \langle \delta y_1 \rangle = y_2$$

$$A_2 = \lim_{\delta t \to 0} \frac{1}{\delta t} \langle \delta y_2 \rangle = -C_T^* y_2 - K_T^* y_1$$

$$B_{12} = B_{21} = \lim_{\delta t \to 0} \frac{1}{\delta t} \langle \delta y_1 \delta y_2 \rangle = 0$$

$$B_{22} = \lim_{\delta t \to 0} \frac{1}{\delta t} \langle \delta y_2 \delta y_2 \rangle = 2D_2$$

where

$$y_1 = \eta$$

$$y_2 = \dot{\eta}$$

Substituting the above expressions for the co-efficients into the Fokker-Planck equation, the following parabolic partial differential equation is obtained

$$D_2 \frac{\partial^2 p^*}{\partial y_2^2} + \frac{\partial}{\partial y_2} [C_T^* y_2 + K_T^* y_1] p^* - \frac{\partial}{\partial y_1} [y_2 p^*] = 0$$

The above equation can be rewritten as [123]

$$\left[C_T^* \frac{\partial}{\partial y_2} - \frac{\partial}{\partial y_1}\right]\left[y_2 p^* + \frac{D_2}{C_T^*} \frac{\partial p^*}{\partial y_2}\right]$$

$$+ \frac{\partial}{\partial y_2}\left[K_T^* y_1 p^* + \frac{D_2}{C_T^*} \frac{\partial p^*}{\partial y_1}\right] = 0$$

A solution of the above partial differential equation is obtained by equating each of the functions following the operators to zero. That is,

$$y_2 p^* + \frac{D_2}{C_T^*} \frac{\partial p^*}{\partial y_2} = 0$$

$$K_T^* y_1 p^* + \frac{D_2}{C_T^*} \frac{\partial p}{\partial y_1} = 0$$

from which the expression for the density function $p^*(\eta,\dot{\eta})$ is obtained as

$$p^*(\eta,\dot{\eta}) = C \exp\left[-\frac{C_T^*}{2D_2}\left\{K_T^*\eta^2 + \dot{\eta}^2\right\}\right]$$

But, by the normality rule

$$\int_{-\infty}^{\infty}\int_{-\infty}^{\infty} C \exp\left[-\frac{C_T^*}{2D_2}\left\{K_T^*\eta^2 + \dot{\eta}^2\right\}\right] d\eta d\dot{\eta} = 1$$

from which

$$C = \frac{(C_T^* K_T^*)^2}{4\pi D_2^2}$$

Therefore, the expression for $p^*(\eta,\dot{\eta})$ becomes

$$p^*(\eta,\eta^1) = \frac{(C_T^* K_T^*)^2}{4\pi D_2^2} \exp\left[-\frac{C_T^*}{2D_2}\left\{K_T^*\eta^2 + \dot{\eta}^2\right\}\right]$$

From the above two dimensional probability density function the mean and mean square value of the response due to the dynamically varying component of torque is obtained from the moment functions written in the form

$$E[\eta] = \int_{-\infty}^{\infty} \eta p(\eta) d\eta = 0$$

$$E[\eta^2] = \int_{-\infty}^{\infty} \eta^2 p(\eta) d\eta = \frac{\pi}{2}\left[\frac{2D_2}{C_T^* K_T^{*2}}\right]^{\frac{3}{4}}$$

Combining the mean value of the response of the system due to the

effective mean value of torque and the dynamically varying component, the mean value of the response due to T(t) is obtained as

$$\eta_S = \frac{(T_m - N)(I_x + \frac{\mu}{c} d_i^2/16)\ell}{X_{11} GJ} \tag{6.15}$$

Since, the variation in the response of the system due to T(t) arises only due to the variation in the response because of the fluctuating component of torque T_t, the variance of the response due to the resultant torque acting on the cutting tool-boring bar system is given by

$$E[\eta^2] = \frac{\pi}{2}\left[\frac{2D_2}{C_T^* K_T^*}\right]^{\frac{2}{4}} = \sigma_{\eta S}^2 \tag{6.16}$$

where

$\sigma_{\eta S}$ represents the angular deviation of the cutting tool from the mean twist.

Equations (6.15) and (6.16) give the mean and mean square value of the response of the cutting tool-boring bar system due to the resultant torque. These equations will be later on employed for obtaining the total response of the system due to the resultant cutting forces.

6.3 Response of the Spindle-Workpiece Assembly due to the Action of the Axial Force

The effect of the axial force on the spindle-workpiece assembly response is determined by solving equation (6.3). This equation is similar to equation (6.1) in that both are parametric stochastic differential equations. So, the response analysis of the spindle-

workpiece system due to the action of the axial force is determined in a manner similar to that followed in Section 6.1, with identical assumptions. Defining

$$K_1^* = \gamma_S^2 = \frac{EI\left[\frac{q_r^4}{\ell_1^3} + \frac{q_r^{*4}}{\ell_2^3}\right]}{m_S(\ell_1 + \ell_2)}$$

and

$$K_2^* F_a = F_\zeta(t) = \frac{(P_{11} + P_{11}^*)}{EI\left[\frac{q_r^4}{\ell_1^3} + \frac{q_r^{*4}}{\ell_2^3}\right]}$$

equation (6.3) can be rewritten as

$$\ddot{\zeta} + C_S^* \dot{\zeta} + \gamma_S [1 - F_\zeta(t)]\zeta = 0$$

Following the procedure described in Section (6.1), the solution to the above equation can be written in the form

$$\zeta = A_S(t) \cos[\gamma_S t + \phi_S(t)]$$

$$\dot{\zeta} = -\gamma_S A_S(t) \sin[\gamma_S t + \phi_S(t)]$$

Combining the above with the original differential equation, and performing certain transformations as explained in Section 6.1, the following expressions for the amplitude and phase of the vibration of the spindle-workpiece assembly are obtained.

$$\frac{\dot{A}_S(t)}{A_S(t)} = \gamma_S F_\zeta(t) \sin[\gamma_S t + \phi_S(t)] \cos[\gamma_S t + \phi_S(t)] + C_S^* \sin^2[\gamma_S t + \phi_S(t)]$$

$$\dot{\phi}_S(t) = C_S^* \sin[\gamma_S t + \phi_S(t)] \cos[\gamma_S t + \phi_S(t)] - \gamma_S F_\zeta(t) \cos^2[\gamma_S t + \phi_S(t)]$$

The above equations for amplitude and phase can be simplified by discarding the terms containing the sine and cosine of the double angle because the total effect of these periodic terms is zero [120]. Thus, the equations for amplitude and phase of the spindle-workpiece assembly can be rewritten as

$$\dot{w} = \zeta_1 + m_{1S} + \frac{C_S^*}{2}$$

$$\phi_S(t) = m_{2S} + \zeta_2$$

where

$$w = \ell n A_S$$

$$\zeta_1 = \gamma_S F_\zeta(t) \sin[\gamma_S t + \phi_S(t)] \cos[\gamma_S t + \phi_S(t)] - m_{1S}$$

$$m_{1S} = \gamma_S \langle F_\zeta(t) \sin[\gamma_S t + \phi_S(t)] \cos[\gamma_S t + \phi_S(t)] \rangle$$

$$\zeta_2 = -m_{2S} - \gamma_S F_\zeta(t) \cos^2[\gamma_S t + \phi_S(t)]$$

$$m_{2S} = \gamma_S \langle F_\zeta(t) \cos^2[\gamma_S t + \phi_S(t)] \rangle$$

In order to obtain a statistical description of the response of the spindle-workpiece assembly, a stochastic characterization of the amplitude and phase of the vibration of the spindle-workpiece assembly has to be obtained. This can be obtained from the equation for the probability density of the phase, for which expressions for m_{1S}, m_{2S}, and the correlation of the processes ζ_1 and ζ_2 have to be derived. The expressions for m_{1S}, m_{2S}, and the correlation of the processes ζ_1 and ζ_2 are obtained in a manner similar to that in Section 6.1. Thus,

$$m_{1S} = \frac{\gamma_S^2}{8}\left[\left\{\frac{(P_{11} + P_{11}^*)F_{am}}{EI\left[\frac{q_r^4}{\ell_1^3} + \frac{q_r^{*4}}{\ell_2^3}\right]}\right\}^2 \delta(2\gamma_S) - \chi(2\gamma_S)\right]$$

$$m_{2S} = \frac{\gamma_S}{2}\left[\frac{(P_{11} + P_{11}^*)F_{am}}{EI\left[\frac{q_r^4}{\ell_1^3} + \frac{q_r^{*4}}{\ell_2^3}\right]}\right]$$

where

$$\delta(2\gamma_S) = \begin{cases} \infty & \text{when the applied frequency} = 2\gamma_S \\ 0 & \text{elsewhere} \end{cases}$$

$$\chi(2\gamma_S) = \int_{-\infty}^{\infty} <F_\zeta(t)F_\zeta(t+\tau)> \cos 2\gamma_S\tau d\tau$$

Further

$$\int_{-\infty}^{\infty} <\zeta_1\zeta_{1\tau}>d\tau = \frac{\gamma_S^2}{8}\chi(2\gamma_S) = \frac{1}{2\lambda_1^*}$$

$$\int_{-\infty}^{\infty} <\zeta_2\zeta_{2\tau}>d\tau = \frac{\gamma_S^2}{4}\left[\chi(0) + \frac{1}{2}\chi(2\gamma_S)\right] = \frac{1}{2\lambda_2^*}$$

Since, the system is observed for a time interval which is much longer than the correlation time of $F_\zeta(t)$, the variation of amplitude and phase can be represented by a Markov Process in phase space [120]. Thus, the equation to compute the porbability density function for the logarithm of the amplitude and phase can be written as

$$\frac{\partial p_S}{\partial t} = \left(m_{1S} + \frac{C_S^*}{2}\right)\frac{\partial p_S}{\partial u} + \frac{1}{4\lambda_1^*}\frac{\partial^2 p_S}{\partial u^2}$$

$$\frac{\partial p_{\phi S}}{\partial t} = m_{2S}\frac{\partial p_{\phi S}}{\partial \phi_S} + \frac{1}{4\lambda_2^*}\frac{\partial^2 p_{\phi S}}{\partial \phi_S^2}$$

The solution to the above equations for the initial conditions

$$p_S(w,0) = \delta(w)$$

$$p_\phi(\phi_S,0) = \delta(\phi_S)$$

are

$$p(w,t) = \sqrt{\frac{\lambda_1^*}{\pi t}}\ e^{-\lambda_1^*[w + (m_{1S} + C_S^*/2)t]^2/t}$$

$$p(\phi_S,t) = \sqrt{\frac{\lambda_2^*}{\pi t}}\ e^{-\lambda_2^*[\phi_S + m_{2S}t]^2/t}$$

from which the first and second moments of the amplitude of vibration, and the phase between the system response and the axial force can be determined. They are

$$E[A] = A_{Sm} = e^{t[1/\lambda_1^* - 2(m_{1S} + C_S^*/2)]} \tag{6.17}$$

$$E[A^2] = A^2_{SMSV} = e^{t[(9/4\lambda_1^*) - 3(m_{1S} + C_S^*/2)]} \tag{6.18}$$

$$E[\phi_S] = \phi_{Sm} = \sqrt{\frac{\lambda_2^*}{\pi t}}\left[\frac{t}{2\lambda_2^*}\ Z_1^*(t) + \frac{m_2 t^{3/2}}{[8\lambda_2^*]^{\frac{1}{2}}}\ Z_2^*(t)\right] \tag{6.19}$$

$$E[\phi_S^2] = \phi^2_{MSV} = \sqrt{\frac{\lambda_2^*}{\pi t}}\left[\sum_{m=0}^{\infty}(-1)^m\left(\frac{\lambda_2}{t}\right)^m \frac{1}{(2m+3)m!}\left\{(2\pi + m_{2S}t)^{2m+3}\right.\right.$$

$$\left.\left. -(m_{2S}t)^{2m+3}\right\} - \frac{m_{2S}t^2}{\lambda_2^*}\ Z_1^*(t) + m_{2S}^2 t^2\sqrt{\frac{\pi t}{8\lambda_2^*}}\ Z_2^*(t)\right] \tag{6.20}$$

A_{Sm} represents the mean amplitude of vibration of the spindle-workpiece system.

A_{bMSV} represents the deviation of the amplitude of vibration of the spindle-workpiece system from the mean.

ϕ_{Sm} represents the mean phase between the applied axial force and the response of the spindle-workpiece system.

ϕ_{MSV} represents the deviation of the phase between the applied axial force and the response of the system from the mean.

Further,

$$Z_1^*(t) = e^{-\lambda_2^* m_{2S}^2 t} - e^{-\lambda_2^* [2\pi + m_{2S} t]^2 / t}$$

$$Z_2^*(t) = e^{-2\lambda_2^* m_{2S}^2 t} - e^{-2\lambda_2^* [2\pi + m_{2S} t]^2 / t}$$

The response of the system under the action of the axial force has been taken as quasi-harmonic. So, a statistical description of the response of the system is known if a statistical description of the amplitude and phase is given through their mean and mean square values. This can then be used subsequently for the determination of the true motion of the tool tip.

6.4 Response of the Spindle-Workpiece System Under the Action of the Resultant Torque

The response of the spindle-workpiece system to the resultant torque is obtained in a manner similar to that described in Section 6.2. Before obtaining a solution to equation (6.4)

$$\ddot{\theta}_S + C_{ST}^* \dot{\theta}_S + K_{ST}^* \theta_S + N^* = T(t)$$

a stability criteria is obtained for the oscillations of the spindle-workpiece assembly based on the expression for the equivalent torsional damping C_{ST}^*. Since

$$C_{ST}^{*} = \frac{[C_{ST} + \Phi'(\omega)/\ell_1 + \ell_2]}{I_x^{*}}$$

and $\Phi'(\omega)$ is always negative, the torsional oscillations of the spindle workpiece will be stable only if

$$\frac{\Phi'(\omega)}{\ell_1 + \ell_2} \leq C_{ST}$$

In order to have a stable machining operation not only the torsional oscillations of the spindle-workpiece system be stable, so also the torsional vibrations of the cutting tool-boring bar system. Therefore, the above mentioned stability criterion has to be combined with the stability criterion for the cutting tool-boring bar system. This yields, the stability criteria for the machining operation as

$$\Phi'(\omega) \leq \text{Min}\,[2\ell C_T,\ (\ell_1 + \ell_2)C_{ST}]$$

where

$\text{Min}\,[2\ell C_T, (\ell_1 + \ell_2)C_{ST}]$ represents the minimum value for the two quantities in the bracket.

Since the system has been modelled as a linear system, the response due to the mean and dynamically varying component can be considered separately. Rewriting, for convencience,

$$-N^{*} + T(t) = T_{em}^{*} + T_t$$

where

T_{em}^{*} represents the effective mean value of torque

T_t represents the dynamically varying component of torque

the response of the system due to the mean value of torque is obtained

by setting $\dot{\theta}_S$ and $\ddot{\theta}_S$ equal to zero. Thus

$$\theta_{Sm} = \frac{T_{em}^*}{K_{ST}^*} = \frac{(T_m - N^*)\ I_X(\ell_1 + \ell_2)}{G^* X_{11}^* J^*}$$

where

θ_{Sm} represents the static twist of the spindle-workpiece assembly due to effective mean torque.

Since, the autocorrelation function of the torque is a delta function, the system response represents a Markov process in phase space and so the Fokker Planck approach can be used to find the system response. The following parabolic partial differential equation in the joint probability density function of θ_S and $\dot{\theta}_S$ is obtained in a manner similar to that described in Section 6.2.

$$D_2 \frac{\partial^2 p_S^*}{\partial \theta_S^2} + \frac{\partial}{\partial \dot{\theta}_S}\left[C_{ST}^* \dot{\theta}_S + K_{ST} \theta_S\right] p_S^* - \frac{\partial}{\partial \theta_S}\left[\dot{\theta}_S p_S^*\right] = 0$$

The solution to the above equation is

$$p_S^*(\theta_S, \dot{\theta}_S) = \frac{(C_{ST}^* K_{ST}^*)^2}{4\pi D_2^2} \exp\left[-\frac{C_{ST}^*}{2D_2}\left\{K_{ST}^* \theta_S^2 + \dot{\theta}_S^2\right\}\right]$$

from which the mean and mean square value of the response of the spindle-workpiece system due to the randomly fluctuating component of torque is obtained and is given by

$$E[\theta_S] = \int_{-\infty}^{\infty} \theta_S p_S(\theta_S) d\theta_S = 0$$

$$E[\theta_S^2] = \int_{-\infty}^{\infty} \theta_S^2 p_S(\theta_S) d\theta_S = \frac{\pi}{2} \left[\frac{2D_2}{C_{ST}^* K_{ST}^*} \right]^{\frac{3}{4}}$$

The mean value of the response of the spindle-workpiece system due to T(t) is obtained by adding the response due to the effective mean value of the torque and the dynamically varying component. Thus

$$\theta_S = (\pi - \theta_S^*) = \frac{(T_m - N^*)\ I_X(\ell_1 + \ell_2)}{GX_{11}^* J^*} \tag{6.21}$$

where

$(\pi - \theta_S^*)$ represents mean twist due to resultant torque acting on the spindle-workpiece system.

Since, the variation of twist arises only due to the fluctuating component of torque T_t, the variance of the response due to the resultant torque acting on the cutting tool-boring bar system is given by

$$E[\theta_S^2] = \sigma_{\theta S}^2 = \frac{\pi}{2} \left[\frac{2D_2}{C_{ST}^* K_{ST}^*} \right]^{\frac{3}{4}} \tag{6.22}$$

where

$\sigma_{\theta S}$ represents the angular deviation of the spindle-workpiece assembly from the mean.

Equations (6.21) and (6.22) give the mean and mean square values of the response of the spindle-workpiece assembly due to the resultant torque. These equations will be coupled with equations (6.11) to (6.20) to obtain the total response of the system and true motion of the tool tip in the following section.

6.5 Motion of the Tool Tip

The true motion of the tool tip describes the path generated on

the workpiece by the cutting tool. Since, long and accurate holes can be drilled in a short time using the BTA deep hole machining process, the determination of the true motion of the tool tip is of prime importance. This can lead to the evaluation of the deviation of the true motion from the ideal motion for assessing the accuracy of the finished hole and for implementation of compensation arrangements. Such implementations are described in the next Chapter.

Under ideal conditions, the motion of any arbitrary point P, on the tool tip (Fig. 6.1), which determines the shape of the curve generated can be described by the following expression:

$$\frac{d}{2}\cos\omega_0 t\ \underline{i} + \frac{d}{2}\sin\omega_0 t\ \underline{j} + f\ \underline{k}$$

where

$\underline{i}, \underline{j}, \underline{k}$ represents the unit vectors along the X,Y and Z directions.

Since, the cutting tool-boring bar system and the spindle-workpiece assembly are elastic systems, they undergo deflections and deformations due to the action of the resultant cutting force system. So, the point P, on the cutting profile of the tool does not generate an ideal curve.

The true motion of the cutting tool tip is obtained by vectorially adding the responses of the cutting tool-boring bar system and the spindle workpiece assembly with the equation for ideal motion. Further, since the gaussian distributed resultant force system acts on linear system, the response of the cutting tool and spindle must have a gaussian distribution. To obtain the true motion of the cutting tool, a point P^* on the spindle-workpiece assembly is considered which coincides with point P (Fig. 6.2) on the cutting tool boring bar system in the absence

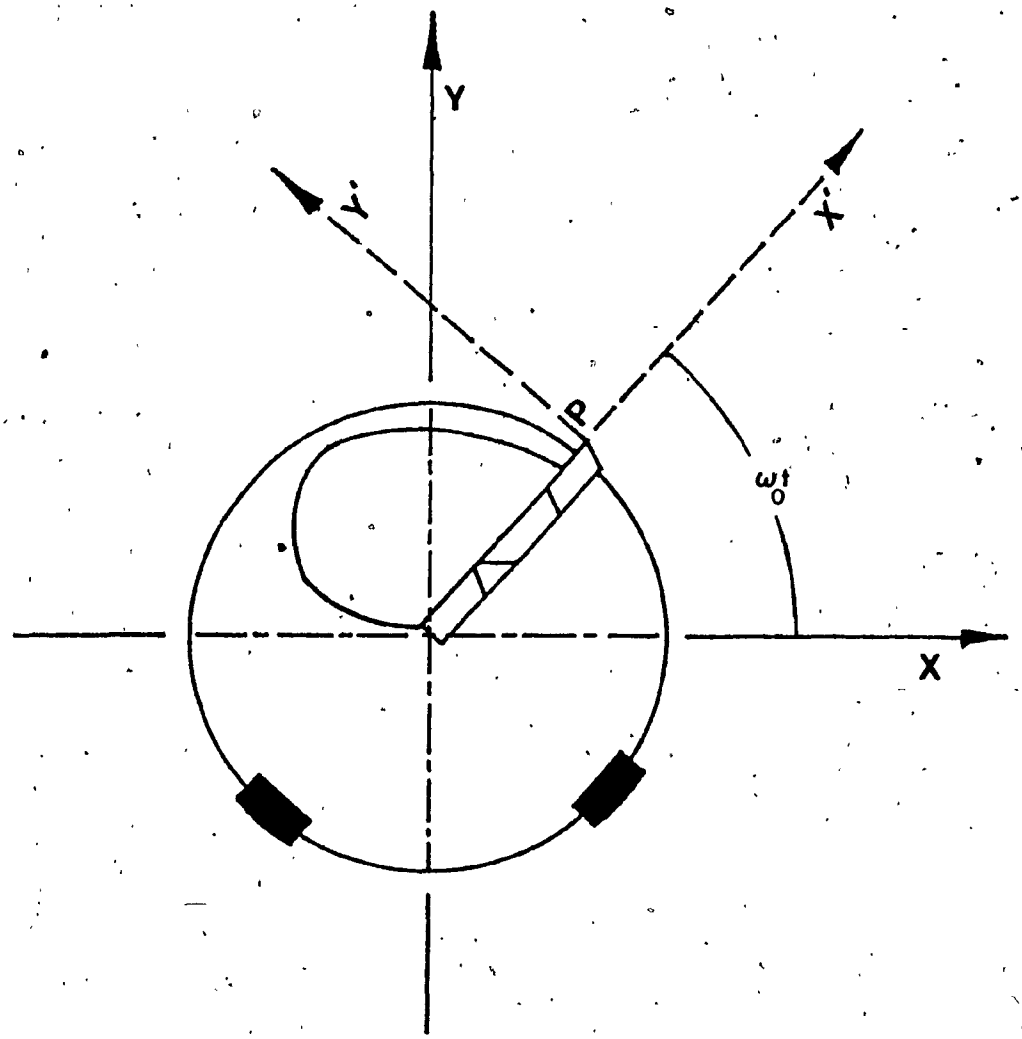

Fig. 6.1: Cross-Sectional View of the Cutting Tool

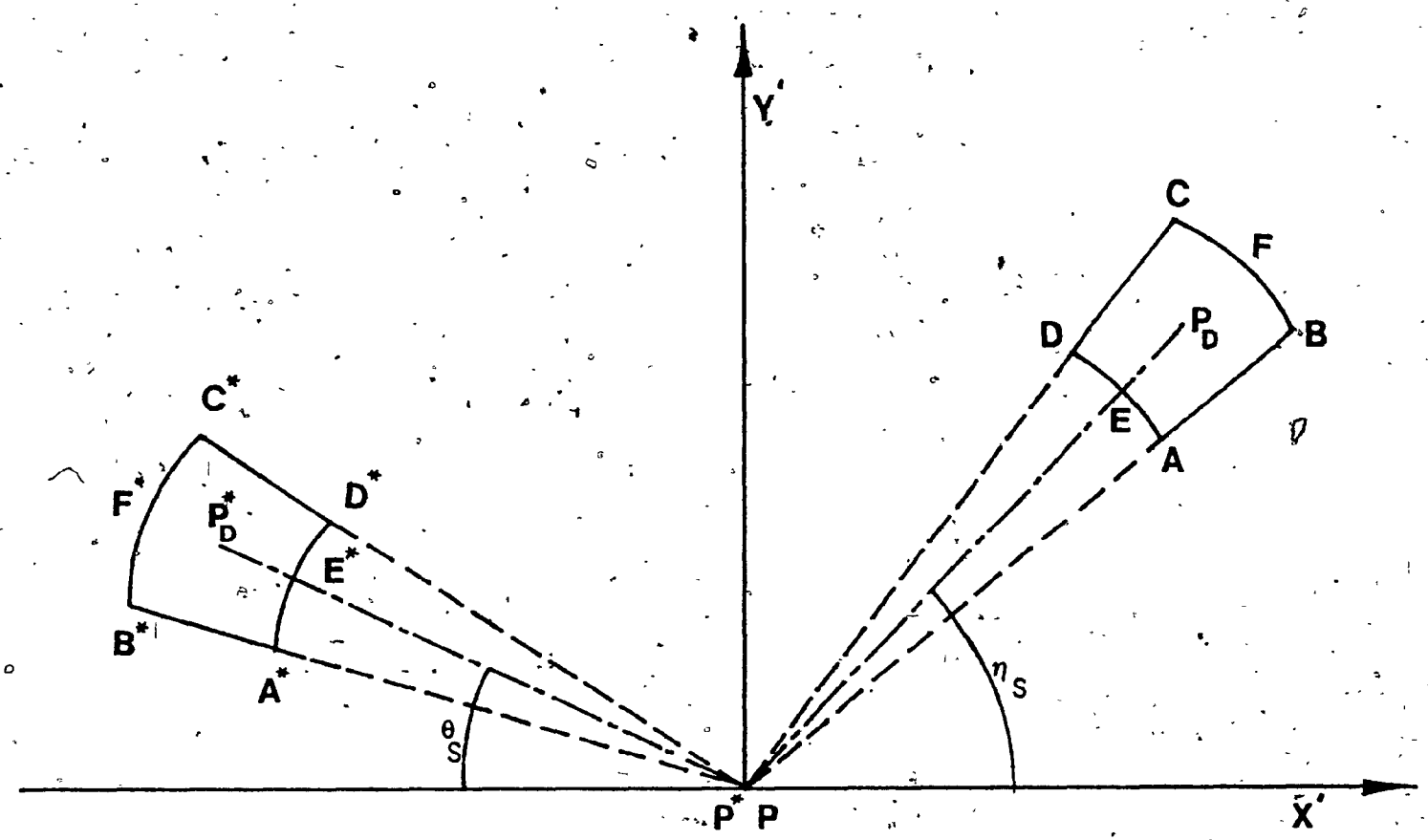

Fig. 6.2: Region of Displacement of Cutting Tool Tip and the Spindle-Workpiece Assembly

of any resultant force system acting on the system. Due to the resultant force system acting on the spindle-workpiece assembly the point P^* gets deflected to P_D^* due to the mean value of torque and the mean axial force. Similarly the point P on the cutting tool-boring assembly will be deflected to P_D due to the effect of the mean axial force and torque on the cutting tool. It has been established in Chapter 4 that the resultant force system is dynamic and that the maximum and minimum values of the torque and axial force are

$$T_p = T_R + 3\sigma_T$$

$$T_{min} = T_R - 3\sigma_T$$

$$F_{ap} = F_{aR} + 3\sigma_{Fa}$$

$$F_{min} = F_{aR} - 3\sigma_{Fa}.$$

Depending upon the magnitude of the axial force and torque acting on the spindle-workpiece assembly and the cutting tool-boring bar system the location of the point P and P^* varies in a given zone. This zone is defined by four extreme points which correspond to

i) maximum Torque and maximum Axial force;

ii) maximum Torque and minimum Axial force;

iii) minimum Torque and maximum Axial force; and

iv) minimum Torque and minimum Axial force.

Thus, the region of deformation of P^* is defined by $A^*B^*C^*D^*$ and the region of deformation of P is given by ABCD. The location of the points A,B,C,D,A^*,B^*,C^*, and D^* are derived from the fact that the system response has a gaussian distribution.

The maximum, average, and minimum x and y components of the deviation of the cutting tool relative to the workpiece can be determined from Fig. 6.2 and are

$$[\Delta_x]_{max} = \left[(q_{bm} + 3\sigma_b)\ \Phi_2(0)\ \cos(\eta_S - 3\sigma_{\eta S}) - (q_{Sm} - 3\sigma_S)\ \Psi_i(x)\ \cos(\theta_S^* + 3\sigma_{\theta S})\right]$$

$$[\Delta_y]_{max} = \left[(q_{bm} + 3\sigma_b)\ \Phi_2(0)\ \cos(\eta_S + 3\sigma_{\eta S}) - (q_{Sm} - 3\sigma_S)\ \Psi_i(x)\ \sin(\theta_S^* - 3\sigma_{\theta S})\right]$$

$$[\Delta_x]_{av} = \left[q_{bm}\ \Phi_2(0)\ \cos\eta_S - q_{Sm}\ \Psi_i(x)\ \cos\theta_S^*\right]$$

$$[\Delta_y]_{av} = \left[q_{bm}\ \Phi_2(0)\ \sin\eta_S - q_{Sm}\ \Psi_i(x)\ \sin\theta_S^*\right]$$

$$[\Delta_x]_{min} = \left[(q_{bm} - 3\sigma_b)\ \Phi_2(0)\ \cos(\eta_S + 3\sigma_{\eta S}) - (q_{Sm} + 3\sigma_S)\ \Psi_i(x)\ \cos(\theta_S^* - 3\sigma_{\theta S})\right]$$

$$[\Delta_y]_{min} = \left[(q_{bm} - 3\sigma_b)\ \Phi_2(0)\ \sin(\eta_S - 3\sigma_{\eta S}) - (q_{Sm} + 3\sigma_S)\ \Psi_i(x)\ \sin(\theta_S^* + 3\sigma_{\theta S})\right]$$

where

$$q_{bm} = A_{bm}\cos[\gamma_b t + \phi_{bm}]$$

$$q_{Sm} = A_{Sm}\cos[\gamma_S t + \phi_{Sm}]$$

$$\sigma_b^2 = [A_{bMSV}^2 - A_{bm}^2]\cos^2(\gamma_b t + \phi_{bm})$$

$$\sigma_S^2 = [A_{SMSV}^2 - A_{Sm}^2]\cos^2(\gamma_S t + \phi_{Sm})$$

Using the vector addition, the maximum, average, and minimum value of

the deviation of the cutting tool tip relative to the spindle-workpiece assembly can be determined and are

$$[\Delta_R]_{max} = \Big\{[\Phi_2(0)q_{bm}]^2 + [\Psi_i(x)q_{Sm}]^2 - 2\Phi_2(0)\Psi_i(x)q_{bm}q_{Sm} \{\cos(\eta_S - 3\sigma_{\eta S})\cos(\theta_S^* + 3\sigma_{\theta S}) - \sin(\eta_S + 3\sigma_{\eta S}) \sin(\theta_S^* - 3\sigma_{\theta S})\}\Big\}^{\frac{1}{2}}$$

$$[\Delta_R]_{av} = \Big\{[\Phi_2(0)q_{bm}]^2 + [\Psi_i(x)q_{Sm}]^2 - 2\Phi_2(0)\Psi_i(x)q_{bm}q_{Sm} \cos(\theta_S^* - \eta_S)\Big\}^{\frac{1}{2}}$$

$$[\Delta_R]_{min} = \Big\{[\Phi_2(0)q_{bm}]^2 + [\Psi_i(x)q_{Sm}]^2 - 2\Phi_2(0)\Psi_i(x)q_{bm}q_{Sm} \{\cos(\eta_S + 3\sigma_{\eta S})\cos(\theta_S^* - 3\sigma_{\theta S}) - \sin(\eta_S - 3\sigma_{\eta S})\cos(\theta_S^* + 3\sigma_{\theta S})\}\Big\}^{\frac{1}{2}}$$

A complete description of the maximum, average, and minimum value of the deviation is obtained if the angles formed by these deviations with the X'Y' axis is known. These are

$$\epsilon_{max} = \tan^{-1}\left[\frac{[\Delta_y]_{max}}{[\Delta_x]_{max}}\right]$$

$$\epsilon_{av} = \tan^{-1}\left[\frac{[\Delta_y]_{av}}{[\Delta_x]_{av}}\right]$$

$$\epsilon_{min} = \tan^{-1}\left[\frac{[\Delta_y]_{min}}{[\Delta_x]_{min}}\right]$$

Since, the deviation of the cutting tool relative to the spindle-

workpiece assembly is not unique, the true equation of motion is not unique. This is because the true motion of the tool tip is obtained by adding the ideal motion of tool with the deviation of the tool relative to the spindle workpiece assembly. Since, the deviation of the cutting tool relative to the workpiece is specified by the maximum deviation, average deviation, and minimum deviation, the true motion of the cutting tool is also specified by the maximum deviation curve, average curve, and minimum curve. Thus, the appropriate expressions are

a) For Maximum Deviation Curve.

$$\left[\frac{d}{2}\cos\omega_o t + [\Delta_R]_{max}\cos(\omega_o t + \varepsilon_{max})\right]\underline{i} + \left[\frac{d}{2}\sin\omega_o t + [\Delta_R]_{max}\sin(\omega_o t + \varepsilon_{max})\right]\underline{j} + f_m\left[\left\{\Phi_2'(0) + \Psi_i'(x)\right\}\Psi_i'(x) + \cos[\Phi_2'(0) + \Psi_i'(x)]\cos\Psi_i'(x)\right]\underline{k} \tag{6.23}$$

b) For Average Curve

$$\left[\frac{d}{2}\cos\omega_o t + [\Delta_R]_{av}\cos(\omega_o t + \varepsilon_{av})\right]\underline{i} + \left[\frac{d}{2}\sin\omega_o t + [\Delta_R]_{av}\sin(\omega_o t + \varepsilon_{av})\right]\underline{j} + f_m\left[\left\{\Phi_2'(0) + \Psi_i'(x)\right\}\Psi_i'(x) + \cos[\Psi_i'(0) + \Psi_i'(x)]\cos\Psi_i'(x)\right]\underline{k} \tag{6.24}$$

c) For Maximum Deviation Curve

$$\left[\frac{d}{2}\cos\omega_o t + [\Delta_R]_{min}\cos(\omega_o t + \varepsilon_{min})\right]\underline{i} + \left[\frac{d}{2}\sin\omega_o t + [\Delta_R]_{min}\sin(\omega_o t + \varepsilon_{min})\right]\underline{j} + f_m\left[\left\{\Phi_2'(0) + \Psi_i'(x)\right\}\Psi_i'(x) + \cos[\Phi_2'(0) + \Psi_i'(x)]\cos\Psi_i'(x)\right]\underline{k} \tag{6.25}$$

The difference between the true motion and the ideal motion gives the error produced on the machined hole. Thus the controlling expressions are

a) For Maximum error

$$\left[[\Delta_R]_{max}\cos(\omega_o t + \varepsilon_{max})\right]\underline{i} + \left[[\Delta_R]_{max}\sin(\omega_o t + \varepsilon_{max}\right]\underline{j}$$
$$+ f_m\left[\left\{\Phi_2'(0) + \Psi_i'(x)\right\}\Psi_i'(x) - 1 + \cos[\Phi_2'(0) + \Psi_i'(x)]\cos\Psi_i'(x)\right]\underline{k} \quad (6.26)$$

b) For Average error

$$\left[[\Delta_R]_{av}\cos(\omega_o t + \varepsilon_{av})\right]\underline{i} + \left[[\Delta_R]_{av}\sin(\omega_o t + \varepsilon_{av})\right]\underline{j}$$
$$+ f_m\left[\left\{\Phi_2'(0) + \Psi_i'(x)\right\}\Psi_i'(x) - 1 + \cos[\Phi_2'(0) + \Psi_i'(x)]\cos\Psi_i'(x)\right]\underline{k} \quad (6.27)$$

c) For Minimum error

$$\left[[\Delta_R]_{min}\cos(\omega_o t + \varepsilon_{min})\right]\underline{i} + \left[[\Delta_R]_{min}\sin(\omega_o t + \varepsilon_{min})\right]\underline{j}$$
$$+ f_m\left[\left\{\Phi_2'(0) + \Psi_i'(x)\right\}\Psi_i'(x) - 1 + \cos[\Phi_2'(0) + \Psi_i'(x)]\cos\Psi_i'(x)\right]\underline{k} \quad (6.28)$$

As seen from the derivations of equations (6.23) to (6.25) the actual path traversed by the cutting tool tip is not unique. That is, the actual path can be helix between and including the minimum deviation curve and maximum deviation curve. Since the true motion of the cutting tool tip is a helix whose boundaries are defined by the maximum deviation curve, and the minimum deviation curve, the surface of the hole produced should have helical grooves. This was in fact observed on all the machined surfaces obtained from laboratory tests. Specimen photographs of these surfaces are shown in Figs. (6.3) and (6.4) for two different diameter holes produced under different machining conditions.

Equations (6.26) to (6.28) give expressions for the error produced on the surface on the machined hole. These errors are explicit functions of time due to the fact that the probability density functions of

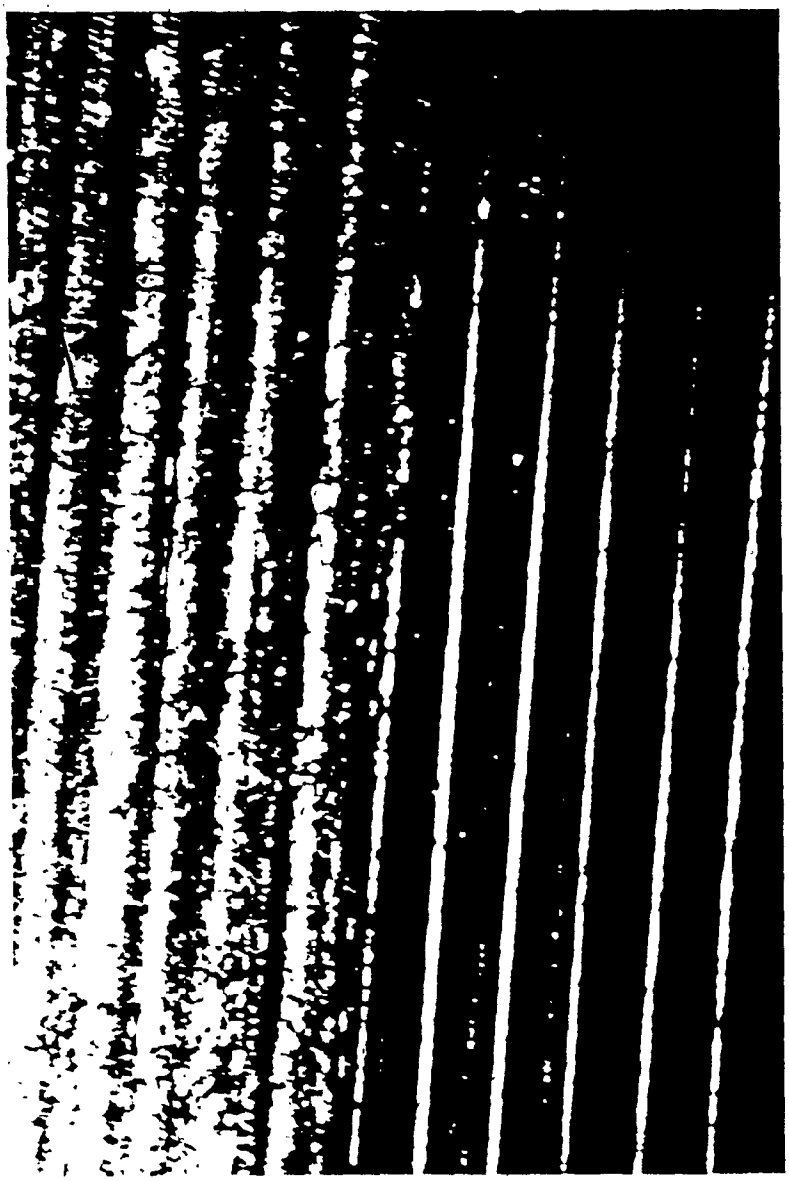

Figure 6.3: Surface Produced on a Workpiece Specimen due to 22.225 mm Tool

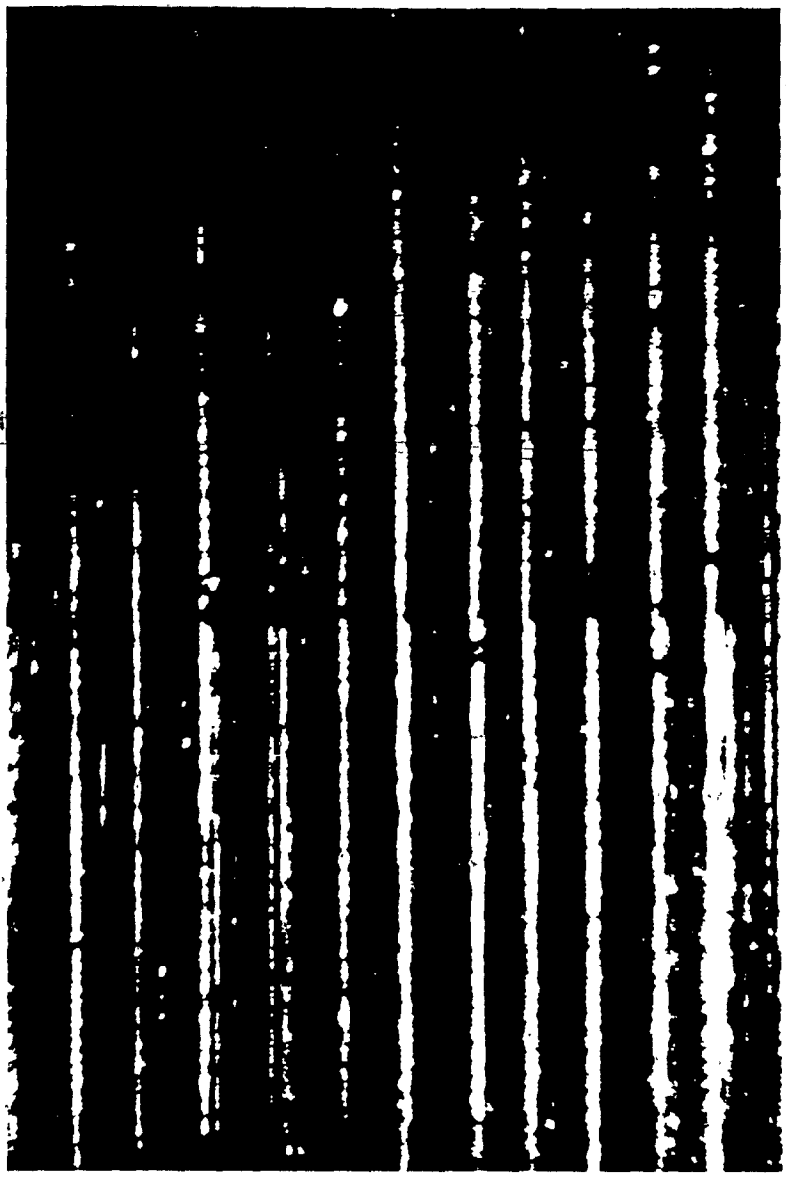

Figure 6.4: Surface Produced on a Workpiece Specimen due to 25.4 mm Tool

$[\Delta_R]_{max}$, $[\Delta_R]_{av}$, $[\Delta_R]_{min}$ are time dependent. Thus, the roundness error at any position, for a given machining condition, can take any value between the minimum error, and the maximum error depending upon the probability denisty function. The measurement of the roundness at different depths of the hole with cutting tools of different diameters, shown in Figs. (6.5) to (6.8) reveal no definite pattern for the roundness error variation with the depth of hole and feed and this in fact confirms the variation of errors between the bounds specified above.

During the roundness measurement, certain grooves were observed at fairly regular intervals along the hole. The roundness was measured at those spots as well but the readings did not show any peculiarities. Therefore it may be concluded that the depth of these grooves are of the same order as that of the surface finish and are caused essentially due to chattering of the tool. This class of chatter, as a result of the undesirable oscillations, occur between the stable and unstable regions of operation during the machining process. Further investigations are to be carried out to understand fully this peculiar phenomenon.

6.6 An Alternate Approach to the Solution of the Parametric Stochastic Differential Equations

The solution to the parametric stochastic differential equations, namely equations (6.1) and (6.3), were performed earlier using the averaging technique. In this section, an alternate method to solve such parametric stochastic differential equations is proposed. This method combines the Fokker-Planck approach to obtain the response on non-linear systems subjected to white random excitation [123] with the

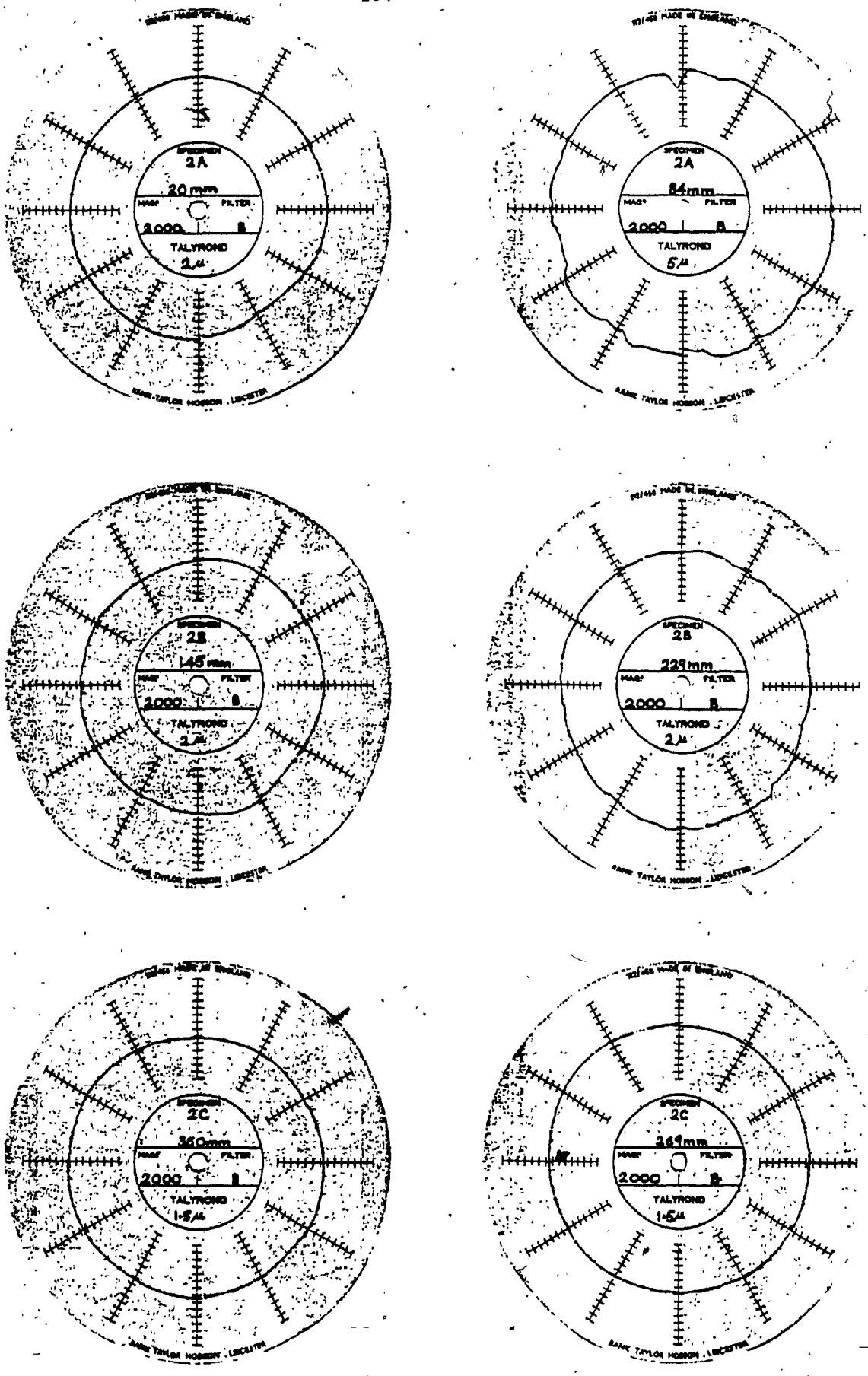

Fig. 6.5: Plots from Talyrond at Different Depths of 19.05 mm Hole at a Particular Feed

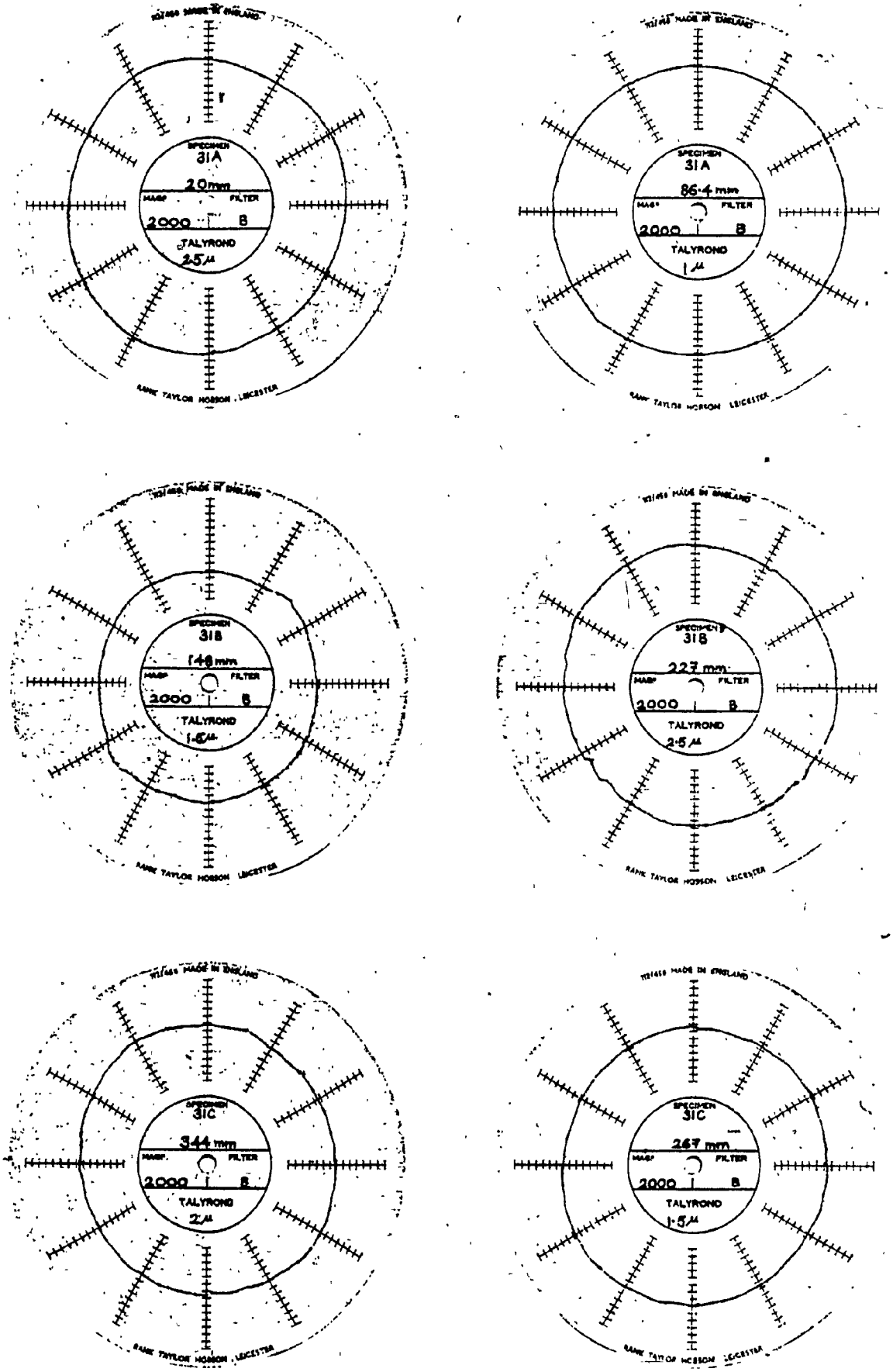

Fig. 6.6: Plots from Talyrond at Different Depths of 28.575 mm Hole at a Particular Feed

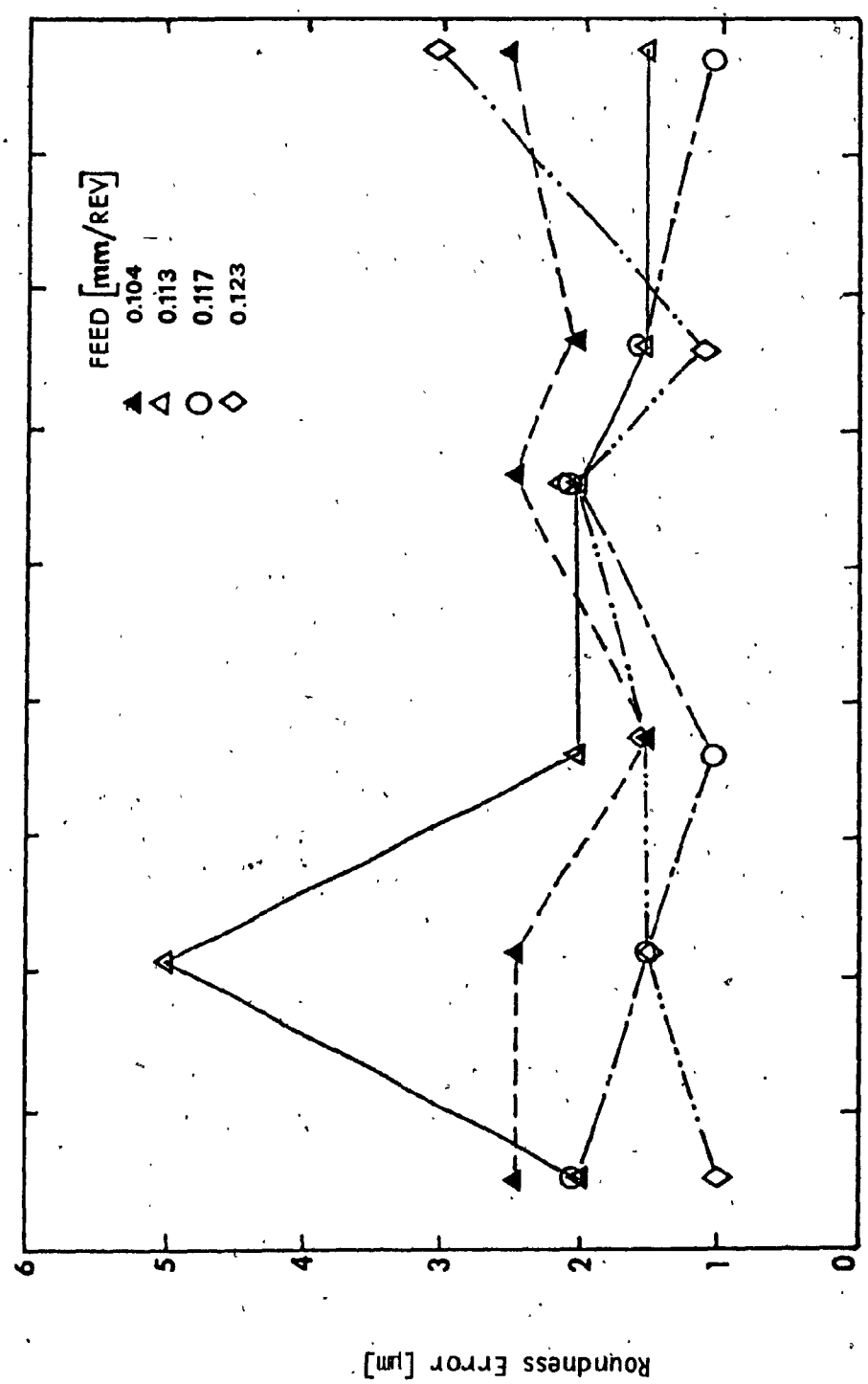

Fig. 6.7: Variation of Roundness Error with Depth of Hole Using a 19.05 mm Cutting Tool

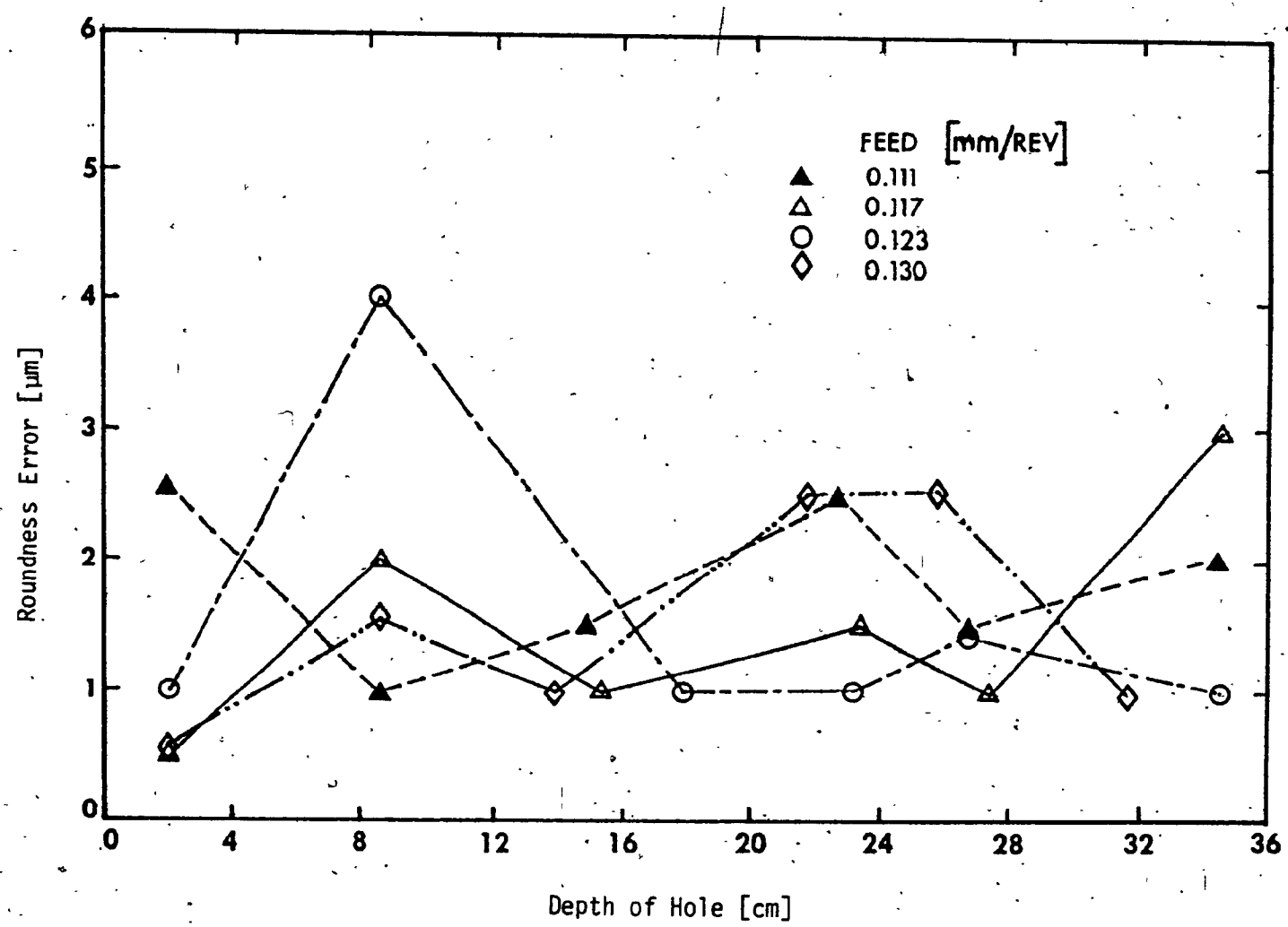

Fig. 6.8: Variation of Roundness Error with Depth of Hole Using a 28.575 mm Cutting Tool

property that the velocity and displacement of the response are statistically dependent in any parametrically excited system. Just for the purposes of illustration, equation (6.1) is solved. This is yet to be fully developed and hence could not be used for obtaining the tool tip motion. Once an expression to evaluate the normality constant is obtained, this method can be easily employed to solve problems involving parametrically excited systems subjected to white random excitation.

Writing equation (6.1) as a set of state equations using

$$y_1 = \xi$$

and $$y_2 = \dot{\xi} ,$$

the following equations are obtained:

$$\dot{y}_1 = y_2 \tag{6.29}$$

$$\dot{y}_2 + C_b y_2 + K^*[1 - Y^* F_a - Z^* F_a^2]\, y_1 = 0 \tag{6.30}$$

Let a small increase in time from t to $t+\delta t$ be considered. δt is taken to be small compared to the response time of the system, but not necessarily small compared to $F_a(t)$ and $F_a^2(t)$. Thus, the state equations can be written in the form

$$\delta y_1 = y_2 \delta t$$

$$\delta y_2 = -C_b y_2 \delta t - K^* y_1 \delta t + K^* Y^* \int_t^{t+\delta t} y_1 F_a(t)dt + K^* Z^* \int_t^{t+\delta t} y_2 F_a^2(t)dt$$

Then, the limiting process $\delta t \to 0$ is used to evaluate A_i and B_{ij} in the equation

$$\sum_{i=1}^{2} \frac{\partial}{\partial x_i}[A_i(\tilde{y})p(\tilde{y})] - \frac{1}{2}\sum_{j=1}^{2}\sum_{i=1}^{2} \frac{\partial^2}{\partial y_i \partial y_j}[B_{ij}(\tilde{y})p(\tilde{y})] = 0 \tag{6.31}$$

Here the co-efficients A_i and B_{ij} are

$$A_1 = \lim_{\delta t \to o} \frac{1}{\delta t} \langle x_2 \delta t \rangle = x_2$$

$$A_2 = \lim_{\delta t \to o} \frac{1}{\delta t} \langle -C_b y_2 \delta t - K^* y_1 \delta t + K^* Y^* \int_t^{t+\delta t} y_1 F_a(t) dt +$$

$$+ K^* Z^* \int_t^{t+\delta t} y_1 F_a^2(t) dt \rangle = -C_b y_2 - K^* y_1 + K^* Y^* \lim_{\delta t \to o} \frac{1}{\delta t} \int_t^{t+\delta t}$$

$$\langle y_1 F_a(t) \rangle dt + K^* Z^* \lim_{\delta t \to o} \frac{1}{\delta t} \int_t^{t+\delta t} \langle y_1 F_a^2(t) \rangle dt$$

Since y_1 is a slowly varying function of time

$$\lim_{\delta t \to o} \frac{1}{\delta t} \int_t^{t+\delta t} \langle y_1 F_a(t) \rangle dt \approx y_1 F_{am}$$

and

$$\lim_{\delta t \to o} \frac{1}{\delta t} \int_t^{t+\delta t} \langle y_1 F_a^2(t) \rangle dt \approx y_1 (F_{am}^2 + \sigma_{Fa}^2)$$

where

F_{am} — represents the mean value of the resultant axial force

σ_{Fa} — represents the deviation of the resultant axial-force from the mean.

Therefore,

$$A_2 = -C_b y_2 - K^* y_1 + K^* Y^* y_1 F_{am} + K^* Z^* (F_{am}^2 + \sigma_{Fa}^2)\, y_1 = -C_b y_2 + \mu y_1$$

$$B_{11} = \lim_{\delta t \to o} \frac{1}{\delta t} \langle x_2 \delta t \cdot x_2 \delta t \rangle = 0$$

$$B_{12} = B_{21} = \lim_{\delta t \to 0} \frac{1}{\delta t} \left\langle (x_2 \delta t) \cdot \left(-C_b y_2 \delta t - K^* y_1 \delta t + K^* Y^* \int_t^{t+\delta t} y_1 F_a(t)dt \right.\right.$$

$$\left.\left. + K^* Z^* \int_t^{t+\delta t} y_1 F_a^2(t)dt \right)\right\rangle = 0$$

$$B_{22} = \lim_{\delta t \to 0} \frac{1}{\delta t} \left\langle \left(-C_b y_2 \delta t - K^* y_1 \delta t + K^* Y^* \int_t^{t+\delta t} y_1 F_a(t)dt \right.\right.$$

$$\left.\left. + K^* Z^* \int_t^{t+\delta t} y_1 F_a^2(t)dt \right)^2 \right\rangle = (K^* Y^* y_1)^2 \cdot 2D_1 + (K^* Z^* y_1^2)$$

$$\cdot 2D_3 + K^{*2} Y^* Z^* y_1^2 \cdot 2D_4 = 2y_1^2 [K^{*2} Y^{*2} D_1 + K^{*2} Z^{*2} D_3$$

$$+ K^{*2} Y^* Z^* D_4] = 2\mu^* y_1^2$$

where

$$\langle F_a(t) F_a(t+\tau) \rangle = 2D_1 \delta(\tau)$$

$$\langle F_a(t) F_a^2(t+\tau) \rangle = 2D_3 \delta(\tau)$$

$$\langle F_a^2(t) F_a^2(t+\tau) \rangle = 2D_4 \delta(\tau).$$

Thus, the Fokker-Planck equation represented by equation (6.31) becomes

$$\mu^* y_1^2 \frac{\partial^2 p}{\partial y_2^2} - \frac{\partial}{\partial y_2} [\{-C_b y_2 + \mu y_1\} p] - \frac{\partial}{\partial y_1} [y_2 p] = 0 \qquad (6.32)$$

Since, the velocity and displacement are statistically dependent

$$p(y_1, y_2) = p_1(y_1) \cdot p_2(y_2 | y_1) \qquad (6.33)$$

Hence, to determine $p(y_1, y_2)$ the two terms $p_1(y_1)$ and $p_2(y_2|y_1)$ have to be individually determined. First, $p_2(y_2|y_1)$ is determined by substituting equation (6.33) into equation (6.32), for any arbitrary but fixed value of y_1. Further

$$p_1(y_1) = \text{constant} = p_0$$

where

$$p_0 < 1$$

for any aribitrary but fixed value of y_1.

Thus,

$$p(y_1,y_2) = p_0 p(y_2|y_1)$$

Substituting $p(y_1,y_2)$ into equation (6.32) the following equation is obtained.

$$p_0\mu^* y_1^2 \frac{d^2p_2}{dy_2^2} - C_b p_0 p_2 - \mu y_1 p_0 \frac{dp_2}{dy_2} + C_b p_0 y_2 \frac{dp}{dy_2} = 0$$

Since $p_0 \neq 0$, the following equation is valid,

$$\mu^* y_1^2 \frac{d^2p_2}{dy_2^2} + (C_b y_2 - \mu y_1) \frac{dp_2}{dy_2} + C_b p_2 = 0$$

The solution to the above equation can be written in the form

$$p_2(y_2|y_1) = e^{-\frac{(C_b y_2 - \mu y_1)^2}{2\mu^* y_1^2 C_b^2}} \left[\alpha_1 + \frac{P(y_1)}{\alpha_1 \mu^* y_1^2 C_b^2} Q(C_b y_2 - \mu y_1)\right],$$

where

$$Q(C_b y_2 - \mu y_1) = \int e^{(C_b y_2 - \mu y_1)^2/2\mu^* y_1^2 C_b^2} d(C_b y_2 - \mu y_1)$$

α_1 represents the constant of integration

$P(y_1)$ arbitrary function of y_1 obtained during integration.

But, $Q(C_b y_2 - \mu y_1)$ is an increasing function which makes the area under the curve $p(y_2|y_1)$ tend to infinity. Since this is impossible, it

follows

$$Q(C_b y_2 - \mu y_1) = 0.$$

Thus

$$p_2(y_2|y_1) = \alpha_1 \exp\left[-\frac{(C_b y_2 - \mu y_1)^2}{2\mu^* C_b^2 y_1^2}\right] \tag{6.34}$$

Substituting $p_2(y_2|y_1)$ into equation (6.33) the following equation for $p(y_1,y_2)$ is obtained.

$$p(y_1,y_2) = \alpha_1 p_1(y_1) \exp\left[-\frac{(C_b y_2 - \mu y_1)^2}{2\mu^* C_b^2 y_1^2}\right] \tag{6.35}$$

Substituting equation (6.35) into equation (6.32), the equation to evaluate $p_1(y_1)$ is obtained, and is

$$y_2 \frac{dp_1(y_1)}{dy_1} - p_1(y_1)\left[(C_b - 1)\left\{1 - \frac{(C_b y_2 - \mu y_1)^2}{\mu^* C_b^2 y_1^2}\right\} - y_2\left\{\frac{(C_b y_2 - \mu y_1)^2}{\mu^* C_b^2 y_1^3} + \frac{(C_b y_2 - \mu y_1)\mu}{\mu^* C_b^2 y_1}\right\}\right] = 0 \tag{6.36}$$

The solution to the above equation can be written in the form

$$p_1(y_1) = \alpha_2 e^{-\left[H_1(y_2)y_1 + H_2(y_2)\ln y_1 + H_3(y_2)y_1^{-1} + H_4(y_2)y_1^{-2}\right]} \tag{6.37}$$

where

α_2 : represents the constant of integration

$$H_1(y_2) = \frac{(1 - C_b)}{y_2}\left\{1 - \frac{\mu^2}{\mu^* C_b^2}\right\} - \frac{\mu^2}{\mu^* C_b^2}$$

$$H_2(y_2) = \frac{2(1 - C_b)\mu}{\mu^*} + \frac{\mu^2}{\mu^* C_b^2} + \frac{\mu}{\mu^* C_b}$$

$$H_3(y_2) = \frac{(1 - C_b)y_2}{\mu^*} + \frac{2\mu}{\mu^{*2} C_b}$$

$$H_4(y_2) = \frac{y_2^2}{2\mu^*}$$

Thus, combining equations (6.34) and (6.37) the equation for the joint probability density of velocity and displacement is obtained, and is

$$p(\xi,\dot{\xi}) = \alpha^* e^{-[T_1(\dot{\xi})\xi + T_2(\dot{\xi})\xi^0 + T_3(\dot{\xi})\ln\xi + T_4(\dot{\xi})\xi^{-1} + T_5(\dot{\xi})\xi^{-2}]} \tag{6.38}$$

where

$$\alpha^* = \alpha_1\alpha_2$$

$$T_1(\dot{\xi}) = \frac{(1 - C_b)}{\dot{\xi}^2}\left\{1 - \frac{\mu^2}{\mu^* C_b^2}\right\} - \frac{\mu^2}{\mu^* C_b^2}$$

$$T_2(\dot{\xi}) = \frac{\mu}{2\mu^* C_b^2}$$

$$T_3(\dot{\xi}) = \frac{2(1 - C_b)\mu}{\mu^*} + \frac{\mu}{\mu^* C_b^2} + \frac{\mu}{\mu^* C_b}$$

$$T_4(\dot{\xi}) = \frac{(1 - C_b)\dot{\xi}}{\mu^*} + \frac{2\mu}{\mu^{*2} C_b}$$

$$T_5(\dot{\xi}) = \frac{\dot{\xi}^2}{2\mu^*}$$

The constant α is evaluated from the normality relation

$$\alpha^* \int_{-\infty}^{\infty}\int_{-\infty}^{\infty} e^{-[T_1(\dot{\xi})\xi + T_2(\dot{\xi})\xi^0 + T_3(\dot{\xi})\ell n\xi + T_4(\dot{\xi})\xi^{-1} + T_5(\dot{\xi})\xi^{-2}]} d\xi d\dot{\xi} = 1 \tag{6.39}$$

Once a method to solve equation (6.39) is ascertained, the normality constant can be determined, and thus the expression for the two dimensional probability density function of displacement and velocity can be completely specified. From the probability density function, the mean and mean square value of not only response of the cutting tool-boring assembly, but also the spindle-workpiece assembly can be determined, from which the tool tip motion can be derived. This needs further investigation.

This approach is presented here purely for the sake of interest and completeness. This would also have provided a comparison for the analytical solutions obtained in Sections 6.1 and 6.3. However, because of analytical difficulties mentioned, and because of the response solutions already obtained in a closed form, this approach is left for further pursuit at a later stage.

6.7 Conclusion

The solutions to the stochastic differential equations, which mathematically represent the machine tool workpiece system are presented. The solutions to the parametric stochastic equations are obtained using the averaging technique, where as the non-parametric non-homogeneous equations are solved using the Fokker-Planck equations. Based on the response of the cutting tool-boring bar system and the spindle-workpiece assembly due to the action of the resultant force system, the deflection of the cutting tool with respect to the workpiece is determined. The

true motion of the cutting tool is then described by the maximum deviation curve, average curve, and the minimum deviation curves, which are in turn obtained from the deflection of the cutting tool with respect to the workpiece. Since, the true motion of the cutting tool is a helix, whose upper and lower boundaries are defined by the maximum deviation and minimum deviation curves, the surface produced on the workpiece should exhibit helical grooves. Such helical grooves were observed on the hole produced when viewed under a microscope. Further, the maximum, average, and minimum values of the deviation of the cutting tool tip, which is a measure of the roundness, are also determined. Based on these, it is seen that the error, at any position, for a given machining condition, can take any value between the maximum error and minimum error depending upon the value of the probability density function. This is confirmed by the roundness measurement, which reveals no definite pattern for the roundness error variation with the depth of hole and feed. Lastly, an alternate closed form method to solve parametric stochastic differential equations is also suggested. The solution obtained using this technique was not used in the determination of the tool tip motion, as the expression to evaluate the normality constants has not yet been determined. Further investigations have to be carried out before this technique is accepted.

The true motion of the tool tip is of prime importance in the determination of the initial state of the machining parameters in the development of an on line adaptive control system. This is described in detail in the next Chapter.

CHAPTER 7

RECOMMENDATION FOR AN ON-LINE ADAPTIVE CONTROL

CHAPTER 7

RECOMMENDATION FOR AN ON-LINE ADAPTIVE CONTROL

Computers add flexibility, reliability and intelligence to manufacturing systems thus making it possible to greatly extend the performance of machine tools. In the past twenty years, since the advent of the first numerically controlled machine in 1952, the expansion of computing power has led to the development of

a) DNC (Direct Numerical Control) where a shared computer is used for distribution of part program data via data lines to remote machine tools,

b) CNC (Computer Numerical Control) where a dedicated computer is used within a numerical control unit with the capability of a local data input,

c) PC (Programmable Controllers) which are microprocessor-based devices that can control many processors on machines or in factory systems.

Recently, computer networks have been developed leading to a full integration of CNC and DNC systems giving a DPM (Distributed Plant Managing) wherein the functions of DNC and CNC are combined into an integrated, interactive factory data management system with flexibility for future expansion and rearrangement. Within such a system the individual machine tool should ideally be able to carry out the machining activities independently and adaptively without human intervention at the machine hardware level. This is the goal of the research in Adaptive Control.

Adaptive Control systems have been used in various machining

operations such as, drilling [124], turning [125], grinding [126], and milling [127,128] and these studies reveal that AC systems can increase metal removal rates by 20-80% and thus improving productivity. Despite the potential for improving productivity, there are still some impediments to the widespread use of AC in industry because of the need for developments in sensor technology, and the variable nature of the machining process [129].

In BTA deep-hole machining, deep and accurate holes are to be produced in a short time. This process involves both roughing and finishing operations in terms of large metal removal rates, maintaining accuracy at the same time. The motion of the tool tip decides the metal removal rate. Also, the efficient functioning of the chip breakers under machining conditions, depends upon the tool tip motion. This is because the tool angles relative to the workpiece depend upon the position and orientation of the tool. Further, the motion of the tool tip decides the nature of the surface produced on the workpiece as explained in Chapter 6. In other words, the motion of the tool tip is a key factor in any adaptive control to be recommended.

This Chapter presents the concept of an on-line low cost adaptive control of machine tools wherein the initial values of the feed and speed are chosen based on the motion of the tool tip. The sensor used for detecting the state variables (the resultant force system acting on the cutting tool) consists of a piezoelectric dynamometer having high natural frequency. It has been shown [130] that these dynamometers can detect the dynamic fluctuations of the cutting force to a very high degree of accuracy. It has also been shown [131,132] that there exists

a clear relation between the probabilistic characteristics of the resultant force system and the resulting surface signals. Based on the random excursion of the resultant force system signals about a specified level, certain statistical parameters describing these excursions can be evaluated by a software package in the microprocessor. The statistical parameters of the surface finish are then evaluated based on a correlation between the parameters of the resulting force system and the surface profile. These are then compared with an acceptable set of values of the respective parameters. Based on the result of the comparison certain changes in the machining conditions take place using the controller software package. The microprocessor can either be a 16 bit or 32 bit system depending upon the accuracy required and economic feasibility. This forms the concept of adaptive control of machine tools using the random function excursion technique [ACRFE]. The advantages of ACRFE are that it combines the characteristics of Adaptive Control of Optimization [ACO] and Adaptive Control of Constraints [ACC] and it takes into account the tool wear without considering it as an explicit variable. Finally, the methodology of applying this technique to BTA deep-hole machining is presented.

7.1 Traditional Adaptive Systems

An adaptive system, in simple terms, can be considered as a system which makes adjustments within itself to accommodate for changes. A more precise definition [133] is that an adaptive system measures a certain performance index using the inputs, the states, and the outputs of the adjustable system. From the comparison of the measured index of performance and a set of given values, the adaption mechanism modifies the parameter of the adjustable system or generates an auxiliary input

in order to maintain the index of performance close to the set of given values. For the purposes of this work in manufacturing systems, adaptive control is defined as a system that allows the machine tool equipped with sensors (a dynamometer) to detect a changing environment (the excursions of the resultant force signals about a specified level) and then take corrective actions (change feed and/or speed).

AC systems can be classified into two types [134,135]:

a) Adaptive Control of Optimization (ACO), in which the performance is optimized according to a prescribed index of performance [IP]. The IP is usually an economic function such as minimum machining cost or maximum production rate by utilizing the well known Taylor equations for the particular tool-workpiece combinations.

b) Adaptive Control of Constraints (ACC), in which machining conditions such as spindle speed and/or feed ratio are maximized within the prescribed limits of machine and tool constraints.

Research and development efforts for adaptive control of machine tools have been underway since the early 1960's. While these early AC systems, which were primarily used in grinding, drilling and milling, demonstrated significant increases in productivity, there were also many practical problems. In particular, there were reliability problems especially with sensors. Also, attempts to mathematically define an economic performance index and to optimize the machining process met with limited success [136]. Many types of AC systems have been proposed and tested, including dimensional correction loops based on inspection of the finished part, systems for controlling tool wear rate [137,138], minimizing tool workpiece impact [137], and detecting and correcting

for chatter [139,140,141]. Successful AC applications in drilling and milling are mainly of ACC type [134], and in grinding the ACO type [126]. An adaptive system for deep-hole machining has been suggested [142], wherein the mean value of the torque is measured and compared with a pre-set value of torque, and changes in the feed, and speed take place depending upon the difference between the measured and pre-set value. Further, an upper bound for feed and speed needs to be specified to avoid tool failure.

7.2 Random Function Excursion of Force and Surface Texture Signals

The concept of random function excursion was used extensively in the area of communication systems and automation [143-148] and formed the basis for profile characterization of manufactured surfaces [149,150], where the mathematical theory of stochastic excursions is employed to obtain parameters describing crest widths and valley spacings about different levels measured in terms of the CLA value. This approach gives a sufficient number of key surface roughness parameters for both height and lengthwise characterization; namely, the CLA and RMS values for amplitude descriptions, and the mean and variance for the intercept excursion descriptions. The method is easily computerized for practical applications and lends itself to automated surface texture data analysis in which surface parameters can be computed continuously and rapidly using low cost instrumentation. The four parameters proposed are [149],

$$MCE = \sum_{i=1}^{n_a} \lambda_i P_c(\lambda_i) \qquad (7.1)$$

$$RMSCE = \left[\sum_{i=1}^{n_a} (\lambda_i - MCE)^2 \, P_c(\lambda_i)\right]^{\frac{1}{2}} \tag{7.2}$$

$$MVE = \sum_{i=1}^{n_a} \Lambda_i P_v(\Lambda_i) \tag{7.3}$$

$$RMSVE = \left[\sum_{i=1}^{n_a} (\Lambda_i - MVE)^2 \, P_v(\Lambda_i)\right]^{\frac{1}{2}} \tag{7.4}$$

If these parameters are evaluated about a specified level, say the CLA value of the roughness profile and are used together with the height indicies, CLA and RMS values, a good knowledge of the mechanical properties of the machined surface can be obtained.

On similar lines the signals representing the resultant force system can be represented by corresponding stochastic excursions about the mean (steady state component) value of the respective components. Thus the four parameters, which along with the mean component, probability density function and power spectral density, which describe the dynamic fluctuations of the resultant force system, are

$$MCEGF = \sum_{i=1}^{m_a} \lambda_{if} \, P_c(\lambda_{if}) \tag{7.5}$$

$$RMSCEGF = \left[\sum_{i=1}^{m_a} (\lambda_{if} - MCEGF)^2 \, P_c(\lambda_{if})\right]^{\frac{1}{2}} \tag{7.6}$$

$$MVEGF = \sum_{i=1}^{m_a} \Lambda_{if} P_v(\Lambda_{if}) \tag{7.7}$$

$$RMSVEGF = \left[\sum_{i=1}^{m_a} (\Lambda_{if} - MVEGF)^2 \, P_v(\Lambda_{if}) \right]^{\frac{1}{2}} \tag{7.8}$$

The flow chart for computing MCEGF, RMSCEGF, MVEGF, RMSVEGF is shown in Fig. 7.1. In addition, two other parameters for the complete force representation are calculated and are

$$CLAGF = \sum_{i=1}^{n} \frac{y_i}{n} \tag{7.9}$$

$$RMSGF = \left[\frac{1}{n} \sum_{i=1}^{n} y_i^2 \right]^{\frac{1}{2}} \tag{7.10}$$

7.3 Adaptive Control by Random Function Excursion

The design of an adaptive control unit involves the choosing of an appropriate sensor, controller computer and obtaining a suitable index of performance considering as many possible variables which effect the machining process. Here, the design of an adaptive control unit for finishing operations with particular reference to finish turning and BTA deep-hole machining is presented.

In any finishing operation, the macro- and micro-geometrical errors on the workpiece should be a minimum. In BTA deep-hole machining, in addition to the surface finish, the roundness error, and the axial run out should be a minimum. Further, the productivity, which depends largely upon tool wear, should be a maximum. All these factors directly depend upon the resultant force system acting on the cutting tool. It

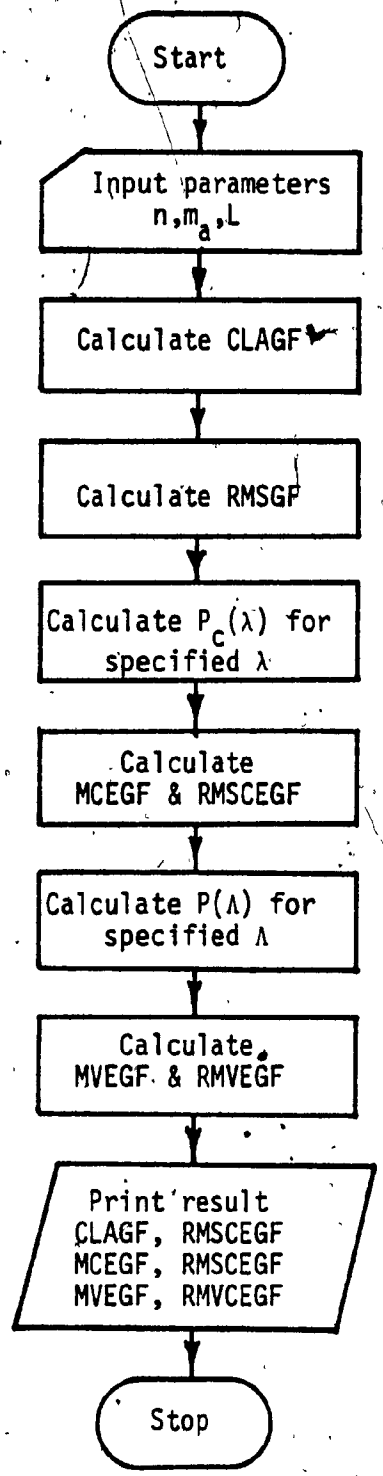

Fig. 7.1: Flow Chart for Computation of Generalized Force Parameters

has been previously shown [116] that the dynamic fluctuations of the resultant force system acting on the cutting tool dictate the nature and trend of the macro- and micro geometrical errors in BTA deep-hole machining. Therefore, the dynamic fluctuations of the resultant force system only, need be sensed. These dynamic fluctuations can be sensed very accurately by the deployment of piezoelectric dynamometers possessing a wide range of frequencies, thus minimizing any error made in sensing. These piezoelectric dynamometers, wherein an electric charge is generated when a force is applied on the faces of a suitably sectioned piezoelectric quartz crystal, have a very high natural frequency and large sensitivity. Based on the dynamic fluctuations, the six parameters described by equations (7.5) to (7.10) are computed from which the six parameters describing the surface texture are evaluated using the following relations:

$$CLA = F_{1i}\,[CLAGF, feed, speed] \quad (7.11)$$

$$RMS = F_{2i}\,[RMSGF, feed, speed] \quad (7.12)$$

$$MCE = F_{3i}\,[MCEGF, feed, speed] \quad (7.13)$$

$$RMSCE = F_{4i}\,[RMSCEGF, feed, speed] \quad (7.14)$$

$$MVE = F_{5i}\,[MVEGF, feed, speed] \quad (7.15)$$

$$RMSVE = F_{6i}\,[RMSVEGF, feed, speed] \quad (7.16)$$

where 'i' is the number of generalized coordinates and functions F_{1i} to F_{6i} vary depending upon the finishing operation. The computations are performed within the microprocessor. The values computed in equations (7.11) to (7.16) are then compared with the acceptable standard and

depending upon the output, the correction in feed and speed is computed using the controller subroutine in the microprocessor. This entire operation is shown in Fig. 7.2. Depending upon the correction signal, the actuators adjust the feed and speed. This entire operation can be performed in milliseconds. The machine tool with adaptive control units is shown in Fig. 7.3.

7.4 Selection of the Initial Machining Conditions

For an effective adaptive control, the choice of the initial machining conditions is of prime importance. This is because the time taken by the system to reach a new state depends not only upon the reliability and structure of the controller, but also upon the initial state. There is no explicit method available to choose this initial state. However, this section presents a methodology of choosing this initial state based on the motion of the tip, derived in the previous Chapter.

The motion of the tool tip, described in Chapter 6 was established in terms of the average curve, minimum and maximum deviation curves. These curves can be displayed on a computer graphics terminal by writing suitable software programs. These curves, when superposed on an ideal cylinder, will give the zone of deviation from the true cylinder. Further, the CLA and RMS values of the surface deviations can be obtained using

$$CLA = \frac{\sum_{i=1}^{m} \left| r_i(t) - \frac{d}{2} \right|}{m} \qquad (7.17)$$

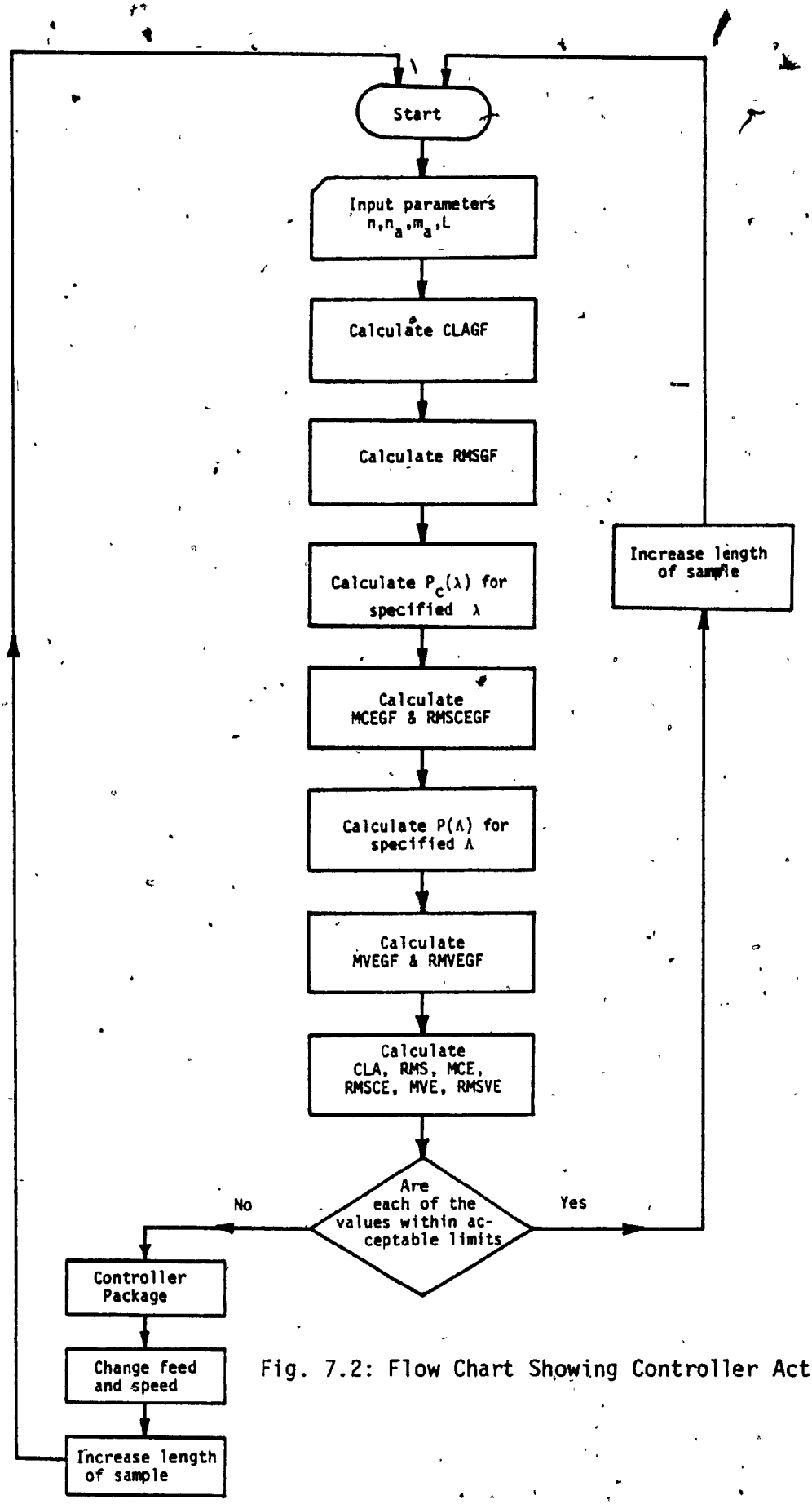

Fig. 7.2: Flow Chart Showing Controller Action

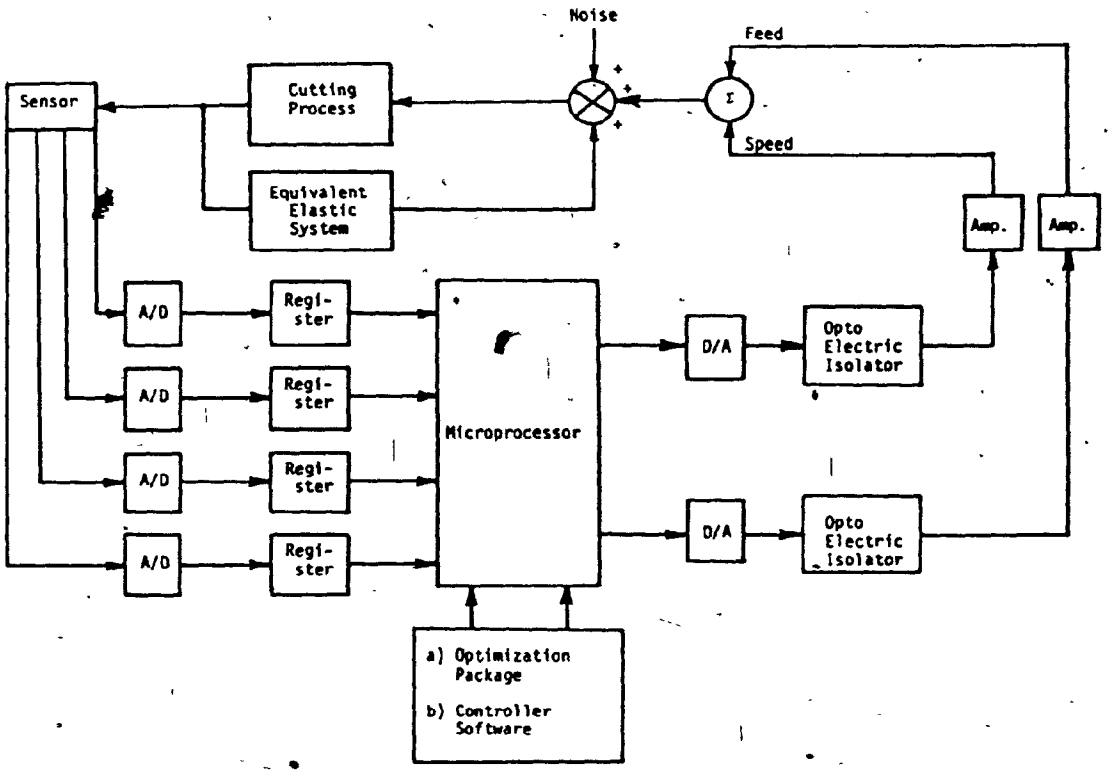

Figure 7.3: A Microprocessor Based Adaptive Control Unit

$$RMS = \left[\frac{1}{m}\sum_{i=1}^{m}\left(r_i(t) - \frac{d}{2}\right)^2\right]^{\frac{1}{2}} \qquad (7.18)$$

where

$r_i(t)$. is the position of the tool tip at the i^{th} sampling point

d is the diameter of the cutting tool

m number of sampling points

Depending upon the shop and product requirements, the accuracy of the finished product will be specified. Therefore, from the CLA, RMS, and the zone of deviation, the motion of the tool tip can be simulated. Based on the deviations of tool tip from the ideal motion, a set of machining parameters can be determined, which represent the initial state of the system. Such a methodology of choosing the machining parameters ensures (a) the accuracy requirements are close to that specified, (b) the time taken for the system to take corrective actions is small, and (c) the stability of the machining operation without going into a chatter zone.

7.5 Conclusions

This Chapter presents the concept of a low cost adaptive control system [ACRFE] suitable for finishing operations as well as for BTA deep-hole machining. The sensor is a piezoelectric dynamometer to detect the dynamic fluctuations of the resultant force system. Based on the stochastic excursions of the dynamic fluctuations of the resultant force system, the statistical characteristics of the surface are

programmed through a software package. These are then compared with an acceptable set of values and based on the output, certain changes in the machining conditions, (feed, speed) using the software package are carried out.

The advantages of such a microprocessor based adaptive control unit, which relies on the random function excursion [ACRFE] are:

a) it combines the characteristics of ACC and ACO;

b) it takes into account tool wear without considering it as an explicit variable;

c) it is relatively inexpensive;

d) it can be easily interfaced with a computer graphics unit so that the actual tool movement can be seen on the screen;

e) such a system could be easily combined in a flexible manufacturing scheme with a data base management as shown in Fig. 7.4.

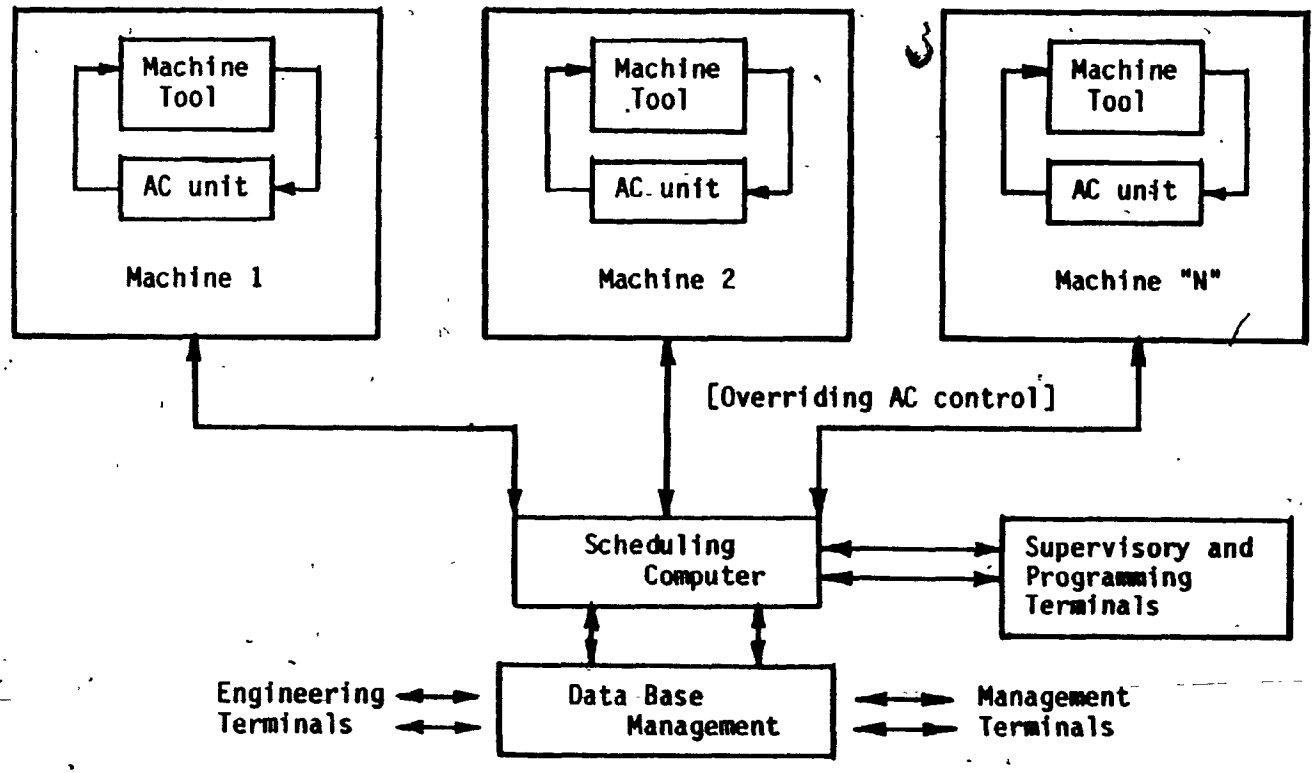

Fig. 7.4: A Flexible Manufacturing Scheme Using the ACRFE Technique

CHAPTER 8

CONCLUSIONS AND RECOMMENDATIONS

CHAPTER 8

CONCLUSIONS AND RECOMMENDATIONS

8.1 Brief Outline of the Work

This thesis investigates, the influence of the resultant force system on the machine tool-workpiece assembly in BTA deep-hole machining. A methodology for the solution is developed, by determining first, the dynamic interaction between the cutting tool and the workpiece, from which the signal properties of the resultant force system are obtained, and are presented in Chapters 2,3, and 4. Then, employing these characterizations of the resultant force system, and setting up an appropriate physical model for the machine tool workpiece assembly, a set of mathematical equations are developed in Chapter 5 to represent the total dynamic system. Finally, these equations are solved in closed form in Chapter 6 to establish the true motion of the tool tip and its influence on the machine tool-workpiece system. As a logical consequence, details required for setting up a microprocessor based adaptive control unit are described in Chapter 7.

8.2 Major Aspects of the Investigations

The highlights of this investigation are the following:

(i) A methodology for representing the steady state cutting forces and torque, using the thin shear plane model and incorporating the key features of the BTA process, is presented. This is subsequently extended to explain the regenerative chatter phenomena in the BTA process.

(ii) The resultant force system, consisting of an axial force and a torque; is found to be highly dynamic in nature, with the magnitude of

the peak values of the axial force and torque being 1.2 and 1.4 times their respective mean values. Their dynamic fluctuations are clearly random in nature, and are modelled as a wide band delta-correlated process with a gaussian distribution, in the frequency range of interest.

(iii) The rotating cutting tool-stationary workpiece working method of the BTA process is mathematically represented by four stochastic differential equations, and they describe the effect of the resultant "cutting" forces on the machine tool-workpiece system.

(iv) The solutions to the system stochastic differential equations are obtained using the Fokker-Planck approach and the averaging technique, from which the motion of the tool tip is evaluated by means of the maximum deviation, average and minimum deviation curves. The deviation of the motion of the tool tip dictates the accuracy of roundness of the hole produced.

(v) A recommendation for an on line adaptive control is presented based on the random function excursion technique. The initial values of the feed and speed, are chosen based on the zone of deviation of the cutting tool tip. This minimizes the possibility of the system becoming unstable during the controlling.

8.3 Detailed Discussion of the Results

In Chapter 2, a methodology for representing the cutting forces is presented, using the thin shear plane model and considering the influence of certain key characteristics of the BTA process. The thin shear plane model is used because (a) high cutting velocities are used; and (b) a chip breaker groove is present.

Such a representation has the following advantages:

(i) The variation of the steady state components of the torque, axial, radial, and tangential forces with the penetration of the cutting tool into the workpiece, can be determined.

(ii) The magnitudes of the steady state components of the torque, the axial, radial, and tangential forces can be evaluated by writing a simple computer programme. The results obtained show that the tangential, axial, and radial forces have magnitudes in the ratio of 10:5:5.1, at different values of the feed. Also, the variation of the radial force shows certain non-linear behaviour with the feed, whereas the torque, axial and tangential forces exhibit a more or less linear variation with the feed. The analytical values obtained here show a fairly good agreement with some of the experimental results published in the past. The small deviations that are observed may be attributed to the fact, that the equations derived to compute the cutting forces do not account for the variations caused in cutting forces due to different tool materials.

(iii) A mechanism for the regenerative chatter in the BTA process is developed, from which the values of the periodically varying component of the torque and cutting forces with respect to time can be determined.

(iv) A chatter analysis and its control, for the machine tool are facilitated, by first obtaining a mathematical model for the randomly varying component of the axial, tangential and radial forces, and torque, and using a combination of the different mathematical models for the periodically varying and randomly varying components, as the forcing function. There are also certain disadvantages in this procedure and they are listed below:

(i) The expression for the forcing function, for carrying out a chatter analysis, becomes very complex.

(ii) The co-efficients, describing the periodically varying components of the cutting forces and the torque, have to be determined by performing a number of metal cutting experiments.

Chapters 3 and 4 present the experimental measurements performed and the analysis of the resultant force system to develop the mathematical model. The experiments conducted achieved the following objectives:

(i) The variation of the resultant axial force and torque, under various machining parameters is established. Without such tests, it is not possible to derive an expression for the resultant force system acting on the cutting tool.

(ii) The variation of the peak axial force and the torque with the machining parameters is obtained. Such an equation is essential to determine the maximum value of the load which each member of the machine tool is subjected to.

(iii) As a result of the above, a mathematical model of the resultant force system is derived so that the performance characteristics of the machine tool under actual working conditions can be evaluated.

A two component piezoelectric dynamometer is chosen to suit the needs of the experiment and it is observed that the static calibration is linear with negligible hysteresis. The natural frequencies of the dynamometer, along the axial force and torque direction, are found to be 4 kHz and 2.8 kHz respectively. The dominant frequency range of the resultant force system is well within the dynamometer range of 2.8 kHz. The frequency response test of the machine tool workpiece system is also

carried out to determine the influence of the machine tool-workpiece system on the measuring accuracy. It is seen that the valid frequency range from the static calibration is 0 to 350 Hz. A close examination of the spectral power distribution of the frequencies of the resultant force system reveals that the power content due to the dynamic fluctuations above 350 Hz is small. Thus, the frequency range of interest becomes 0 to 350 Hz and the error contained in neglecting frequencies of greater than 350 Hz is negligible. Over this frequency range, the dynamic fluctuations of the resultant force system is modelled as a stationary wide band process with a gaussian density function. The assumptions included in arriving at this model are:

(i) The given sample record will properly reflect any non-stationary characteristics, if at all present.

(ii) The given sample record is very long compared to the lowest frequency component.

(iii) The actual random characteristics of the resultant force system has been idealized as a first order Markov process. Such an assumption is valid because the power content of the dynamic fluctuations in the desired frequency range of 0 to 350 Hz is significant.

The steady state component of the resultant force system is measured by setting the time constant of the measuring system to a large value. It is observed that the variation of the axial force and the torque with the feed and the diameter, is not linear. This non-linearity arises mainly because the burnishing action taking place between the workpiece and the pads involves a plastic deformation, which is essentially non-linear. Also, it is observed that the total axial force is about 1.3

times the value of the cutting axial force, whereas the total torque is approximately 2 times the value of the cutting torque.

Chapters 5 and 6 present a procedure for deriving a comprehensive mathematical model and obtaining closed form solutions to the equations representing such a mathematical model. Such an approach is helpful in the

(a) selection of the parameters of a drive;

(b) analysis of the machine tool behaviour upon travel of the components without cutting action;

(c) analysis of the machine tool behaviour during machining operation;

(d) development of control system to prevent a tendency of the machine tool to go into an unstable region during machining;

(e) development of an appropriate adaptive control unit.

The model for the deep-hole machining system is obtained by first identifying the major components. Each component is then modelled separately using discrete elements such as springs and dampers by considering

(i) the location of each component in the machine tool system;

(ii) their functional characteristics;

(iii) the effect of clearances and tolerances on the performance;

(iv) the stiffness and damping present at different key locations along the component.

Since, the aim of this investigation is to determine the effect of the resultant force system on the dynamics of the machine tool-workpiece system, a mathematical model, based on an appropriately simplified model of the BTA deep-hole machining system is obtained using the assumed modes

method. This is because, the solution to the exact stochastic partial differential equations, obtained here, using the Hamilton's principle, is difficult. The mathematical model consists of two non-homogeneous stochastic differential equations and two parametric stochastic differential equations. The non-homogeneous partial differential equations are solved using the Fokker-Planck approach as the system response can be represented by a Markov process in phase space. The solutions to the parametric stochastic differential equations are obtained using the well known averaging technique. The assumptions made regarding the excitation process:

(i) The intensity of the exciting force is not large; that is, it does not lead to a large change in amplitude during one period of system oscillation.

(ii) The exciting force differs from a sine wave because of slowly varying but constantly accumulating deviations of amplitude and phase.

(iii) The accumulating deviations in amplitude and phase are small for one or several periods, but after a large number of periods the amplitude and phase change significantly.

(iv) The changes in amplitude and phase after a large number of periods makes the sinusoidal wave function completely different from the original shape.

(v) The time derivatives of the amplitude and phase are small. The solutions to the four stochastic differential system equations are then combined, using vector addition, to obtain the motion of the tool tip in terms of maximum deviation curve, average curve, and minimum

deviation curve. The deviation of the tool tip from the ideal motion dictates the accuracy of roundness, or the error in the produced hole.

Finally, a recommendation for an on-line adaptive control is presented in Chapter 7, based on the random function excursion technique and using the fact that there exists a direct relation between the probabilistic characteristics of the resultant force and the surface texture produced on the workpiece. Since, the controller is a software package in a microprocessor, the entire controlling action is carried out in milliseconds, making the ACRFE very feasible for finishing operations. The CLA and RMS values required on a surface are usually specified. So, the zone of deviation of the cutting tool tip is determined from the expression for tool tip motion, from which the initial values of the feed and the speed are determined. Such a specification of the initial state minimizes the possibility of the system becoming unstable during the stage of controlling.

8.4 A Comparison of Roundness Errors

A comparison between the experimentally measured roundness error and the theoretically obtained roundness error, due to deviation of the tool tip from the ideal motion, establishes the validity of the mathematical model representing the BTA deep-hole machining system. For this purpose, based on the equations representing the tool tip motion, an index is defined which gives an upper bound for the roundness error. This is stated as

$$[OOR]_{ub} = \left\{[\Phi_2(0)A_{bm}]^2 + [\Psi_i(x)A_{sm}]^2\right\}^{\frac{1}{2}} \qquad (8.1)$$

with i = 1 or 2, depending upon the region in the spindle-workpiece assembly being considered.

The values of $[OOR]_{ub}$ are calculated using the following data for the constants, which are obtained from the experiments carried out.

Density of the oil-chip mixture = 7848 N/m^3

Power spectral density of the axial force = 0.05 W/Hz

Volume flow rate of oil = 0.035 $\frac{m^3}{min}$

Upon calculating the values of A_{bm} and A_{sm}, it is found that A_{bm} is always zero, because m_1 approaches infinity, and A_{sm} is given by

$$A_{sm} = e^{t[5.28\times10^{-9} - 9294\zeta]} \quad \text{meters}$$

Therefore, the expression for $[OOR]_{ub}$ becomes

$$[OOR]_{ub} = \Psi_i(x)\, e^{t[5.28\times10^{-9} - 9294\zeta]} \quad \text{meters} \qquad (8.2)$$

The out-of-roundness values are plotted for different values of ζ as shown in Fig. 8.1, and are compared with some experimentally obtained values. The following observations can be made based on Fig. 8.1.

(i) The roundness error is largely dependent upon the value of ζ.

(ii) The zone of large roundness error corresponds to the zone where the probability of displacement of the tool is the greatest. Since, the first moment of this probability density distribution is an exponential function, the roundness error also decays exponentially.

(iii) The value of the roundness error at zero depth is dictated by the value of $\Psi_i(x)$ at $x = 0$. Since $\Psi_i(x)$ is zero, the roundness error is obviously zero.

(iv) Although, theoretically the roundness error is zero beyond a certain depth of hole, the roundness error measured gives a finite

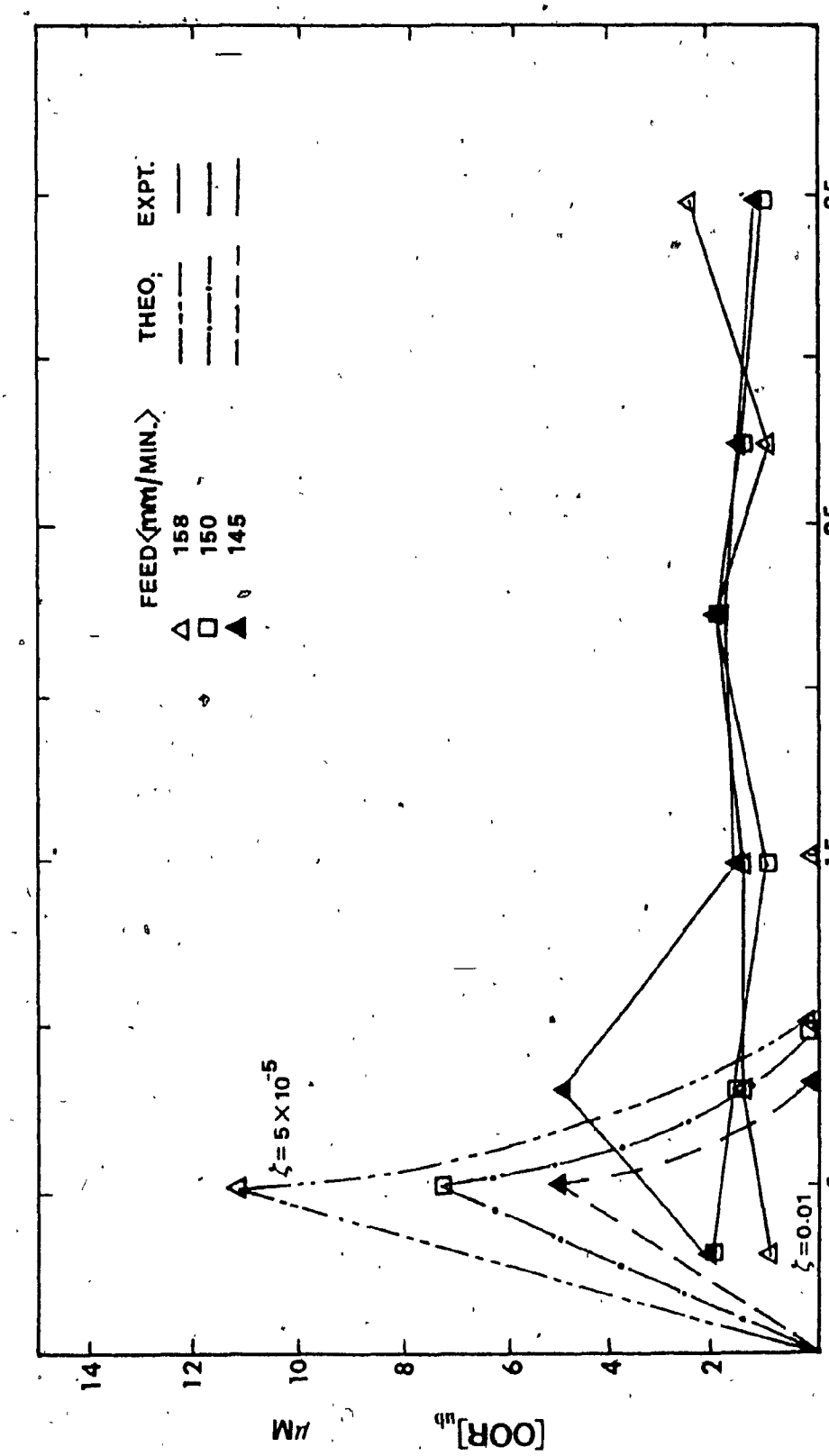

Figure 8.1: Variation of Theoretically Predicted Roundness Error with Depth of Hole

value. This difference arises due to the following limitations in the model:

(a) The resultant force system acting on the cutting tool has been assumed to consist of a resultant axial force and a torque. This is valid, if the damping between the cutting tool and the workpiece due to burnishing, stick-slip, and friction is neglected, and the stiffness is assumed to be very large as is the case in the present analysis. But actually, this stiffness at the pads is finite, and so, the resultant force system acting on the cutting tool will consists of a radial and tangential force in addition to the axial force and torque.

(b) The bearings at the rest and drive unit are considered to be infinitely stiff, but ideally this is not true. A finite stiffness present at the various bearing supports will cause a whirling of the boring bar, which leads to a greater deflection of the cutting tool.

(c) The impacting force on the cutting tool due to the pressure fluctuations in the pressure head also causes the tool to deflect more than usual. This has not been accounted for in the theoretical model developed here.

Based on these observations, it is speculated that the resultant force system is not completely balanced at the pads. The validity of this statement can only be determined by performing a number of experiments to measure the radial and tangential forces acting on the cutting tool.

8.5 Recommendations for Future Work

Based on the present investigation the following recommendations are suggested for future development of research on the problem considered in this thesis. They are:

(a) This investigation presents only the influence of the tool tip motion on the roundness of the hole produced in the workpiece. Such an analysis can be extended to correlate the tool tip deflection with the surface texture of the produced workpiece. For this, a series of experiments have to be carried out to determine:

(i) the stiffness and damping between each of the pads, cutting profile and the workpiece;

(ii) The complete characteristics of the resultant force system in such cases. Based on the results obtained, a mathematical model for the machine tool workpiece system is to be obtained similar to the present method, from which the true motion of the tool tip may be determined. Indicies for identifying the surface texture can then be defined from the deviation error of the tool tip. This has to be compared with experimentally observed values to check the range of applicability of the theoretical model developed.

(b) The physical models for the three working methods have been suggested, out of which a detailed mathematical analysis has been carried out only for the stationary workpiece-rotating cutting tool method, neglecting any rotor dynamic effects. The rotor dynamic effects may be included and analysis for the three working methods may be carried out. Based on the results obtained, the results of the three working methods can be compared and the best working method for a particular application chosen for best performance of the machine system.

(c) To reduce the vibration and to improve the surface finish of the product, passive dampers, namely, an impact type damper, can be considered. The applicability of impact dampers at high feeds should be

examined to improve upon the productivity of the BTA process. The design and implementation of these impact dampers should be envisaged and the effective location determined from vibration analysis. The performance of the machining operation with and without the impact dampers may be analyzed in terms of chip thickness, force and/or torque fluctuations and the produced surface texture on the workpiece. A theoretical analysis can then be carried out to support the experimental findings.

(d) The forces acting on a standard twist drill consist of an axial force and torque. But, due to the shape of the drill it may be expected that there is a coupling between the axial force and the exerted torque. A mathematical expression to identify this coupling may be developed in terms of the drill geometry. Next, the projected profile of the twist drill can be represented by an equation using an appropriate least square algorithm. Based on the result obtained, an appropriate model for the drill has to be established. It is already indicated that the dynamic fluctuations of the resultant force system on the drill can be represented by a stationary wide band process with a gaussian density function. This then becomes the forcing function on the drill. Based on the physical model, a mathematical model to represent the influence of the axial force and torque can be developed. The solution to these equations may be able to answer the walking phenomenon observed in most drills.

(e) In BTA deep-hole machining a very good surface finish on the hole produced is obtained only with a particular value of feed. This value of the feed varies with the diameter of the cutting tool. If the feed is increased, a chatter phenomenon results. To reduce this chatter, an active control of the boring bar is to be implemented. This can be

done by sensing the vibration signals at key locations of the boring bar and analyzing them on-line through either an FFT analyzer or a software package incorporating a certain performance index in a microprocessor. Based on the output, the vibration of the bar can be minimized by the superposition of an appropriate external disturbance. This may lead to securing a better surface finish of the machined hole at higher feeds, thus improving the productivity in BTA machining.

REFERENCES

REFERENCES

1. Latinovic, V., "An Investigation of the Theoretical and Design Aspects of Unsymmetrical Multi-Cutting Action in Deep-Hole Machining", D.Engg. Thesis, Concordia University, Montreal, 1978.

2. Steeds, W., "A History of Machine Tools 1700-1910", Oxford Press, 1969, p. 1.

3. Armarego, E.J.A., and Brown, R.H., "The Machining of Metals", Prentice Hall, New York, 1969.

4. Galloway, D.F., "Some Experiments on the Influence of Various Factors on Drill Performance", Trans. ASME, Vol. 79, 1957, p. 191.

5. Haggerty, W.A., "Effect of Point Geometry and Dimensional Symmetry on Drill Performance", Int. J. of Mac. Tool. Des. Res., No. 1, 1961, p. 41.

6. Swinehart, H.J., "Gundrilling, Trepanning, and Deep-Hole Machining", ASTME, Dearborn, 1967.

7. Merchant, M.E., "Mechanics of the Cutting Process", J. of App. Phy., 16, 1945, pp. 267 & 318.

8. Kobayashi, S., and Thomsen, E.G., "Some Observations of the Shearing Process in Metal Cutting", Trans. ASME, J. of Engg. for Indus., 81, 1959, p. 251.

9. Palmer, W.B., and Oxley, P.L.B., "Mechanics of Orthogonal Machining", Proc. Inst. Mech. Engrs., 173, 1969, p. 263.

10. Okushima, K., and Hitomi, K., "An Analysis of the Mechanics of Orthogonal Cutting and Its Application to Discontinuous Chip Formation", Trans. ASME, J. of Engg. for Indus., 83, 1961, p. 545.

11. Shaw, M.C., Cook, N.H., and Smith, P.A., "The Mechanics of Three-Dimensional Cutting Operations", Trans. ASME, 74, 1952, p. 1055.

12. Brown, R.H., and Armarego, E.J.A., "Oblique Machining with a Single Cutting Edge", Int. J. of Mac. Tool Des. Res., 4, 1964, p. 9.

13. Kronenberg, M., "Machining Science and Application", Pergamon Press, 1966.

14. Shaw, M.C., and Oxford, C.J. Jr., "On the Drilling of Metals II: The Torque and Thrust in Drilling", Trans. ASME, 79, 1957, p. 139.

15. Boston, O.W., and Kraus, C.E., "Elements of Milling", Trans. ASME, 54, 1932, p. 71.

16. Koenigsberger, F., and Sabberwal, A.J.P., "An Investigation into the Cutting Force Pulsations During Milling Operations", Int. J. of Mac. Tool Des. Res., 1, 1961, p. 15.

17. Arnold, R.N., "The Mechanism of Tool Vibration in Cutting Steel", Proc. Inst. Mech. Engr., 154, 1946, p. 261.

18. Doi, S., and Kato, S., "Chatter Vibration of Lathe Tools", Trans. ASME, 78, 1956, p. 1127.

19. Tobias, S.A., and Fishwick, W., "Chatter of Lathe Tools Under Orthogonal Cutting Conditions", Trans. ASME, 80, 1958, p. 1079.

20. Tobias, S.A., and Fishwick, W., "Vibrations of Radial Drilling Machines under Test and Working Conditions", Proc. Inst. Mech. Engg., 170, 1956, p. 232.

21. Tobias, S.A., "Vibrations of Vertical Milling Machines under Test and Working Conditions", Proc. Inst. Mech. Engg., 173, 1959, p. 474.

22. Smith, J.D., and Tobias, S.A., "The Dynamic Cutting of Metals", Int. J. of Mac. Tool Des. Res., 1, 1961, p. 283.

23. Albrecht, P., "Dynamics of Metal Cutting Process", Trans. ASME, Ser. B., J. of Engg. for Indus., 87, 1965, p. 429.

24. Wallace, P.W., and Andrew, C., "Machining Forces: Some Effects of Removing a Wavy Surface", J. of Mech. Engg. Science, 8, 1966, p. 129.

25. Wallace, P.W., and Andrew, C., "Machining Forces: Some Effects of Tool Vibration", J. of Mech. Engg. Science, 7, 1965, p. 152.

26. Das, M.K., and Tobias, S.A., "The Relation Between the Static and Dynamic Cutting of Metals", Int. J. of Mac. Tool Des. Res., 7, 1967, p. 63.

27. Knight, W.A., "The Universal Machinability Index and the Prediction of Machine Tool Stability", Int. J. of Mac. Tool Des. Res., 7, 1967, p. 91.

28. Kainth, G.S., "Dynamics of Metal Cutting Process", Sixth AIMTDR Proceedings, 1970, p. 249.

29. Kainth, G.S., "Dynamic Shear Angle Approach to the Prediction of Machine Tool Stability", Sixth AIMTDR Proceedings, 1970, p. 262.

30. Nigm, M.M., Sadek, M.M., and Tobias, S.A., "Dimensional Analysis of the Steady State Orthogonal Cutting Process", Int. J. of Mac. Tool Des. Res., 17, 1977, p. 1.

31. Nigm, M.M., Sadek, M.M., and Tobias, S.A., "Determination of Dynamic Cutting Co-efficients from Steady State Cutting Data", Int. J. of Mach. Tool Des. Res., 17, 1977, p. 19.

32. Rubenstein, C., "An Analysis of Dynamic Cutting when a Plane Surface is Cut with an Oscillating Tool I: General Equations", Int. J. of Mac. Tool Des. Res., 12, 1972, p. 179.

33. Rubenstein, C., "An Analysis of Dynamic Cutting when a Plane Surface is Cut with an Oscillating Tool II: Linearized Equations", Int. J. of Mac. Tool Des. Res., 12, 1972, p. 249.

34. Grieve, R.J., and Rubenstein, C., "An Experimental Investigation into the Dynamic Cutting of Steel", Int. J. of Mac. Tool Des. Res., 13, 1973, p. 1.

35. Sarnicola, J.F., and Boothroyd, D., "Machine Tool Chatter: Effect of Surface Slope on Machining Forces during Wave Removing", Trans. ASME, Ser., B, J. of Engg. for Indus., 96, 1974, p. 1102.

36. Boothroyd, G., "Fundamentals of Metal Machining and Machine Tools", McGraw Hill, 1975.

37. Sarvanja-Fabris, N., and D'Souza, A.F., "Nonlinear Stability Analysis of Chatter in Metal Cutting", Trans. ASME, Ser. B, J. of Engg. for Indus., Vol. 96, 1974, p. 670.

38. Hanna, N.H., and Tobias, S.A., "A Theory of Non-linear Regenerative Chatter", Trans. ASME, Ser. B, J. of Engg. for Indus., Vol. 96, 1974, p. 247.

39. Grasso, V., Nato LaDiega, S., and Passannanti, A., "Dynamic Cutting Co-efficients in Three-Dimensional Cutting", Int. J. of Mac. Tool Des. Res., 20, 1980, p. 325.

40. Bickel, E., "Die Wechselnden Kräfte bei der Spanbildung", Annals CIRP, Vol. 12, No. 4, 1966, p. 206.

41. Margos, S.K., "Measurement and Modelling of Cutting Force Fluctuations during Machining", M. Engg. Thesis, Sir George Williams University, Montreal, 1973.

42. Rakhit, A.K., Sankar, T.S., and Osman, M.O.M., "The Influence of Metal Cutting Forces on the Formation of Surface Texture in Turning", Int. J. of Mac. Tool Des. Res., Vol. 16, 1976, p. 281.

43. Osman, M.O.M., Xistris, G.D., and Chahil, G.S., "The Measurement and Stochastic Modelling of Torque and Thrust in Twist Drilling", Int. J. of Prod. Res., Vol. 17, No. 4, 1979, p. 359.

44. Wallichs, F., and Optiz, H., "Schu-β - Defries: Bediemmgsanweisungzun Me-β - Stahlhater", Dusseldorf, 1936.

45. Shaw, M.C., Cook, N.H., and Lowen, E.G., "Machine Tool Dynamometer- a Current Appraisal", American Machinist, Vol. 98, 10, 1954, p. 125.

46. Shaw, M.C., Lowen, E.G., and Marshall, E.R., "Electric Strain Gauge Tool Dynamometers", Proceedings S.E.S.A., Vol. 8, No. 2, 1951.

47. Okushima, K., and Hitomi, K., "A Design of a Three Component Tool Dynamometer", Trans. JSME, 1961.

48. Michelletti, G.F., Von Turkovich, B., Rossetto, S., "Three Force Component Piezoelectric Dynamometer [ITM-Mark 2]", Int. J. of Mac. Tool Des. Res., Vol. 10, 1970, p. 305.

49. Boston, O.W., and Gilbert, W.W., "The Torques and Thrusts in Small Drills Operating in Various Metals", Trans. ASME, Vol. 58, 1936.

50. Boston, O.W., and Oxford, C.J., "Power Required to Drill Cast Iron and Steel", Trans. ASME, Vol. 52, 1930.

51. Galloway, D.F., "Some Experiments on the Inlfuence of Various Factors on Drill Performance", Trans. ASME, Vol. 79, No. 2, Feb. 1957, p. 191.

52. Dean, S.K., and Kilburn, M.A., "Simple Torquemeter", The Engineer, Vol. 200, No. 5027, 1955, p. 686.

53. Schmidt, A.O., "Measurements and Controls that Enhance Machinability", Proceedings of the Exploratory Clinic on New Instrumentation Requirements for Metal Cutting", Michigan, 1958.

54. Ghosh, A., Mukherjee, S.C., and Bhattacharya, A., "A New Electronic Drill Dynamometer", Journal of Institution of Engineers (India), Vol. XLIII, No. 1, Part ME-1, 1962.

55. Boston, O.W., Gilbert, W.W., and Kaiser, K.B., "Power and Forces in Milling S.A.E.-3150 Steel with Helical Mills", Proceedings ASME, Vol. 59, 1937, p. 545.

56. Schmidt, A.O., "Determination of Tool Forces in High Speed Milling by Thermo-Analysis", Mech. Engg., Vol. 66, 1942.

57. Bendixen, I., "Face Milling-Power Measurements Guide Tool Selection", Tool Engr., Vol. 42, 4, 1959, p. 102.

58. Roubik, J.R., "Milling Torquemeter of Planetary Gear Design", Proceedings ASME, Vol. 83, No. 22, 1961, p. 155.

59. Cook, N.H., Lowen, E.G., and Shaw, M.C., "Machine Tool Dynamometer", American Machinist, July 1954.

60. Griffths, B.J., "The Measurement of Thrust and Torque in Deep-Hole Boring", Symposium Brünel University, Feb. 1973.

61. Sakuma, K., Taguchi, K., and Kinjo, S., "Study on Deep-Hole Drilling with Solid Boring Tool-The Effect of Tool Materials on the Cutting Performance", Bull. of the JSME, Vol. 21, No. 153, March 1978, p. 532.

62. Del Taglia, A., and Tani, G., "A Method for Measuring Cutting Forces in Boring Operation", Int. J. of Mac. Tool Des. Res., Vol. 22, No. 1, 1982, p. 23.

63. Sun, P.Y., Chang, Y.K., Wang, T.C., and Lui, P.T., "A Simple and Practical Piezo-electric Shank Type Dynamometer", Int. J. of Mac. Tool Des. Res., Vol. 22, No. 2, 1982, p. 111.

64. Tobias, S.A., "Machine Tool Vibration", Blackie and Son Ltd., Glasgow, U.K., 1965.

65. Koenigsberger, F., and Tlusty, J., "Machine Tool Structures", Vol. 1, Pergamon Press, 1970.

66. Peters, J., "Dynamic Analysis of Machine Tools using Complex Modal Method", Annals CIRP, Vo.. 25, No. 1, 1976, p. 257.

67. Tlusty, J., Lau, K.C., and Parthiban, K., "Use of Shock Compared with Harmonic Excitation in Machine Tool Structure Analysis", Trans. ASME, J. of Engg. for Indus., Ser. B, Vol. 96, 1974, p. 187.

68. Sexton, J.S., and Stone, B.J., "An Investigation of the Transient Effects During Variable Speed Cutting", J. of Mech. Engg. Science, Vol. 22, No. 3, 1980, p. 107.

69. Nigm, M.M., "A Method for the Analysis of Machine Tool Chatter", Int. J. of Mac. Tool Des. Res., Vol. 21, No. 3/4, p. 251.

70. Merritt, H.E., "Theory of Self-Excited Machine Tool Chatter", Trans. ASME., Ser. B, Vol. 87, 1965, p. 477.

71. Kwiatkowski, A.W., and Bennett, F.E., "Application of Random Force Excitation to the Determination of Receptances of Machine Tool Structures", Advances MTDR Conference, 1965.

72. Kwiatkowski, A.W., and Bennett, F.E., "Correlation Methods of System Identification, Computer Program and Experimental Design Considerations", Advances MTDR Conference, 1966.

73. Samaha, M., and Sankar, T.S., "Dynamic Acceptance Test for Machine Tools Based on a Non-linear Stochastic Model", Trans. ASME, Paper No. 79-DET-21.

74. Kwiatkowski, A.W., and Al Samarai, H.M., "Progress in the Application of Random Signal Analysis Methods to the Identification of Machine Tool Structures", Advances MTDR, 1968, p. 591.

75. Opitz, H., and Weck, M., "Determination of Transfer Function by Means of Spectral Density Measurements and Its Application to the Dynamic Investigation of Machine Tools Under Working Conditions", Advances in MTDR., 1969, p. 349.

76. Osman, M.O.M., and Sankar, T.S., "Short-Time Acceptance Test for Machine Tools Based on the Random Nature of the Cutting Forces", Trans. ASME, Jol. of Engg. for Indus., Vol. 94, No. 4, 1972, p. 1020.

77. Peklenik, J., and Kwiatkowski, A.W., "New Concepts in Investigating the Manufacturing by Means of Random Process Analysis", Proc. IMTDR Conference, 1965, p. 683.

78. Sharan, A.M., Sankar, T.S., and Sankar, S., "Dynamic Behaviour of Lathe Spindles with Elastic Supports Including Damping of Finite Element Analysis", The Shock and Vibration Bulletin, No. 51, Part 1, 1981, p. 83.

79. Burney, F.A., Pandit, S.M., and Wu, S.M., "A Stochastic Approach to Characterization of Machine Tool System Dynamics under Actual Working Condition", Trans. ASME, J. of Engg. for Indus., Ser., B, Vol. 98, 1976, p. 614.

80. Griffths, B.J., "An Investigation into the Role of the Burnishing Pads in the Deep-Hole Drilling Process", Ph.D. Thesis, Brunel University, 1982.

81. Ramamurthi, V., and Srinivasan, V., "Machine Tool Vibration-A Review", Shock and Vibration Digest, p.3.

82. Osman, M.O.M., "The BTA Technique - Fast Hole Machining", Tooling and Production, Feb. 1975, p. 49.

83. Corney, J., and Griffths, B., "A Study of the Cutting and Burnishing Operation during Deep-Hole Drilling and its Relationship to Drill Wear", Int. J. of Prod. Res., Vol. 14, No. 1, p. 1.

84. Tlusty, J., "Analysis of the State of Research in Cutting Dynamics", Annals CIRP, Vol. 27, No. 2, 1978, p. 583.

85. Osman, M.O.M., and Latinovic, V., "On the Development of Multi-Edge Cutting Tools for BTA Deep-Hole Machining", Trans. ASME, J. of Engg. for Indus., Ser. B, Vol. 98, No. 2, 1976, p. 474.

86. Latinovic, V., and Osman, M.O.M., "Unsymmetrical Multi-Edge Cutting in Deep-Hole Machining-Design Concept and Analysis", Proc. NAMRC-IV, 1976, p. 255.

87. Latinovic, V., and Osman, M.O.M., "On the Performance of Unsymmetrical Multi-Edge Tools for BTA Deep-Hole Machining-Test Results", Proc. NAMRC-IV, 1978, p. 317.

88. Latinovic, V., Blakely, R., and Osman, M.O.M., "Optimal Design of Multi-Edge Cutting Tools for BTA Deep-Hole Machining", Trans. ASME, J. of Mech. Des., Vol. 101, 1979, p. 281.

89. Kahng, C.H., and Ham, I., "A Study on Sequential Quality Improvement in Hole Making Processes", Annals of the CIRP, Vol. 24, No. 1, 1975, p. 27.

90. Sakuma, K., Taguchi, K., and Katsuki, A., "Study on Deep-Hole Drilling with Solid Boring Tool-The Burnishing Action of Guide Pads and Their Influence on Hole Accuracies", Bull. of the JSME, Vol. 23, No. 185, 1980, p. 1921.

91. Sakuma, K., Taguchi, K., and Katsuki, A., "Study on Deep-Hole Boring by a BTA System Solid Boring Tool-Behaviour of Tool and Its Effects on the Profile of the Machined Hole", Bull. of the JSPE, Vol. 14, No. 3, 1980, p. 143.

92. Sakuma, K., Taguchi, K., and Katsuki, A., "Self Guiding Action of Deep-Hole Drilling Tools", Annals CIRP, Vol. 30, No. 1, 1981, p. 311.

93. Osman, M.O.M., Latinovic, V., and Greuner, B., "On the Performance of Cutting Fluids for BTA Deep-Hole Machining", Int. J. of Prod. Res., 1981, Vol. 19, No. 5, p. 491.

94. Zorev, N.N., "Metal Cutting Mechanics", Pergamon Press, 1966.

95. Gautschi, G.H., "Cutting Forces in Machining and Their Routine Measurement with Multi-Component Piezo-Electric Force Transducers", Adv. in MTDR, 1971, p. 113.

96. Sen, G.C., and Bhattacharya, A., "Principles of Metal Cutting", New Central Book Agency, 1969.

97. Shigley, J.M., "Mechanical Engineering Design", McGraw Hill, N.Y., 1977.

98. Piezo-Instrumentation KISTLER, "2-Component Load Washer (F_z,M_z) - Type 9065", Nr. 6.9065de.

99. Kistler Piezo-Messtechnik, "Kistler Instrument AG Data Catalogue", Nr. 1.002e.

100. Knight, W.A., and Sadek, M.M., "The Correction for Dynamic Errors in Machine-Tool Dynamometers", Annal CIRP, Vol. 19, 1971, p. 237.

101. Garcia-Gardea, E., Burney, F.A., and Wu, S.M., "Determination of True Cutting Signal by Separation of Instrumentation Dynamics from Measured Response", Trans. ASME, J. Engg. for Indus., Vol. 101, 1979, p. 264.

102. Field, J.S., "Investigating the Frequency Response of Cutting Force Dynamometers by Transient Loading", Int. J. of Prod. Res., Vol. 20, No. 1, 1982, p. 57.

103. Bendat, J.S., and Piersol, A.G., "Random Data: Analysis and Measurement Procedures", Wiley Interscience, 1971.

104. Bendat, J.S., and Piersol, A.G., "Measurement and Anslysis of Random Data", Wiley Interscience, 1966.

105. Acherkan, N., "Machine Tool Design-Vol. 3", Mir Publishers, Moscow, 1973.

106. Meirovitch, L., "Elements of Vibrations Analysis", McGraw Hill, New York, 1975.

107. Thomson, W.T., "Theory of Vibration with Applications", Prentice Hall, New Jersey, 1981.

108. Henry, R.F., and Tobias, S.A., "Instability and Steady State Coupled Motions in Vibration Isolation Systems", J. of Mech. Engg. Science, Vol. 1, 1959, p. 19.

109. Optiz, H., and Salje, E., "Reibwertmessung an kunstoffgleitführungen für werkzeugmaschinen", Industrie-Anzeiger, No. 63, 1952, p. 116.

110. Griffths, B.J., "The Machining Action during Deep-Hole Boring and the Resultant Hole Form and Force System", Proc. Second Int. Con. on Prod. Res., 1973.

111. Chandrashekhar, S., Osman, M.O.M., and Sankar, T.S., "An Analytical Time Domain Evaluation of the Cutting Forces in BTA Deep-Hole Machining using the Thin Shear Plane Model", To be Published in the Int. J. of Prod. Res.

112. Chandrashekhar, S., Osman, M.O.M., and Sankar, T.S., "An Experimental Investigation into the Stochastic Modelling of the Resultant Force System in BTA Deep-Hole Machining", To be published in the Int. J. of Prod. Res.

113. Harris, C.M., and Crede, C.E., "Shock and Vibration Handbook", McGraw Hill, New York, 1976.

114. Tso, W.K., "Parametric Torsional Instability of a Bar under Axial Excitation", Trans. ASME, J. of App. Mech., 35, 1968, p. 13.

115. Greenwood, D.T., "Classical Dynamics", Prentice Hall, New Jersey, 1977.

116. Chandrashekhar, S., Osman, M.O.M., and Sankar, T.S., "A Stochastic Characterization of the Machine Tool Workpiece System in BTA Deep-Hole Machining - Part I: Mathematical Modelling and Analysis" To be published in the Trans. I.Mech.E.

117. Ibrahim, R.A., and Roberts, J.B., "Parametric Vibration, Part V: Stochastic Problems", Shock and Vibration Digest, Vol. 10, No. 5, 1978, p. 17.

118. Stratonovich, R.L., "Topics in the Theory of Random Noise-Vol. 1", Gordon and Breach, New York, 1963.

119. Stratonovich, R.L., "Topics in the Theory of Random Noise-Vol. 2", Gordon and Breach, New York, 1963.

120. Kuznetsov, P.I., Stratonovich, R.L., and Tikhonov, V.I., "Non-Linear Transformations of Stochastic Processes", Pergamon Press, Oxford, 1965, p. 322.

121. Chuang, K., and Kazda, F., "A Study of Non-Linear Systems with Random Inputs", Amer. Inst. Elec. Engg., No. 42, 1959, p. 100.

122. Ariaratnam, S.T., "Random Vibration of Non-Linear Suspensions", J. Mech. Engg. Science, Vol. 2, No. 3, 1960, p. 195.

123. Caughey, T.K., "Derivation and Application of the Fokker Planck Equation to Discrete Non-Linear Dynamic Systems Subjected to White Random Excitation", J. of Acous. Soc. of America, Vol. 35, No. 11, 1963, p. 1683.

124. Bedini, R., Pinotti, P.C. and Presciuttini, G., "Adaptive Control in Drilling", Int. J. of Mac. Tool Des. Res., Vol. 17, 1977, p. 91.

125. Bedini, R., and Pinotti, P.C., "Experiments on Adaptive Constrained Control of a CNC Lathe", Trans. ASME, J. of Engg. for Indus., Ser., B, Vol. 104, 1982, p. 139.

126. Amitay, G., Malkin, S., and Koren, Y., "Adaptive Control Optimization of Grinding", Trans. ASME, J. of Engg. for Indus., Ser. B, Vol. 103, No. 1, 1981, p. 102.

127. Bedini, R., and Lisini, G., "Experiments on Adaptive Control of a Milling Machine", Trans. ASME, J. of Engg. for Indus., Ser. B, 1976, p. 235.

128. Tlusty, J., and Elbestarvi, M., "Constraints in Adaptive Control with Flexible End Mills", Annals of CIRP, Vol. 28, No. 1, 1979, p. 253.

129. Ulsoy, A.G., Koren, Y., and Rasmussen, F., "Principal Developments in the Adaptive Control of Machine Tools", Trans. ASME, J. of Dy. Sys., Mea., and Control, Vol. 105, 1983, p. 107.

130. Venkatesh, V.C., and Chandrasekaran, H., "Experimental Methods in Metal Cutting", Prentice Hall of India, New Delhi, 1982.

131. Rakhit, A.K., Sankar, T.S., and Osman, M.O.M., "The Influence of Metal Cutting Forces on the Formation of Surface Texture in Turning", Int. J. of Mach. Tool Des. Res., Vol. 16, 1976, p. 281.

132. Frazao, J., Chandrashekhar, S., Osman, M.O.M., and Sankar, T.S., "On the Correlation Between the Dynamic Fluctuations of the Resultant Force System and Surface Texture in BTA Deep-Hole Machining", To be published.

133. Landau, Y.D., "Adaptive Control: The Model Reference Approach", Marcel Dekker, New York, 1979.

134. Wick, C., "Automatic Adaptive Control of Machine Tools", Manu. Engg., Vol. 79, No. 3, 1977, p. 38.

135. Yen, D.W., and Wright, P.K., "Adaptive Control in Machining-A New Approach Based on the Physical Constraints of Tool Wear Mechanisms", Trans. ASME, J. of Engg. for Indus., Ser. B, Vol. 105, 1983, p. 31.

136. De Felippi, A., and Ippolito, R., "Adaptive Control in Turning: Cutting Forces and Tool War Relationship for P10, P20 and P30 Carbides", Annals of the CIRP, Vol. 17, 1969, p. 377.

137. Brecker, J.N., and Shum, L.Y., "Tool Collision and Machine Considerations in Adaptive Control Systems", Annals of the CIRP, Vol. 25, No. 1, 1976, p. 319.

138. Arsovski, S.M., "Wear Sensors in the Adaptive Control of Machine Tools", Int. J. of Prod. Res., Vol. 21, No. 3, 1983, p. 347.

139. Weck, M., et al, "Adaptive Control of Face Milling Operations with Strategies for Avoiding Chatter Vibrations and for Automatic Cut Distributions", Annas of the CIRP, Vol. 24, No. 1, 1975, p. 405.

140. Inamura , T., Senda, T., and Sata, T., "Computer Control of Chattering in Turning Operation", Annals of the CIRP, Vol. 25, No. 1, 1977, p. 181.

141. Srinivasan, K., and Nachtigal, C.L., "Analysis and Design of Machine Tool Chatter Control Systems using the Regeneration Spectrum", Trans. ASME, J. of Dyn. Sys. Meas. and Control, Vol. 100, 1978, p. 191.

142. Tuffentsammer, K., "Feasibility of Controlled Adaption in Deep-Hole Boring", International Conference of Deep-Hole Boring and Drilling, Brunel University.

143. Kuznetsov, P.I., Stratanovitch, R.L., and Tikhonov, V.I., "On the Duration of Excursions of Random Functions", Non-Linear Transformations of Stochastic Processes, Pergamon Press, Oxford, 1965, p. 341.

144. Tikhonov, V.I., "The Distribution of the Duration of Excursions of Normal Fluctuations", Non-Linear Transformations of Stochastic Processes, Pergamon Press, Oxford, 1965, p. 354.

145. Tikonov, V.I., "An Experimental Study of the Length Distribution Law of Fluctuation Excursions", Non-Linear Transformations of Stochastic Processes, Pergamon Press, Oxford, 1965, p. 368.

146. Tikhonov, V.I., "Fluctuation Excursion and Their Correlation", Non-Linear Transformations of Stochastic Processes, Pergamon Press, Oxford, 1965.

147. Tikhonov, V.I., "Probability Densities for the Duration of Fluctuation Excursions", Non-Linear Transformations of Stochastic Processes, Pergamon Press, Oxford, 1965, p. 382.

148. Tikhonov, V.I., "The Effect of Differentiating and Integrating on the Average Number of Excursions", Non-Linear Transformations of Stochastic Processes, Pergamon Press, Oxford, 1965, p. 396.

149. Sankar, T.S., and Osman, M.O.M., "Profile Characterization of Manufactured Surfaces Using Random Function Excursion Technique - Part I: Theory", Trans. ASME, J. of Engg. for Indus., Ser. B, 1975, p. 190.

150. Osman, M.O.M., and Sankar, T.S., "Profile Characterization of Manufactured Surfaces Using Random Function Excursion Technique-Part II: Application", Trans. ASME, J. of Engg. for Indus., Ser. B, 1975, p. 196.

151. Chandrashekhar, S., Sankar, T.S., and Osman, M.O.M., "A Stochastic Characterization of the Machine Tool Workpiece System in BTA Deep-Hole Machining - Part II: Response Analysis and Evaluation of the Tool Tip Motion", To be published in Trans. I.Mech.E.